



Universität Hamburg  
DER FORSCHUNG | DER LEHRE | DER BILDUNG

# Interaction of polyurethane with wood-based sandwich panels

## Dissertation

with the aim of achieving a doctoral degree (Dr. rer. nat)  
at the Faculty of Mathematics, Informatics and Natural Sciences

Department of Biology  
Institute of Wood Science  
of Universität Hamburg

submitted by

**Kanokorn Sae-Ueng**  
born in Surat Thani, Thailand

Hamburg 2021

1. Examiner: Prof. Dr. Andreas Krause  
Institute of Wood Science, Department of Biology,  
Universität Hamburg / Thünen Institut of Wood Research,  
Germany

2. Examiner: Prof. Dr. Bodo Saake  
Institute of Wood Science, Department of Biology,  
Universität Hamburg,  
Germany

Date of defense: 25<sup>th</sup> March 2021

Vicki Marais  
Dorfstr. 31  
23881 Koberg  
Germany

21.01.2021

**Letter of confirmation**

I, Vicki Marais, being an English teacher at the Berlitz Language school, located in Hamburg, Germany; hereby confirm that I have assisted Kanokorn Sae-Ueng with her dissertation *Interaction of polyurethane with wood-based sandwich panels*.

Having grown up and resided in South Africa for twenty one years with English as my home language, after which I spent 14 years in England, I can confirm that I am a native speaker of the English language. Additionally, all of the my schooling and further studies were completed in English.

I assisted Kanokorn by correcting the language and grammar of her dissertation, in order to clarify her thoughts and the results of her study. I reviewed the complete dissertation, from the first page to the conclusion.



Vicki Marais

**Eidesstattliche Versicherung / Declaration on oath**

Hiermit erkläre ich an Eides statt, dass ich die vorliegende Dissertationsschrift selbst verfasst und keine anderen als die angegebenen Quellen und Hilfsmittel benutzt habe.

*I hereby declare upon oath that I have written the present dissertation independently and have not used further resources and aids than those stated.*

Hamburg, den 22.01.2021

Unterschrift|Signature

# Abstract

---

The continuous one-step production process for light wood-based panels patented by Lüdtke et al. (2007) allows for the expansion of a foam core in a hot press after the compaction of surface layers. Thermoplastic materials have been successfully applied as the core material but require a final cooling phase in a production unit in order to stabilize the expanded polymer foam after pressing. Polyurethane (PUR), as a thermoset, does not require this process step. The self-adhesive property, low thermal conductivity and tailor-made preparation based on selected components and formulations, make PUR an attractive core layer. However, isocyanate's high reactivity challenges the control of PUR foam reaction in the one-step production of wood-based panels. Besides, PUR may be fluid when compressed due to its liquid nature, so it does not remain static during the pressing process. The potential PUR components need to be scattered, able to mix well with wood chips and inactive under normal conditions, yet have the ability to be triggered by external parameters in the process. In order to develop PUR components into an efficient precursor to fulfill the core material requirements of the one-step production process, this thesis focuses on chemical and physical solutions: blocked isocyanates to trigger the foaming reaction thermally and wood filler addition to improve the distribution within the core layer.

Blocked isocyanates are an adduct formed by the reaction of isocyanate with an active hydrogen compound, stable at normal temperature. The isocyanate group could be re-released at elevated temperatures. Regarding the mechanism, blocked isocyanates from pMDI and 4,4'-MDI were prepared using  $\text{NaHSO}_3$  and  $\epsilon$ -caprolactam as blocking agents. Blocked isocyanates were mixed with sucrose-based polyether polyol to prepare the one-component (1-C) PUR mixture, which must be cured at high temperatures in the hot press to polymerize and create a foam core. Blocked isocyanates were successfully prepared according to FTIR. The deblocking temperatures measured by DSC and TGA for both blocked adducts by  $\text{NaHSO}_3$  and  $\epsilon$ -caprolactam were 90-127 and 180-226 °C respectively. The NCO release from deblocked products was not so intensive as that in the pure isocyanate. Polyol was mixed into the 1-C PUR mixture with blocked isocyanates and cured in the DSC using different times and temperatures. For  $\text{NaHSO}_3$ -blocked isocyanates, the IR results exhibited the closest similarity to PUR using the weight ratio of 2:1 of blocked isocyanate per polyol.  $\epsilon$ -caprolactam-blocked isocyanates showed better IR results in the mixture with a 1:1 ratio. However, a high curing temperature of 250 °C was applied in both cases. Other factors (curing time,

heating rate and isocyanate types) did not affect the cured mixture's IR results significantly.

Wood addition was another intriguing concept used to adjust the PUR formulations for an application in the process. In the following study, wood-mixed PUR foams were produced by thermal curing and investigated for foaming properties. The addition of wood affected the physical and mechanical properties of PUR foam but not the chemical characteristics. PUR containing a wood content of 40 % achieved the highest density of ca.  $90 \text{ kgm}^{-3}$  due to the mixture's higher viscosity. It also had a significantly decreased compressive strength with ca. 0.009 MPa compared to that of 10 % filler containing PUR, which is 0.190 MPa. The compressive properties did not change significantly by varying the wood flour content between 0–12 % in the PUR foam. The curing temperature also had a considerable influence on foam properties. The density of wood-mixed PUR foam decreased significantly from an average of 146 to  $70 \text{ kgm}^{-3}$  when a curing temperature from room temperature (20-25 °C) to 100 °C was applied. Considering both factors, an addition of 10 % wood and a curing temperature of 100 °C appeared to be the optimal parameters for further study.

The thermally activated PUR reaction was infeasible due to the low reactivity of deblocked isocyanates. In the practical application, the time for the pressing hot plates was measured and observed during foam growth in the core layer, being used afterwards as a reference for the duration of foam growth, in order to control foam expansion in the core layer in further experiments. PUR with 10 and 20 % wood contents was added to the middle layer of sandwich panels surfaced by MDF sheets. The plate-closing or pressing time was identified by time to foam rise. Panels were produced without pressing (100X) and with a plate-opening distance of 50 % (50X). The foam densities were measured between 33-90 and 32-153  $\text{kgm}^{-3}$  from the PUR cores with 10 and 20 % wood content, respectively. The target panel thickness was achieved only in 100X panels. Inserting the plate-closing distance in 50X panels, the PUR did not have sufficient resistance against pressing, which led to material compaction and unapproachable thickness. 100X panels exhibited higher deviation in compressive properties and internal bond than 50X panels due to the free but irregular foam expansion.

This thesis has revealed possible solutions for preparing a PUR foam core within wood-based panel production, which should be considered and researched further to improve the aforementioned continuous process.

# Zusammenfassung

---

Der von Lüdtké et al. (2007) patétierte kontinuierliche Prozess zur Herstellung von holzbasierten Leichtbauplatten ermöglicht die Expansion des Schaumkerns durch Heißpressen während der Verdichtung der Deckschichten in einem Schritt. Als Kernmaterial wurden erfolgreich thermoplastische Materialien eingesetzt. Bei der Verwendung dieser Kunststoffe benötigt der Produktionsprozess jedoch eine zusätzliche Kühleinheit zur Stabilisierung der Platten nach dem Pressen. Als Duroplast benötigt Polyurethan (PUR) diesen Stabilisierungsschritt nicht. Die selbstklebende Eigenschaft, die geringe Wärmeleitfähigkeit und die maßgeschneiderte Aufbereitung durch Auswahl der Komponenten und Rezepturen machen PUR zu einer attraktiven Kernschicht. Allerdings stellt die hohe Reaktivität des Isocyanats eine Herausforderung für die Steuerung der PUR-Schaumreaktion dar. Aufgrund der flüssigen Beschaffenheit von PUR besteht außerdem das Problem, dass dieses beim Komprimieren herausfließen kann. Die potenziellen PUR-Komponenten müssen gleichmäßig verteilt, gut mit Holzspänen mischbar, unter normalen Bedingungen inaktiv sein und während des Pressvorgangs durch externe Parameter reaktiviert werden können. Die Arbeit konzentriert sich auf chemische und physikalische Lösungen für die Entwicklung von PUR-Komponenten zu einem effizienten Vorprodukt. Als chemischer Ansatz werden blockierte Isocyanate zur thermischen Auslösung der Schaumreaktion untersucht, während sich der physische Ansatz mit dem Zusatz von Holzfüllstoff zur Verbesserung der Verteilung innerhalb der Kernschicht befasst.

Blockiertes Isocyanat ist ein Addukt, das durch die Reaktion von Isocyanat mit einer aktiven Wasserstoffverbindung gebildet wird und bei Normaltemperatur stabil ist. Die Isocyanatgruppe kann bei erhöhten Temperaturen wieder freigesetzt werden. Die blockierten Isocyanate wurden aus pMDI und 4,4'-MDI mit NaHSO<sub>3</sub> und ε-Caprolactam als Blockierungsmittel hergestellt. Zum Nachweis der erfolgreichen Blockierung wurde FTIR-Spektroskopie verwendet. Diese blockierten Isocyanate wurden danach mit Polyetherpolyol auf Saccharosebasis gemischt, um die Einkomponenten-(1-K)-PUR-Mischung herzustellen, die durch hohe Temperaturen in der Heißpresse ausgehärtet wird, um den Schaumkern zu polymerisieren. Die mittels DSC und TGA gemessenen Deblockierungstemperaturen für beide blockierten Addukte durch NaHSO<sub>3</sub> und ε-Caprolactam lagen bei 90-127 bzw. 180-226 °C. Die NCO-Freisetzung aus den entblockten Produkten war nicht so intensiv wie bei reinem Isocyanat. Polyol wurde mit blockierten Isocyanaten in das 1-K-PUR-Gemisch eingemischt und im DSC mit unterschiedlichen Zeiten und Temperaturen ausgehärtet. Für NaHSO<sub>3</sub>-blockierte

Isocyanate zeigten die IR-Ergebnisse die größte Ähnlichkeit mit PUR bei einem Gewichtsverhältnis von 2:1 von blockiertem Isocyanat pro Polyol.  $\epsilon$ -Caprolactam-blockierte Isocyanate zeigten bessere IR-Ergebnisse bei einem Mischverhältnis von 1:1. Allerdings wurde in beiden Fällen eine hohe Härtungstemperatur von 250 °C angewendet.

In der zweiten Studie wird das Konzept der Holzbeimischung untersucht. Es wurden dabei holzgemischte PUR-Schäume durch thermische Aushärtung hergestellt und auf die Schaumeigenschaften getestet. Der Holzzusatz beeinflusste die physikalischen und mechanischen Eigenschaften des PUR-Schaums, nicht aber die chemischen Eigenschaften. PUR mit 40 % Holzanteil erreichte aufgrund der höheren Viskosität der Mischung eine hohe Dichte von ca.  $90 \text{ kgm}^{-3}$ . Es hatte auch eine deutlich verringerte Druckfestigkeit mit ca. 0,009 MPa im Vergleich zu 0,190 MPa bei 10 % füllstoffhaltigem PUR. Die Druckeigenschaften änderten sich bei einer Variation zwischen 0-12 % Holzmehlanteil im PUR-Schaum nicht signifikant. Auch die Aushärtetemperatur hatte einen erheblichen Einfluss. Die Dichte von holzgemischtem PUR-Schaum sank signifikant von durchschnittlich 146 auf  $70 \text{ kgm}^{-3}$ , wenn die Aushärtetemperatur von Normaltemperatur auf 100 °C erhöht wurde. Der Holzzusatz von 10 % und die Aushärtungstemperatur bei 100 °C schienen optimale Parameter für weitere Untersuchungen zu sein.

Die thermisch aktivierte PUR-Reaktion war aufgrund der geringen Reaktivität der deblockierten Isocyanaten nicht durchführbar. In der praktischen Anwendung wurde die Schaumreaktion über die Presszeit im Verhältnis zum Schaumanstieg gesteuert. PUR mit 10 und 20 % Holzanteil wurde in die Mittelschicht von Sandwichplatten, die mit MDF-Platten belegt waren, eingebracht. Der Plattenschluss bzw. die Presszeit wurde über die Zeit bis zum Schaumaufstieg ermittelt. Die Platten wurden ohne Verpressung (100X) und mit 50 % Plattenöffnungsabstand (50X) hergestellt. Die Schaumdichten wurden zwischen 33-90 und 32-153  $\text{kgm}^{-3}$  aus den PUR-Kernen mit 10 bzw. 20 % Holzanteil gemessen. Die Zielplattendicke wurde nur bei 100X-Platten erreicht. Aufgrund des mangelnden Widerstands des PUR Schaums führte der Pressvorgang bei 50X-Platten zu Materialverlust und unzureichender Dicke. 100X-Platten wiesen aufgrund der freien aber ungleichmäßigen Schaumausdehnung eine höhere Abweichung der Druck- und Quergeigenschaften auf, als 50X-Platten. Die Arbeit zeigt die Ergebnisse aus der Anwendung möglicher Varianten zur Vorbereitung des PUR-Schaumkerns innerhalb des kontinuierlichen Herstellungsprozesses von Leichtbauplatten. Diese Ergebnisse sollten bei Anwendung des Prozesses berücksichtigt werden und dienen als Grundlage zur weiteren Prozessoptimierung.

# Contents

|  |           |
|--|-----------|
| Abstract   |           |
| Zusammenfassung  |           |
| Abbreviations and Terms  |           |
| <b>Chapter 1 Introduction</b>                                      | <b>1</b>  |
| <b>Chapter 2 Background &amp; current state of knowledge</b>       | <b>5</b>  |
| 2.1 Lightweight sandwich panel and production processes            | 5         |
| 2.1.1 Lightweight wood-based panel                                 | 7         |
| 2.1.2 Sandwich panel   | 9         |
| 2.1.3 Production processes   | 15        |
| 2.1.3.1 Application of PUR foam                                    | 15        |
| 2.1.3.2 Production process of wood-based panel with foam core      | 17        |
| 2.1.3.2.1 Discontinuous production                                 | 17        |
| 2.1.3.2.2 Continuous production                                    | 18        |
| 2.2 Polyurethane (PUR)   | 21        |
| 2.2.1 PUR rigid foam   | 22        |
| 2.2.1.1 Important PUR reactions                                    | 25        |
| 2.2.1.2 Foaming process  | 26        |
| 2.2.1.3 Foam development   | 27        |
| 2.2.1.4 Reaction kinetics  | 28        |
| 2.2.2 Interaction with wood  | 31        |
| 2.2.2.1 Effects of wood addition in PUR foam                       | 31        |
| 2.2.2.2 Chemical interaction between wood and isocyanate           | 33        |
| 2.3 Blocked isocyanates  | 35        |
| 2.3.1 Mechanisms of blocked isocyanates                            | 36        |
| 2.3.2 Deblocking temperature                                       | 38        |
| 2.3.3 Blocking agents and their applications                       | 40        |
| 2.3.3.1 Sodium bisulfite (NaHSO <sub>3</sub> )                     | 41        |
| 2.3.3.2 ε-caprolactam  | 42        |
| <b>Chapter 3 Objectives and research plan</b>                      | <b>43</b> |
| 3.1 Study I: Blocked isocyanates for PUR rigid foam                | 44        |
| 3.2 Study II: Effects of wood addition and temperature on PUR foam | 45        |
| 3.3 Study III: PUR foaming within the one-step panel production    | 46        |
| <b>Chapter 4 Materials and methods</b>                             | <b>47</b> |
| Materials  | 47        |
| Methods  | 48        |
| 4.1 Sample production  | 48        |
| 4.1.1 Study I: Blocked isocyanates for PUR rigid foam              | 48        |

|   |  |           |
|---|--|-----------|
| 4.1.1.1                                       | Synthesis of blocked isocyanates .....                               | 48        |
| 4.1.1.1.1                                     | Blocking by NaHSO <sub>3</sub> .....                                 | 49        |
| 4.1.1.1.2                                     | Blocking by ε-caprolactam .....                                      | 49        |
| 4.1.1.2                                       | CO <sub>2</sub> detection test during the blocking process.....      | 49        |
| 4.1.1.3                                       | NCO conversion of deblocked isocyanates .....                        | 50        |
| 4.1.1.4                                       | PUR curing via reaction with polyol.....                             | 51        |
| 4.1.2   | Study II: Effects of wood addition and temperature on PUR foam ..... | 52        |
| 4.1.3   | Study III: PUR foaming within the one-step panel production.....     | 54        |
| 4.1.3.1                                       | Design of press program .....  | 54        |
| 4.1.3.2                                       | Panel production .....   | 54        |
| 4.2   | Sample preparation .....   | 57        |
| 4.2.1   | PUR from cup testing .....   | 57        |
| 4.2.2   | Panel sample.....  | 57        |
| 4.3   | Sample characterization.....   | 59        |
| 4.3.1   | Chemical characterization .....                                      | 59        |
| 4.3.1.1                                       | FTIR spectroscopy .....  | 59        |
| 4.3.1.2                                       | DSC analysis.....  | 60        |
| 4.3.1.3                                       | TGA .....  | 60        |
| 4.3.2   | Physical characterization.....                                       | 61        |
| 4.3.2.1                                       | Density and density profile .....                                    | 61        |
| 4.3.2.2                                       | Microscopic and elemental analysis.....                              | 61        |
| 4.3.2.3                                       | Cell size measurement.....   | 62        |
| 4.3.2.4                                       | Open-cell content .....  | 62        |
| 4.3.2.5                                       | Thermal conductivity and resistance.....                             | 64        |
| 4.3.3   | Mechanical characterization.....                                     | 65        |
| 4.3.3.1                                       | Compression properties .....   | 65        |
| 4.3.3.2                                       | Internal bond .....  | 65        |
| 4.4   | Data analysis.....   | 66        |
| <b>Chapter 5 Results and discussion .....</b> |  | <b>67</b> |
| 5.1   | Study I: Blocked isocyanates for PUR rigid foam .....                | 67        |
| 5.1.1   | Characterization of blocked isocyanates.....                         | 67        |
| 5.1.1.1                                       | Commercial blocked isocyanate .....                                  | 67        |
| 5.1.1.2                                       | Blocked isocyanates by NaHSO <sub>3</sub> .....                      | 68        |
| 5.1.1.3                                       | Blocked isocyanates by ε-caprolactam .....                           | 72        |
| 5.1.2   | CO <sub>2</sub> detection test during blocking process .....         | 77        |
| 5.1.3   | NCO conversion of deblocked isocyanates .....                        | 79        |
| 5.1.4   | PUR curing .....   | 82        |
| 5.1.4.1                                       | Reaction of NaHSO <sub>3</sub> -blocked isocyanates with polyol..... | 84        |
| 5.1.4.2                                       | Reaction of ε-caprolactam-blocked isocyanates with polyol .....      | 87        |

|         |  |     |
|---------|--|-----|
| 5.1.5   | Discussion .....   | 92  |
| 5.2     | Study II: Effects of wood addition and temperature on PUR foam .....     | 94  |
| 5.2.1   | PUR foam reaction analysis .....   | 94  |
| 5.2.2   | PUR foam characterization .....  | 95  |
| 5.2.2.1 | FTIR characterization .....  | 95  |
| 5.2.2.2 | Foam morphology .....  | 96  |
| 5.2.2.3 | Material characterization by EDX .....                                   | 99  |
| 5.2.2.4 | Open-cell content .....  | 100 |
| 5.2.2.5 | Cell size .....  | 103 |
| 5.2.2.6 | Foam densities .....   | 107 |
| 5.2.2.7 | Compressive properties .....   | 110 |
| 5.2.2.8 | Relationship between compressive strength, cell size and densities ..... | 113 |
| 5.3     | Study III: PUR foaming within the one-step panel production .....        | 116 |
| 5.3.1   | Foam rise analysis .....   | 116 |
| 5.3.1.1 | Temperature development during the foaming reaction .....                | 116 |
| 5.3.1.2 | Relationship between internal temperature and foam rise .....            | 117 |
| 5.3.1.3 | Effects of foam formulation on the internal temperature .....            | 119 |
| 5.3.2   | Designing the press program .....  | 121 |
| 5.3.3   | Properties of produced PUR sandwich panels .....                         | 123 |
| 5.3.3.1 | Foam morphology .....  | 123 |
| 5.3.3.2 | Cell size .....  | 124 |
| 5.3.3.3 | Foam density .....   | 126 |
| 5.3.3.4 | Apparent density and thickness .....                                     | 126 |
| 5.3.3.5 | Compression properties .....   | 128 |
| 5.3.3.6 | Internal bond .....  | 130 |
| 5.3.3.7 | Thermal resistance and conductivity .....                                | 131 |
| 5.4     | Overall discussion .....   | 134 |
|         | <b>Chapter 6 Conclusion</b> .....  | 140 |
|         | <b>Chapter 7 Outlook</b> .....   | 142 |
|         | Appendix I: FTIR absorbance units of PUR .....                           | 144 |
|         | Appendix II: Calculation of atom ratios in different materials .....     | 145 |
|         | Appendix III: Internal temperature of PUR mixture during pressing .....  | 146 |
|         | List of Tables .....   | 147 |
|         | List of Figures .....  | 148 |
|         | References .....   | 152 |
|         | Acknowledgements   |     |

## Abbreviations and Terms

|                    |   |                                     |
|--------------------|---|-------------------------------------|
| 1-C, 2-C           | one-component, two-component              |                                     |
| ANOVA              | one-way analysis of variance              |                                     |
| CFC                | chlorofluorocarbon                        |                                     |
| CO <sub>2</sub>    | carbon dioxide                            |                                     |
| DBTDL              | dibutyltin dilaurate                      |                                     |
| DSC                | differential scanning calorimetry         |                                     |
| EDX                | energy dispersive X-ray spectroscopy      |                                     |
| EPS                | expanded polystyrene                      |                                     |
| FJ                 | finger-jointed lumber                     |                                     |
| FRD/FRH            | free rise density/free rise height        |                                     |
| FTIR               | fourier transform infrared                |                                     |
| Glulam             | glue-laminated lumber                     |                                     |
| hr                 | hours                                     |                                     |
| HCFCs              | hydrochlorofluorocarbons                  |                                     |
| HDF                | high-density fiberboard                   |                                     |
| HDI                | hexamethylene diisocyanate                |                                     |
| HFCs               | hydrofluorocarbons                        |                                     |
| IPDI               | isophorone diisocyanate                   |                                     |
| IR                 | infrared                                  |                                     |
| LSD                | least significant difference              |                                     |
| LSP                | light structural panel                    |                                     |
| LVL                | laminated veneer lumber                   |                                     |
| MDF                | medium-density fiberboard                 |                                     |
| MDI                | methylene diphenyl diisocyanate           |                                     |
| min                | minutes                                   |                                     |
| MS                 | microsphere                               |                                     |
| NaHSO <sub>3</sub> | sodium bisulfite                          |                                     |
| NCO                | isocyanate                                |                                     |
| OSB                | oriented strand board                     |                                     |
| PAPI               | polyaryl polymethylene isocyanate         |                                     |
| PBA                | physical blowing agent                    |                                     |
| PE                 | polyethylene                              |                                     |
| PIR                | polyisocyanurate                          |                                     |
| PMDI               | polymeric methylene diphenyl diisocyanate |                                     |
| PS                 | polystyrene                               |                                     |
| PUR                | polyurethane                              |                                     |
| PVC                | polyvinyl chloride                        |                                     |
| SEM                | scanning electron microscope              |                                     |
| TDI                | toluene diisocyanate                      |                                     |
| TGA                | thermogravimetric analysis                |                                     |
| UF                 | urea-formaldehyde                         |                                     |
| VOCs               | volatile organic compounds                |                                     |
| WPC                | wood plastic composite                    |                                     |
| $\alpha$           | isocyanate conversion                     | [%]                                 |
| $\lambda$          | thermal conductivity                      | [Wm <sup>-1</sup> K <sup>-1</sup> ] |
| $R$                | thermal transfer resistance               | [m <sup>2</sup> KW <sup>-1</sup> ]  |
| $T$                | temperature                               | [°C]                                |

# 1 Introduction

---

Weight reduction in structures became significantly important in World War II due to the demand for lightweight building materials in aircraft. The Mosquito aircraft utilizing veneer faces with a balsa core was produced in England by mass production of sandwich panels for the first time during the 1940s, due to the shortage of other materials as well as an appreciation of the structural efficiency of the concept (Zenkert, 1995). Since that time, lightweight construction has been widespread in various applications and continues to grow rapidly owing to a variety of motivations. In addition to improving the functionalities – as in vehicles and saving material and related material costs, the lightweight concept reduces ecological degradation i.e. indirectly decreased energy or higher loading volume for transportation. Therefore, the concept is motivated by functional, economic and environmental aspects (Wiedemann, 2007).

Many strategies have been applied as regards for the weight reduction of conventional particleboard and other wood-based panels, such as using lightweight wood species, adding light fillers, hollow profiles or less compaction of the wood mat. However, reduction in material weight is usually challenged by the decreased mechanical properties and limitations in production i.e. consumption of a higher amount of resin or more complicated post-processing in terms of surface finishing and post-forming (Monteiro et al., 2018). The sandwich concept is one of the weight reduction strategies that faces challenges in the production process. The multi-layer structure has its advantages in the selection of facing and core material. The combination of thickness ratio and different layer materials leads to the desired characteristics of the end product. Additionally, joining the face and core layers is a critical step that determines defects due to loading. Concerning the features of the end product and production costs, the respective production process can play an essential role in qualitative and economic terms.

In the discontinuous or batch process, the prefabricated layers are assembled with the adhesive under pressure and at a specific temperature. The layers are separately prepared from different wood-based panels such as plywood and fiberboards with foam cores from various plastic types. Plywood and fiberboard are produced and prepared before they are fixed with the foams by adhesives. The continuous process of sandwich panels has more advantages for facilitating both productions in the same unit and the adjustable length of produced panels. While the foam liquid is introduced by injection in

the panel line, thin layers such as metal foils or impregnated paper used as face material, can run through the roll into coils. The production of wood-based panels with a foam core inhibits the production unit's feeding system in the same way as thin layers due to the increased thickness. The one-step continuous process patented by Lüdtke et al. (2007), however, allows expansion of foam by hot pressing during the compaction of surface layers. The process is similar to the conventional particleboard process, in which three layers are formed and pressed in one step. Surface layers are densified by pressing, while the core material can be triggered to expand by heat transferred from the hot plates. Thermoplastic granulates have been successfully applied as the core material, after all, the production unit requires a cooling phase to stabilize the panels after pressing using this type of plastic. The purpose here is to decrease the temperature of the foam core to its glass transition point for solidification.

Polyurethane (PUR) as a thermoset does not require this process, potentially increasing efficiency in the production line. Using PUR for the core material, surface layers can be fixed, and the foam in the form of mixed liquid components poured to fill an area between both strained panels that does not require adhesives. Aside from this, PUR has the potential for low thermal conductivity of closed-cell and tailor-made preparations based on selecting components and formulations. The self-adhesive property of PUR results in a strong bond. Moreover, the possibility to produce PUR from biomaterials is on the increase. Polyols derived from renewable resources have been successfully used to obtain different PUR types, including porous composites (Kurańska et al., 2013), which can substitute polyols from the petrochemical source. Specific properties and the potential for bio-based sandwich structures make PUR rigid foam an attractive choice for the core layer.

Controlling the PUR foaming reaction is a big challenge in the one-step production process. The high reactivity of isocyanate leads to PUR formation as soon as it is mixed with polyol without catalysts. PUR uses reactive foaming, namely the chemical reaction of mixed components to induce the foaming. The reaction of isocyanate with water releases carbon dioxide gas ( $\text{CO}_2$ ), which exists in a polymer matrix for foaming the structure. For this reason, controlling the foam rise is supposed to be facilitated chemically so that the mixture is non-active for a specific time before adding it into the hot pressing process. The high reactivity of isocyanate is possibly inhibited by blocking its functional group via the formation of a weak bond with an active hydrogen compound, a so-called blocking agent, to create blocked isocyanate. It can be mixed with polyol without reactivity under normal conditions. Then, the isocyanate group can be regenerated at an elevated temperature.

Blocked isocyanates are widely used in powder coatings, elastomers and adhesives on account of their longer shelf life and lower toxicities when compared with free isocyanates. Commercial blocked isocyanates are available based on toluene diisocyanate (TDI), isophorone diisocyanate (IPDI), hexamethylene diisocyanate (HDI), which do not serve a purpose for rigid foam production. For PUR rigid foam production, different polyols like aromatic or aliphatic polyesters and polyethers can be used. They have a wider variety of choices than isocyanate, which is commonly limited to polymeric methylene diphenyl diisocyanate (pMDI). The preparation of blocked pMDI could be a possible solution with the following considerations.

The releasing point of isocyanate or the deblocking temperature, is determined by the type and ratio of isocyanate and blocking agent, as well as the blocking process. Applying a mixture of blocked pMDI and polyol can be complicated due to the deblocking equilibrium and reaction rate of all components, resulting in overall time and curing temperature. Meanwhile, the curing reaction needs to accommodate the requirements of the hot-pressing process. The temperature in the core layer reaches approximately 90-120 °C depending on wood adhesives applied for wood-based surface layers (Lüdtke, 2011). At this point, the reaction of released isocyanate and polyol in the mix will form thermally stable bonds and cross-linked foam structure. Furthermore, to apply the PUR mixture during the process, the core material requires critical properties – including pressure resistance – in its unexpanded state, ability to expand, and especially the foaming controllability by pressing conditions.

The pressure resistance of the core material is challenging since PUR raw components are present in liquid form. The addition of solid fillers to the components may reduce the fluidness of the materials. In recent years, research into PUR reinforced with synthetic and natural fillers has been increased due to their degradability, lightness, reduced cost and favorable mechanical properties (Atiqah et al., 2017). Natural fillers from agricultural residues i.e. oil palm empty fruit bunch, rice husk and wood flour, have advantages over synthetic materials due to their availability and economical production, as well as their renewable and biodegradable properties. On the other hand, they pose some processing restrictions, such as variation in properties, limited operation temperatures regarding biological components and high moisture content.

Having said that, the existence of moisture in bio-fillers is not always unfavorable. Wood moisture can feature as a blowing agent in a thermoplastic composite, based on the physical blowing process, which utilizes the evaporation of added blowing agents with a low boiling point (Matuana & Mengeloglu, 2002; Rizvi et al., 2000). For PUR, water plays

an important role in the chemical foaming, primarily by the reaction with isocyanate. Applying wood moisture in foaming PUR could differ from thermoplastics since wood filler, water and polyol are all hydroxyl-containing components that could potentially react with isocyanate. A higher amount of isocyanate could therefore be required due to this repetitive reaction. Although wood filler has been investigated for its effect on PUR foam in past studies (Krishnamurthi et al., 2003; Kurańska et al., 2015; Mosiewicki et al., 2012; Yuan & Shi, 2009), the results of wood moisture on the foam properties were rarely considered. In most publications, PUR foams were produced under standard conditions without additional energy input, the exception being mechanical turbulence. For PUR foaming during the hot pressing of wood-based sandwich panels, it is necessary to examine the influence of heat on the PUR foam properties produced.

Blocked isocyanates and wood addition are intriguing concepts that potentially transform the PUR formulations for application in the one-step production process. They should not only fulfill the requirements of the core material but also the quality of the produced panels, since the formation of the expanded core and the connection between core and face can govern the stability and basic properties of panels. PUR rigid foam production by filler addition has been proven to be possible. However, using blocked isocyanate for PUR foam is still unclear. There remains a need for the investigation of PUR foaming in the one-step hot pressing production using both concepts.

To enhance the understanding of the experiment, the next chapter (Background and current state of knowledge) will explore the basic ideas for the abovementioned studies. The background and current state of knowledge will be reviewed in separate topics: lightweight sandwich panel and production process, PUR rigid foam and blocked isocyanates. The research problems and objectives will be addressed in Chapter 3 (Objectives and research plan), in which the research outline and plan, divided into three studies is presented. The experimental details i.e. parameters and limitations for different studies, will be described in Chapter 4 (Materials and methods). The results of each study will be revealed and discussed separately in Chapter 5 (Results and discussion). Results from three studies will be evaluated altogether in the overall discussion at the end of the chapter. Chapter 6 (Conclusion) summarizes the findings and problems discovered during the research and uses these to answer the main questions of whether new PUR formulations can be used for one-step pressing production. Finally, new ideas for further development and subsequent research will be suggested in Chapter 7 (Outlook).

## 2 Background & current state of knowledge

### 2.1 Lightweight sandwich panel and production processes

As the world population continues to increase steadily, the concern about the availability of wood on a sustainable basis becomes clear. In the last decades, the woody crop area in the world did not increase as much as the demanded production of wood-based panels (FAOSTAT, 2020). Fig. 1 indicates the continuous increase in the production volume since 2000 from ca. 178 to 400 million m<sup>3</sup>, compared with the relatively unchanged woody crop area of an average 200 million ha over the same period. Wood biomass is becoming scarcer and thus more expensive; compounding this, the global raw material situation in terms of wood-based materials is further being influenced by the economic growth in emerging countries, since this leads to an increased demand for furniture (Hellmann, 2012). Furthermore, a competition between the demands for wood energy and traditional forest-based industries is emerging. There may not be enough wood to satisfy the combined needs of the forest-based industries and the wood energy producers from domestic sources in 2030 (Mantau et al., 2010).

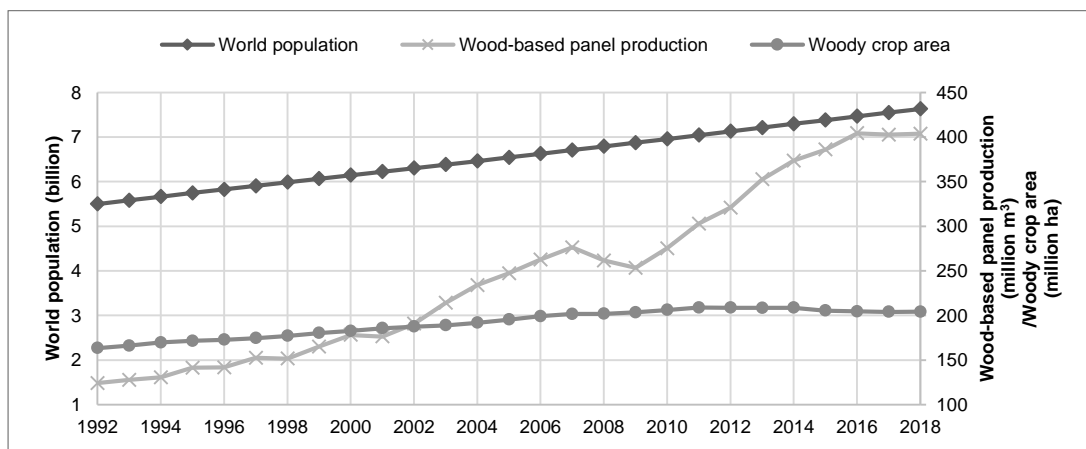


**Fig. 1 Development of world population and global wood-based panel production compared with woody crop area over 1992-2018 (FAOSTAT, 2020)**

Current situations challenge the manufacturer of wood-based panels, especially classic furniture builds as regards increasing energy prices, the rising cost of raw materials, as well as the necessary reduction of logistics costs. Aside from that, the legal restrictions regulate permissible contract weights and customs duties based on weight at some national borders outside the EU to only 25 kg weight per cargo package (Stosch, 2009). The lightweight concept in furniture construction is driven by these situations and became more dominant due to changes in the furniture market and design as well as the general trend towards mass and material reduction (Thoemen, 2008). The share of

furniture in the takeaway sector has increased since IKEA's successful model emerged. Weight reduction for the thicker components is preferable in the design. Low consumption of materials and fuel for transportation supports environmentally friendly aspects. Therefore, lightweight material brings many advantages for producers, designers and consumers, as described by Shalbahafan (2013) e.g. lower costs regarding mass reduction and transportation, corresponding design trends, more rational use of wood and ease of transportation. The motivation of lightweight construction can be summarized into three different aim dimensions, according to Wiedemann (2007), as follows:

1. Functional dimension: to achieve specific functions e.g. in aviation and aeronautics, support structure without much increase in loading weight
2. Economic dimension: to save material costs, especially for thick panels
3. Ecological dimension: to reduce energy and fuel consumption by higher loading volume

Regarding the manufacturing efficiency for industries, lightweight wood composites may come into consideration as reviewed by Hellmann (2012) for the following important resources:

1. Personnel efficiency: relation of income to personnel expenses
2. Material efficiency: relation of product output to material input
3. Processing efficiency: provision of all necessary resources according to demand, ultimately the ratio of income to expense
4. Energy efficiency: energy input needed to achieve a defined benefit e.g. product

Personnel and material efficiency were examined in his study concerning furniture production. For personnel efficiency, a load of the lightweight board for workers during manual handling becomes lower than that of standard chipboard. In terms of 25 kg component weight, a 38 mm thick chipboard ( $600 \text{ kgm}^{-3}$ ) will gain a panel area of 1.1 to  $3.7 \text{ m}^2$  for the same thickness with lower density ( $180 \text{ kgm}^{-3}$ ). Carrying a lightweight panel will subject the workers to a lower load, compared to conventional boards with an equal dimension. It will lead to fewer recovery breaks, rarer causes of faults and component damage and presumably increased employee motivation. In respect of material efficiency, the production costs of modern chipboard products comprise about 40-44 % of the cost of wood. Therefore, the raw material cost of wood has a decisive influence on the price of the chipboard. From both aspects, a material reduction in lightweight wood composite could be an attractive solution and developing trends for industries. However, processing and energy efficiency must be taken into account. The requirements for lightweight processing in conventional manufacturing can lead to increased production

costs. Additionally, the reduction of mechanical properties due to lower density is another restriction found in a lightweight structure.

### **2.1.1 Lightweight wood-based panel**

Wood-based composites have been a solution for the biomass shortage from the beginning due to the flexibility of input raw materials. Small diameter trees or waste wood from industrial processing and agriculture residues can be used as raw materials. The various sizes and shapes of wood elements starting from largest to smaller elements: the log, thin lumber, veneer, chips, flakes, particles and wood flour, are main components in different classifications of wood based-composites (layered composite, particle composites, fiber composites, flour composites) (Bodig & Jayne, 1982). A wood composite is commonly produced by bonding wood elements using adhesive and suitable processing depending on the types of wood elements and end-product. The requirements for wood quality are highly varied in different wood-based composites. In general, the demands on the wood quality decrease as the degree of wood dissociation increases i.e. lower wood qualities are more likely to be used in chipboard than in laminated timber. Related to solid wood, wood-based composites are more uniform, defect-free and can be designed for specific qualities or performance requirements such as unique shapes and dimensions, improved fire resistance and better biological durability.

Panels with a density below  $600 \text{ kgm}^{-3}$  are classified as lightweight materials (DIN CEN/TS 16368). Another work defined lightweight wood-based panels with a density below  $500 \text{ kgm}^{-3}$  (Thoemen, 2008). Fig. 2 shows the density ranges for wood-based materials compared to solid wood and cell wall. The difference in densities and corresponding properties resulting from production parameters i.e. particle wood size, layer assembly and gluing/pressing methods, can fulfill specific application purposes compared to solid wood. Nearly all main types of wood-based composites have higher densities than the defined lightweight. As illustrated here, materials such as tubular board, honeycomb panel and foam core panels are included in lightweight materials. These strategies are used to obtain weight reduction in the production of wood-based materials.

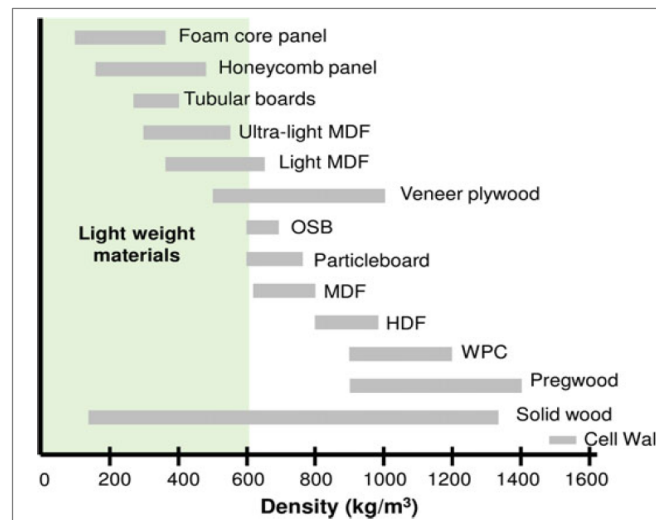


Fig. 2 Density of wood-based materials and cell wall (Monteiro et al., 2018)

The strategies for weight reduction in wood-based composites available in the market were previously reviewed by Monteiro et al. (2018). A basic approach is to use plant species with a low density below  $450 \text{ kgm}^{-3}$  for the production of wood composites such as balsa (*Ochroma* spp.), ceiba (*Ceiba* spp.), poplar (*Populus* spp.), which are native species from North America, South America and Europe, respectively. The densities of MDF and particleboards can be decreased by processing such as less compaction of the wood mat or fabricating hollow-tube profile within the panel. Extruded tubular boards may have a density between  $250$  to  $400 \text{ kgm}^{-3}$ , with the density reductions achieved by most of these techniques about  $150$  to  $200 \text{ kgm}^{-3}$  (Shalbafan, 2013).

Compared with the conventional panels, some general limitations in the lightweight structure should be taken into consideration during the processing (Monteiro et al., 2018; Shalbafan, 2013). The increase in production cost is anticipated due to the limited availability of low-density wood species, the substituting of raw materials, more complicated production technology and a higher amount of resin due to using agricultural residues. Notably, the reduction in the mechanical properties of lightweight panels resulting from lower density, disallows the use in applications requiring load-bearing capacity.

The particleboard properties are influenced by the following five structural parameters in the macroscopic scale as follows (Benthien et al., 2019),

1. raw material selection,
2. particle geometry (dimension and shape),
3. particle orientation perpendicular to and in the panel plane direction,
4. cross-section structure (density profile and distribution of particle sizes perpendicular to the plane direction/type of layer-wise assembly), and
5. kind of particle adhesion (adhesive type, content and distribution).

Lightweight panels with wood material reduction can sustain their properties in the same way as conventional particleboards with reference to these structural parameters. The adjustments needed when constructing the lightweight particleboard can be divided into two sections: material and structural adjustments (Benthien et al., 2019), as shown in Fig. 3. Material adjustment involves the particle geometry depending on mat's layers or the material used, based on wood species and applied adhesives. Structural adjustment is associated with the density distribution and particle orientation. Density adjustment includes vertical, horizontal and periodical changes in the density profile. Particle orientation combines the position and direction of particles related to the panel plane direction. Both types of adjustment are employed for lightweight particleboard simultaneously; for example, incorporating non-wood light fillers in the core layer, the substitution of wood by annual plant residues (e.g., straw), the use of thin strands instead of conventional particles and variations of the horizontal density profile (dual-density board).

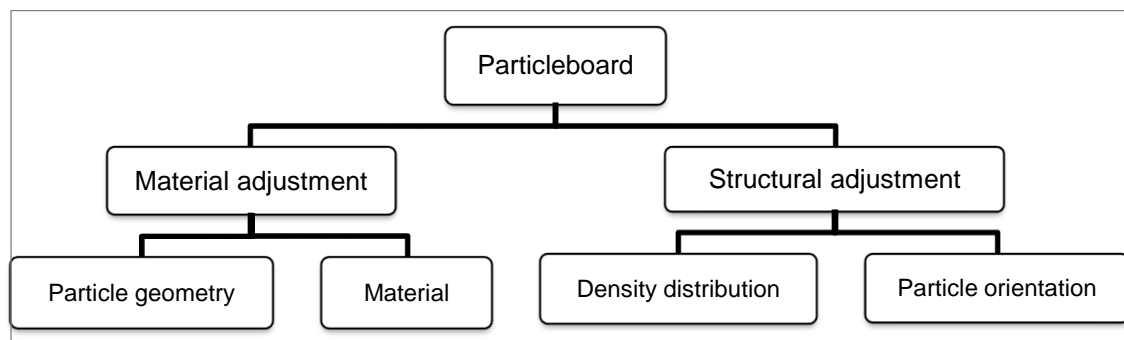


**Fig. 3 Classification of measured employed to maintain the properties of wood-reduced particleboards at those of commercially manufactured panels (Benthien et al., 2019)**

The sandwich panel uses both adjustments to reduce the panel weight. It is combined of two surfaces with high densities and a high-volume core with a low density. This method is used to increase the strength and stiffness by achieving densities in the final panel ranging from 100 to 350 kgm<sup>-3</sup>. Other existing strategies as regards material selection are not widely applied, such as using starch granules or foamable adhesives to create low-density spaces between the particles, while maintaining the inter-particle (Shalbafan, 2013).

### 2.1.2 Sandwich panel

Combining two different materials for both the outer and core layers make the sandwich concept more adjustable compared to other strategies. A thick, lightweight core separates two thin yet stiff and strong skins. The thick, lightweight core absorbs shear stress, while the stiff skins absorb tensile and compression stress under force bending, which leads to an increase of strength, stiffness and resistance of bending and bucking

loads without considerable weight gain (Gibson & Ashby, 1999; Zenkert, 1995). Using this concept, it can achieve a remarkable weight reduction while maintaining acceptable mechanical properties.

The sandwich structure is an essential strategy for weight reduction in material design, especially where weight saving weight is critical, as in aircraft, portable structures and sports equipment. The anatomical evolution also uses the same concept for body improvement to support specific functions as seen in a human's skull, the wing of a bird or even in a leaf. In all these examples from nature, the face and core are made from the same material in the faces, which are almost entirely dense and the lightweight core body (Gibson & Ashby, 1999). Sandwich panels are different from nature, as they extract efficiency from the various core and layer materials.

Owing to their bonded structures, sandwich panels were popular way back in the 1930s when structural adhesives were first invented, becoming widespread in England and the United States. The first time mass production of sandwich panels in England utilized veneer faces with a balsa core for the Mosquito aircraft operated during World War II due to the shortage of other materials (Zenkert, 1995). Since then, the inventions, technology and applications of sandwich panels have progressed, while the core materials continue to develop. Exceeding natural raw materials like balsa wood, honeycomb cores, or polymer foam core is used for a wide range of applications. Compared to balsa, the properties of the latest core types are more tailor-made and developed for a specific application.

Sandwich panels with foam cores (made of PUR or PS foam) or paper-based honeycomb structures are a major trend in the industry. Two groups of sandwich core materials can be distinguished: the homogeneous and the structured cores or non-homogeneous cores, as shown in Fig. 4 (Monteiro et al., 2018; Pflug et al., 2002). The first group includes cores made from hardwood strips (*Ochroma* spp., *Populus* spp., low-density *Pinus* spp.). Thermosetting or thermoplastic foams with open or closed cells are also used to produce a sandwich panel with the homogeneous core. Typical properties of polymer types used for the core layer such as PUR, PS and PVC are shown in Tab. 1. The group of non-homogenous cores includes textiles, corrugated and honeycomb cores. Honeycomb cores can be comprised of metal plastic or paper (Monteiro et al., 2018).

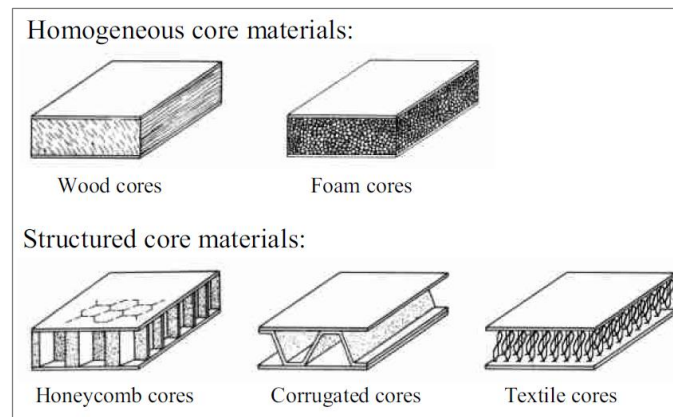


**Fig. 4 Homogeneous and structured core materials (Pflug et al., 2002)**

A simple structure of a sandwich element is one with a homogeneous core. The following prerequisites should apply to the behavior of such a component (Reich, 1962):

- The skins exhibit linearly elasticity.
- The core is homogeneous, also showing linear elastic elasticity.
- The core layer is not compressible, so that shear forces can be transmitted preferentially due to the low modulus of elasticity.

**Tab. 1 Properties of polymer core materials (Klein, 2009; Kollmann et al., 1975)**

| Core material | Density<br>(kgm <sup>-3</sup> ) | Elastic modulus<br>(MPa) | Shear modulus<br>(MPa) | Tensile strength<br>(MPa) | Compression strength<br>(MPa) |
|---------------|---------------------------------|--------------------------|------------------------|---------------------------|-------------------------------|
| PUR foam      | 100                             | 9-25                     | 5-20                   | 0.7                       | 0.9                           |
|               | 200                             | 15-95                    | 5-20                   | 2.0                       | 3.0                           |
| PVC foam      | 50                              | 18                       | 5                      | 0.8                       | 0.2                           |
|               | 80                              | 30                       | 10                     | 2.0                       | 0.5                           |
| PS foam       | 20                              | -                        | 4                      | 0.3                       | 0.1                           |
|               | 28                              | 8                        | 8                      | -                         | -                             |
|               | 48                              | 14                       | 12                     | -                         | -                             |
|               | 72                              | 21                       | 18                     | -                         | -                             |

Despite the various core structure types, they possess one common crucial characteristic that supports the shear loads, whereas the surface serves to support bending loads (compression and tension). The type of surfaces chosen for a particular application is determined by the functional requirements, such as strength, stiffness, damage tolerance and appearance with a minimum overall cost (Nilsson & Nilsson, 2002). In addition to foil and paper surfaces, panels with wood-based surfaces are used widely for general constructions such as door, furniture, general panel industries and interior design.

Different types of wood-based composites are employed for the surface layers of sandwich panels, depending on the area of application. OSB or plywood combined with a plastic foam core namely structural insulated panel (SIP), originated in the United States. The standard SIP panels consist of a foam core insulation material, commonly

PS, sandwiched between two OSB sheets and adhered with glue. Panels are applied for wall, foundation, floor or roof systems for high level of thermal insulation (Parker, 1986). Plywood and fiberboards, with different types of plastic foam cores (PVC, PE), are commonly used in decorative, soundproofing and thermal insulation, as well as in an area where a lightweight material is required as in ship ceilings, shelving and suspended panels. Tab. 2. shows examples of products and the application areas of the wood-based panels with foam core from producers of some selected countries.

**Tab. 2 Product examples of sandwich wood panel with plastic foam core and their application areas**

| <b>Surface</b>                 | <b>Core</b>                | <b>Application</b>   | <b>Commercial name<br/>(country)</b> |
|--------------------------------|----------------------------|--|--------------------------------------|
| <b>Plywood</b>                 | PE foam                    | soundproofing, thermal insulation  | GISATEX® Thermo Isocell (Germany)    |
| <b>Plywood</b>                 | PVC foam                   | yachts, ship partition walls, decorative, ship ceilings  | COMPOCEL® WF (Italy)                 |
| <b>Plywood</b>                 | Rubber, PUR mat            | soundproofing, thermal insulation  | SONOPANEL L/L (Belgium)              |
| <b>Plywood</b>                 | Closed cell thermoplastics | decorative   | AIREX XT-90 (Netherlands)            |
| <b>Hardboard, MDF, Plywood</b> | PS                         | ceiling beams, architectural panels, displays, doors, shelving, suspended panels, store fixtures | Foam Light®, Foamkore® (USA)         |

In the furniture industry, weight reduction was driven by the increasing share of takeaway furniture and the changing design trends for furniture, including a shift towards thicker components. Since the successful launch of the furniture line LACK in 1982 by IKEA, which had relatively thick components made of honeycomb sandwich panels with internal frames, particleboard and MDF have increased in popularity as regards the sandwich concept (Thoemen, 2008).

Corresponding to this, BASF offered a light filler for the core layer under the commercial name Kaurit® Light. The innovative product was developed to decrease the quantity of wood consumed in the production of chipboard for furniture. The filler consists of chipped wood, EPS polymer (expanded polystyrene) and binding agents. Polymer foam is used to fill the hollow and connect with the wood chips, allowing for the densification of the surface layer. According to the producer, the new panel will weigh 30 % less than conventional chipboard. The product attracts the panel manufacturer, as it can be processed conventionally in the same way as particleboard. An example of that is the Rheinspan® Airmaxx lightweight panel from Nolte, which uses this light filler for the area

of takeaway furniture and stand construction (Nolte Holzwerkstoff GmbH & Co. KG, 2009).

Another innovative research for core material for lightweight panels has been done, making use of sustainable resources, in which popcorn grains were applied for the core layer of panels (Kharazipour & Bohn, 2013; Stosch, 2009). Forestry scientists at the University of Göttingen have developed a lightweight composite material consisting of wood chips and corn in the form of popcorn granules. The material is called Balanceboard and was made in cooperation with Pfleiderer AG in Neumarkt, Bavaria. According to Pfleiderer, the Balanceboard has a bulk density of  $500 \text{ kgm}^{-3}$ , markedly lower than a typical standard board of  $630 \text{ kgm}^{-3}$  (Sponholz, 2017).

Furthermore, other experiments involving the core material of sandwich panels were mentioned by Stosch (2009). WoodPOP comprises a core made of granulate formed from wood sanding dust, which is expanded by the added foaming agent. The project was developed by student Johannes Ebner from Ostwestfalen-Lippe University of applied science and arts. The application of a suitable temperature also helps the natural adhesion of the wood. Core materials from food such as rice waffles and sugar puffs, were used for the core layer, which appears to produce sandwich panels with a low density. However, these findings are also disadvantageous, in that it may take food away from the food supply system. Residues from the agricultural sector, like cocoa shells and groundnut shells, can be used in sandwich panels yielding densities of 260 and  $220 \text{ kgm}^{-3}$ , respectively (Stosch, 2009).

### ***Theory of sandwich structure***

Sandwich structure is defined as a special form of a laminated composite, comprising a combination of different materials bonded to each other in order to utilize each separate component's properties, to the structural advantage of the whole assembly. Despite the possibilities of material selection in a sandwich structure, face and core layers have their specific characteristics and functions (Klein, 2009; Zenkert, 1995).

The faces are usually two thin, stiff and strong layers. They are bonded to the core in order to obtain a load transfer between the components. Both faces act together to form an efficient stress pairing, counteracting external bend. The aim is to use skins with the highest possible degree of elasticity. The core material is thick and light with a higher volume, which spreads out as continuous support for the faces rather than being concentrated on a narrow web. The core resists shear and stabilizes the faces against buckling or wrinkling. It may possess either a lower shear modulus or open-worked core structures with low force-conducting cross-sectional areas.

The mechanical behavior of a sandwich panel depends on the properties of the face and core materials and its geometry (Gibson & Ashby, 1999). After the combination, the bond between the faces and the core must be strong enough to resist the shear and tensile stresses set up between them. The adhesive that bonds the faces to the core is thus of critical importance. Furthermore, the use thereof also requires some design precautions. These consist mainly of the force application, the corner joints and connections and the overall shape (e.g., angles, curvatures) (Klein, 2009).

The goal of the design is to achieve a panel with minimum weight, while still meeting the constraints of stiffness and strength. The optimization can be carried out on the core and skin thicknesses and materials as well as the core density. Different failure modes are described and analyzed for rectangular sandwich beams in failure-mode equations, using the stress distribution model by Allen (1969). The way in which a failure will present itself in a sandwich, is determined by the lowest load that meets the criteria of the failure type. As the geometry and loading change, the failure mode can change, too. The failure modes of a sandwich beam or panel (see Fig. 5) are defined (Gibson & Ashby, 1999) as follows:

- Face yield occurs when the normal stress in the face equals the strength of the face material.
- Face wrinkle: a local buckling of skin into the core, occurring when the normal stress in the compressive face reaches the local instability stress.
- Core failure (core shear/core fracture): the core will usually fail in shear; though compressive or tensile failure is also possible. This occurs in a foam with a plastic–yield point when the principal stresses satisfy the yield criterion. If the shear stress in the core is high when compared to the normal stress, failure occurs when the shear stress equals the yield strength of the foam in shear.
- Bond failure between the face and core: debonding occurs by brittle fracture, since adhesives are usually brittle. Failure of the adhesive bond between the skin and the core is the most difficult of the mechanisms to analyze.

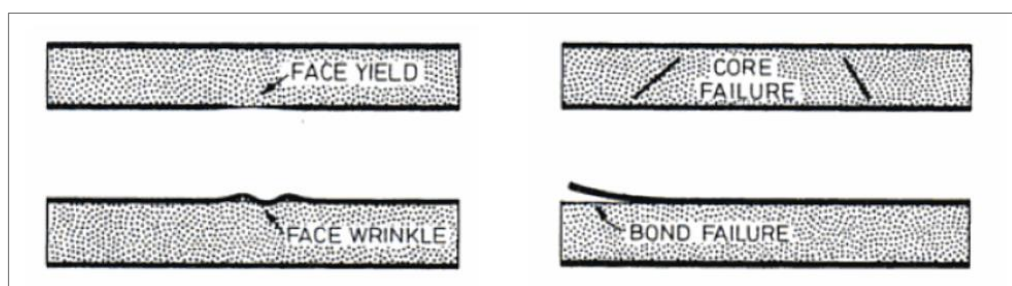


**Fig. 5 Failure modes of sandwich beam (Gibson & Ashby, 1999)**

Equations for failure load for each of the mechanisms contain three sets of variables, which are related to the loading configuration, material properties and the solid from which the core is foamed, and the beam design. Gibson and Ashby (1999) determined

how the failure mode is dependant on the beam design. The failure mode map loaded in 3-point bending is shown in Fig. 6. The axes are the design parameters of the beam. The diagram is divided into fields, within which one failure mechanism is dominant. The fields are separated by field boundaries (heavy lines), which are the loci of design points, for which two mechanisms have the same failure load. Two design parameters:  $t/l$  and  $p_c/p_s$  are used as the axes for the diagram. The beam width and core thickness cancel out because all of the mechanisms depend on them in the same way.

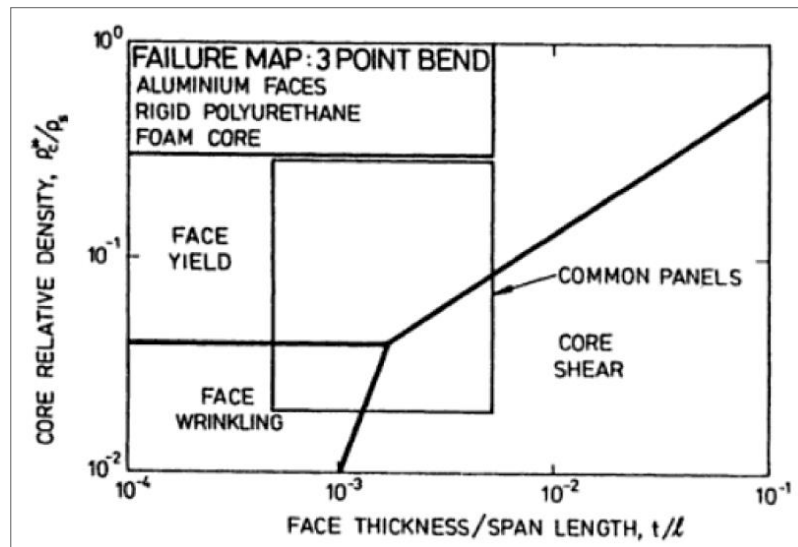


Fig. 6 Failure mode map loaded in 3-point bending (Gibson & Ashby, 1999)

### 2.1.3 Production processes

The production processes of sandwich panels are as diverse as the variety of sandwich products, depending on the types of core and surface layers and their combination. In this research, the sandwich panel production involves the processing of wood-based panels with a foam core, specifically PUR rigid foam. Due to its distinct properties as a thermoset, PUR foam application processes are reported in this next section. The related background for the sandwich panel production will be given in the subsequent section.

#### 2.1.3.1 Application of PUR foam

PUR foams can be employed in different stages. Reacted rigid foam produced in slabstock is used in the form of sheets and other cut-to-size pieces. Slabstocks produced by hand-foaming or foaming machines can be stuck on facings and cut into a great variety of composite elements. Unreacted liquid-state PUR is applied in *in-situ* operations, where the production takes place directly at the site by pouring or spraying; for instance, flat roofs, walls of buildings and storage tanks. The advantage of *in-situ* foam is that it is not necessary to transport large volumes of foam, simply the raw materials

and the foaming machine. Even complicated surfaces can be coated with a relatively uniform foam layer using this method (Szycher, 2012).

Kapps and Buschkamp (2004) described the qualities of the PUR component mix in different uses. PUR one-component (1-C) foam is suitable for filling cavities and openings in walls providing sound and heat insulation. The component contains moisture-curing resin with a blowing agent and catalyst. The resin is based on a pre-adduct (prepolymer), produced from isocyanate and a polyol formulation and consists of additives (catalysts, stabilizers, flame retardants) necessary for foaming. Foaming occurs due to spontaneous evaporation of the blowing agent, dissolved or emulsified in the prepolymer. The foam cures as a result of the free NCO groups of the prepolymer reacting with the ambient humidity. 1-C foams have been used in the building industry since the beginning of the 1970s. Various types of foam are available for diverse applications i.e. for assembly, insulating, filling, bonding, and sealing. 1-C foam is operated in *in-situ* foam by pour-in-place or layer-by-layer applications. Pour-in-place is ideal for filling defined areas such as curtain wall sandwich panels, wall cavities, and irregularly shaped voids (Szycher, 2012). Whereas layer-by-layer application is used when cavities cannot be filled with foam by a single filling process due to the limited performance of the foaming machine and the insufficient foam pressure (Kapps & Buschkamp, 2004).

The widely used PUR application by spraying, is particularly useful for applications in a large area or on plain surfaces such as tanks or building walls. The reaction mix for spraying consists of two components, polyisocyanate and polyol with all additives, including blowing agents. The machines are transportable and equipped with long delivery hoses attached to the mixing head. The hoses are sheathed in a heat-retaining device and the mixing head is integrated into a gun so spraying can be started and stopped as desired. The reaction mix is adjusted for quick reaction and curing of the foam by addition of the appropriate catalysts. The reaction mix is produced by high-pressure machines and sprayed without an air supply.

Another operation of PUR was mentioned by Szycher (2012), namely plastic stage forming. During manufacture, the foam will reach the plastic stage after the expansion but still not be set for the final state. In this second phase, thin sheets of foam can be shaped in the desired form and maintained in the position until the set stage is achieved. The shaped foam is free of densification because the cells are not ruptured during bending; it exhibits no evidence of internal stress or strain. This technique is commonly used to shape rigid urethane foam into pipe insulation.

The major construction application for rigid PUR foam is PUR sandwich-structure composites, known as sandwich panels (Engels et al., 2013). They consist of stiff skins with the core filled with rigid PUR foam, the self-adhesive properties of the PUR resulting in a strong bond. The resulting panels have excellent insulating properties and, thanks to their stability, can serve as walling and roofing elements in constructing industrial, warehouse, and refrigerated buildings. The following section will discuss the manufacturing of wood-based sandwich panels with a PUR core in a discontinuous or continuous process.

### **2.1.3.2 Production process of wood-based panel with foam core**

Regarding the selection of core and surface materials, the sandwich assembly can be carried out differently. Surfacing with wood-based boards requires the prefabrication in a separate production unit from the sandwich production due to the different suppliers or limitations in production. When compared with the complexity in the production of fiberboard, particleboard, chipboard or OSB, the preparation of foam polymer core material is simpler, since the polymer materials are available in a more ready-to-use form. Plastics are applied to the sandwich assembly in form of slab stock or expandable granules. This section reviews the production process of sandwich panels in discontinuous and continuous processes and the application of PUR material into those processes.

#### **2.1.3.2.1 Discontinuous production**

Methods for manufacturing a sandwich panel with a foam core were reviewed by Monteiro et al. (2018). The discontinuous process includes batch process and mold foaming. In the batch process, the prefabricated layers are assembled with adhesive. The pre-expanded foam is prepared and sliced from the block before the stack is pressed, to cure the adhesive and form the final sandwich product. It is possible to use wood-based facings in this process. However, they must be cut in the desired dimensions before being glued with foam core. Their limited sizes, including at least three necessary individual steps for the panel production, induce the high production costs (Barbu et al., 2010). In the discontinuous process of mold foaming, two faces are combined to create the cavity. After that, an exact amount of foam is introduced to fill the mold. Spacers support the upper face to maintain it in position and if edge profiles are required, these must be placed at this stage. The mold structure must be rigid enough to withstand the high pressures reached during foam formation. This method allows for the production of panels with complex shapes. As the foam reacts within the cavity, the adhesion between core and surfaces is not necessary, which is more advantageous than the batch process.

However, this is a relatively slow process that can cause void spaces within the panel due to the non-uniformity of foam flow (Monteiro et al., 2018).

### 2.1.3.2.2 Continuous production

When compared to the last process, continuous production uses fewer individual steps for the assembly of sandwich panels. In this process, materials can be fed into a processing unit in a virtually endless manner, from a coil for example. Only prefabricated facings like foils or impregnated papers can be used, while the core is foamed between the facings during the production process. PUR foam is usually used, since the additional adhesive layer is not required in this case (Barbu et al., 2010). Due to its liquid components, the foam can be injected directly into the panel line. The principles for mass production were described by Davies (2008), as shown in Fig. 7. Two metal strips that form the faces are run-off coils and pass through roll formers, where the surface profile and edge details are formed. They are then heated to the required temperature, which is a pre-requisite for an optimal chemical reaction. The two-component foam mixture is then introduced before the strips enter a double conveyor, a type of traveling mold that resists the foaming pressure and keeps the faces at the required distance apart. When the continuous panel emerges, the foam has hardened and it may be cut to the required lengths by a flying saw. The production allows for flexible panel length. Thus, the main advantages are fewer production steps and a corresponding higher output, which leads to a higher efficiency with regards to time, material and human resources. This aspect has a considerable effect on the final panel cost (Shalbfan, 2013).

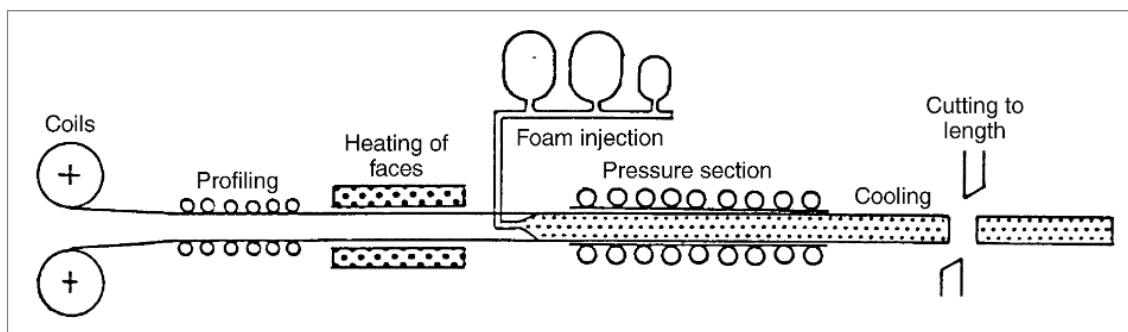


Fig. 7 Continuous line of foam production (Davies, 2008)

#### ***One-step production of foam core panel***

Barbu et al. (2010) reported a novel approach for the continuous production of foam core sandwich panels with wood-based facings. At University of Hamburg, a novel method for the continuous production of foam core sandwich panels with wood-based facings was patented (Lüdtke et al., 2007). In this approach, the manufacture of the facings and the core takes place during the continuous hot pressing of the sandwich panel. The process is derived from the conventional production technique of wood-based panels

(particleboard and MDF). It was designed for the continuous production of foam core panels, where the surface and core layers are fabricated in the same production unit collaterally. Therefore, the process is also called one-step production.

Fig. 8a shows the principle of a conventional particleboard process. A three-layered mat composed of resinated wood particles, coarse particles in the core and fine particles in the surface layers, is formed using three individual forming heads. The mat is then pressed in a continuous hot press. In comparison, Fig. 8b shows the novel foam core process. A three-layered mat is formed consisting of two resonated, yet not compacted face layers and one unexpanded core layer. The face layers comprise of resinated wood fibers or particles. The core layer is composed of a dry expandable thermoplastic material, which is triggered by temperature. The entire mat is compressed and heated. Sufficient time is needed for the adhesive in the surface layers to be cured. Once the conditions for expansion have been reached inside the core material, the press is opened to the target thickness of the final panel, so that space is given for the core material to expand. The last part of the pressing process is for solidifying the core material. The conditions for this solidification may differ, depending on whether a thermoplastic or a thermosetting core material is used.

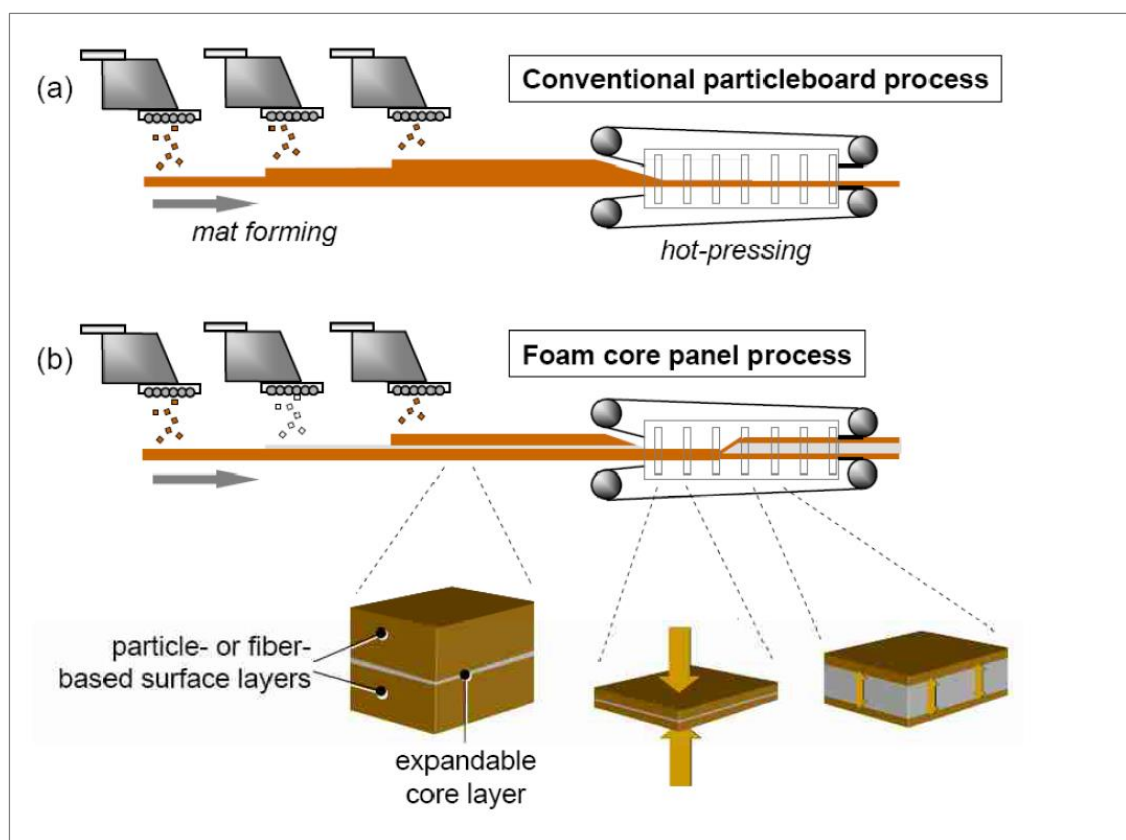


**Fig. 8 Schematic of (a) the conventional particleboard process in comparison to (b) the foam core panel process (Thoemen, 2008)**

One of the requirements the core material has to fulfill, is that its expansion should be triggered for example by temperature or chemicals. It is supposed to be pressure resistant in an unexpanded state and free-flowing for regular distribution in mat-forming, so that the compaction of face layers, as well as the connection between core and face can be achieved.

The new one-stage process improves efficiency and can be used to produce lightweight sandwich panels with wood-based facings continuously. The mechanical properties of the panels are, in terms of weight, comparable to classic wood-based panels. The panel composition can be varied in a broad scope of ranges. At the same time, the panels are not dependant on frame construction. Against the background of growing freedom in design for furniture manufacturers and the need for efficient production techniques, this development seems to be an alternative for recently used production techniques (Barbu et al., 2010).

Owing to the requirements of core materials, that should be an expandable solid-state granular shape, granules from thermoplastics have been used under the obligation of the cooling phase for panel stabilization. On the other hand, thermosetting foam materials as core layer materials do not require this. Thermosetting PUR is available as a liquid raw material and cannot fulfill the requirements. Shalbafan et al. (2016) developed an ideal industrial one-step manufacturing process for a PUR foam core, as described in Fig. 9. The process includes the four consecutive stages: layer compaction, surface layer separation, foam injection and panel stabilization. Here, surface layer separation and foam injection are additional steps from the last one-step continuous process.

Firstly, the two surface layers are compacted until the UF resin was cured. Then, the surface layers are separated. Various separation techniques are carried out after the bottom layer formation and before the face layer formation using either unresinated wood particles or the water spray technique. A higher amount of sprayed water would possibly influence the foam formation and the connectivity between face-core layers. The level of sprayed water is controlled to be as low as possible. For removing the unresinated wood particles or poorly bonded particles between the surface and the bottom layer, suction (vacuum cleaner) is used after surface layer separation but before the foam injection stage.

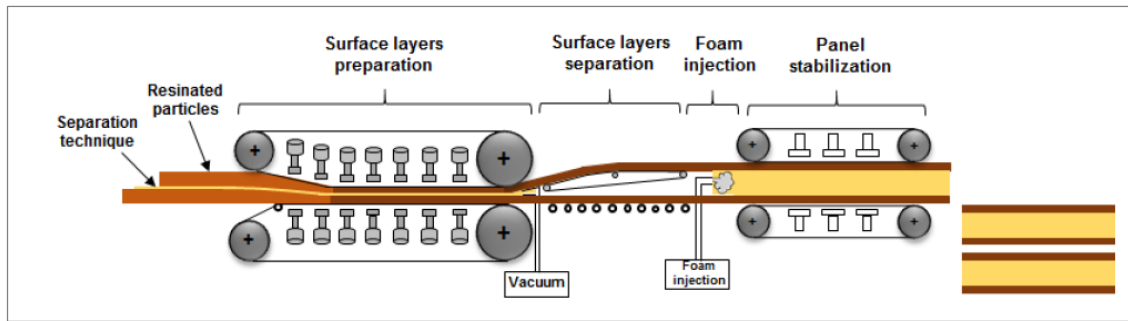


**Fig. 9 Development of a production process for foam core particleboards in an industrial scale (Shalbahfan et al., 2016)**

This study showed that foam core particleboards using rigid PUR as a core layer could be produced in a simulated one-step manufacturing process. Generally speaking, the PUR foam core particleboards showed good potential for use in the furniture industry. Further research in PUR formulation is needed to enhance the foam structure, which can affect the panel characteristics proportionately.

## 2.2 Polyurethane (PUR)

PUR was discovered for the first time via the reaction of a polyester diol with a diisocyanate by Bayer and his coworkers in 1937 (Delebecq et al., 2012). PUR was initially used in World War II as a replacement for rubber. From that day on, PUR grew in its applications as adhesives, elastomers and foams and became one of the most important classes of polymers in use today. The demand for PUR appears in various end-segment industries varying from construction, medical, packaging, furnishing and electronics and automotive to textiles, in which the furniture market is the most dominant sector. The versatility of PUR led to its global end-segment demand for 16 million tons in 2016 (PlasticInsight). A quarter of the total amount is attributed to Europe, where the demand for PUR from the converter reached to 4 million tons in 2017. PUR represents 7.7 % of the total plastic consumption (Fig. 10), which is lower only than the common types of thermoplastics (PP, PE, PVC) (PlasticsEurope). Among all polymer types, PUR has the most variations in properties. It can display thermoplastic, elastomeric and thermoset behavior depending on its chemical and morphological makeup (Engels et al., 2013). PUR in thermoplastic elastomers or thermosets is determined by whether linear or cross-linked networks are prepared. For this reason, different forms of PUR can provide a broad range of applications. The market share of its various forms is revealed in the following diagram.

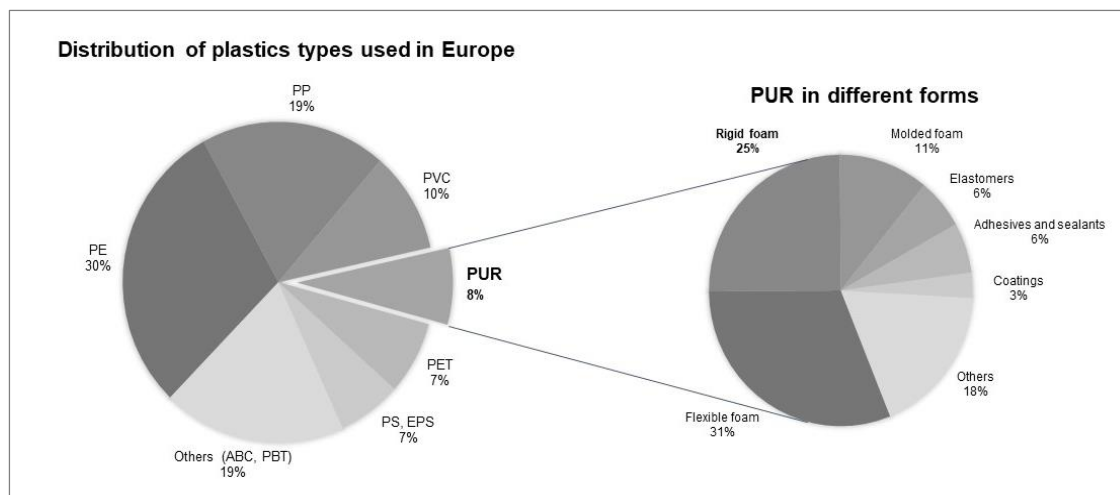


**Fig. 10 (left) European plastic converter demand by polymer types in 2017 adapted from PlasticsEurope, (right) PUR consumption in different forms 2016 adapted from PlasticInsight**

### 2.2.1 PUR rigid foam

PUR foams are an important commercial application of PUR chemistry, evidenced by their share of 67 % in PUR total consumption. The flexible foam features the maximum usage among other forms used in mattresses, cushions and car seats. Aside from this, PUR rigid foam commonly used for insulation, possesses a large range, comprising 25 % of the total share. PUR foams have been in use for over 60 years in a variety of applications and diverse fields. Two types of foam are based on similar chemistry; however, the type and degree of polymerization create the difference in product and property. PUR rigid foams are strongly cross-linked due to short polyol with higher hydroxyl content compared to flexible foams. To be more precise, the molar mass of the polyol component is less than  $10^3 \text{ gmol}^{-1}$  for rigid foam and between 2 and  $8 \times 10^3 \text{ gmol}^{-1}$  for the flexible ones (Delebecq et al., 2012). Moreover, the selection of isocyanate type distinguishes both types of foam i. e. PUR flexible foam employs TDI, whereas MDI is mostly required for the manufacture of a rigid one. While the PUR flexible foam contains mostly open pores, rigid PUR foam is the closed-pore structure that supports its application for construction, refrigeration and piping/tubing industry.

PUR rigid foam exhibits a broad range of physical properties; the foams are made in densities as low as 8 and up to  $320 \text{ kgm}^{-3}$  or even higher (Szycher, 2012). The typical PUR rigid foam properties are reviewed in Tab. 3.

Tab. 3 Typical properties of PUR rigid foams transformed in the metric system (Szycher, 2012)

| Properties                    | Method     | Value                   |
|-------------------------------|------------|-------------------------|
| Density                       | ASTM D1622 | 24-32 kgm <sup>-3</sup> |
| Tensile strength              | ASTM D1623 | 207-276 kPa             |
| Compression strength at yield | ASTM D1621 |                         |
| Parallel to foam rise         |            | 138-310 kPa             |
| Perpendicular to foam rise    |            | 69-172 kPa              |
| Compression at yield          |            | 5-10 %                  |
| Closed cell                   | ASTM D1940 | 92-98 %                 |
| Dimension stability           |            |                         |
| at 70 °C, 100 % RH, 2 weeks   |            | 7-15 % volume change    |
| at 100 °C, 2 weeks            |            | 5-10 % volume change    |
| at -40 °C, 2 weeks            |            | 0-2 % volume change     |

The combination of its high strength and light weight is not the only reason for its legitimate use in structural materials. Compared to commercially available insulating panels made of PS or wool, PUR rigid foam displays better insulating properties, as revealed in Fig. 11. Additionally, the self-adhesive properties of PUR serve a beneficial purpose in the production of a sandwich composite. PUR rigid foam displays thermoset behavior, which supports the application for this research in the continuous process of sandwich wood-based panels. The system does not require a cooling phase as in thermoplastics.

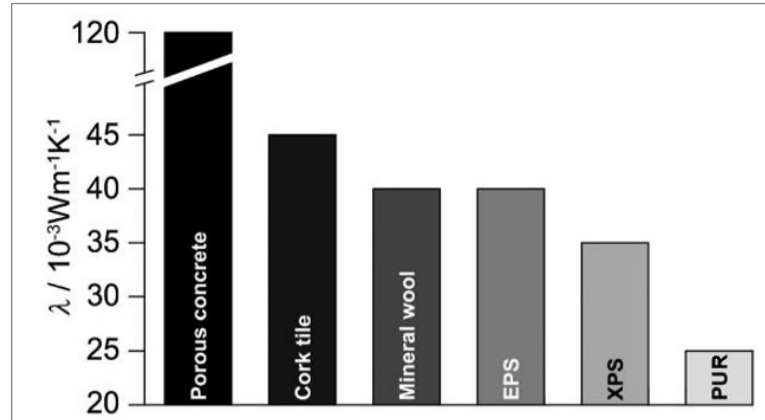


Fig. 11 Thermal conductivity values of various insulating materials (Engels et al., 2013)

The production of PUR rigid foams requires polyether or polyester polyols with polymer MDI grades as the main components. The choice of the MDI and polyol and isocyanate indexes are two specific points that come into consideration in PUR rigid foam production. Randall and Lee (2002) described the properties of both main PUR components. Generally, standard polymeric MDI (pMDI) is selected to correctly balance viscosity and the reactivity that makes optimal physical properties for most applications. PMDI is a mix of MDI (mainly 4,4'-MDI and 2,4'-MDI) and higher molecular components of MDI, which can be seen in Fig. 12. High functionality polymeric MDI is used when

improved physical properties are required. Low functionality MDI provides better flow during foam formation and results in improved impact resistance in structural foam.

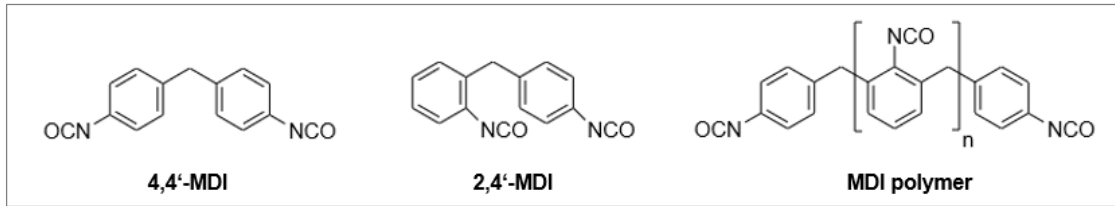


Fig. 12 MDI and MDI polymer

Polyols have more variety of choices than polymeric MDIs. The essential products are polyether based on sorbitol and sucrose as they are cost-effective and have a high degree of functionality, ranging from four to seven in terms of polyol. Polyethers based on glycerol are added to modify the reactivity and improve the processing, whilst amine-based polyols are used for specific applications such as spray foam, where high reactivity is required. Aromatic polyester polyols are widely used as they produce foam with better fire properties than polyethers. Still, their high viscosity limits their use in an application where the flow is not critical. The choice of polyol also depends on the compatibility of the blowing agents.

The isocyanate (NCO) index measures the excess isocyanate used relative to the theoretical equivalent amount required for 1:1 reaction with all active hydrogen, defined as follows:

$$NCO \text{ index} = \frac{\text{Actual amount of isocyanate used}}{\text{Theoretical amount of isocyanate required}} \quad (1)$$

The required amount of isocyanate is primarily calculated from the amount of polyol of active hydrogen groups. For water-blown foams, one molecule of water can consume two equivalents of isocyanate, so this molecular number of water is included in the theoretical amount of isocyanate required. The NCO index has a high impact on the processing and end properties. PUR foams typically have an index range of 0.9 to 1.3, whereas polyisocyanurate (PIR) has an MDI/polyol ratio higher than 1.8 (Randall & Lee, 2002).

Apart from the main components, the surfactant is another important reactant in PUR foam production, despite its need in a small amount. The word surfactant is a contraction of the surface-active agent. A surfactant functions as the name suggests, by lowering the surface tension. For the application in rigid foams, high surface activity is necessary for the nucleation and stabilization of the cells, as well as good emulsifying abilities for the raw materials and the blowing agent. Without a surfactant, the foam may collapse or

have a coarse cell structure (Szycher, 2012). Surfactants significantly affect cell size and foam air permeability (Lee & Ramesh, 2004). Owing to diverse functions, surfactants have been called stabilizers, cell control additives, foam stabilizers and cell control agents, among other titles. The choice of surfactant is governed by factors such as polyol type and method of foam preparation. A typical surfactant is a copolymer composed of a silicone backbone and poly(ethylene oxide-co-propylene oxide) grafts (Lee & Ramesh, 2004). Typically, surfactants, including other additives, are pre-blended into polyol before combination with MDI.

Other additives are employed to achieve the desired properties e.g. antioxidants, flame retardants and catalysts that control the selectivity of the targeted isocyanate reactions (Kapps & Buschkamp, 2004). One of the essential additives, namely the blowing agent, will be reviewed in the following section with its responsibility in the foaming process.

### 2.2.1.1 Important PUR reactions

The term 'Polyurethane' does not accurately represent its chemical background and may lead to a great deal of confusion. The polymer is not derived by polymerizing a monomeric urethane reactant, nor does it primarily contain urethane linkage. The name 'Polyurethane' comes from the trivial name urethane, which is used for the organic compound ethyl carbamate ( $\text{CH}_3\text{CH}_2\text{OC}(\text{O})\text{NH}_2$ ). PURs contain the same linkage, carbamate or urethane ( $-\text{RNHCOOR}'-$ ) as in ethyl carbamate, but they are reacted by two basic components: isocyanate and polyol. The reaction of both components in the formation of PUR form aliphatic and aromatic hydrocarbons, esters, ethers, amides, urea and isocyanurate groups in addition to urethane linkages.

Fig. 13 illustrates important reactions in water-blown PUR. The foaming process involves two competing reactions, blowing and gel reaction (polymerization reaction). Water serves as a chemical blowing agent for reaction with isocyanate that creates carbamic acid ( $\text{RNHCOOH}$ ) as a primary addition product. As it is not stable, amine and gaseous  $\text{CO}_2$  split off. Generated gas fills the cellular structure of the bubbles and expands the matrix polymer. Released heat from the exothermic reaction drives the evaporation process (Al-Moameri et al., 2016). Amine immediately reacts with additional isocyanate to give urea. Other secondary reactions arise i.e. urea reacts with additional isocyanate to form biuret and amine reacts with more isocyanate to form a polyurea. At the same time, the reaction of the isocyanate group and the alcohol groups in polyol leads to urethane linkage—the further reaction of the urethane with additional isocyanate forms allophanates. Additional to this, isocyanates can react with carbodiimide,  $\text{CO}_2$  forming at

high temperatures. In case of sufficient isocyanates or a very high NCO index, isocyanate groups may react with themselves for the trimerization of PIR foam. As PUR foams usually utilize polyfunctional reactants, this leads to the formation of a cross-linked polymer. The formed  $\text{CO}_2$  and the addition of low boiling physical blowing agents (PBAs), which evaporated during the exothermic reaction, assemble cellular plastics (Demharter, 1998). During this phase, the center of the foam can reach temperatures as high as  $190\text{ }^\circ\text{C}$ . The reactions are not complete at the end of the foam rise and can go for several hours until the center of the foam completely cools down to ambient temperature (Randall & Lee, 2002).

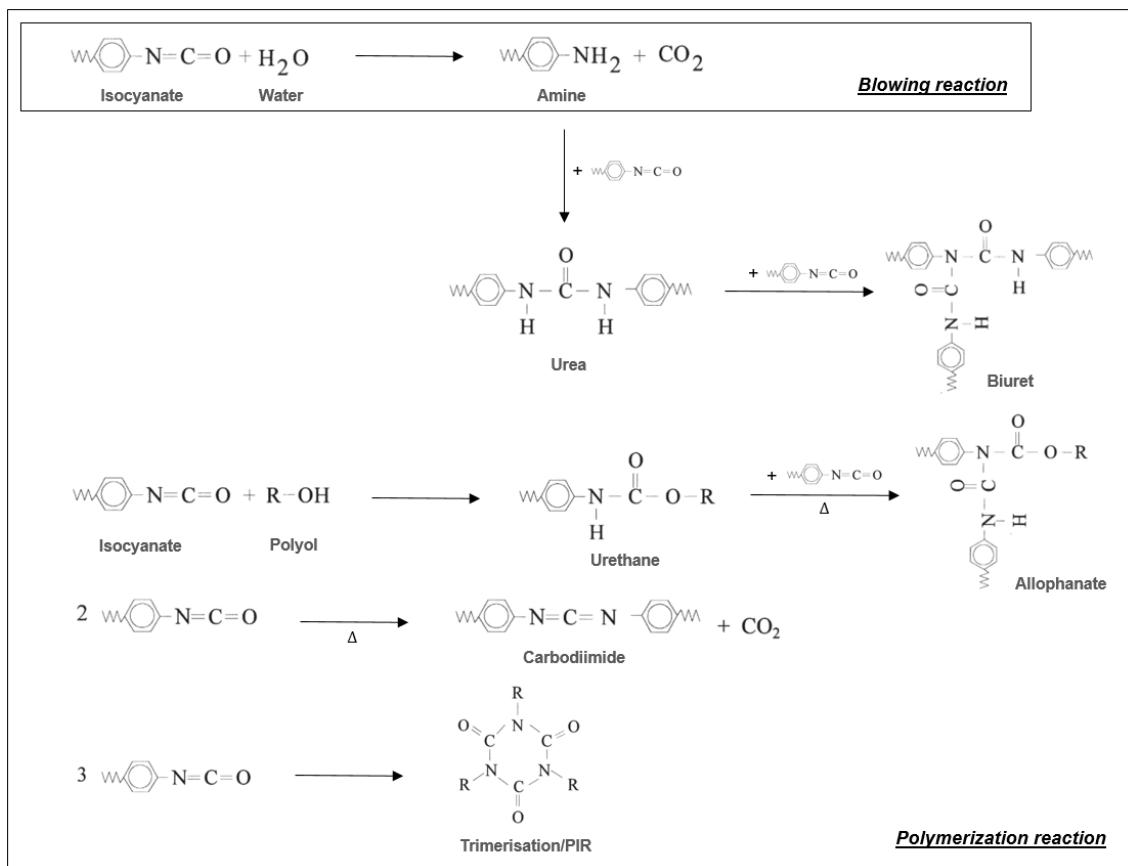


Fig. 13 Important PUR reactions (blowing and polymerization) adapted from Demharter (1998)

### 2.2.1.2 Foaming process

Foaming in polymers can be processed chemically or physically. Chemical blowing refers to the participation of reactive foaming that generates through a chemical reaction. Gas can evolve out of simple reactions between reactants or by thermally induced decomposition. The amount of gas is governed by the reactant quantity and ratio, reaction rate of a catalyst and thermal condition and foam stability by additives (Lee & Ramesh, 2004). Chemical blowing is a basic reaction in PUR production, occurring due to the  $\text{CO}_2$  produced from the reaction between isocyanate and water, as mentioned earlier. Physical blowing can exist if a physical blowing agent (PBA) is added to assist in

the foaming process physically. A mixture of chemical and physical blowing agents can be used to enhance either agent alone (Al-Moameri et al., 2016).

PBAs are low boiling point substances used in the extrusion – mostly in thermoplastic processing – to generate the cellular structure. Due to the heat of the reaction, they vaporize and leave the trapped gas in the foam cells. One of the well-known PBAs, chlorofluorocarbon (CFCs), has been phased out because of its effects on the depletion of the stratospheric ozone layer. Following the ban on the use of CFCs in 1996, the foam industry began to use other groups of chemicals. Currently, hydrochlorofluorocarbons (HCFCs), hydrofluorocarbons (HFCs) and volatile organic compounds (VOCs) – mostly hydrocarbons such as pentane – are the major chemicals used as blowing agents (Lee & Ramesh, 2004). These PBAs are metered and dissolved in the polymer melt during processing. Bubbles often expand owing to the presence of nucleating agents. Suddenly releasing the system pressure generates the super-saturation and diffusion of gas into the nucleated bubbles. When followed by subsequent cooling, polymer cell walls become solidified, leading to the stabilization of the resultant cellular structure.

### 2.2.1.3 Foam development

The foaming process is described in four steps (Al-Moameri et al. 2016, Lee and Ramesh 2004):

1. Dissolution of foaming agent
2. Cell nucleation (bubble formation)
3. Bubble growth
4. Stabilization

In the first step, after the evolution of CO<sub>2</sub> gas by chemical reaction, developed gas – including air – is dissolved in the polyol component. A gas-polymer solution is formed. These phenomena can induce the nucleation of bubbles in PUR systems in the next step. The mechanical agitation of polyol and isocyanate mixture provides microbubbles of air that serve as sites for bubble growth. Self-nucleating CO<sub>2</sub> from a mixture of polyol and TDI was proven unachievable without aid i.e. physically mixing the air (Kanner & Decker, 1969). The bubble growth starts, in which blowing-agent gas diffuses from the liquid–gas interface into the bubbles before stabilizing cell bubbles in the final step.

Fig. 14 illustrated the mentioned foam development starting from the bubble nucleation stage to the stabilization. The dispersed spherical gas bubbles initially grow due to the diffusion of blowing gas. This process lasts until a certain volume is achieved, in which the spherical cells are at the most densely packed in the liquid matrix. In the case of exceeded volume, spherical cells will convert to polyhedral cells. The majority of polymer

liquid is located here, in the struts and walls, while thin membranes separate the individual cells from one another (Kapps & Buschkamp, 2004). The rigid foam polymer becomes self-supporting once enough network formation has taken place. The additional expansion of the foam is then driven by the difference between the internal cell gas pressure and the external atmospheric pressure. The growth stops when the foam has built sufficient strength to withstand the pressure difference or molded foams, once the mold is filled (Randall & Lee, 2002).

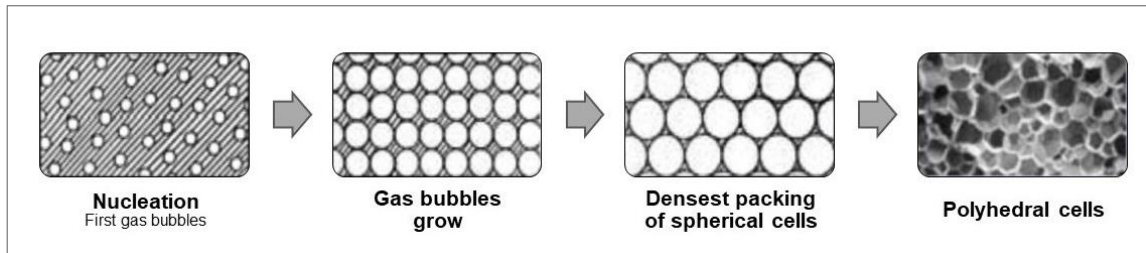


**Fig. 14 Production of PUR rigid foam adapted from Kapps & Buschkamp (2004)**

Variables accounted for during these stages of the foaming process are complex. For instance, the viscosity of the polymer, the gas concentration, the foaming temperature and the amount of nucleating agent and its nature are some of the variables that control the foam growth process (Lee & Ramesh, 2004). These factors do not only have effects on foaming, but some of them could also influence each other.

Physical processes during the foam formation are characterized by a period in which alternation of the mixture can be observed. With the start of mixing set at zero, characteristic times measured during the foaming process are described by Randall and Lee (2002) and defined in ASTM D7487 as follows:

- Cream time or initiation time is when the mix starts to foam or the point at which bubbles begin to appear.
- String time or pull time or gel time is identified as the point when strings of polymer can be withdrawn by dipping a pointer into the foam mix or pulled away from the surface of the foam if the surface is touched by the edge of a tongue depressor or similar implement.
- The tack-free time is when the surface of the foam stops being tacky to touch.
- The end-of-rise is the point of maximum foam height.

The determination of these characteristic times helps to predict the foaming stage.

#### **2.2.1.4 Reaction kinetics**

To produce PUR foam under the varying conditions of wood-based panel manufacture, it is crucial to understand the foaming process in terms of time and temperature. Typical foam expansion and exothermic development are plotted against time, for a formulation

blown by CO<sub>2</sub>, as seen in Fig. 15. After 57 s of stirring, the string time was reached, while volume expansion was nearly complete. From this status, the mixture temperature continued to rise by almost 50 °C to the final value of more than 160 °C. This implied that resin formation is far from complete when the foam has fully risen. It also suggests that polymer strength is built up in the later stage, despite the early start of reaction kinetics immediately after mixing polyol and pMDI (Lee & Ramesh, 2004).

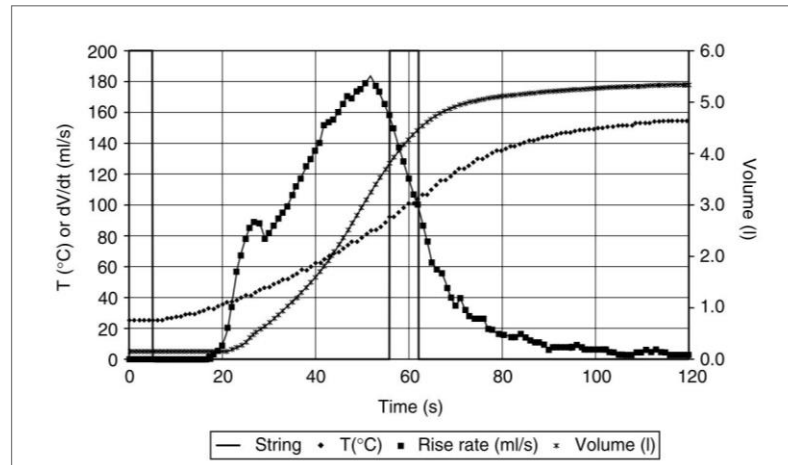


**Fig. 15 Rise rate, volume expansion, and reaction exotherm of a water-blown rigid foam (Lee & Ramesh, 2004)**

The reaction kinetics of the PUR foaming process was modeled by Zhao et al. (2013), in that the relationship of the internal temperature versus time was represented. As the volume changes, polymer chains stretch and the elastic energy stored in the chains during this deformation will contribute to the total internal energy. They predicted the foam height according to the volume of foam at different temperatures, as shown in the following equation. Both CO<sub>2</sub> and methyl formate (MFL) contribute to foam volume rise. The model allows for dynamic heat transfer primarily from the exposed top surface of the foam.

$$\frac{dh}{dt} = \frac{dV}{dt} \times \frac{1}{A} = \left( \frac{22.4 \times T}{273.15} \right) \times \left( \frac{dn_{\text{CO}_2}}{dt} + \frac{dn_{\text{MFL}}}{dt} \right) \times \frac{1}{A} \quad (2)$$

where

- $A$  : the surface area of the foam related to different foam height,
- $-\frac{dn_{\text{MFL}}}{dt}$  : the evaporation rate of methyl formate,

The equation created the model for foam temperature as a function of time in their research. The study confirmed that the maximum temperature substantially indicates the completion of the reactions. Findings based on this research (Lee & Ramesh, 2004; Zhao et al., 2013) support the correlation between the foam rise profile and the PUR mixture's internal temperature during the foaming process.

In addition to temperature, viscosity and bubble pressure are parameters within foam that change remarkably during the foaming process. Experimental data for foam height was compared via simulated data concerning viscosity and time by Al-Moameri et al. (2016), as summarized in Fig. 16a. They implied that as the water loading in the formulation increases, more CO<sub>2</sub> is generated and a higher foam is obtained. The result from Fig. 16a suggests that the viscosity remains constant at the reaction start until it increases distinctly at a specific point approximately before the maximal foam height. From their experiment, bubble pressure was simulated, as shown in Fig. 16b. The results show that the bubble pressure increases when the resin sets because of the increase in viscosity. This increase is only due to the continued growth in the temperature of the system.

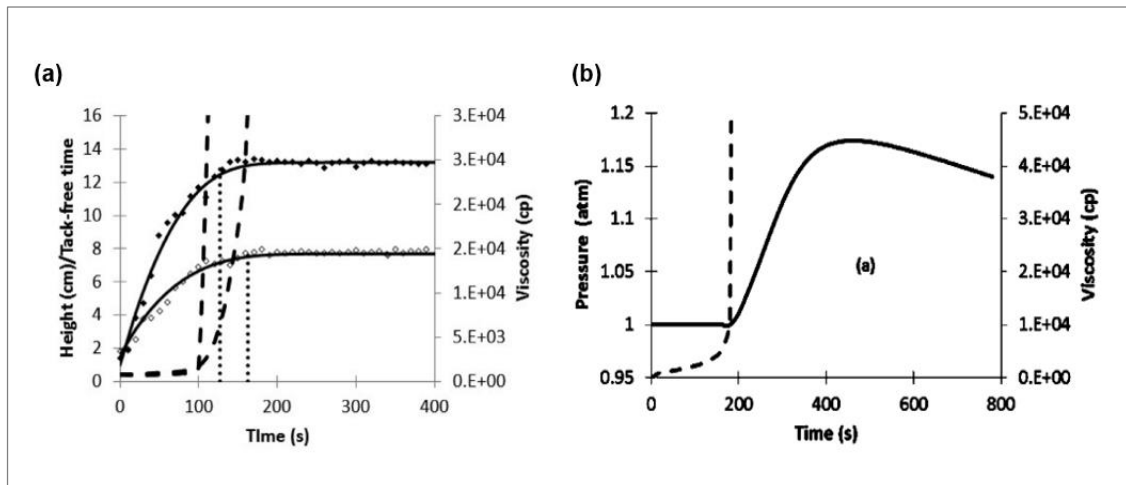


**Fig. 16 (a)** Symbols represent experimental results for foam height using (◆) 1 and (◇) 0.5 g of water. Solid lines represent simulation results for foam height. Dashed and dotted lines from left to right represent viscosities and tack-free times, respectively, for foams blown by 0.5 and 1 g of water. **(b)** Bubble pressure simulation, solid and dashed lines represent the pressure inside the bubble and the resin viscosity, respectively (Al-Moameri et al., 2016).

Much of the research in recent years has focused on reaction kinetics in the foaming process, specifically the temperature profile, foam height (Lee & Ramesh, 2004; Zhao et al., 2013) as well as blowing agent performance and cell morphology (Al-Moameri et al., 2016; Choe et al., 2004; Hee Kim et al., 2008; Lim et al., 2010). As the PUR foam reaction is self-activating under normal conditions and requires only mechanical agitation for bubble nucleation, the curing temperature was not considered an influencing factor in those studies. There remains a need to investigate the effect of the curing temperature on PUR foaming, particularly for the foaming process under the hot pressing machine, where different conditions will be regulated.

## 2.2.2 Interaction with wood

### 2.2.2.1 Effects of wood addition in PUR foam

Many types of fillers have been used in PUR production for improving the structural and mechanical properties of PUR foams. Different fillers such as cellulose and lignocellulose fibers, glass wool, glass microsphere or glass fibers, eggshell wastes, date palm particles, walnut and hazelnut shells and esparto wool have been reported being used to improve the structural and mechanical properties of PUR foams (Gama et al., 2018). In recent years, fillers were not only used in PUR foams however. Many studies showed that natural fillers such as kenaf fiber, oil empty fruit brunch, rice husk and wood flour could also be used to produce both thermoplastic and thermoset PUR (Atiqah et al., 2017). The input of lignocellulose materials is more beneficial than synthetic ones, as it reduces costs and increases the utilization of natural resources in components, such as polyols, which are derived from a natural origin like vegetable oils such as rapeseed, palm and soybean (Petrović, 2008). Most lignocellulose fillers are obtainable from the agricultural sector, thus reducing cost and attracting the manufacturing industry. The application of biomaterials in polymers can be advantageous due to their low density, economical production, renewable and biodegradable properties, CO<sub>2</sub> neutral character-combustion as well as their availability. On the contrary, it possesses some disadvantages; for instance, poor dispersion of fibers in the matrix, high moisture content inducing the decreased properties, variation in properties, little microbial resistance, and thermal degradation at high temperatures i.e. during ranges between 220-280 °C and 280-300 °C for hemicellulose and lignin respectively (Abdellaoui et al., 2018).

Moisture in wood fiber was examined as a blowing agent for producing PS/wood-fiber composite foams (Rizvi et al., 2000). Hygroscopic wood-fibers used as filler were utilized as a carrier to distribute water in the polymer matrix due to the low solubility of water in hydrophobic plastic. The study showed that the wood-fiber moisture could be effectively used as a blowing agent during the extrusion foaming of composites. An expansion ratio of up to 20 was achieved. It was explained by the transformation of moisture into the gaseous state at temperatures exceeding 100 °C. Bound water located within the cell walls was quickly converted into gas and lost from the extruder's hopper. Then, about 3 % of the rest of the wood moisture, which was the remaining water in part of the molecular structure of the wood, namely water of constitution, was utilized as a foaming agent. Matuana and Mengeloglu (2002) confirmed the function of wood moisture as a blowing agent, by which rigid PVC/wood flour composites could be foamed at lower processing temperatures. Unlike the prior study, they suggested that bound water was

used as the foaming agent, as it required less energy to remove from wood cell walls than the water of constitution present in the molecule of cell wall components.

PUR rigid foam, changes in mechanical and thermal properties affected by the addition of various fillers derived from agricultural residues e.g. flax and hemp fibers (Kuranska & Prociak, 2012), ground walnut shell (Prociak et al., 2015) have been discussed. Both wood fiber and flour were applied to investigate for effects on foam properties. Some cases showed degraded properties when increasing wood contents; for example, a reduction in compressive properties of PUR foam by the addition of wood flour was found by Krishnamurthi et al. (2003) and Mosiewicki et al. (2009). At the same time, other literature confirmed the improved properties when a lower amount of wood contents were added to the foam (Gu & Sain, 2013; Yuan & Shi, 2009). However, it could be possible to apply wood filler into PUR foam at an optimal concentration. 15 – 20 % wood flour was proven to produce PUR foam with acceptable properties in research by Yuan and Shi (2009) and Mosiewicki et al. (2009) respectively. Kurańska et al. (2015) confirmed the application of wood fibers in PUR-PIR foam formulations from about 22 to 27 % by weight.

In general, the incorporation of fillers to PUR caused a higher modulus due to the stiffness of particles (Casado et al., 2009). The result could differ in PUR foam, where the foam nucleation makes a difference. Despite the advantages mentioned above and a broad spectrum of high possibilities, the application of wood flour can affect PUR foam formulation, especially in terms of viscosity. It causes the mixture to be less expandable, giving rise to the more distorted cells' structure, with a more extensive cell size distribution. This effect increases with filler content when wood flour particles are large enough, purported to be 64  $\mu\text{m}$  diameter on average, to interfere with cell development (Mosiewicki et al., 2009). Furthermore, the increase of wood fillers content caused more of them to be located in the cell walls, causing increased open-cell content in these foams (Kurańska et al., 2015).

Aside from wood-based contents, other filler features e.g. filler size and shape, can alter both the morphology and the characteristics of the PUR foam (Mosiewicki et al., 2009; Prociak et al., 2015). This is owing to the fact that it induces a difference in the arrangement of fibers, the dispersion of filler in the polyol matrix, and the interaction between the polymer matrix and the surface of the fibers (Kuranska & Prociak, 2012). Therefore, it can be said that the mechanical properties of PUR foam depend on the concentration, size, shape, position and orientation of the filler and the incorporation of filler into the cell wall.

The presence of filler contributes to changes in PUR foam properties as regards the physical features mentioned. However, using a filler could alter parts of the chemical characteristics of PUR as well. Principally, the addition of any fillers to the PUR matrix can affect the reaction between the polyol and the isocyanate due to at least two resultant interactions (Gama et al., 2018):

- The hydroxyl groups on the surface of the filler can alter the NCO index, thus affecting the consumption of isocyanate groups.
- The interference of the filler on the rate of polymerization is associated with the rheological behavior of the reaction mixture and the coupling of the filler surface groups with either the isocyanate, the polyol, and/or the water.

Therefore, the presence of fillers may lead to an increase or decrease of the urethane/urea linkage ratio, altering the cross-linking density and affecting the morphology of the foams. Wood addition in PUR fundamentally affects PUR properties because of the existence of hydroxyl groups. The representative probable chemical structure of the PUR and the cellulose fiber was suggested by Mothé et al. (2009), as illustrated in Fig. 17. It implies that the first reaction begins from the combination of polyol and isocyanate to produce PUR. After that, the hydroxyl group from cellulose reacts with urethane linkage in PUR and enlarges the molecule. This idea agrees with Casado et al. (2009), who concluded that wood flour co-reacted with PUR could act as a chain extender, in the same way that short diols added to segmented PUR formulations do.

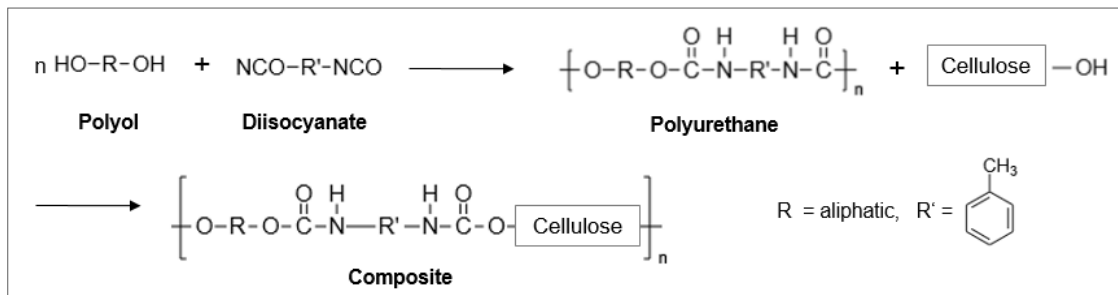


Fig. 17 Probable reaction between isocyanate group of PUR and cellulosic fiber adapted from Mothé et al. (2009)

### 2.2.2.2 Chemical interaction between wood and isocyanate

The importance of PUR in the wood industry was established in the 1960s when moisture-cured isocyanate-based resins were first introduced. In the field of wood-based panels for exterior applications specifically, formulated resins from PUR are used in glue-laminated lumber (Glulam), finger-jointed lumber (FJ) and laminated veneer lumber (LVL), as they have good gap filling properties and improved resistance to creep. For wood composites, polymeric grades of MDI were utilized in MDF, Particleboard and OSB with product differentiation (Randall & Lee, 2002). Aside from that, PUR coatings are the

most preferred systems for coating wood, with a market share exceeding 40 %. The TDI-based coating is used most frequently in both 1-C and 2-C formulations (Engels et al., 2013).

The study of isocyanate in wood is complicated, since wood is a complex material containing three main components with varied contents: cellulose (38-50 %), hemicelluloses (23-32 %) and lignin (15-25 %), in which

- Cellulose is a linear biopolymer that derives from  $\beta$ -1,4 linked glucose monomers (Fig. 18). Each repeated unit is composed of three hydroxyl groups, in which the crystallinity is conditioned by the aptitude of these groups to make hydrogen bonds (Siqueira et al., 2010).
- Hemicelluloses are heterogeneous polysaccharides based on pentoses (D-xylose and L-arabinose), hexoses (D-glucose, D-galactose, D-mannose, L-rhamnose) and uronic acid units (D-galacturonic acid and D-glucuronic acid).
- Lignin is the third polymeric main constituent of wood and structurally derives from *p*-hydroxycinnamyl alcohols. The lignin is completely amorphous and hydrophobic. It forms large three-dimensional networks embedding and gluing the polysaccharides together.

Structurally, if the fiber is treated as a composite material, where the cellulose is the fiber reinforcement and the lignin is the matrix, the hemicellulose acts as a normalizer at the interface between the cellulose and the lignin elements (Abdellaoui et al., 2018; Zuckerstätter et al., 2010).

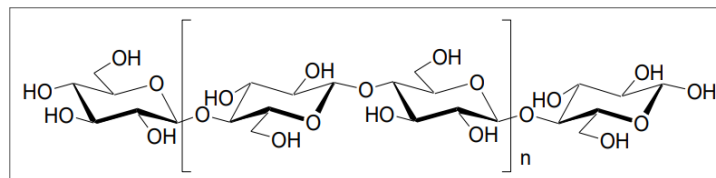


**Fig. 18 Cellulose structure (Siqueira et al., 2010)**

All main wood components contain hydroxyl groups; therefore, the reaction of isocyanate with this functional group in wood will form carbamate, the same linkage that results from the reaction between isocyanate and polyol. This chemical reaction is employed for bonding isocyanate adhesive with wood. Owing to the high reactivity of isocyanate, another competitive reaction with water coexists. The former reaction is preferred for wood-bonding, as forming more carbamate signifies better bonding results. Gao et al. (2005) investigated the reaction of phenyl isocyanate and cellulose with different moisture contents to compare the reaction rate in both components. They found that the reaction rate between isocyanate and water is faster than the isocyanate and hydroxyl groups of wood. An increase in the moisture content of cellulose raises the reaction rate of isocyanate and water; in contrast, the reaction rate of isocyanate and cellulose

decreases. For this reason, the high hydrophilicity of cellulose could be undesirable in the reaction between wood and isocyanate when a high level of bonding is required.



Fig. 19 Reaction schemes of isocyanate with or bonded to wood containing water (Gao et al., 2005)

Isocyanate was used to reduce the hydrophilic characteristic of lignocellulose fibers in order to improve compatibility with the hydrophobic matrices. The reaction between isocyanate and water present on the fiber surface forms urea, that can further react with the hydroxyl groups of the celluloses. This secondary reaction results in higher moisture resistance properties in the fiber and better bonding with the matrix, thereby enhancing the composite's properties. From these typical PUR reactions (Fig. 13), it can be seen that isocyanate serves as a coupling agent in fiber-reinforced composites.

### 2.3 Blocked isocyanates

The high reactivity of isocyanates produces a variety of reactions, which originate a wide range of PUR products in the form of elastomers, foams, adhesives, binders and coatings cross-linked plastics. On the contrary, the high reactivity of isocyanate with nucleophiles as alcohol and amines causes a negative impact on the environment. Further practical problems such as sensitivity towards moisture limit the storage time, dosage in a 2-C system challenged industries due to their effects on the manufacturing process and quality of the end products. To overcome these obstacles, there was an attempt to isolate the active isocyanate group from the reaction. This method is called blocking, and is divided into chemical and physical processes. Generally, when the term 'blocked isocyanate' is used in literature, it refers to a chemical blocking process. Blocked isocyanates are widely used in powder coatings, elastomers and adhesives (Tang et al., 2013), purported to be fine particles, well distributed with a simple configuration and harmless to the environment.

Chemical blocking utilizes two components, basically isocyanate and a nucleophilic substance. Both react at normal temperature into the adducts, which can be separated at elevated temperatures. Consequently, the isocyanate will be re-released and prepared for further reaction with an available reactant in the system. The coating industry uses

this concept to make 1-C PUR formulations for thermal curing, which is preferred for end users when compared with the 2-C system. It is possible to prepare a mixture of blocked isocyanate with polyol in an optimal ratio as regards the reactant dosage. As the adduct is stable at room temperature, it will only react with mixed polyols at high temperatures in order to form the urethane linkage bond. Owing to the low reactivity, blocked isocyanates are insensitive to moisture and have a high level of stability in storage, which is user friendly and more environmentally acceptable.

Instead of using the chemical bond with blocking agents, the physical blocking aims to shield isocyanate from direct contact with reactive environments by spatial separation. One physical blocking technique is microencapsulation, where the isocyanate is enclosed in a microsphere, enabling its dispersion yet preventing a reaction with another component. In activated circumstances, a micro-crack can potentially proliferate through the material, it then ruptures the microcapsules and releases the healing agent into the damaged region, where it undergoes polymerization upon mixing with the catalyst phase (Yang et al., 2008). This concept of self-healing material was used in various fields, including nanomaterials, agricultural, pharmaceuticals, cosmetics and in textile industries (Ma et al., 2017). Physical blocking by microencapsulation was investigated with different isocyanates. Microcapsules of IPDI with PUR shell wall were investigated for self-healing polymers for advanced coating purposes (Yang et al., 2008). PAPI (polyaryl polymethylene isocyanates) microcapsules were prepared by the new energy-efficient strategy (Ma et al., 2017). In their study, isocyanate was reacted with small-molecule active hydrogen via interfacial polymerization under agitation in an oil-in-water emulsion.

Consequently, PUR and polyurea were used to form the microcapsule's shell without the addition of any other material. In their next study, PAPI release was controlled by encapsulation with the UF resin shell (Ma et al., 2019). The microcapsules were used in wood adhesive as a functional crosslinker, enabling the isocyanate to cross-link in plywood. In the publication, pressure was used to destroy the microcapsules, controlling the release of the liquid core in plywood production.

### **2.3.1 Mechanisms of blocked isocyanates**

Delebecq et al. (2012) analyzed the high reactivity of isocyanate by the electronegativity of structured atoms. The isocyanate group is a strained linear structure with two cumulated double bonds  $N=C$  and  $C=O$ . The isocyanate group reactivity is based on the polarization induced by the high electronegativities of nitrogen and oxygen atoms, which delocalize the electron density toward the nitrogen and oxygen atoms. For this reason,

isocyanate reacts easily with active nucleophilic reagents XH; the nucleophilic center X attacks the electrophilic carbon of isocyanate. The most important reactions involving isocyanate are additions of alcohol, thiol or amine: the isocyanate group reacts with a hydroxyl group to yield urethane, with a thiol to produce thiourethane and with an amine to give urea bonds (Fig. 20).

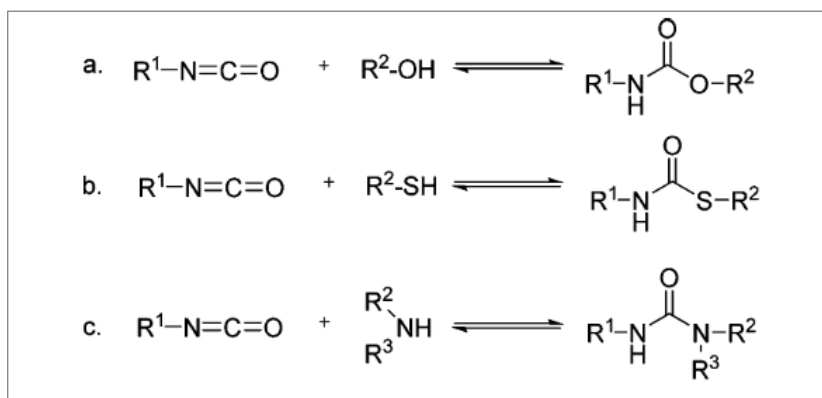


Fig. 20 Common reactions used in PUR chemistry (Delebecq et al., 2012)

Blocked isocyanate is described as an adduct containing a weak bond formed by an isocyanate reaction with an active hydrogen compound. Since it is an equilibrium, this reaction tends to regenerate the isocyanate group at elevated temperatures (see Fig. 21 a). The adduct must be stable at room temperature and very reactive at high temperatures (Delebecq et al., 2012). As the temperature rises, the isocyanate unblocks liberating NCO groups, free to react with polyols to form the urethane polymer. The process is called curing reaction when free isocyanate reacts with a substrate containing nucleophile to form thermally more stable bonds (see Fig. 21 b). This phenomenon in the curing reaction was described by Jones (2008). The free blocking agent then either remains in the coating or is removed by evaporation. The overall cure reaction will not be instantaneous—the combination of both molecular processes deciding in the overall time and cure temperature. Typically, cure times are 20 min to 1 hr at the unblocked temperature, which is the fastest time achieved using catalysis. Curing can be effected at lower temperatures if the curing time is increased. However, the balance of the curing speed, energy requirement and temperature sensitivity of the substrate needs to be considered. Some concerns over the misunderstanding of the deblocking temperature in actual use with polyol were also expressed (Jones, 2008). Because the overall process during curing results from two different molecular functions i.e. the unblocking equilibrium reaction and the subsequent reaction of the unblocked isocyanate with polyol, the curing temperature at the end may differ from the deblocking temperature.

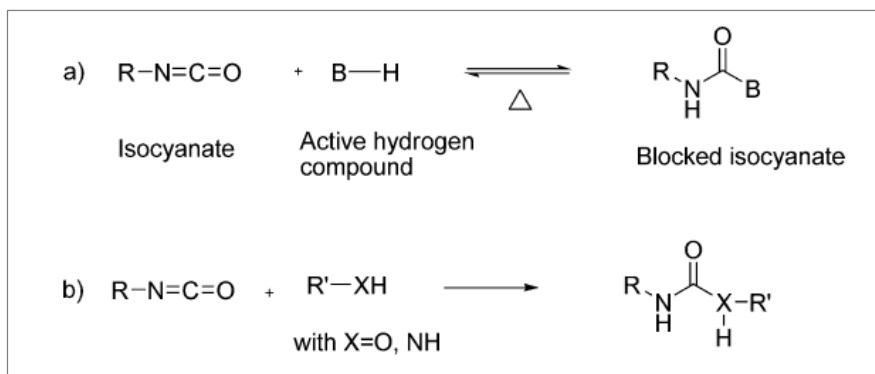


Fig. 21 a Blocking and deblocking reaction of isocyanate, b Curing reaction (Delebecq et al., 2012)

### 2.3.2 Deblocking temperature

The blocking and unblocking reaction is a chemical equilibrium. Hence, the deblocking temperature is not a fixed point. The initial deblocking temperature describes the temperature at which the feature of deblocking can be observed. In practical applications, it is possible to generate a deblocking temperature according to the adduct's onset temperature of dissociation (Delebecq et al., 2012). Different analytical techniques have been used to characterize the deblocking temperature. This will be discussed at the end of this section.

Delebecq et al. (2012) discussed the deblocking temperature in a theoretical view of a kinetic mechanism. The blocking and deblocking reaction are described by the Arrhenius relationship, where the reaction is dependant on temperature ( $T$ ) and activation energy ( $E_a$ ).

$$k = A e^{-E_a/(RT)} \quad (3)$$

According to the above equation, the exponential factor ( $A$ ) is increased by  $T$  and for a given temperature variation, the higher the  $E_a$ , the more important the change. To get an accentuated threshold temperature between blocked and free isocyanate,  $E_a$  should be increased. Since the elevated dissociation temperature does not comply with industrial requirements for economic reasons, a compromise is necessary. Moreover, large  $E_a$  makes the unblocking reaction too slow unless  $A$  is large enough to counteract  $E_a$ . The ideal reaction should have a large positive entropy change, such as the cleavage of a ring system to a ring-opened system, to take advantage of the temperature effect.

Basically, the rate and extent of the deblocking reaction depends on the structure of the isocyanate and blocking agent, including substituents. The thermal dissociation temperature of a urethane bond varies with the involved functional groups. The following decomposition temperature order is given (Simon et al., 1988):

- n-Alkyl–NHCOO–n-alkyl: 250 °C
- Aryl–NHCOO–n-alkyl: 200 °C
- n-Alkyl–NHCOO–aryl: 180 °C
- Aryl–NHCOO–aryl: 120 °C

The thermal stability of the isocyanate-blocking agent bond caused by their chemical structures is not the only factor influencing the deblocking reaction. The wide range of deblocking temperatures can be accomplished by varying operating and reaction conditions (Delebecq et al., 2012) i.e. the presence of catalysts and other additives (Rolph et al., 2016) or the mole ratio of blocking agents per isocyanate (Lubis et al., 2017). Furthermore, different results of deblocking temperatures from the same adducts can be reported, depending on the method of analysis e.g. heating rate, gas flow, sensibility or sealed reactor cup (Delebecq et al., 2012). Consequently, the deblocking temperature can be specific and varied despite having the same blocking agent.

The deblocking temperature can be measured by different techniques. Features of standard techniques are described as follows:

- Infrared (IR) spectroscopy and Fourier Transform Infrared (FTIR) spectroscopy can detect strong bands between  $\nu = 2230 \text{ cm}^{-1}$  and  $\nu = 2270 \text{ cm}^{-1}$  (attributed to free N=C=O), the appearance of which can be compared to the disappearance during deblocking of the bands associated with the blocked isocyanate (C=O between  $\nu = 1640 \text{ cm}^{-1}$  to  $\nu = 1720 \text{ cm}^{-1}$  and N–H band at approximately  $\nu = 1535 \text{ cm}^{-1}$ ) (Rolph et al., 2016).
- Differential scanning calorimetry (DSC) measures heat flow into or out of a sample over a specified temperature range. This technique is applicable due to the different adduct structures of synthesized compounds. Therefore they exhibit a significant difference in energy (endothermic) during unblocking (Lee et al., 2005).
- Thermogravimetric analysis (TGA) measures the changes in sample weight over a specific temperature range. Thus, TGA is unsuitable for compounds that do not exhibit volatility over the unblocking temperature range (Lee et al., 2005).

Their advantages and disadvantages are compared as listed in Tab. 4.

**Tab. 4 Advantages and disadvantages of commonly used techniques to determine the deblocking temperatures (Rolph et al., 2016)**

| <b>Technique</b>             | <b>Advantages</b>   | <b>Disadvantages</b>  |
|------------------------------|---|---|
| <b>IR, FTIR spectroscopy</b> | Immediate result,<br>easy to determine 100 %<br>completion of blocking/deblocking.<br>High resolution instruments<br>allow for ppm detection. | Strongly influenced by heating rate.<br>Sample preparation and evaporation<br>can cause discrepancies in results.<br>Results need to be normalized for<br>analysis. |
| <b>DSC analysis</b>          | Relatively high temperature<br>capability (up to 700 °C).<br>No additional sample preparation.  | High temperatures may influence the<br>baseline and signal: noise ratio.  |

|            |  |   |
|------------|--|---|
| <b>TGA</b> | High temperature capability (up to 1500 °C).<br>Samples require no additional preparation. µg sensitivity. | High temperatures may influence the baseline and signal: noise ratio.<br>Boiling point of the blocking group must fall within the probed temperature range. |
|------------|--|---|

The high deviations in deblocking temperatures and rate determined by using different methods were highlighted in their work. So the direct comparison between two deblocking temperatures should be carefully considered. Despite the importance of the deblocking point in industrial applications, it does not provide information on the deblocking rate.

### 2.3.3 Blocking agents and their applications

Despite the great variety in types, blocking agents have one common feature as they contain an active hydrogen atom within the molecule. This is exceptional for diethyl malonate that has a reactive methylene group containing two active hydrogen atoms. Several compound groups with an active hydrogen atom have been reported as blocking agents: alcohols and phenols (OH), amines (NH), oximes (C=N-OH), and other N-based compounds such as amides (R-CO-NR), imides (R-C-NR-C-R) and imidazole, pyrazole and triazole. All of them have the bonding of an active hydrogen atom with an atom of N or O. Those additional compounds used for blocking are called external agents. In the case of internal blocking, the isocyanate is used to block itself, such as in the case of uretdione – a self-condensation product – and transform into a trimer (isocyanurates) (Jones, 2008; Rolph et al., 2016).

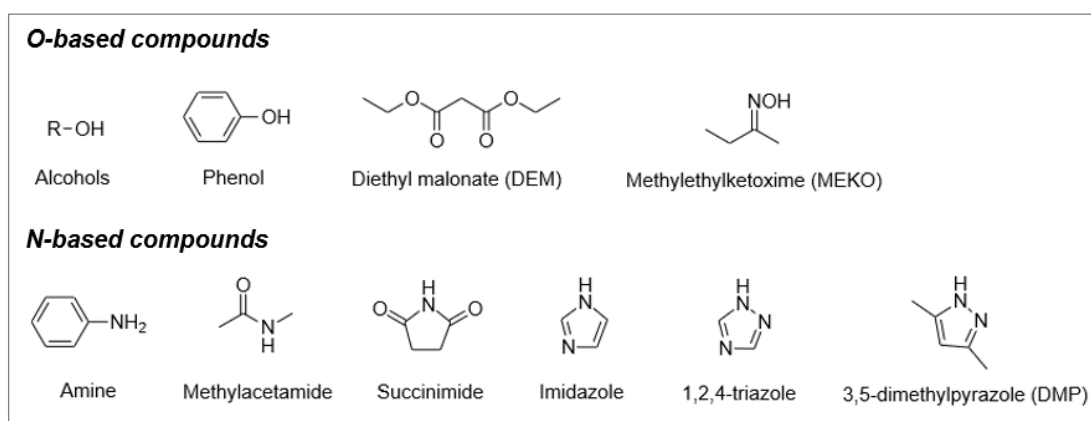


**Fig. 22 Blocking agents divided into O-based and N-based compounds, considered by the atom that reacts to C-atom of NCO group in the formation of blocked adducts**

The vast array of blocking agents enables a wide range of deblocking temperatures. This can happen as the deviated temperature in combination with the changing of the experimental conditions and isocyanate type (Rolph et al., 2016). Aromatic isocyanates are those in which the isocyanate function is directly bonded to an aromatic ring, as in

TDI or MDI. This influences unblocking at a lower deblocking temperature than an aliphatic isocyanate blocked with the same blocking agent (Jones, 2008). Regardless of the wide variety in adduct properties, blocking agents have significant limitations from relatively high curing temperatures in some cases and the evolution of undesirable volatile blocking agents such as phenol (Lee et al., 2005). Also, free blocking agents may remain in the product material unless the deblocking range is similar to their boiling points. This can cause the formation of bubbles in the product material, which is especially disadvantageous for the coating application, as highlighted by Rolph et al. (2016).

### 2.3.3.1 Sodium bisulfite ( $\text{NaHSO}_3$ )

Among other blocking agents,  $\text{NaHSO}_3$  attracts users for its low price and pollution-free characteristic. The chemical properties are distinct because of the hydrophilicity and the water-solubility of the adducts, which are frequently required in waterborne coatings or solutions. Adducts from bisulfites have hydrophilic molecules by anionically charged sulphonate systems of the general formula  $\text{R-NH-C(=O)-SO}_3\text{Na}$  (see Fig. 23) (Barruet et al., 2007), whereas most blocked isocyanates are hydrophobic. For this reason, it is a favored blocking group for isocyanates in waterborne solutions (Wicks & Wicks Jr, 1999). Compared with alcohols, phenols, oximes and caprolactam, bisulfites have relatively low deblocking temperatures.

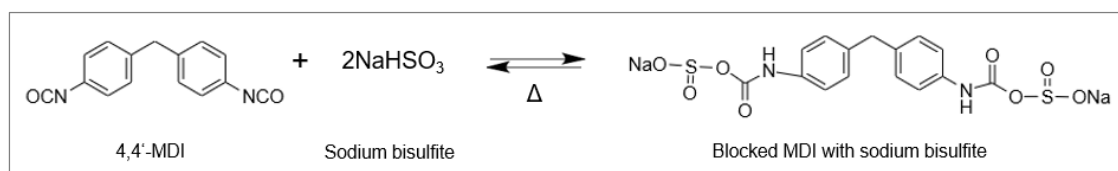


**Fig. 23 Blocking and deblocking reaction of isocyanate and  $\text{NaHSO}_3$**

The deblocking temperatures of  $\text{NaHSO}_3$  can vary greatly, ranging between 50-160 °C (Rolph et al., 2016). Blocked pMDI could release isocyanate using heating temperatures between 95-105 °C (Zhang et al., 2011). In another study by Lubis et al. (2017), this appeared to be lower between 78-82 °C under certain circumstances, as blocked pMDI in their research was obtained for the modification of UF resin adhesive. UF/blocked pMDI resin in powder form was prepared for plywood adhesives in the hot pressing, where the core temperature in the composite is not much higher than 100 °C (105-120 °C). As the  $\text{HSO}_3^-/\text{-NCO}$  mole ratios increased from 0.9 to 1.8; higher deblocking temperatures of blocked pMDI were observed by DSC.

Adduct prepared by another isocyanate type as IPDI did not seem to have a high deviation in the deblocking range. Zhou et al. (2013) confirmed the deblocking

temperature between 85-117 °C. The blocked IPDI in liquid and solid states are stable after being stored for 12 months at room temperature.

### 2.3.3.2 $\epsilon$ -caprolactam

$\epsilon$ -caprolactam is the most widely used blocking molecule in the coating and paint industries (Delebecq et al., 2012), since caprolactam-blocked isocyanate powder coatings show good package stability and good leveling. The good leveling results from favorable rheological behavior at melt temperatures and due to part of the caprolactam remaining in the film (Wicks & Wicks, 2001). The existing  $\epsilon$ -caprolactam that does not volatilize after deblocking can act as plasticizer. Due to its low price, relatively low toxicity and outstanding resistance to discoloration, it is also reported as being used in glass fiber coating (Lee et al., 2005). As  $\epsilon$ -caprolactam is non-corrosive, it shares a part of the major market that exists between the variety of blocking agents available (Libni et al., 2018).

$\epsilon$ -caprolactam-blocked isocyanate forms linkage (-NH-CO-) as seen in Fig. 24. Due to its flexibility, this linkage causes better combinations of thermomechanical properties that make  $\epsilon$ -caprolactam-blocked isocyanate suitable for the fabrication of polymer composites. With flexible linkage, the blocked diisocyanate is expected to function as the best thermoplastic toughener for epoxy resin (Premkumar et al., 2008).

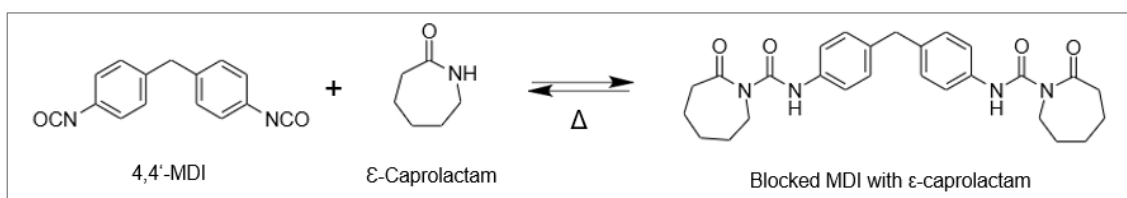


**Fig. 24 Blocking and deblocking reaction of isocyanate and  $\epsilon$ -caprolactam**

A deblocking temperature in the range between 70-170 °C was reported by Rolph et al. (2016). Between the different isocyanate types, MDI adduct exhibited a higher deblocking temperature (>158 °C) than TDI adduct (>130 °C), which was found in commercial blocked isocyanates (Subramani et al., 2004). Compared by Lee et al. (2005) using DSC and TGA techniques, the deblocking temperature ranges of blocked isocyanates from MDI and TDI showed a minor difference in the range of 5-10 °C. Using TGA provided a broader range of deblocking temperatures than with DSC, measuring 140-200 °C and 150-210 °C in TDI and MDI respectively.

### 3 Objectives and research plan

This thesis aims to develop PUR components for application as the core layer in the one-step continuous process according to Lüdtkke et al. (2007). The requirements for core layer materials are listed in the following table:

**Tab. 5 General ambient conditions and requirements for the core layer material**

| <b>Surrounding conditions during the process</b>   |  |
|--|--|
| <u>High-pressure phase</u>   | <u>Expansion phase</u>   |
| <ul style="list-style-type: none"> <li>• Pressure: up to 4 Nmm<sup>-2</sup></li> <li>• Temperature: increase in the core between 90-120 °C</li> <li>• pH-value: light acidic due to the hardening reaction in the cover layers</li> </ul>  | <ul style="list-style-type: none"> <li>• Temperature reduction to &lt;90 °C</li> </ul> |
| <b>Technological properties</b>  |  |
| <ul style="list-style-type: none"> <li>• Homogeneous cell structure after expansion</li> <li>• Formation of proper adhesion, in order to produce a sufficient bonding to the boundary layer and foam formation without additional adhesives</li> <li>• Foaming process either triggered by external parameters (temperature, humidity) or influenced chemically/temporally</li> <li>• Formation of a stable foam matrix entirely within the pressing process</li> <li>• At the very least, acceptable emissions during production and use</li> <li>• Fulfillment of the required mechanical and physical properties after the expansion</li> </ul> |  |
| <b>Integration into existing processes</b>   |  |
| <ul style="list-style-type: none"> <li>• Ability to be scattered, similar to the top layer particles</li> <li>• Good miscibility with wood chips to improve the spreading properties</li> </ul>  |  |

Thermoplastic materials such as microsphere (MS) and expanded polystyrene (EPS) were used in the process due to possessing the required characteristics. Within these conditions in the production process, one of the core material properties is the foaming process by the controlling of parameters. The expansion should be sufficient to adhere to surface layers without additional bonding, while still creating the homogeneous foam structure. Though PUR has been used in sandwich panel production's continuous processes, the processes include more steps, such as separation of surface layers, which require the investment of new equipment into an existing production unit. PUR foaming process in the one-step production is challenging due to the chemical reaction of PUR preparation. The high reactivity of isocyanate initiates the polymerization reaction once it comes into mixing with polyol. PUR raw materials should be prepared in a suitable formulation to fulfill those criteria for applying in the one-step process.

The overall objective of this thesis is to improve PUR components as an efficient precursor for the core layer in the one-step panel production. Therefore, this study focuses on both chemical and physical solutions, which are the concepts of blocked isocyanates and wood filler addition, respectively. Blocked isocyanate has shown high industrial applicability, evidenced by a high number of patents related to the literature on the topic (Rolph et al., 2016). However, currently available blocked isocyanates are incapable of producing PUR rigid foam due to the different isocyanate types. In this study, blocked pMDI was synthesized and investigated for the reactivity of polymerization, with a view to creating the 1-C precursor for core layer materials that fulfills the requirements of a one-step process. Apart from this, the effects of the addition of wood and processing temperature need to be investigated.

The thesis outline with different research questions and objectives is divided into three areas of study as follows:

### 3.1 Study I:

#### **Blocked isocyanates for PUR rigid foam**

- **Research question:**  
How to prepare 1-C PUR formulation based on blocked isocyanates for the production of PUR rigid foam by thermal activation
- **Objective:**  
To develop blocked isocyanates which can release an isocyanate group at high temperatures ranging between 90-120 °C, in order to initiate the reaction with polyol and establish PUR rigid foam.

PMDI for the production of PUR rigid foam was used to synthesize blocked adducts with  $\text{NaHSO}_3$  and  $\epsilon$ -caprolactam as blocking agents. Both non-toxic chemicals have differing ranges of deblocking temperatures. Additionally, 4,4'-MDI was selected as another isocyanate type with which to compare the result. The  $\text{CO}_2$  detection test using  $\text{Ba}(\text{OH})_2$  solution was set during the blocking process, to monitor the reaction between isocyanate and water during the blocking process. Because of the high reactivity of free isocyanate, the reaction of isocyanate with other nucleophilic compounds in the system may decrease its content. Thus, adduct samples were investigated for NCO conversion by heating in the DSC to control the precise curing time, temperatures and heating rate and characterized by FTIR spectrometry. Both techniques were employed to mixture samples of blocked adducts and polyol with different NCO/OH ratios. FTIR spectra of the mixture were compared with polyol and PUR to observe new bonds between the isocyanate and polyol within cured samples.

Tab. 6 Overview of Study I

| <b>Synthesis</b>  |                                       |
|---|---------------------------------------|
| <u>Blocked isocyanate and mixture with polyol for PUR curing</u>  |                                       |
| <ul style="list-style-type: none"> <li>• NaHSO<sub>3</sub>-blocked pMDI and 4,4'-MDI</li> <li>• <math>\epsilon</math>-caprolactam-blocked pMDI and 4,4'-MDI</li> <li>• PUR component mix containing blocked isocyanates and polyol</li> </ul> |                                       |
| <b>Investigating parameter</b>  |                                       |
| <ul style="list-style-type: none"> <li>• Mix ratio between blocked isocyanate and polyol</li> <li>• Curing temperature</li> <li>• Curing time</li> <li>• Heating rate</li> </ul>  |                                       |
| Measurement   | Technique/Method                      |
| • Confirmation of blocking process  | ➤ FTIR                                |
| • Characterization of blocked adducts: $T_{\text{deblock}}$   | ➤ DSC, TGA                            |
| • CO <sub>2</sub> detection during blocking process   | ➤ Ba(OH) <sub>2</sub> solution method |
| • NCO conversion  | ➤ DSC, FTIR                           |
| • PUR curing by DSC   | ➤ DSC, FTIR                           |

### 3.2 Study II:

#### Effects of wood addition and temperature on PUR foam

- **Research question:**  
How to apply the wood-mixed PUR formulation for the PUR foam production by thermal curing, whether the difference in temperature and wood contents affects the foam properties
- **Objective:**  
To examine the properties of PUR rigid foam prepared by the addition of wood flour and thermal curing and evaluate the possibilities of using wood-mixed PUR components within the following hot-pressing process.

Wood flour was used as the filler to increase the pressure resistance of the PUR formulation. PUR samples with different filler contents were investigated for the chemical and physical properties of the foam. Additionally, they were prepared at high temperatures to investigate the foaming process in the hot press. The effects from the curing temperature were investigated by comparing the foam properties of samples cured at room temperature with heat-cured samples. The curing temperature was tested between 100 to 160 °C.

Tab. 7 Overview of Study II

| <b>Synthesis</b>   |                  |
|--|------------------|
| <ul style="list-style-type: none"> <li>• Heat-cured PUR rigid foam with wood flour addition</li> </ul> |                  |
| <b>Investigating parameter</b>   |                  |
| <ul style="list-style-type: none"> <li>• Curing temperature</li> <li>• Wood flour content</li> </ul>   |                  |
| Measurement  | Technique/Method |
| • Chemical characteristics   | ➤ FTIR, EDX      |

|                          |                           |
|--------------------------|---------------------------|
| • Cell size              | ➤ SEM, optical microscopy |
| • Open cell              | ➤ ASTM D6226              |
| • Foam densities         | ➤ ASTM D7487              |
| • Compressive properties | ➤ ISO 844                 |

### 3.3 Study III:

#### PUR foaming within the one-step panel production

- **Research question:**  
How to implement the 1-C PUR precursor by chemical (Study I) or physical (Study II) methods into the continuous production of foam-cored panels
- **Objective:**  
To introduce the PUR component mixture developed from the results of prior studies within the core layer of wood-based panels in the one-step production and evaluate the possibilities of concepts within conditions of the hot press.

Sandwich panel one-step production requires a press program that temporarily regulates the distance of hot plates, pressure and temperature during panel formation. Temperature data could help optimize time for plate closing and opening regarding the relationship between internal temperature and foam rise. So it needed to be confirmed first before designing the optimal press program for the prepared PUR formulation in the following tests. The pressing step was determined depending on the distance of pressing plates and varied for different foam formulation. Finished wood-based panels were used as surfacing, as this helps to focus the foaming process in the core layer without any effects from the surface formation. Sandwich panels produced by different press programs were investigated for optical characteristics by microscopy, physical and mechanical properties in the same way as in Study II.

Tab. 8 Overview of Study III

| <b>Synthesis</b>  |   |
|---|---|
| <ul style="list-style-type: none"> <li>• Sandwich panel with PUR foam core</li> </ul>   |   |
| <b>Investigating parameter</b>  |   |
| <ul style="list-style-type: none"> <li>• PUR formulation</li> <li>• Press program</li> </ul>  |   |
| <b>Measurement</b>  | <b>Technique/Method</b>   |
| <u>Temperature data</u>   |   |
| <u>Panel properties</u>   |   |
| <ul style="list-style-type: none"> <li>• Foam morphology</li> <li>• Cell size</li> <li>• Density</li> <li>• Compression</li> <li>• Internal bond</li> <li>• Thermal conductivity</li> </ul> | <ul style="list-style-type: none"> <li>• Thermocouple elements</li> <li>• SEM</li> <li>• Optical microscopy</li> <li>• ISO 844</li> <li>• DIN EN 319</li> </ul> |

# 4 Materials and methods

## Materials

PUR main components were provided by Covestro Company. Selected polyol (Desmophen 1240N) is a sucrose-based polyether polyol of high functionality for the production of rigid polyurethane foam. For isocyanate, pMDI (Desmodur 44P16), di-/poly-isocyanate-component for PUR rigid foam production was used. Blocked isocyanates were prepared from two types of isocyanate, pMDI and 4,4'-MDI. MDI consisting of the mixture from di- and triisocyanate for synthesis, was provided by Merck KGaA company (Darmstadt, Germany). The supplied application information of polyol and isocyanates is presented in Tab. 9.

Tab. 9 Specifications of polyol (Desmophen 1240N) and isocyanates (Desmodur 44P16, 4,4'-MDI)

| Specification      | Unit                   | Desmophen 1240N | Desmodur 44P16 (pMDI) | 4,4'-MDI |
|--------------------|------------------------|-----------------|-----------------------|----------|
| Density at 20 °C   | g·cm <sup>-3</sup>     | 1.16            | 1.238                 | 1.239    |
| Viscosity at 25 °C | mPa·s                  | 6600±600        | 1900                  | 210      |
| Water content      | % by wt.               | max. 0.20       | -                     | -        |
| Hydroxyl number    | mg KOH g <sup>-1</sup> | 445±25          | -                     | -        |
| Acidity (HCl)      | mg·kg <sup>-1</sup>    | -               | 198                   | -        |
| NCO                | %                      | -               | 26.33                 | -        |
| Boiling point      | °C                     | 233             | 255                   | 196      |

Another isocyanate type used in the experiment was blocked TDI (Desmodur BL 1100/1) from Covestro Company. The blocked aromatic polyisocyanate based on TDI is commonly used as a hardener for coating materials for industrial or trade applications with  $\epsilon$ -caprolactam concentration <5 wt.%, free NCO content <0.2 %, blocked NCO ca. 3 %. Two chemicals, NaHSO<sub>3</sub> and  $\epsilon$ -caprolactam, were used as blocking agents. Their properties are shown in Tab. 10.

Tab. 10 Specifications of blocking agents

| Specification    | Unit                | NaHSO <sub>3</sub> | $\epsilon$ -caprolactam |
|------------------|---------------------|--------------------|-------------------------|
| Molecular weight | g·mol <sup>-1</sup> | 104.061            | 113.16                  |
| Density          | g·cm <sup>-3</sup>  | 1.48               | 1.02                    |
| Melting point    | °C                  | 150                | 70                      |
| Boiling point    | °C                  | 315                | 270                     |

The blocking reaction with  $\epsilon$ -caprolactam required a catalyst, namely dibutyltin dilaurate (DBTDL) 95 %, provided by Sigma-Aldrich Chemi GmbH (Taufkirchen, Germany) with formula  $C_{32}H_{64}O_4Sn$ . Furthermore, the following additives were applied in PUR foam production:

- Surfactant is the only chemical additive used for rigid foam preparation. The silicone surfactant for PUR/PIR insulating panels (Dow Corning 2938) was obtained from Dow Chemical Company.
- Wood flour under the trade name Arbocel C100 was supplied by the company J. Rettenmeier & Söhne GmbH and Co. KG. The material comprises raw cellulose with a grain size between 70-150  $\mu m$ . Screen analysis under DIN 734 by the supplier confirms an amount of screen residue with an interior mesh aperture of 250  $\mu m$  with max. 0.5 %, 100  $\mu m$  with max. 45 % and 32  $\mu m$  with max. 95 %.

## Methods

### 4.1 Sample production

#### 4.1.1 Study I: Blocked isocyanates for PUR rigid foam

##### 4.1.1.1 Synthesis of blocked isocyanates

Blocked isocyanates were prepared using two types of blocking agents,  $NaHSO_3$  and  $\epsilon$ -caprolactam. The blocking processes with  $NaHSO_3$  and  $\epsilon$ -caprolactam were methods referred to and described by Lubis et al. (2017) and Lee et al. (2005), respectively. In both blocking processes, the mole ratio between the blocking group and NCO was 1.0. The blocking method and some adjustments from the literature are mentioned in the following steps. After blocking, the dry weight of blocked isocyanate was measured and calculated for the yield percentage of products based on raw materials and kept in the closed container under normal conditions until further characterization.

Tab. 11 Weight ratios of raw chemicals used for preparation of blocked isocyanates

| Component                                  | Blocked with $NaHSO_3$ |          | Blocked with $\epsilon$ -caprolactam |          |
|--|------------------------|----------|--------------------------------------|----------|
|  | pMDI                   | 4,4'-MDI | pMDI                                 | 4,4'-MDI |
| <b>Isocyanate</b>                          | 6.157 g                | 4.829 g  | 3.190 g                              | 2.502 g  |
| <b>Blocking agent</b>                      | 4.041 g (0.0386 mol)   |          | 2.260 g (0.02 mol)                   |          |
| <b>DBTDL</b>                               | none                   |          | 0.1 g                                |          |
| <b>%w/w isocyanate from blocked adduct</b> | 60.37%                 | 54.44%   | 58.53%                               | 52.54%   |

#### 4.1.1.1.1 Blocking by NaHSO<sub>3</sub>

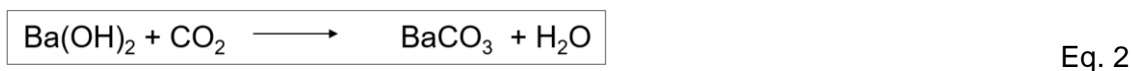
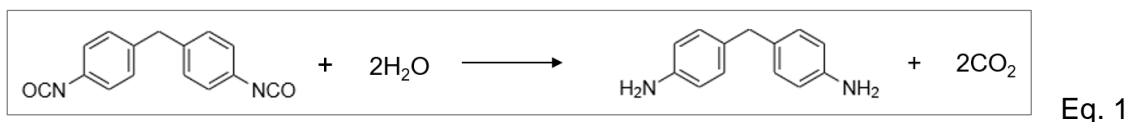
40wt% aqueous solution of NaHSO<sub>3</sub> was prepared. 10.1 g solution containing 4.041 g NaHSO<sub>3</sub> was mixed with the same amount of acetone 10.1 g in a three-neck flask to obtain a 20 wt% aqueous NaHSO<sub>3</sub> solution. The flask was purged with nitrogen to remove air via a neck and connected with a condenser and a dropping funnel through the remaining necks. The solution was mixed by a magnetic stirrer. During the mixing, the isocyanate solution was prepared by mixing 0.0386 mol of isocyanates with acetone to make a 20 ml solution. The solution was poured into the dropping funnel. After mixing the NaHSO<sub>3</sub> solution for ca. 15 min time, the first drop of isocyanate solution was introduced under agitation. The dropping period was controlled for 20 min. The blocking reaction was maintained at a normal temperature for 2 hr. At the end of the reaction, the white precipitate was filtered by polyethersulfone filter type GPWP04700 with a 47 mm diameter using vacuum filtration to obtain a solid powder. During the filtration, the product was washed once with 250 ml acetone, then dried in a vacuum cabinet for at least 18 hr.

#### 4.1.1.1.2 Blocking by $\epsilon$ -caprolactam

The blocking agent solution was prepared by mixing 2.26 g  $\epsilon$ -caprolactam into 80 ml acetone in a 250 ml 3-necked flask. The flask was equipped with a magnetic stirrer, temperature regulator, and condenser and set in an oil bath above the magnetic heat plate, which helped to stir and control the reaction temperature. The temperature of reactants was raised to the reflux temperature of acetone. After the blocking agent had been completely dissolved in the acetone, 0.1 g DBTDL was added to fasten the reaction and the isocyanate was added slowly. Previous to this, isocyanate was dissolved in 20 ml acetone, put into a dropping funnel and set in a flask neck. The solution was then dropped into the flask over 20 min. The oil bath temperature was controlled in a range of 65-75 °C, which is higher than acetone's reflux temperature at 56 °C, since the reflux within the condenser could not be observed before that point. The reaction time starting from the last drop of isocyanate solution was 5 hr. After that, the white precipitate would be expected to appear. The adduct was filtered in the same manner as mentioned in the blocking process with NaHSO<sub>3</sub>. The solid product was dried in an air circulating oven at 60 °C for at least 18 hr.

#### 4.1.1.2 CO<sub>2</sub> detection test during the blocking process

The reaction of isocyanate and water can form amine and CO<sub>2</sub> (Eq. 1). Saturated Ba(OH)<sub>2</sub> solution was prepared and connected via the rubber tube to the flask, where the blocking reaction continued. CO<sub>2</sub> gas can react with Ba(OH)<sub>2</sub> into BaCO<sub>3</sub> forming a white solid, which makes the solution cloudy (Eq. 2).

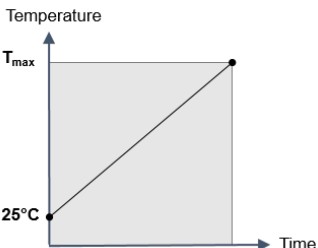
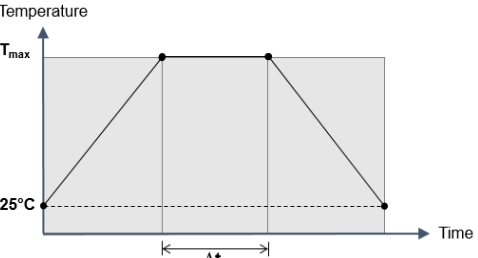


The CO<sub>2</sub> detection test was settled in the blocking reaction of 4,4'-MDI with NaHSO<sub>3</sub>. The blocking reaction of 4,4'-MDI with ε-caprolactam was also inspected for CO<sub>2</sub> as a control group, since their reaction did not use water as a solvent. In the case the appearance of BaCO<sub>3</sub>, the solution would be dried at 105 °C for 24 hr. The dry weight was measured and calculated for the isocyanate ratio that reacted with water during the blocking process.

#### 4.1.1.3 NCO conversion of deblocked isocyanates

In order to measure the NCO conversion during the unblocking, blocked isocyanates were heated by the DSC instrument. ε-caprolactam blocked isocyanates were heated using the following heating programs, to prepare the deblocked samples for investigating the NCO conversion affected by temperatures and time.

**Tab. 12 Heating programs applied on deblocked isocyanates for the measurement of NCO conversion rate**

| Heating program   | $T_{\max}$<br>(°C) | Heating rate<br>(Kmin <sup>-1</sup> ) | Duration at $T_{\max}$<br>(min) |
|---|--------------------|---------------------------------------|---------------------------------|
|  | 200                | 5                                     | -                               |
|   | 225                | 5                                     | -                               |
|   | 250                | 5                                     | -                               |
|  | 200                | 20                                    | 10                              |
|   | 200                | 20                                    | 20                              |
|   | 220                | 20                                    | 10                              |
|   | 220                | 20                                    | 20                              |

#### 4.1.1.4 PUR curing via reaction with polyol

To investigate the PUR reaction of prepared adducts, blocked isocyanates were hand mixed with polyol in different weight proportions in a small glass beaker. Mixture samples were heated using the DSC technique, from 25 °C to curing temperature, with a constant heating rate for the specific period; all tested factors are listed in Tab. 13. Most tests were performed by blocked pMDI, as it is the main isocyanate for PUR foam production. Blocked 4,4'-MDI was therefore tested here as a reference.

Tab. 13 Mixture samples prepared by different factors for PUR curing

| Blocked isocyanate                | Blocked isocyanate per polyol (w/w) | Temperature (°C) | Curing time (min) | Heating rate (Kmin <sup>-1</sup> ) | Weight (g) |
|-----------------------------------|-------------------------------------|------------------|-------------------|------------------------------------|------------|
| <b>NaHSO<sub>3</sub>-pMDI</b>     | 1:1                                 | 150              | -                 | 2                                  | 26.26      |
|                                   | 1:1                                 | 250              | -                 | 5                                  | 13.67      |
|                                   | 2:1                                 | 200              | -                 | 5                                  | 8.67       |
|                                   | 2:1                                 | 200              | -                 | 10                                 | 10.42      |
|                                   | 2:1                                 | 200              | -                 | 20                                 | 10.10      |
|                                   | 2:1                                 | 200              | 15                | 20                                 | 7.99       |
|                                   | 2:1                                 | 200              | 30                | 20                                 | 8.02       |
|                                   | 2:1                                 | 200              | 45                | 20                                 | 10.81      |
|                                   | 2:1                                 | 200              | 60                | 20                                 | 9.74       |
|                                   | 2:1                                 | 250              | -                 | 5                                  | 7.81       |
|                                   | 2:1                                 | 250              | 15                | 20                                 | 10.41      |
|                                   | 2:1                                 | 250              | 30                | 20                                 | 10.10      |
| <b>NaHSO<sub>3</sub>-4,4'-MDI</b> | 3:1*                                | 250              | -                 | 5                                  | 8.90       |
|                                   | 1:1                                 | 150              | -                 | 2                                  | 33.26      |
|                                   | 1:1                                 | 250              | -                 | 5                                  | 12.81      |
|                                   | 2:1                                 | 250              | -                 | 5                                  | 13.80      |
| <b>ε-cap.-pMDI</b>                | 3:1*                                | 250              | -                 | 5                                  | 14.30      |
|                                   | 1:1                                 | 200              | -                 | 5                                  | 7.40       |
|                                   | 1:1                                 | 200              | 30                | 20                                 | 6.30       |
|                                   | 1:1                                 | 225              | -                 | 5                                  | 10.10      |
|                                   | 1:1                                 | 250              | -                 | 5                                  | 6.3        |
|                                   | 1:1                                 | 250              | 15                | 20                                 | 6.9        |
|                                   | 2:1*                                | 200              | 30                | 20                                 | 7.1        |
|                                   | 2:1*                                | 250              | -                 | 5                                  | 5.8        |
|                                   | 3:1*                                | 250              | -                 | 5                                  | 3.2        |
|                                   | 1:2.5                               | 200              | 30                | 20                                 | 7          |
|                                   | 1:2.5                               | 225              | 15                | 20                                 | 8.1        |
|                                   | 1:2.5                               | 250              | -                 | 5                                  | 8.1        |
| <b>ε-cap.-4,4'-MDI</b>            | 2:1*                                | 250              | -                 | 5                                  | 3.2        |

\*prepared by using acetone as solvent for mixing

The proportion of blocked isocyanates and polyol was selected based on weight, which is chemically inaccurate. For the PUR reaction, it was important to notice the ratio between NCO and OH groups that will react with each other for bonding urethane and further linkages. Mostly, there should be a surplus isocyanate content in the component mixture, especially for PUR foam production in that high cross-linking is required. To prepare a mixture with 1 g polyol with NCO index of 1.0, the mass of blocked isocyanate can be calculated by the following formulation:

$$\begin{aligned} & \text{Required isocyanate mass (g)} \\ & = 1 \text{ g polyol} \cdot \frac{\% \text{ OH in polyol}}{\frac{17 \text{ g OH}}{1 \text{ mol OH}}} \cdot \frac{1 \text{ mol NCO}}{1 \text{ mol OH}} \cdot \frac{\frac{42 \text{ g NCO}}{1 \text{ mol NCO}}}{\% \text{ NCO in isocyanate}} \end{aligned} \quad (4)$$

where %OH in polyol of Desmophen 1240N is 13.49 %,  
%NCO in isocyanate of pMDI and 4,4'-MDI is 26.33 %, 33.57 %, respectively.

For mixing with 1 g polyol, it requires 1.265 g neat pMDI or 0.992 g neat 4,4'-MDI.

Regarding isocyanate share in different blocked isocyanates (see Tab. 11),

$$\text{blocked isocyanate mass (g)} = \frac{\text{required isocyanate mass (g)}}{\% \text{ isocyanate in adduct}} \quad (5)$$

required mass of blocked isocyanates will be calculated for

|  |                            |                 |
|--|----------------------------|-----------------|
| <b>NaHSO<sub>3</sub>-blocked pMDI :</b>    | 1.265 g pMDI / 60.37 %     | = <b>2.09 g</b> |
| <b>NaHSO<sub>3</sub>-blocked 4,4'-MDI:</b> | 0.992 g 4,4'-MDI / 54.44 % | = <b>1.82 g</b> |
| <b>ε-capro.-blocked pMDI:</b>              | 1.265 g pMDI / 58.53 %     | = <b>2.16 g</b> |
| <b>ε-capro.-blocked 4,4'-MDI:</b>          | 0.992 g 4,4'-MDI / 52.54 % | = <b>1.89 g</b> |

From this calculation, the optimal ratio between blocked isocyanate and polyol is estimated to be 2:1. For the PUR curing reaction, different ratios of 1:1, 2:1, 3:1 were tested in adducts from NaHSO<sub>3</sub>. An increased proportion of blocked isocyanate from 2:1 to 3:1 caused inhomogeneity in the mixture due to an inadequate amount of polyol in the liquid-state when combined with a solid blocked isocyanate. For this reason, samples with a high ratio of blocked isocyanate were prepared by adding ca. 5-10 ml acetone to aid for blending. Later, samples containing acetone were left within a fume hood under normal conditions for at least 2 hr, until the acetone had evaporated thoroughly before PUR curing in the DSC. Using acetone in a 2:1 mixture of ε-caprolactam-blocked pMDI has the same explanation.

Some of the above-listed samples did not display the curing time. In this case, samples were heated up by a constant heating rate to their specific curing temperatures. Once this point was reached, curing would be terminated. After preparing adducts in the DSC, samples were characterized by FTIR analysis (see 4.3.1.1). FTIR spectrometry of polyol and PUR was also examined for reference with the sample results.

#### 4.1.2 Study II: Effects of wood addition and temperature on PUR foam

In this study, wood-mixed PUR foams cured by heat were investigated for foaming during the process and foam properties. For preparation, Desmophen 1240N was dehydrated by heat before use. Wood flour was oven-dried at 103 °C for 24 hr and moisturized according to the required wood moisture content. In the mixing step, components with OH groups were mixed first. Here, Desmophen 1240N was mixed with water, followed

by the surfactant and wood flour respectively. After that, Desmodur 44P16 was added to the polyol mixture. The components were mixed by an electric hand mixer in aluminum cups; then placed into the oven at 100 °C for 15 min. Reacted foam samples were removed from the oven and left at room temperature for at least 24 hr before conditioning at 20 °C with 50 % relative humidity.

The experiment was conducted in different parts (see Tab. 14). The surfactant ratio was fixed at three parts per hundred parts polyol (pphp). No differences existed in foam preparation among samples, though depending on study objectives, in some parameters. The pretest was designed to observe the foaming reaction and foam properties affected by water adding methods. Absolutely dried wood flour was used in group A (with distilled water) and group C (without water), then water was added in polyol for group A. For group B, moisturized wood flour was prepared by water spraying on absolutely dried wood flour in a closed container and was kept under normal conditions for 24 hr. Wood flour with an equilibrium moisture content was obtained directly from the wood material kept in stock at room temperature, with moisture content values between 8-12 %.

Experiments OVEN1 and OVEN2 determined the optimal wood flour content in PUR components and their influence on foam properties. The hydroxyl group from wood flour was neglected in calculating the NCO index. For water, the hydroxyl number was not included in only the OVEN1 experiment. The NCO index was increased from 1.0 to 1.1 in next experiments for higher chemical bonding via the isocyanate group. PUR rigid foam was prepared at varied curing temperatures to investigate the effect of temperature on the foam characteristics in the OVEN3 experiment. All samples were produced in the same manner as the OVEN2 experiment. The description of variables used in all tests is presented in the following table:

**Tab. 14 Applied parameters in experiments of PUR foam production**

| <b>Experiment Name</b> | <b>Water adding method</b>                                 | <b>NCO index</b> | <b>Water content (pphp*)</b> | <b>Wood flour content (% w/w)</b>                | <b>Temperature (°C)</b>                       |
|------------------------|--|------------------|------------------------------|--|---|
| <b>Pretest</b>         | A. distilled water<br>B. wood moisture<br>C. without water | 1.0              | 5                            | 0, 5, 10, 15, 20<br>per total weight             | 100   |
| <b>OVEN1</b>           | equilibrium wood moisture                                  | 1.0              | not fixed                    | 0, 10, 20, 30, 40<br>per chemicals               | 100   |
| <b>OVEN2</b>           | distilled water  | 1.1              | 3                            | 0, 2, 4, 6, 8, 10, 12<br>per chemicals           | 100   |
| <b>OVEN3</b>           | distilled water  | 1.1              | 3                            | 10<br>per total weight<br>20<br>per total weight | normal, 100,<br>120, 140, 160<br>90, 120, 150 |

\*pphp: parts per hundred parts polyol

### 4.1.3 Study III: PUR foaming within the one-step panel production

#### 4.1.3.1 Design of press program

The one-step continuous process included three steps: plate closing, plate opening, and stabilization. To create the press program, the time required for each step needed to be determined. The test procedure was divided into four parts, as illustrated in Fig. 25.

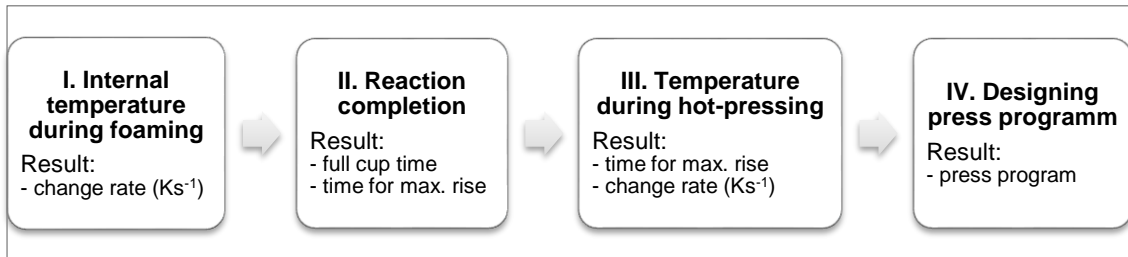


Fig. 25 Procedure for designing press program divided in four steps

First (I), PUR foam samples were prepared using different temperatures in the drying cabinet, in order to observe the temperature changes taking place during foaming. Additionally, the foam rise was recorded by camera to monitor for the reaction completion (II). The end of the reaction means that the foaming process has terminated; shortly after that, pressing plates open. However, the environmental factors in the drying cabinet differ from those in the hot pressing machine. For this reason, the following step (III) was used to consider the internal temperature the PUR mixture developed during hot pressing. A change in PUR temperature may indicate a specific time for plate closing and opening, but creating a press program requires another critical parameter: the distance between hot plates. In the final test (IV), the distance between pressing plates was specified at 100 % and 50 % of the end-opening distance of hot plates. After that, the pressing time and the period from start to end of foaming, was optimized in the press program.

#### 4.1.3.2 Panel production

All components used for preparing wood-mixed PUR and their proportion per total weight are shown in Tab. 15. NCO index of 1.1 was applied here as in the OVEN2 experiment. The same surfactant was used. First, components in the polyol-side (polyol, water and surfactant) were mixed, then dry wood flour and isocyanate were added. After that, they were mixed through by a kitchen machine for at least 30 s until the mixture became homogeneous. The mixture of components was filled into aluminum cups for testing in the drying cabinet. The internal temperature in the foam mass was measured by thermocouple elements, equipped with a temperature data logger Testo 176 T4.

Tab. 15 Formulations of PUR components used for panel production

| Component                    | Content of component (% w/w total) |                         |
|------------------------------|------------------------------------|-------------------------|
|                              | 10 % wood mixture (10W)            | 20 % wood mixture (20W) |
| <b>Polyol</b>                | 29.65                              | 26.36                   |
| Water                        | 3 pphp                             | 3 pphp                  |
| Surfactant                   | 3 pphp                             | 3 pphp                  |
| <b>Isocyanate</b>            | 58.58                              | 52.07                   |
| <b>Oven-dried wood flour</b> | 10                                 | 20                      |

After the same PUR foam preparation method, each part of this section was operated according to the following details:

For part I, the 10W PUR component mixture was filled separately into two sample cups, one for curing at room temperature and another for testing in the drying cabinet at 140 °C. Heat-cured samples were set in the drying cabinet for 15 min. For the reaction in normal conditions, curing time was extended to be at least 2 hr. Temperature changes within PUR mixture in both conditions were recorded along with the reaction.

For part II, two aluminum cups containing PUR mixture with 10 % wood content were set in the drying cabinet at 140 °C. Changes in foam rise height per running time were recorded by a digital camera equipped with a tripod standing outside the drying cabinet. The internal temperature of PUR was measured during the reaction, so that it could be compared against the rate of foam rise. The time from start to maximal foam height was determined for the completed foaming reaction. The change in the internal temperature of the mixture and foaming rate were measured.

For part III, the PUR component mixture was spread between MDF layers, framed by PIR foam to protect foam loss during the reaction. The specifications of all materials used in sandwich panel production are shown as follows:

- Surface layer: 245x245x2 mm<sup>3</sup> MDF sheets from Finsa, 650-670 kgm<sup>-3</sup> density
- Middle layer: 10W mixture with different input weight of 83, 100, 125 g
- Pressing frame: PIR rigid foam for application at high temperature (-80 to 200 °C) with a density of 37-40 kgm<sup>-3</sup> provided by F.Willich Isoliersystem GmbH & Co.KG

To measure PUR temperature during hot-pressing, thermocouple elements were plugged into the foam mass between MDF layers (see Fig. 26). After that, the combined layers were placed into a computer-controlled lab-scale single opening hot press (Siempelkamp, Germany) to form a panel. Different press temperatures were set for 140 and 160 °C. In this test, the plate-opening distance was controlled to be constant at 20 mm along with the production without the pressing phase (Fig. 27), where both hot plates were moved closer to increase the pressure within the composite layers. The

temperature data from this test was required to create the press program with a pressing phase in the next step.



**Fig. 26 (from left to right) Component mixture, scattering on the surface layers, compaction of surface layers, a finished panel with frame**

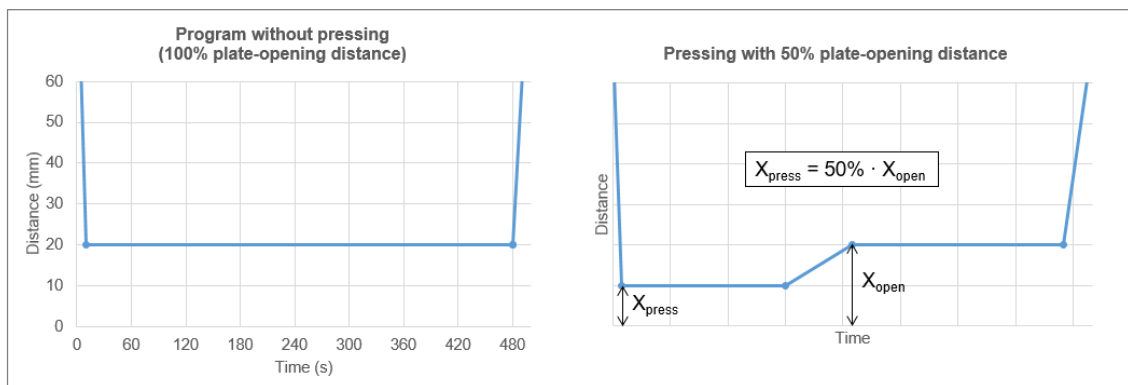


**Fig. 27 Press programs, (left) without pressing and (right) with 50% plate-opening distance**

For part IV, temperature data from the last program (100 % plate-opening distance) was analyzed for maximal pressing time, which was defined from the time when the internal temperature of PUR became constant. The duration was set for pressing in a new press program with a 50 % plate-opening distance (Fig. 28). During the new production, the PUR mixture's temperature was measured again for its change because of higher heat transferred from closer distance to the hot plate. Press programs with varied pressing times were created using 10W and 20W components as material for the middle layer with the pressing temperature of 140 °C. After that, panels produced by different programs were evaluated for their physical and mechanical properties and foam characteristics.

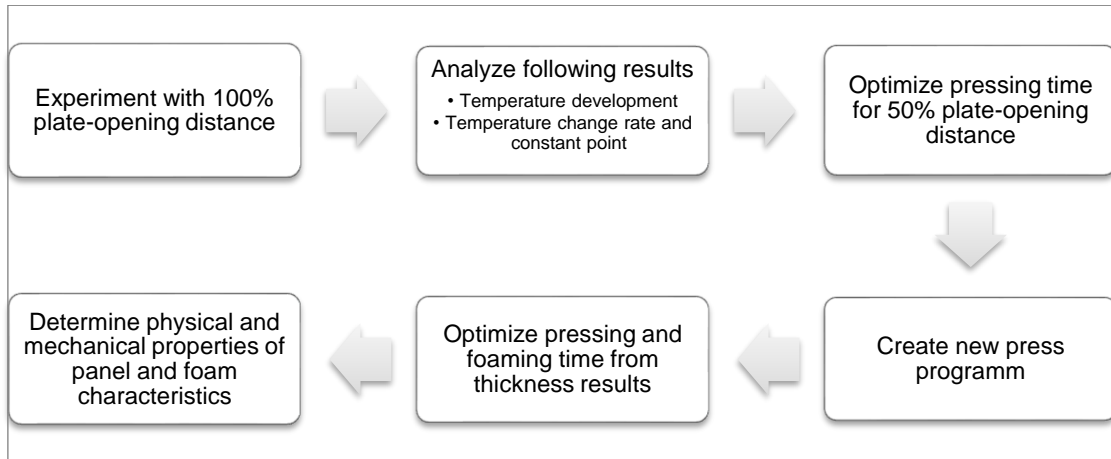


Fig. 28 Procedure for the development of press program

## 4.2 Sample preparation

### 4.2.1 PUR from cup testing

After the conditioning, PUR foam in an aluminum cup was prepared by the pillar drill to obtain a sample in cylinder form. It was then cut into samples, the largest having a height of 25 mm, which was used for the compression test. Another sample was cut into six cubes for the determination of open-cell content. The remainder of the foam was sliced into thin layers for microscopic analysis. Fig. 29 shows the steps of sample preparation as described.

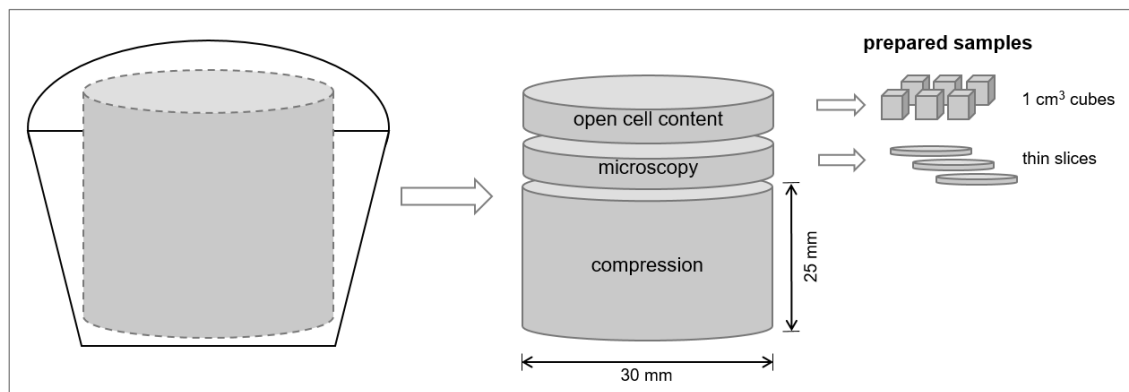


Fig. 29 Preparation steps of PUR samples for property testing

### 4.2.2 Panel sample

The following panels were produced based on 10 and 20 % wood-mixed PUR foam core (10W, 20W) with various press programs. A press program without pressing (100X) and with 50 % plate-opening distance (50X) was applied. In the 50% plate-opening distance, the duration of the plate closing was varied in second test which appears here in the last position of the sample name.

- 10W 100X
- 10W 50X180
- 10W 50X90
- 10W 50X60
- 20W 100X
- 20W 50X90
- 20W 50X70

The sample name represents wood ratio, plate-opening distance and pressing time (time from the beginning to plate-opening); for this reason, pressing time is not shown for 100 % plate-opening distance. Each panel board had an area of 245x245 mm<sup>2</sup> with different thicknesses. Test specimens were prepared according to the cutting scheme (Fig. 30) by a cutting saw. They had been conditioned at 20 °C and 65 % relative humidity for at least 6 hours before any property determination. The thickness of test specimens was measured using an electronic digital caliper.

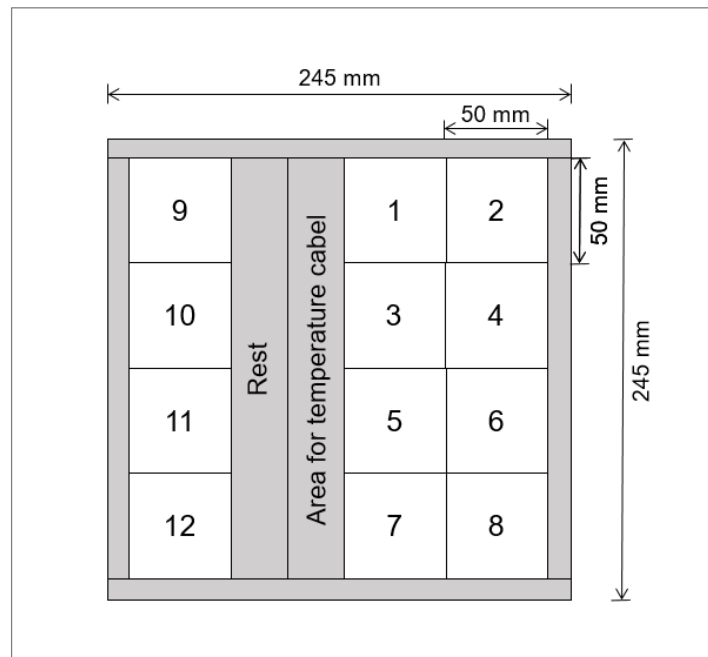


**Fig. 30 Sample cutting profile for panel characterization**

Since the density profile and thermal conductivity examination was non-destructive, both tests were executed before the mechanical tests. Three samples (no. 1, 5, 8) were used for the compression test. Five samples randomly selected from each panel were used for testing the internal bond. Two samples were selected for microscopic analyses, each for determining cell size and the foam expansion in the core layer, aiming to observe the foam structure, which would expand during the hot-pressing process. Since some panels were not thick enough, the examination of open-pore content was not executed in Study III.

### 4.3 Sample characterization

#### 4.3.1 Chemical characterization

The FTIR technique was used to characterize unblocked, blocked and deblocked isocyanates, including the mix of isocyanate and polyol. The deblocking temperature of isocyanates was examined by the DSC technique. The instrument was used to prepare samples of deblocked isocyanates and cured mixtures of blocked isocyanate and polyol. Furthermore, PUR foam produced according to Study II was analyzed for its characteristic IR spectra as reference.

##### 4.3.1.1 FTIR spectroscopy

Blocked isocyanates were characterized by FTIR spectroscopy to confirm the blocking reaction. A FTIR spectrophotometer Bruker Vector 33 (Mettler-Toledo GmbH) was used in conjunction with ATR sampling technology, based on 2 cm<sup>-1</sup> resolutions with the spectrum range between 600-3800 cm<sup>-1</sup>. The provided software, Opus 6.5, was available to measure and evaluate the results. The NCO group strongly absorbs between 2250-2270 cm<sup>-1</sup> (Delebecq et al., 2012), which is the region of cumulated double bond strength (Silverstein & Bassler, 1962). The disappearance of this band indicates the completion of the blocking reaction and therefore can characterize the adducts between isocyanates and blocking agents. Unblocked, blocked and deblocked isocyanates were characterized for their IR spectra in every stage, specifically the existence of an isocyanate group.

Typically, the variations of absorbance are normalized to the C-H stretching at 2946 cm<sup>-1</sup>, in order to compensate for the changes in thickness during the course of the reaction. Tang et al. (2013) defined lower absorbance at 2929, 2934 cm<sup>-1</sup> as an inner standard band in their work. Related to the reference absorbance, the isocyanate conversion is then calculated as follows (Delebecq et al., 2012),

$$\text{Isocyanate conversion } \alpha = 1 - \frac{(A_{NCO}/A_{ref})_t}{(A_{NCO}/A_{ref})_{t=0}} \quad (6)$$

Isocyanate conversion of  $\epsilon$ -caprolactam-blocked isocyanates was calculated using the previous equation. However, NaHSO<sub>3</sub>-blocked isocyanates did not show the clear absorbance for C-H stretching at 2946 cm<sup>-1</sup>. Instead, the reference absorbance was selected at ca. 1700 cm<sup>-1</sup> representing C=O band frequencies. This frequency can be shifted to lower vibration frequencies depending on hydrogen bonding.

Additionally to this, the remaining PUR foam from the sample preparation (4.2.1) was characterized. Foam material was ground before the analysis. Neat PUR and wood-mixed samples were realized for the difference in structural characterization by the FTIR-ATR technique, as mentioned earlier. The resulting absorbance was compared to the results described in the literature. The identical absorption bands of isocyanate and polyol segments can be found in Appendix I.

#### 4.3.1.2 DSC analysis

The DSC technique measures heat flow within the sample of blocked isocyanates. The initial deblocking temperature was defined as the temperature where sudden heat flow increases. The deblocking process leads to a significant change in energy within the endothermic transition, which is measured as the deblocking temperature. Modulated DSC instrument model Mitterer Toledo DSC 3+ Star System was used for the characterization under  $10 \text{ mLmin}^{-1} \text{ N}_2$  gas flow rate. Approximately 3-5 mg weight of the sample was inserted in a sealed pan with a hole to prevent the blocking molecule evaporation from blowing up the cell. The measuring temperature and heating rate were adjusted to types of blocked isocyanates.

Commercial blocked TDI (Desmodur BL 1100/1) was investigated for a deblocking reaction, to compare the isocyanate conversion with the prepared blocked isocyanates in this research. The measuring temperature was set from 25-250 °C with a constant heating rate of  $5 \text{ Kmin}^{-1}$ . For  $\text{NaHSO}_3$ -blocked isocyanates, the same measuring temperature range was applied with a constant heating rate of  $2 \text{ Kmin}^{-1}$ . To prove the back-reaction between isocyanates and blocking agents, the measuring temperature was reduced to 25 °C after heating to 150 °C, for reheating with a constant rate of  $\pm 4 \text{ Kmin}^{-1}$ .

For  $\epsilon$ -caprolactam-blocked isocyanates, the measuring temperature was increased from 25 °C to a higher point of 300 °C with a constant heating rate of  $3 \text{ Kmin}^{-1}$ . The maximal measuring temperature was set higher than that in the former test, as  $\epsilon$ -caprolactam-blocked isocyanates generally have higher deblocking temperatures than  $\text{NaHSO}_3$ -blocked isocyanates.

#### 4.3.1.3 TGA

TGA was performed with a TGA analyzer (Model STA 409 C/CD, Netzsch-Gerätebau GmbH, Germany) using the differential thermal analysis (DTA)/TGA measurement mode. In the analysis, ca. 20 mg of sample in  $\text{Al}_2\text{O}_3$  crucible was heated from 20-600 °C with a  $5 \text{ Kmin}^{-1}$  heating rate under  $50 \text{ mLmin}^{-1} \text{ N}_2$  gas flow rate.

### 4.3.2 Physical characterization

#### 4.3.2.1 Density and density profile

In the foam cup test, foam density was determined using two definitions of density: free rise density (FRD) and apparent density. FRD of the foam is an important parameter since it determines the expansion capability of the foam and hence the final overall density in the cabinet or door (Randall & Lee, 2002). FRD is the density in  $\text{kgm}^{-3}$  of PUR foam prepared in an open cup, determined from the remaining foam in the cup (ASTM D7487).

$$\text{Free Rise Density (kgm}^{-3}\text{)} = W_{\text{foam}}/V_{\text{cup}} \quad (7)$$

Where  $W_{\text{foam}}$ : weight in grams of the remaining foam in the cup  
 $V_{\text{cup}}$ : the volume of the cup

Apparent density can be categorized into two definitions, according to ASTM D1622. Apparent core density is the weight in the air per unit volume of a sample after forming skins have been removed. In contrast, apparent overall density is the same measurement, including all forming skins. In this study, foam density was defined from the sample density, which was prepared for the compression test. The volume was calculated from the cut cylinder foam. Therefore, when apparent density is mentioned in this study for foam, it shall be interpreted as being a core density.

The determination of density profile was performed using the laboratory density profile measuring system DENSE-LAB X from the company Electric Wood Systems (EWS). The instrument determines the density distribution over the sample thickness (perpendicular to the panel surface). The measurement is non-destructive and non-contact, using X-ray technology. Five samples with an area of  $50 \times 50 \text{ mm}^2$  were randomly selected from a panel board for the testing. Results from the density profile were calculated for average and deviation of foam density.

#### 4.3.2.2 Microscopic and elemental analysis

A scanning electron microscope SEM-LEO1505 (Zeiss) was used to obtain micrographs of the features of the foam structure and cell density. Foam specimens in thin slices were cut into small rectangular samples and glued on stubs, which helped to position the sample during the analysis. The specimen surface was coated with platinum before the analysis. An InLens-detector was applied with an acceleration voltage of 5.0 kV. SEM shots provided positions for element analysis by way of the EDX (Energy-dispersive spectroscopy) technique using an octane plus silicon drift detector (Octane plus SDD).

Optical microscope Keyence VHX5000 was used to observe the visual morphology of the foam cut surface and to determine cell diameter. The foam from Study II was cut into as thin a sample as possible, taking care that it did not take apart. Samples from the sandwich panel in Study III were prepared by removing the surface layers before slicing into a thin specimen. The cut specimen was inserted onto a microscope desk and examined using the following parameters: 250X magnification, light entry at 100 % with ring illumination, 4-6 mm<sup>2</sup> observed area. 2D-panorama images were created from 3D capture in all positions, then processed using the provided software.

Furthermore, the sandwich panel was observed for the PUR foam expansion. To examine this, foam specimens were cross-cut diagonally to the layer alignment into small rectangular samples. The specimen surface was coated with gold and then glued on stubs; in this manner the PUR layer could be investigated from the side. The scanning electron microscope Quanta FEG Type 250, Serial number D9122 (FEI Germany) was used, with an acceleration voltage of 7.0 kV.

#### 4.3.2.3 Cell size measurement

Cell diameter was measured manually on the program from Keyence. For each photo, the largest cells were selected. Two values were detected from each cell. Most cells were polyhedral. Therefore, the longest and shortest cell sides were measured and calculated for the average diameter. In the end, the measurement was executed in at least 50 cells.

To determine the cell density, SEM photos within the specified area were used; foam cell numbers were also measured. Cell density is the cell number that appears in a specified volume. The foam cell density can be calculated according to the formula proposed by Karlsson and TomasÅström (1997) (Choupani Chaydarreh et al., 2017):

$$D_{cell} = (N \times M^2 / A)^{3/2} \quad (8)$$

where  $D_{cell}$  : foam cell density (cells cm<sup>-3</sup>),  
 $N$  : cell number in the defined area,  
 $M$  : microscope magnification,  
 $A$  : measured area.

#### 4.3.2.4 Open-cell content

The measurement of open-cell content was conducted following ASTM D6226. This method considers only open cells, defined by a cell not enclosed by its walls and open to the surface either directly or by interconnecting with other cells according to ASTM D883. In contrast, closed cells and cell walls include inaccessible internal volume, consisting of an aggregate of solid polymer volume (cell walls, struts), filler volume, the

volume of individual closed cells and the volume of small cell groups interconnected by ruptured cell walls but otherwise inaccessible.

According to ASTM D6226, this test method is based on a determination of porosity. The accessible cellular volume of a cellular plastic is determined by the application of Boyle's Law, which states that the increase in the volume of confined gas results in a proportionate decrease in pressure. The apparatus consists of two chambers of known volume connected by a valve. One of the chambers, the calibrated sample chamber, is accessible for the insertion of the test specimen and is connected to a source of high purity dry gas, such as nitrogen or helium. The pressure in the sample chamber is increased to a predetermined pressure and this value,  $P_1$ , is noted. The valve between the two chambers is then opened and the second, lower pressure,  $P_2$ , is again noted. The ratio of the pressure change  $P_1/P_2$  is directly related to the volume of the sample chamber displaced by the specimen. The difference between this volume and the geometric volume of the specimen is a measure of the open-cell volume.

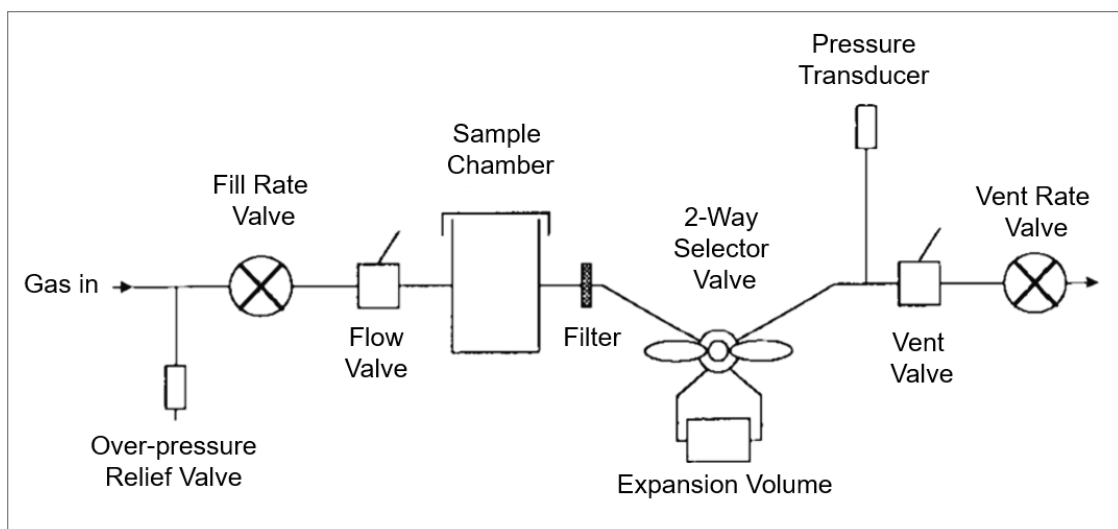


**Fig. 31 Schematic diagram of gas pycnometer (ASTM D6226)**

The test specimen consisted of two cubes, each having a dimension of  $1 \times 1 \times 1 \text{ cm}^3$ , which differed from the nominal dimension of  $2.5 \times 2.5 \times 2.5 \text{ cm}^3$  since this using specimen dimension could fit into the sample chamber of 10 ml accurately. Specimens were conditioned at the standard laboratory temperature of  $23 \text{ }^\circ\text{C}$  and 50 % relative humidity, for a minimum of 24 hr as in the previous test. At least three sets of two specimens were tested for each variation.

Open-cell content was measured using an Accupyc II 1340 gas displacement pycnometry system. The machine determines density and volume by measuring the pressure change of helium within calibrated volumes. Installed software FoamPyc was

applied to analyze the PUR foam samples. The software provides different testing modes; method B was selected for the measurement. This method corrects the cut cells by using two separate measurements. For the second measurement, each cube is recut into eight smaller pieces (trisecting) to double the cut surface. The observed difference in the cut open cell volume is applied as a correction to the initial measured volume. Purge and cycle fill pressure of 2.9 psig or 0.2 bar was used and the end equilibrium time was set to 15 s.

#### 4.3.2.5 Thermal conductivity and resistance

Thermal conductivity ( $\lambda$ ) and thermal transfer resistance ( $R$ ) of PUR foam-core panel were measured using the thermal conductivity test tool  $\lambda$ -Meter EP500, produced by Lambda-Messtechnik GmbH, Dresden, Germany. Tests are possible following ISO 8302, EN 12667, ASTM C177 (DIN 52612). The guarded hot plate apparatus measures the thickness ( $d$ ) of the inserted sample, the temperature difference ( $\Delta T$ ) over the sample and the heat flux ( $Q$ ) which is equivalent to the electrical power of the measuring heating ( $P = U \cdot I$ ). The thermal conductivity is determined based on a defined measurement area ( $A$ ) and the one-dimensional thermal conduction as follows:

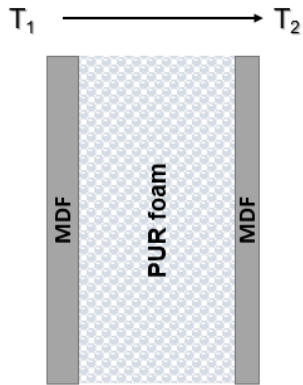
$$\lambda = \frac{Q \cdot d}{A \cdot \Delta T} = \frac{U \cdot I \cdot d}{A \cdot \Delta T} \quad (9)$$

where  $R$  is inversely proportional to  $\lambda$  and calculated by

$$R = \frac{A \cdot \Delta T}{Q} = \frac{d}{\lambda} \quad (10)$$

Nine cut samples of 50x50 mm<sup>2</sup> were aligned in a quadratic of 3x3 on the measuring circle area, embedded by the PIR foam frame, which expanded the testing area to 500x500 mm<sup>2</sup> and protected it from the external heat transfer. The test pressure of 250 Nm<sup>-2</sup> was applied. The temperature difference between measuring plates was set for 10 K with a coefficient time of 60 min.

The thermal conductivity ( $\lambda_{tot}$ ) and resistance of composite panels ( $R_{tot}$ ) were measured by the instrument. The thermal conductivity of PUR foam layer ( $\lambda_{PUR}$ ) was calculated from  $R_{tot}$  and the thickness of PUR layer ( $d_{PUR}$ ) based on the known resistance of applied MDF sheet ( $R_{MDF} = 0.0225 \text{ m}^2\text{KW}^{-1}$ ).



$$R_{tot} = R_{MDF} + R_{PUR} + R_{MDF} \quad (11)$$

$$R_{tot} = 2 \cdot R_{MDF} + R_{PUR} , \quad (12)$$

$$\text{where } R_{PUR} = \frac{d_{PUR}}{\lambda_{PUR}}$$

$$R_{tot} = 2 \cdot R_{MDF} + \frac{d_{PUR}}{\lambda_{PUR}} \quad (13)$$

$$\rightarrow \lambda_{PUR} = \frac{d_{PUR}}{R_{tot} - 2 \cdot R_{MDF}} \quad (14)$$

### 4.3.3 Mechanical characterization

#### 4.3.3.1 Compression properties

The compressive properties were determined according to ISO 844. For Study II, cylinder specimens from cup testing with a smaller size than specified in the standard were used. From Study III, specimens no. 1, 5, 8, as shown in the cutting profile, were used. After the specimens had been prepared, they were conditioned at 20 °C with 50 % relative humidity until testing. Samples were measured for their weight and dimension directly before the test. The measurement was performed by the universal testing machine Zwick Roell RetroLine including software for data acquisition. The testing speed of the machine was set to 10 % per min with a maximal loading force of 0.5 or 5 kN, depending on the sample properties. They were set into the compression testing machines and tested in the manner in which compression is carried out parallel to the foam rise direction or perpendicular to the plane of layer alignment in the case of sandwich samples.

#### 4.3.3.2 Internal bond

For the determination of internal bonding, five faultless specimens of 50x50 mm<sup>2</sup> were selected. The internal bond property was determined, according to DIN EN 319. Specimens were attached to hardwood-plywood jokes on both surfaces before testing. To prepare this, the surfaces of both samples and wood jokes needed to be sanded, after which they were set at 150 °C in a drying cabinet for 2 hr and 15 min respectively before gluing, respectively. This method helped prolong the hot-melt adhesive's hardening time, which can be distributed more regularly on interconnected surfaces. Samples glued with testing jokes on both sides were then conditioned at 65 % and 20 °C. After a minimal 24 hr of conditioning, the internal bond testing was performed using the universal testing machine Zwick Roell RetroLine. The testing speed of the machine was set for 0.5 mmmin<sup>-1</sup> with a maximal loading of 500 N.

#### **4.4 Data analysis**

Design-Expert software was used to evaluate the foaming reaction from different water adding methods. To compare the two sample groups as in between the densities of PUR produced by wood moisture vs. distilled water and FRD vs. sample density, a two samples F-test was first performed to prove the variances of the two independent populations. After that, a two-sample t-test for measuring the difference of means was applied. A one-way analysis of variance (ANOVA) was performed in the remainder of the results that contained more than two sample groups. Statistical differences between variations were evaluated by multiple comparisons based on the least significant difference (LSD) test (Fischer's LSD test statistic). The statistical significance was set to  $P < 0.05$ . All the data analysis was executed using the Microsoft Excel program.

# 5 Results and discussion

## 5.1 Study I: Blocked isocyanates for PUR rigid foam

### 5.1.1 Characterization of blocked isocyanates

#### 5.1.1.1 Commercial blocked isocyanate

Since the deblocking range of blocked TDI (Desmodur BL 1100/1) was unmentioned in the company datasheet, DSC was investigated, as shown in Fig. 32. The chemical contains 3 % of blocked isocyanate from the provided data and requires 10 min at the maximal curing temperature of 180 °C. However, the DSC curve did not reveal the endotherm transition that indicated the deblocking reaction. FTIR spectra of blocked TDI before and after heating in the DSC are shown in Fig. 33 in blue and red spectra, respectively. The characteristic absorption of NCO appeared around 2274  $\text{cm}^{-1}$  after heating. Although the absorption was low compared to other existing bands, the isocyanate group's release could be confirmed. The heating temperature in DSC at 250 °C was much higher than the curing temperature represented in the company data. The low percentage of containing blocked isocyanate in the product and high heating temperature in DSC could be reasons for this low absorbance after deblocking.

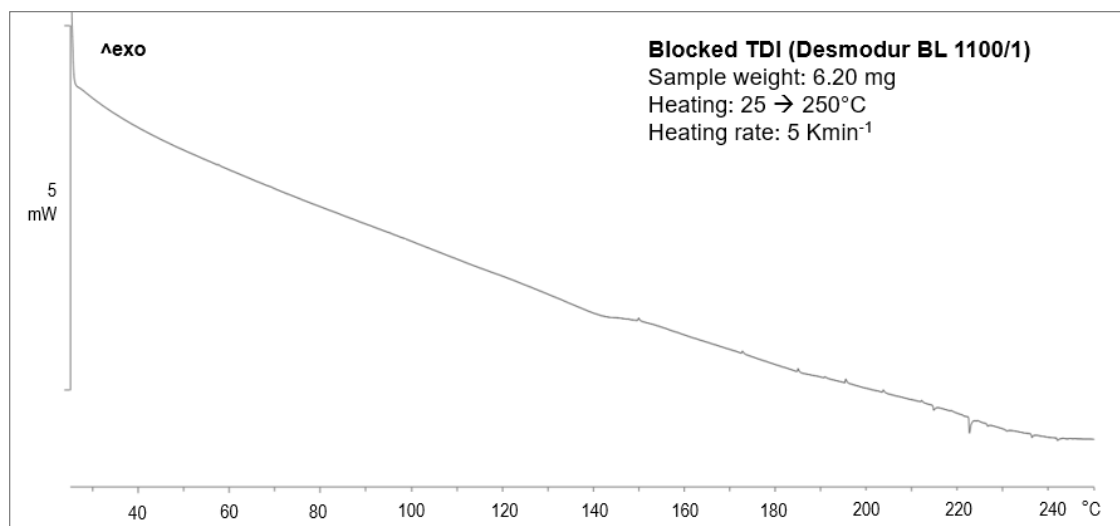


Fig. 32 DSC curve of commercial blocked TDI

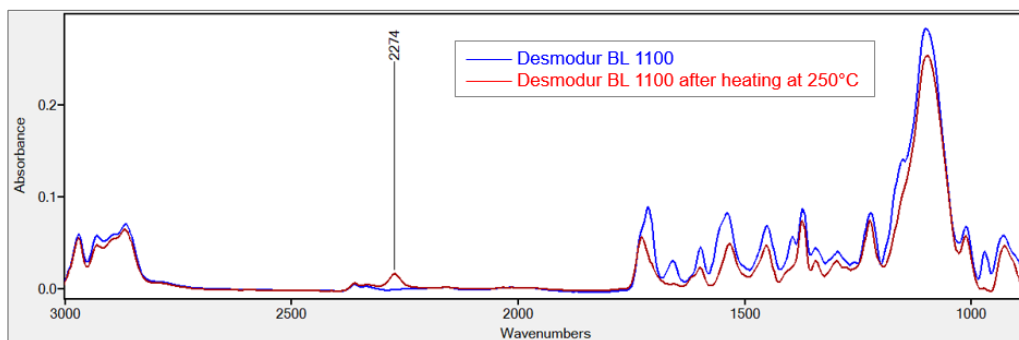


Fig. 33 FTIR spectra of commercial blocked TDI before and after heating up to 250 °C by DSC

### 5.1.1.2 Blocked isocyanates by NaHSO<sub>3</sub>

Yield percentage of blocked isocyanates was calculated as follows,

$$\% \text{ yield} = \frac{\text{mass of dried adduct}}{\text{mass of isocyanate and blocking agents before reaction}} \cdot 100 \% \quad (15)$$

- For NaHSO<sub>3</sub>-blocked pMDI, it was calculated for **107.23 %** by 10.97 g adduct after drying / [6.19 g pMDI + 4.04 g NaHSO<sub>3</sub>]
- For NaHSO<sub>3</sub>-blocked 4,4'-MDI, it was calculated for **98.53 %** by 8.74 g adduct after drying / [4.83 g MDI + 4.04 g NaHSO<sub>3</sub>]

NaHSO<sub>3</sub>-blocked pMDI had a higher yield mass related to the used reactants, whereas the adduct of 4,4'-MDI had a great yield ratio of almost 100 %, which was supposedly caused by the existence of water during the blocking process. Water was required to dissolve bisulfite and act as a co-solvent; however, the reaction between water and isocyanate may lead to undesirable side reactions. Despite using acetone as another co-solvent, water was able to partly react with the isocyanate. This hypothesis was proven by testing for CO<sub>2</sub>, as it is a product of the reaction between water and isocyanate. The results can be found in 5.1.2.

NCO bands were observed at 2250 and 2265 cm<sup>-1</sup> in neat pMDI and 4,4'-MDI, as revealed in Fig. 34 and 35, respectively. After blocking with NaHSO<sub>3</sub>, NCO bands in both types of isocyanate disappeared. The absence of this band indicated the completion of the reaction. An absorption band between 1770 and 1700 cm<sup>-1</sup> in the pure isocyanate spectrum, was assigned to the C=O group. The C=O bond frequencies can be shifted to lower vibration frequencies depending on the hydrogen bonding (Delebecq et al., 2012). It may describe the presence of an absorption band at 1678 cm<sup>-1</sup> in blocked pMDI, which refers to C=O stretching of urethane and carboxylic groups. Strong absorption bands between 3401 and 3195 cm<sup>-1</sup> (N-H stretching), 1700 cm<sup>-1</sup> (-C=O stretching of urethane and carboxylic groups), 1521 cm<sup>-1</sup> (N-H bending) confirmed the formation of urethane, which was not the urea that formed by the reaction of isocyanate with water (Zhang et

al., 2011). FTIR results suggested that all the NCO groups had reacted with the bisulfite group of NaHSO<sub>3</sub>.

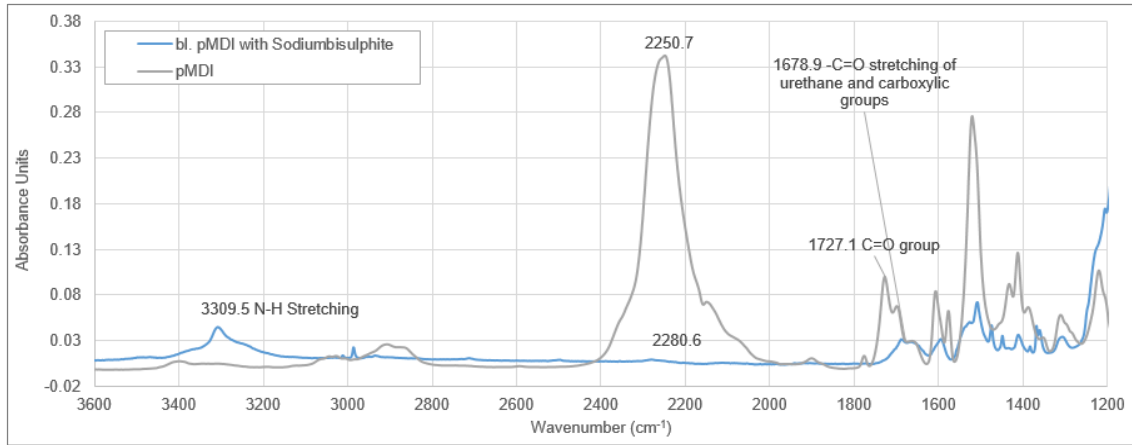


Fig. 34 FTIR spectra of pure pMDI (grey line) and NaHSO<sub>3</sub>-blocked adduct (blue line)

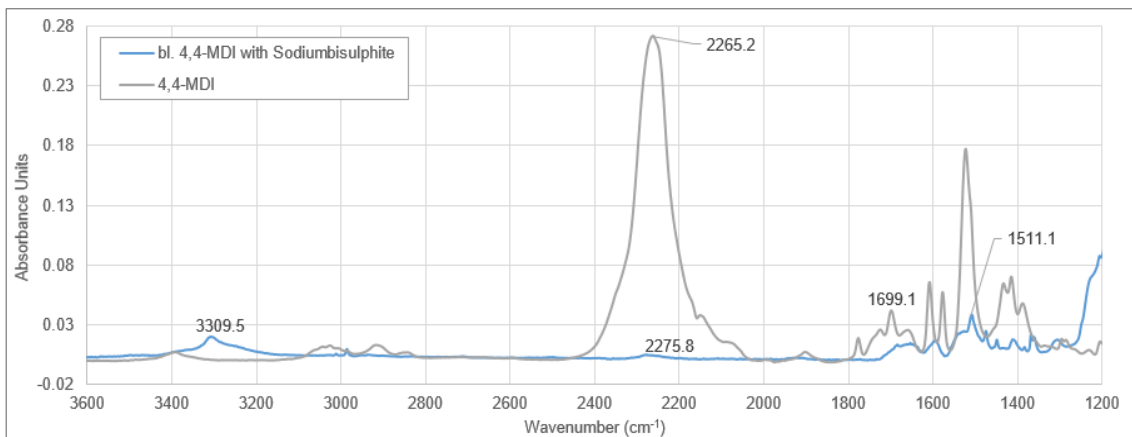


Fig. 35 FTIR spectra of pure 4,4'-MDI (grey line) and NaHSO<sub>3</sub>-blocked adduct (blue line)

The isocyanate conversion ( $\alpha$ ) was calculated from the absorbance change of the isocyanate group related to carboxyl groups, as shown in Tab. 16. The isocyanate conversion can specify the blocking rate of isocyanate, which was found to be 91 and 95 % in pMDI and 4,4'-MDI, respectively. Approximate blocking rates of 91.8 and 96.8 % were mentioned earlier (Lubis et al., 2017; Zhang et al., 2011), though without a description of the applied method.

Tab. 16 Absorbance of C=O and NCO frequencies in pure and NaHSO<sub>3</sub>-blocked isocyanates

| Isocyanates             | Absorbance at wavenumbers   |                                      | $A_{NCO}/A_{ref}$                 |
|-------------------------|---|--------------------------------------|-----------------------------------|
|                         | C=O<br>at 1770-1700 cm <sup>-1</sup> in -NCO<br>at 1710-1640 cm <sup>-1</sup> in -NH-(C=O)- | NCO<br>at 2250-2270 cm <sup>-1</sup> |                                   |
| <b>PMDI</b>             | 0.0994  | 0.3418                               | 3.44                              |
| <b>Blocked pMDI</b>     | 0.0315  | 0.0093                               | 0.30                              |
|                         |   |                                      | <b><math>\alpha = 0.91</math></b> |
| <b>4,4'-MDI</b>         | 0.0420  | 0.2719                               | 6.47                              |
| <b>Blocked 4,4'-MDI</b> | 0.0148  | 0.0049                               | 0.33                              |
|                         |   |                                      | <b><math>\alpha = 0.95</math></b> |

DSC and TGA techniques were used to investigate the deblocking reaction of blocked isocyanates. The DSC results are shown in Fig. 36 and 37. In both isocyanate types, an endothermic signal at ca. 118 °C existed. The broad endothermic transition, starting from around 90 °C, corresponds to the slow deblocking rate of blocked isocyanates. Blocked isocyanates in this research have common results when compared to the study by Zhang et al. (2011), where the onset temperature of the same adduct was 95.6 °C to the signal at 109.5 °C. An absolute comparison between deblocking temperatures from different studies should be done carefully, since factors such as preparation methods and analytical techniques impact the adduct and its deblocking temperature. Furthermore, the deblocking temperature increased with the ratio between  $\text{HSO}_3$ -/NCO mole. The deblocking temperatures between 78.3 to 82.4 °C were discovered by Lubis et al. (2017) on an increased proportion of a  $\text{HSO}_3$ -/NCO mole from 0.9 to 1.8.

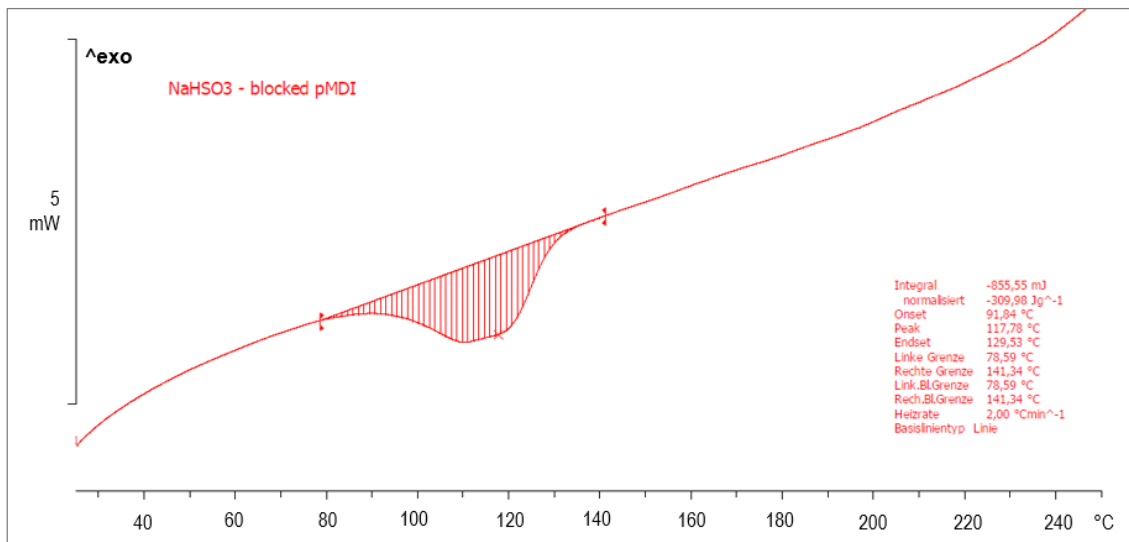


Fig. 36 DSC curve of NaHSO<sub>3</sub>-blocked pMDI

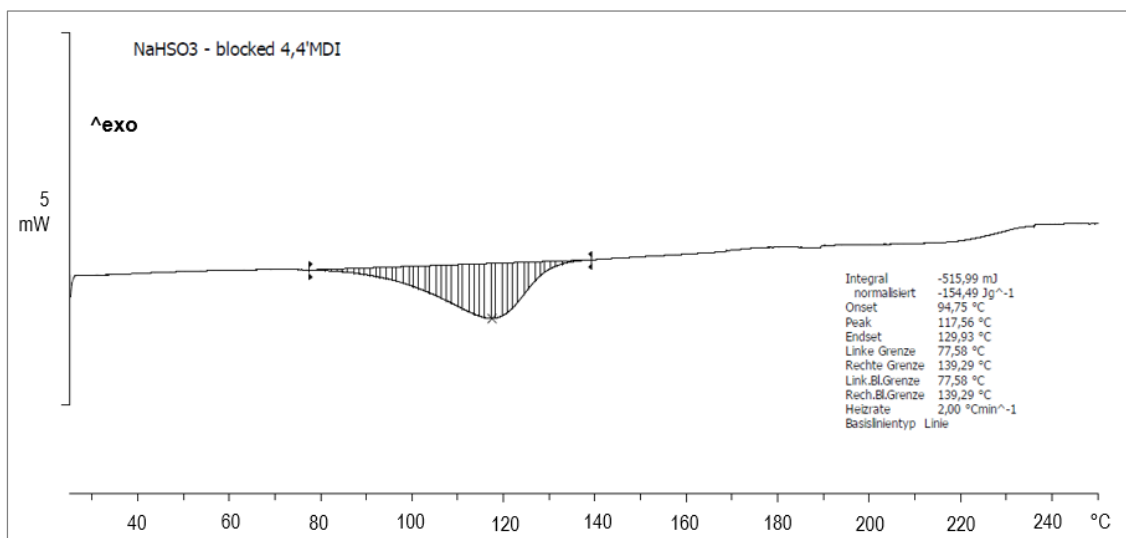
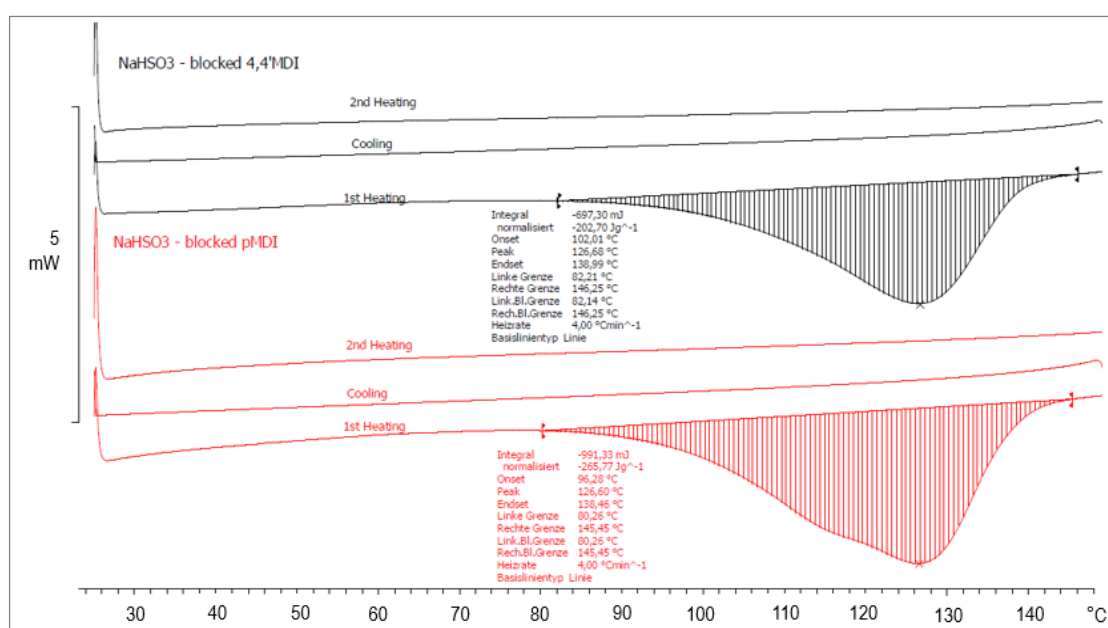


Fig. 37 DSC curve of NaHSO<sub>3</sub>-blocked 4,4'-MDI

NaHSO<sub>3</sub>-blocked isocyanates were proven for the re-blocking reaction after deblocking by DSC. Fig. 38 represents DSC curves from heating, cooling-down and reheating phase of both isocyanates. The reversal points are observed at 126-127 °C within the endotherm, higher than the last results in Fig 36 and 37. The measuring sensitivity probably became lower at a higher heating rate. It can shift an endotherm to the higher range during the rising temperature since the heating rate of 4 Kmin<sup>-1</sup> is applied here instead of 2 Kmin<sup>-1</sup> in the last experiment, due to the measurement's shorter duration. Since the endothermic transition could not be found in the decline of the temperature from 150 to 0 °C, it is assumed that there was no re-blocking reaction between free isocyanates and NaHSO<sub>3</sub>.



**Fig. 38 DSC curve of NaHSO<sub>3</sub>-blocked pMDI (red line) and 4,4'-MDI (black line) in the range of 0-150 °C with cooling-down and reheating phases, measured by heating rate of 4 Kmin<sup>-1</sup>**

Fig. 39 and 40 show TGA plots of blocked isocyanate adducts of pMDI and 4,4'-MDI, respectively. The deblocking temperature was observed by the reduction rate of DTG, which appeared in blocked adduct of pMDI from 58-162 °C and 4,4'-MDI from 63-146 °C. The highest DTG was measured at around 126 °C in both isocyanate types. The first stage decompositions were 23.4 and 18.6 % in blocked pMDI and 4,4'-MDI, respectively. The results conformed to the endothermic curve of DSC, where the possible degradations by melting or evaporation of blocked isocyanate took place. The result was comparable to the reported deblocking temperature of NaHSO<sub>3</sub>-blocked pMDI (Zhang et al., 2011), where the deblocking temperature ranged from 80 to 151 °C. In their research, temperatures from 150-200 °C indicated the decomposition of sodium bisulfite by the release of sulfur dioxide, causing a loss weight of 7 %. The isocyanate began to self-crosslink during the temperature range of 150 to 250 °C.

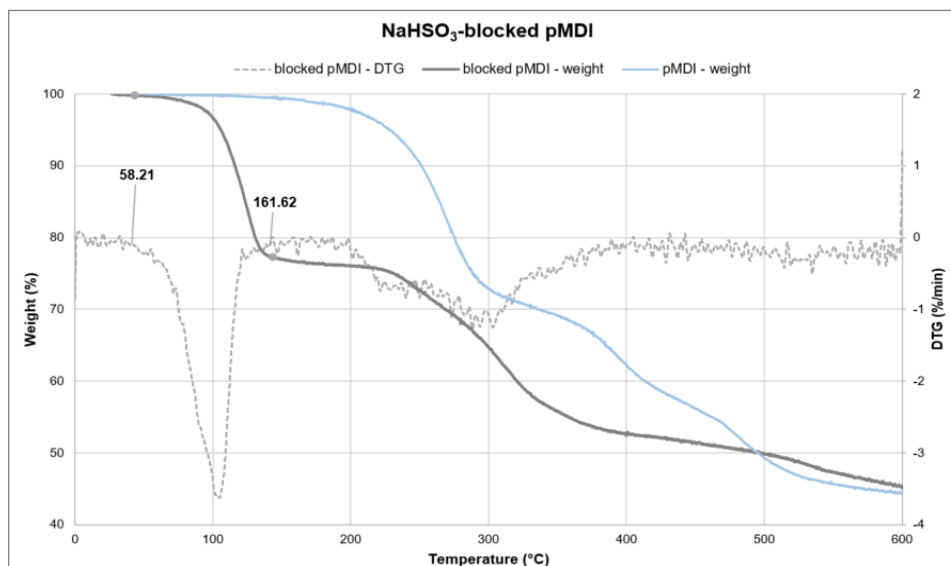


Fig. 39 TGA and DTG curve of NaHSO<sub>3</sub>-blocked pMDI

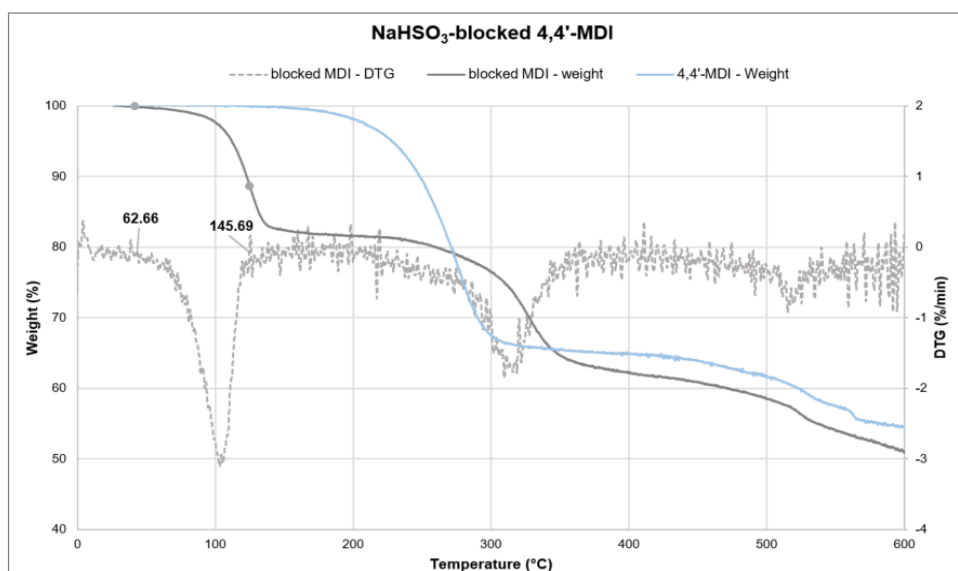


Fig. 40 TGA and DTG curve of NaHSO<sub>3</sub>-blocked 4,4'-MDI

### 5.1.1.3 Blocked isocyanates by $\epsilon$ -caprolactam

The yield percentage of blocked isocyanates was calculated as in the formula (15) as follows,

- For  $\epsilon$ -caprolactam-blocked pMDI, it was calculated for **56.88 %** by  $3.10 \text{ g adduct after drying} / [3.19 \text{ g pMDI} + 2.26 \text{ g caprolactam}]$
- For  $\epsilon$ -caprolactam-blocked 4,4'-MDI, it was calculated for **57.98 %** by  $2.76 \text{ g adduct after drying} / [2.50 \text{ g MDI} + 2.26 \text{ g caprolactam}]$

Approximately, 60 % of the final product of  $\epsilon$ -caprolactam-blocked isocyanates was obtained from the raw materials, much lower than the yield of NaHSO<sub>3</sub>-blocked isocyanates. This can be attributed to differences in the blocking reaction. Blocking with NaHSO<sub>3</sub> can be operated at normal temperatures without the use of a catalyst but uses

water as a co-solvent. On the other hand, the blocking reaction with  $\epsilon$ -caprolactam was more complicated. The reaction period was markedly extended and therefore required both a catalyst and a high reaction temperature. However, the water did not take part in the blocking with  $\epsilon$ -caprolactam as a solvent. Different yield percentages could be connected to the discrepancy in preparation methods of isocyanates blocked by both agents.

The FTIR spectra of neat isocyanates and blocked adducts of pMDI and 4,4'-MDI are represented in Fig. 41 and 42, respectively. Spectra of both blocked adducts did not show a high absorption band at  $2260\text{ cm}^{-1}$  as in unblocked isocyanates, which indicated that the most NCO characteristic groups of pMDI and 4,4'-MDI molecules were blocked. The formation of blocked adducts was confirmed by the existence of the following absorption bands (Lee et al., 2005): C=O stretching at  $1690\text{--}1725\text{ cm}^{-1}$ , N-H stretching at  $3200\text{--}3400\text{ cm}^{-1}$ , N-H bending at  $1530\text{--}1560\text{ cm}^{-1}$  and the stretching vibration of the C=O group of urea combined with the N-H group at  $1210\text{--}1240\text{ cm}^{-1}$ . All regions of absorbance were observed in spectra of blocked adducts from pMDI and 4,4'-MDI.

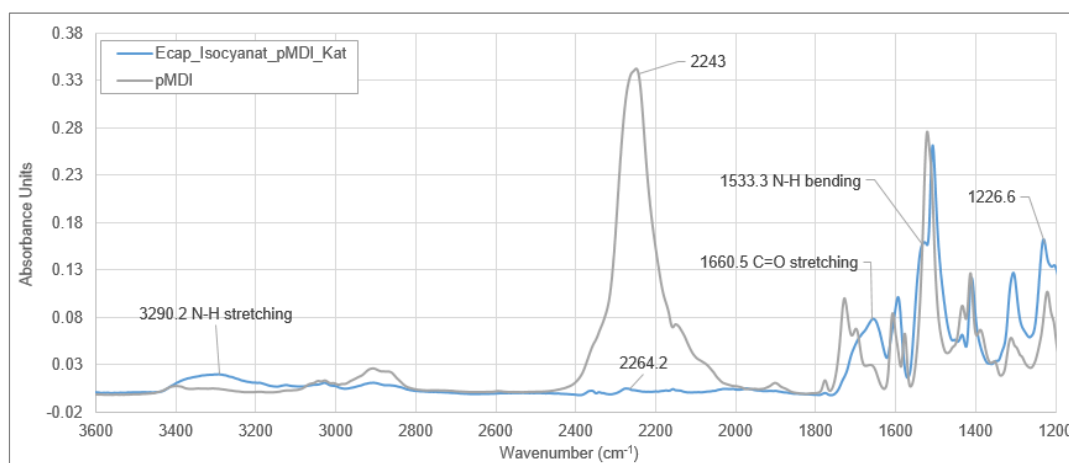


**Fig. 41** FTIR spectra of pure pMDI (grey line) and  $\epsilon$ -caprolactam-blocked adduct (blue line)

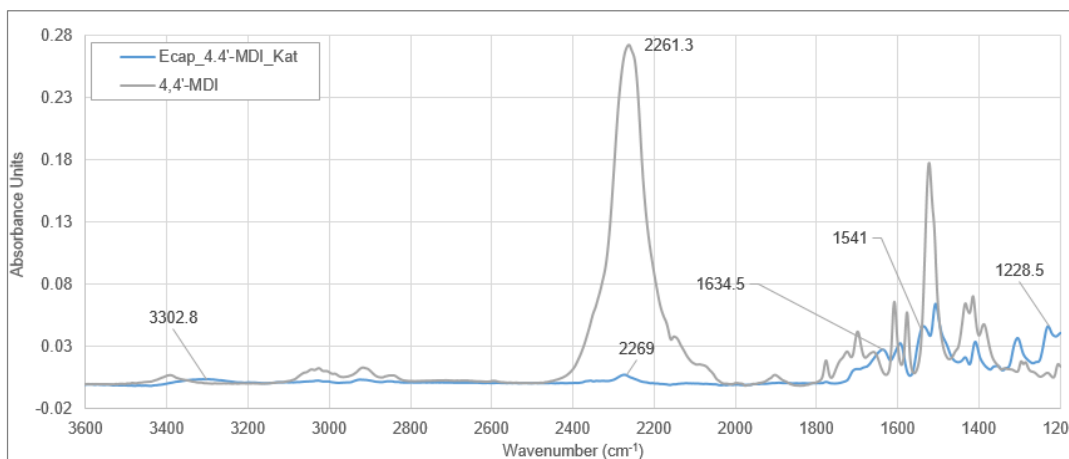


**Fig. 42** FTIR spectra of pure 4,4'-MDI (grey line) and  $\epsilon$ -caprolactam-blocked adduct (blue line)

The absorbance of C-H and NCO was measured by the provided software during FTIR analysis. The absorbance of the NCO band at 2250-2270  $\text{cm}^{-1}$  was normalized to the C-H stretching (Delebecq et al., 2012). Tab. 17 shows the isocyanate conversion ( $\alpha$ ) of both isocyanate types that are 97 and 88 % for pMDI and 4,4'-MDI, respectively. This high blocking rate confirmed the blocking reaction by  $\epsilon$ -caprolactam.

**Tab. 17 Absorbance of C-H and NCO frequencies in pure and  $\epsilon$ -caprolactam-blocked isocyanates**

| Isocyanates             | Absorbance at wavenumbers         |                                   | $A_{NCO}/A_{ref}$                 |
|-------------------------|-----------------------------------|-----------------------------------|-----------------------------------|
|                         | C-H<br>2910-2940 $\text{cm}^{-1}$ | NCO<br>2250-2270 $\text{cm}^{-1}$ |                                   |
| <b>PMDI</b>             | 0.0257                            | 0.3389                            | 13.19                             |
| <b>Blocked pMDI</b>     | 0.0107                            | 0.0047                            | 0.44                              |
|                         |                                   |                                   | <b><math>\alpha = 0.97</math></b> |
| <b>4,4'-MDI</b>         | 0.0131                            | 0.2718                            | 20.75                             |
| <b>Blocked 4,4'-MDI</b> | 0.0023                            | 0.0057                            | 2.52                              |
|                         |                                   |                                   | <b><math>\alpha = 0.88</math></b> |

The deblocking behavior of blocked isocyanates was investigated by DSC, as can be seen in Fig. 43. Here, DSC curves of  $\epsilon$ -caprolactam blocked adducts did not show a sharp deblocking range as in the  $\text{NaHSO}_3$ -blocked adducts. The obvious endothermic transition was unobserved as in common results of blocked isocyanate adducts. The reversal points were measured at 213 and 226  $^{\circ}\text{C}$  for blocked 4,4'-MDI and pMDI adducts, respectively. They are much higher than the deblocking point of  $\epsilon$ -caprolactam-blocked MDI found by Lee et al. (2005), 155-180  $^{\circ}\text{C}$  measured by DSC and 150-210  $^{\circ}\text{C}$  by TGA. In their study, the broad endotherm that existed at 222  $^{\circ}\text{C}$  was implied to be the melting point of decomposed products. Indeed, the melting points of  $\epsilon$ -caprolactam at 68  $^{\circ}\text{C}$  and MDI at 40  $^{\circ}\text{C}$  are much lower than that, so the decomposed product in their study was not supposed to be these two reactants. In this study, only one broad endotherm was found for each adduct. It can be assumed that the reversal ranges between 180-225  $^{\circ}\text{C}$  could be either the melting point of  $\epsilon$ -caprolactam-blocked isocyanates or dissociation temperatures of blocked adducts.

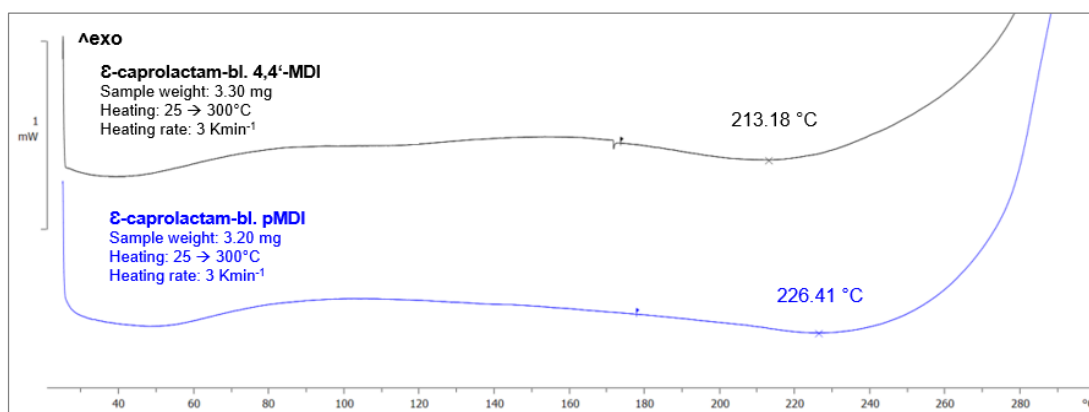


**Fig. 43 DSC curve of  $\epsilon$ -caprolactam-blocked pMDI (blue line) and 4,4'-MDI (black line)**

The following diagrams indicate TGA plots of  $\epsilon$ -caprolactam-blocked pMDI and 4,4'-MDI, respectively. The first stage decomposition appeared at 179-265 °C and 153-254 °C with a weight loss of approximately 3 and 11 % for  $\epsilon$ -caprolactam-blocked pMDI and 4,4'-MDI, respectively. This range is supposed to be the deblocking temperature. However, the weight loss appeared to be much less than reported earlier at 30-80 % (Lee et al., 2005). Here, the further weight loss in the second decomposition appeared to be higher than appeared in the deblocking stage. TGA measurement is based on the evaporation of the blocking molecule. Since the boiling point of both pMDI and DBTDL starts at ca. 250 °C and that of  $\epsilon$ -caprolactam is much higher, the minimal weight loss in the first stage of decomposition at around 180 °C in blocked pMDI could not be the dissociation of those components; it could, however, be explained by 1) low content of blocked isocyanate in the adducts and 2) another possible degradation reaction of the urethane bond. The CO<sub>2</sub> detection test could verify the first reasoning in the next section of the results. The test can confirm whether and how much the isocyanate reacts with water during the blocking process. For the latter explanation, the urethane bond can transform to different degradation reactions starting from 150 °C, which possibly release CO<sub>2</sub> gas and re-bond the rest substance (Delebecq et al., 2012). The low weight loss during the deblocking process confirmed the broad endotherm found in  $\epsilon$ -caprolactam-blocked isocyanate in the DSC.

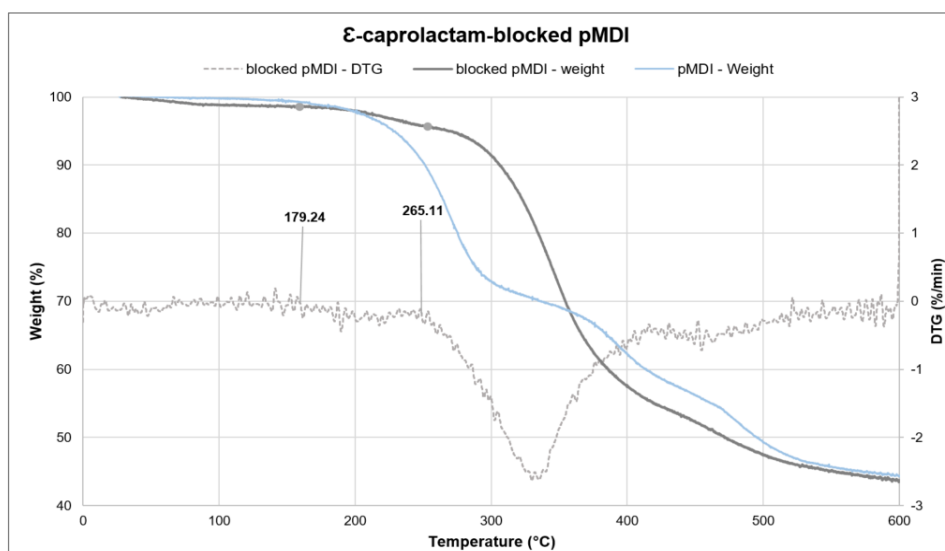


**Fig. 44 TGA and DTG curve of  $\epsilon$ -caprolactam-blocked pMDI**

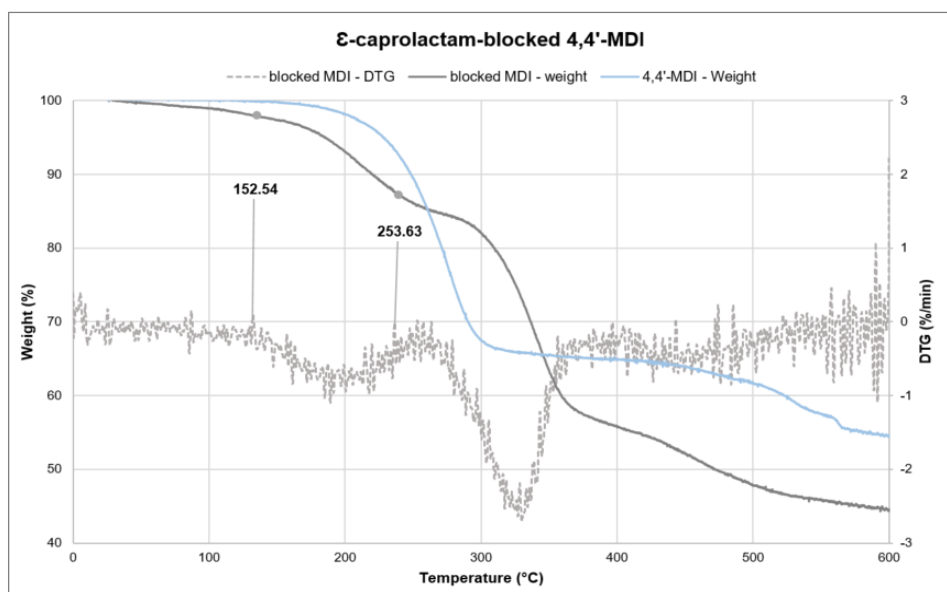


**Fig. 45 TGA and DTG curve of  $\epsilon$ -caprolactam-blocked 4,4'-MDI**

The determined deblocking temperatures of blocked isocyanates with  $\text{NaHSO}_3$  and  $\epsilon$ -caprolactam are summarized in Tab. 18. From this table,  $\text{NaHSO}_3$ -blocked isocyanates show lower temperatures than  $\epsilon$ -caprolactam based blocked adducts in all cases, which correspond to a review by Rolph et al. (2016). Apart from operating conditions and the presence of additives and solvents, the nucleophilicity of blocking agents is one of the critical factors. Their active hydrogen compounds can govern the reactivity toward isocyanate. Delebecq et al. (2012) presented the relative reaction rate of different active hydrogen compounds against isocyanate, in which amine compounds have a higher reaction rate than hydroxyl groups.

For this reason, the deblocking temperature of  $\epsilon$ -caprolactam adducts, blocked via -NH group, is higher than that of  $\text{NaHSO}_3$  adduct via -OH group. Despite the dependency of deblocking temperatures on isocyanate types, the discrepancy in the deblocking ranges of blocked adducts between pMDI and 4,4'-MDI did not appear. A minor difference in  $\epsilon$ -caprolactam-blocked adducts can be seen, in which blocked pMDI exhibits a slightly higher deblocking temperature than that of blocked 4,4'-MDI. Lee et al. (2005) compared the deblocking temperatures among the aromatic diisocyanates. The study concluded that the steric effect and electron-withdrawing nature of the benzene ring are the main reasons for the lower deblocking temperature of the TDI based blocked isocyanate than that of MDI based blocked adducts. A benzene ring of aromatic isocyanate attracts the electron pair of a nitrogen atom. It increases the positive charge density of nitrogen atom, making lower dissociation temperatures of blocked aromatic isocyanates (TDI, MDI) than blocked aliphatic isocyanates (IPDI,  $\text{H}_{12}$ MDI) in general. These effects could not be detected when comparing the deblocking temperatures of pMDI and 4,4'-MDI, as shown

in Tab. 18. It could be explained by the similarity in chemical structures of both isocyanate types.

Tab. 18 Summary of deblocking temperatures measured in the research compared to reported values from literature a. Zhang et al. (2011), b. Lee et al. (2005)

| Blocked isocyanate                   | Technique | Heating rate<br>(Kmin <sup>-1</sup> ) | Deblocking temperature<br>(°C) | Reported values<br>(°C) |
|--------------------------------------|-----------|---------------------------------------|--------------------------------|-------------------------|
| NaHSO <sub>3</sub> -blocked pMDI     | DSC       | 2                                     | 91 – 118                       | a. 96 – 110             |
|                                      |           | 4                                     | 100 – 127                      |                         |
|                                      | TGA       | 5                                     | 58 – 162                       | a. 80 – 151             |
| NaHSO <sub>3</sub> -blocked 4,4'-MDI | DSC       | 2                                     | 92 – 118                       |                         |
|                                      |           | 4                                     | 100 – 127                      |                         |
|                                      | TGA       | 5                                     | 63 – 146                       |                         |
| ε-caprolactam-blocked pMDI           | DSC       | 3                                     | 180 – 226                      |                         |
|                                      | TGA       | 5                                     | 180 – 265                      |                         |
| ε-caprolactam-blocked 4,4'-MDI       | DSC       | 3                                     | 180 – 213                      | b. 155 – 180            |
|                                      | TGA       | 5                                     | 153 – 254                      | b. 150 – 210            |

### 5.1.2 CO<sub>2</sub> detection test during blocking process

The side reaction between isocyanate and water during the blocking reaction was proven using Ba(OH)<sub>2</sub> solution, according to Eq. 1 and 2.

The reaction was confirmed by the appearance of white solid barium carbonate (BaCO<sub>3</sub>) in the solution, which indicated the CO<sub>2</sub> gas from the side reaction. The dry weight of BaCO<sub>3</sub> was measured and calculated for the isocyanate ratio that reacted with water, as follows:

$$\text{Amount of NCO reacted with H}_2\text{O (\%)} = \frac{NCO_{\text{reacted with H}_2\text{O}} \text{ (mol)}}{NCO_{\text{start}} \text{ (mol)}} \cdot 100 \quad (16)$$

$$\text{where } NCO_{\text{reacted with H}_2\text{O}} \quad (17)$$

$$= \frac{\text{dry weight BaCO}_3 \text{ (g)}}{\text{molecular weight BaCO}_3 \text{ (197.34 g/mol)}} \cdot \frac{1 \text{ mol NCO reacted with H}_2\text{O}}{1 \text{ mol BaCO}_3}$$

- For blocking of 4,4'-MDI with NaHSO<sub>3</sub>,  
0.3 g (1.52 mmol) dry weight of BaCO<sub>3</sub> was measured,  
divided by 0.039 mol used NCO from the beginning.  
NCO ratio reacted to water is obtained for **3.94 %** from the total isocyanate.
- For blocking of 4,4'-MDI with ε-caprolactam,  
1.37 g (6.94 mmol) dry weight of BaCO<sub>3</sub> was measured,  
divided by 0.020 mol used NCO from the beginning.  
NCO ratio reacted to water is obtained for **34.71 %** from the total isocyanate.

Although water was used as a solvent in the blocking process with  $\text{NaHSO}_3$ , the increased content of reacted isocyanate with water was found to be greater during the blocking with  $\epsilon$ -caprolactam. It seems that using water in blocking with  $\text{NaHSO}_3$  did not raise the side reaction as significantly as predicted. The side reaction in the blocking process with  $\epsilon$ -caprolactam is evidenced by the high amount of  $\text{BaCO}_3$ , suggesting the presence of unknown water in the reaction. It appeared that the added acetone contained water up to the maximal amount of 0.05 %, according to the product information, which represents 27.8 mmol water in the blocking process with  $\epsilon$ -caprolactam. This sufficient content of water was available to react with isocyanate. Still, a high water content is not the only factor for the side reaction. Other operation factors, such as the reaction period, should be determined. The longer reaction time of 7 hr in the blocking process of  $\epsilon$ -caprolactam induced a higher possibility of side reaction than the blocking process of  $\text{NaHSO}_3$  based on 2-3 hr. The high rate of side reaction in blocking with  $\epsilon$ -caprolactam conformed with the low yield percentage of the blocked adduct (see 5.1.1.3). Via the reaction with water, isocyanate groups of MDI will split carbon and oxygen atoms. The total mass of both atoms is higher than that of two hydrogen atoms that MDI receives afterward to form an amine-MDI product (see Eq. 1).

Therefore, the more an amine side product is generated, the lower the yield weight of the dry product will be. To make this obvious, the molecular weight of targeted  $\epsilon$ -caprolactam blocked MDI is calculated for  $476.6 \text{ g mol}^{-1}$ , while that of the side product, amine-MDI, is approximately  $198 \text{ g mol}^{-1}$ . The production of  $\text{CO}_2$  as another side product also takes some carbon atoms from the blocked adduct. So the side reaction between isocyanate and water in blocking with  $\epsilon$ -caprolactam can reduce the yield percentage of the end product significantly. However, the appearance of the MDI-amine product was untraceable from the IR spectra of blocked adducts by  $\epsilon$ -caprolactam (Fig 41 and 42). Primary amines have two N-H bonds, which generally show two well-defined signals due to asymmetric and symmetric N-H stretching, separated by  $80\text{-}100 \text{ cm}^{-1}$ , making this band resemble a molar tooth between  $3200\text{-}3600 \text{ cm}^{-1}$ . It could be possible that the MDI-amine product reacts with the remainder of the isocyanate to give urea bond, as it happens in the common PUR reaction.

### 5.1.3 NCO conversion of deblocked isocyanates

The deblocking signal of NaHSO<sub>3</sub>-blocked pMDI was found to be at 117.8 °C, as illustrated in Fig. 36. Blocked adduct was heated by the DSC to prepare the deblocked isocyanate. After heating, the adduct sample was placed into the FTIR instrument in a sealed pan with a hole for characterization. The FTIR spectra of blocked pMDI samples before and after deblocking at 120 °C are visible in Fig. 46. The results indicated that blocked pMDI has an even higher absorbance of the NCO group than deblocked products. In general, a lower absorbance was detected in the deblocked pMDI, though both FTIR results have the remainder of the signals in common. The isocyanate group in blocked isocyanate should be re-released when exposed to a high temperature. In this experiment, the IR band of the NCO group did not show up as much as expected in the deblocked isocyanate. Zhang et al. (2011) experienced a different result. In their study, an NCO band at 2280 cm<sup>-1</sup> was given after deblocking at 70, 80, and 100 °C using an oven attached to a hermetic container; however, an obvious signal could only be seen in the IR band of the deblocked sample at 70 °C from their spectra diagram. A new small double band around 2341-2349 cm<sup>-1</sup> close to the characteristic NCO signal was found in deblocked samples from both studies. The signal could be disordered with NCO absorbance. It is probably referred to as O=C=O stretching of CO<sub>2</sub>, which came from the atmosphere.

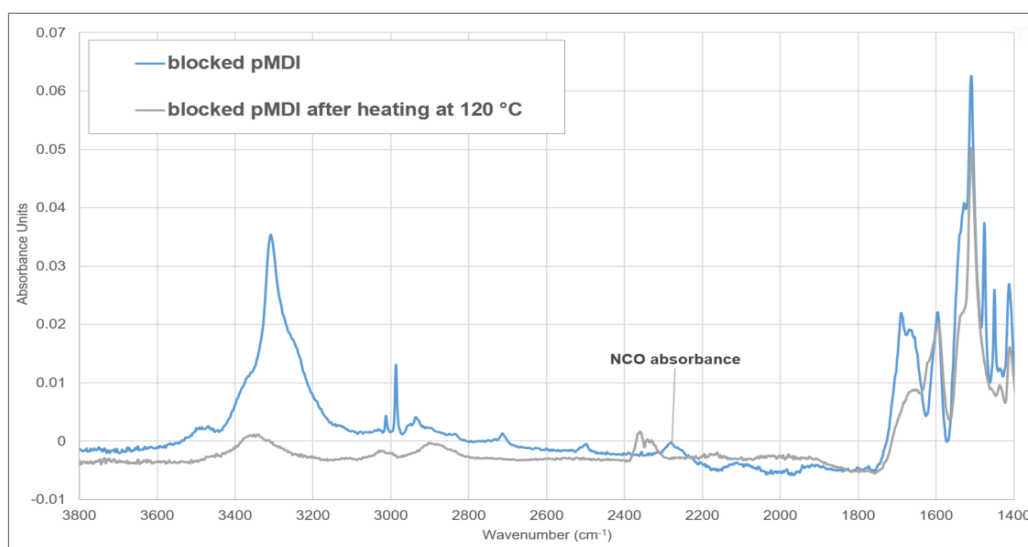
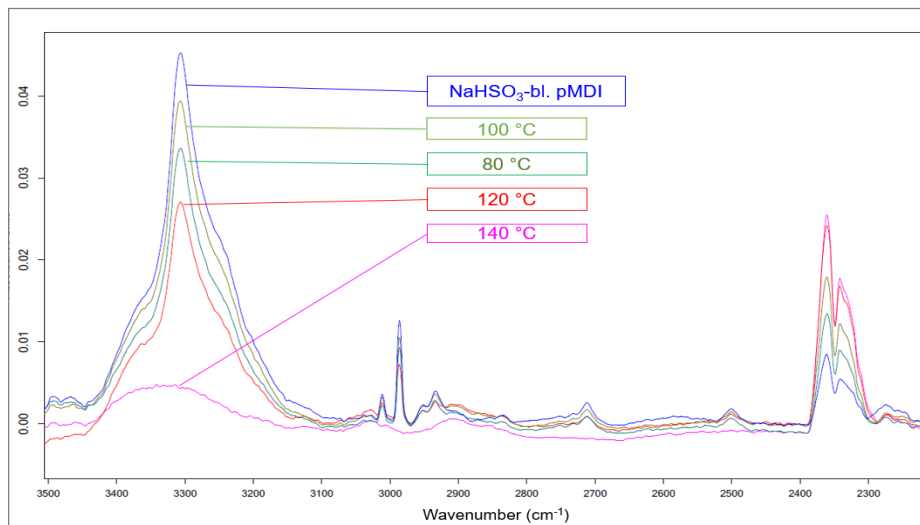


Fig. 46 FTIR spectra of NaHSO<sub>3</sub>-blocked pMDI and after heating at 120 °C by DSC

Gradual changes in the IR spectrum after deblocking using different temperatures can be seen in Fig. 47. NaHSO<sub>3</sub>-blocked pMDI was deblocked at 80, 100, 120 and 140 °C by DSC. The N-H stretching signals at 3401 and 3195 cm<sup>-1</sup> became reduced at increasing temperatures until the appearance of the broad band at 140 °C. At this temperature, the spectrum exhibited less intensive signals than that of lower

temperatures. Still, the NCO signal of re-released isocyanate at  $2250\text{-}2270\text{ cm}^{-1}$  could not be detected in various deblocking temperatures.



**Fig. 47 FTIR curves of  $\text{NaHSO}_3$ -blocked pMDI at different temperatures**

Isocyanates blocked by  $\epsilon$ -caprolactam exhibited more alteration in the NCO conversion than those by  $\text{NaHSO}_3$  during deblocking, as shown in Fig. 48.  $\epsilon$ -caprolactam pMDI adduct was set in DSC for deblocking at different temperatures and times. Regarding NCO absorbance at  $2250\text{-}2270\text{ cm}^{-1}$ , deblocked products featured lower intensity than the blocked pMDI. NCO absorbance changes were compared to those of C-H stretching at  $2910\text{-}2940\text{ cm}^{-1}$ , the same as for determining NCO conversion as mentioned earlier in Tab. 17. It can be seen that both C-H and NCO groups in the deblocking state revealed lower absorbance than in the blocked adduct. Ratios between the absorbance of NCO related to the C-H group of ( $A_{\text{NCO}}/A_{\text{ref}}$ ) various deblocking samples were summarized in Fig. 49 and 50 for pMDI and 4,4'-MDI, respectively.

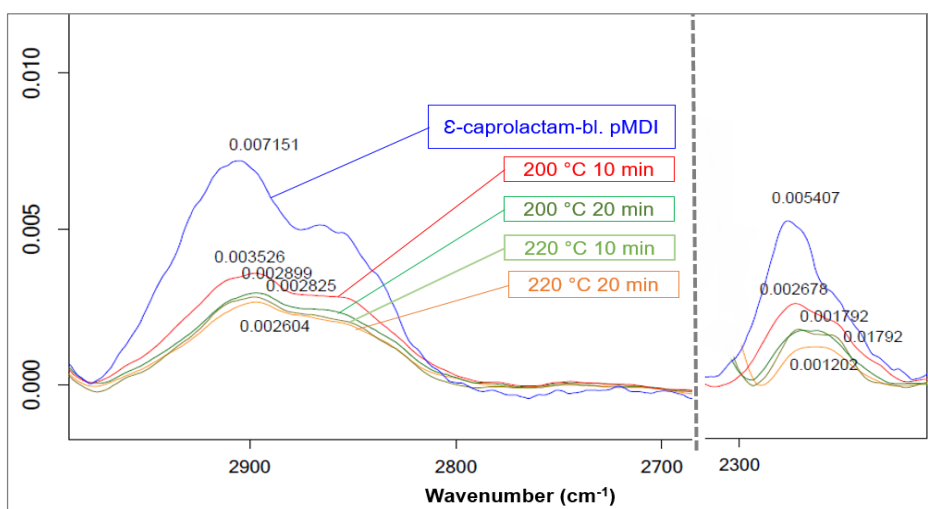


**Fig. 48 FTIR curves of NCO absorption band from  $\epsilon$ -caprolactam-blocked pMDI at different time and temperatures**

According to Fig. 49, the normalized NCO absorbance of  $\epsilon$ -caprolactam pMDI deblocked at 200 and 225 °C (see dark blue bars) was increased from 0.69 in blocked pMDI to 1.11 at 225 °C. Then, it was dropped by heating at 250 °C. It can be related to the deblocking temperature of  $\epsilon$ -caprolactam-blocked pMDI, which was found before at 226.4 °C (see Fig. 43). Thus, the adduct deblocked at 225 °C had the highest normalized NCO absorbance. That was in the case without heating time, which means the deblocking process was terminated after the specific temperature was reached. Other deblocked samples within the heating periods showed different results (see the light blue bars). By extending the heating time, the isocyanate group tended to reveal a lower absorbance ratio. It could be assumed that the deblocking reaction is measurable at a specific temperature and time. After this point, the re-released NCO group can further react to available aliphatic substances in the system. Consequently, measuring changes in the absorbance ratio of NCO could be deviated because of the time gap between the deblocking in DSC and FTIR characterization and access of sample to the atmosphere.

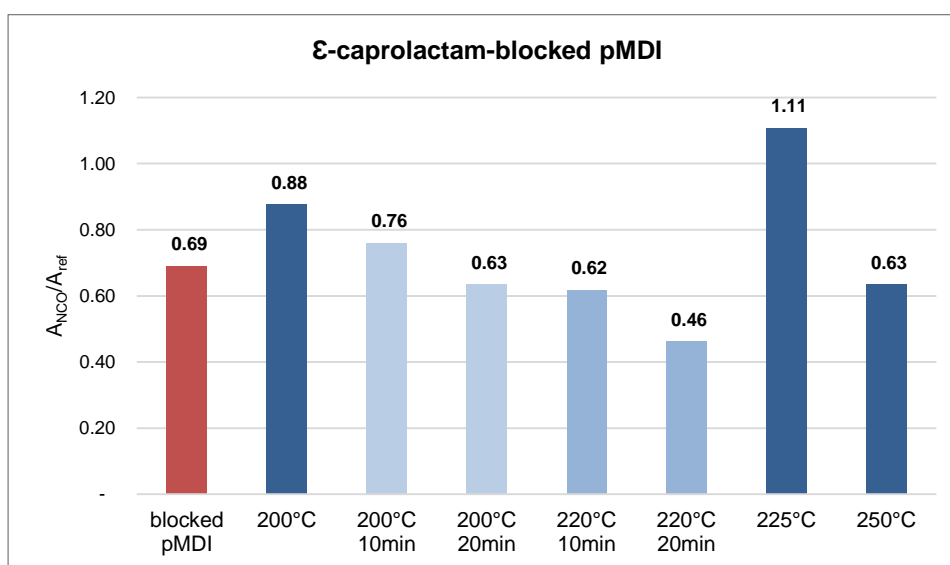


**Fig. 49 Absorbance ratios of NCO normalized to C-H in blocked and deblocked pMDI**

$\epsilon$ -caprolactam-blocked 4,4'-MDI appeared to have the same tendency as blocked pMDI after setting at 225 and 250 °C. As the deblocking temperature of blocked 4,4'-MDI was identified for 213.2 °C, heating with a constant rate up to the specific temperature has proven to increase the normalized NCO absorbance. It was then reduced in deblocked samples with heating periods. Here, the normalized NCO absorbance ratio of heated adducts at 200 °C is lower than that of the blocked adduct. Since this temperature was below the deblocking point, the absorbance ratio is supposed to be constant or slightly increased. In contrast, it was reduced from 2.52 to 0.93 at 200 °C.

The confusing result could be explained by the blocking rate of blocked 4,4'-MDI, which was 88 % (see Tab. 17). Consequently, the rest amount of unblocked NCO appeared in a high absorbance ratio of 2.52 in blocked 4,4'-MDI; after that, it was abruptly reduced in samples heated at 200 and 225 °C due to evaporation or further reactions of unblocked isocyanate. The absorbance ratios in deblocked adducts will become larger than blocked 4,4'-MDI when the gain in deblocked NCO amount is enough to compensate the fled unblocked group, as appeared in deblocked adduct at 225 °C. Evaporation could be a critical point depending on the measurement techniques (Delebecq et al., 2012). In TGA measurements, evidently performed in an open pan, the blocking molecule evaporation will pull the reaction toward free isocyanate formation. On the contrary, in DSC, the sample is analyzed either in a sealed pan if the boiling point of the blocking molecule is higher than the temperature range or in a pan with a hole to prevent the blocking molecule evaporation from blowing up the cell. The same phenomenon will rarely occur.

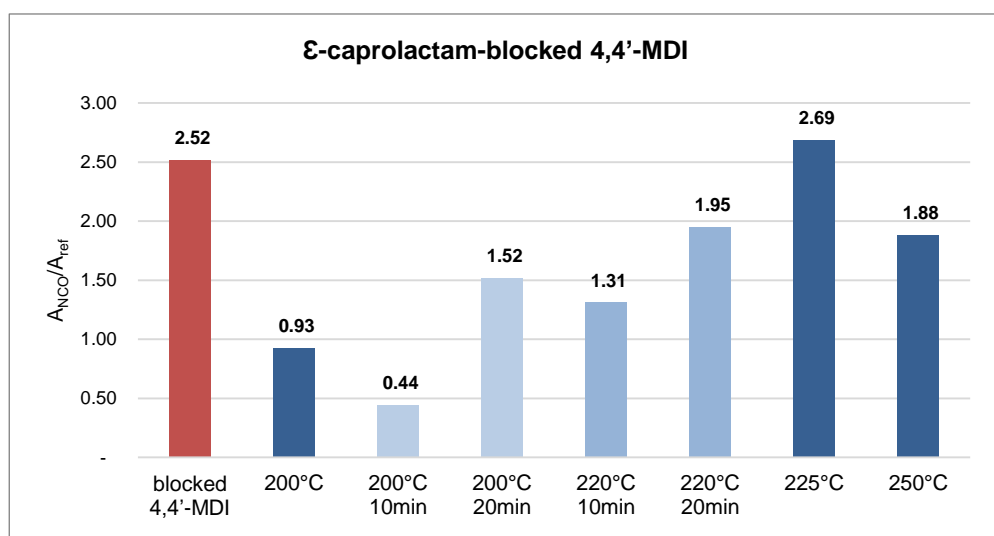


Fig. 50 Absorbance ratios of NCO normalized to C-H in blocked and deblocked 4,4'-MDI

#### 5.1.4 PUR curing

To investigate the PUR curing reaction, PUR foam was prepared from polyol (Desmophen 1240N) and pMDI (Desmodur 44P16) according to the described method in 4.2.1. Polyol and PUR foam were characterized for characteristic groups by FTIR spectrometry. Both IR spectra are represented in Fig. 51 and 52 and are used as a reference for comparison with other IR results of products from blocked isocyanates and polyol.

Polyol has its characteristic bands, which also appears as the soft segment in the IR result of PUR. For example, there are two bands between 2970 and 2873 cm<sup>-1</sup>, attributed to the symmetrical and nonsymmetrical stretching of the C–H bond. Some bands became weakened in the PUR spectra, such as a broad and strong signal from the ether

bond C-O-C stretch at  $1082\text{ cm}^{-1}$  or the loss of  $\text{-OH}$  absorbance at  $3413\text{ cm}^{-1}$ , as the band became blended with the stretching vibration of N-H from isocyanate at  $3310\text{ cm}^{-1}$ .

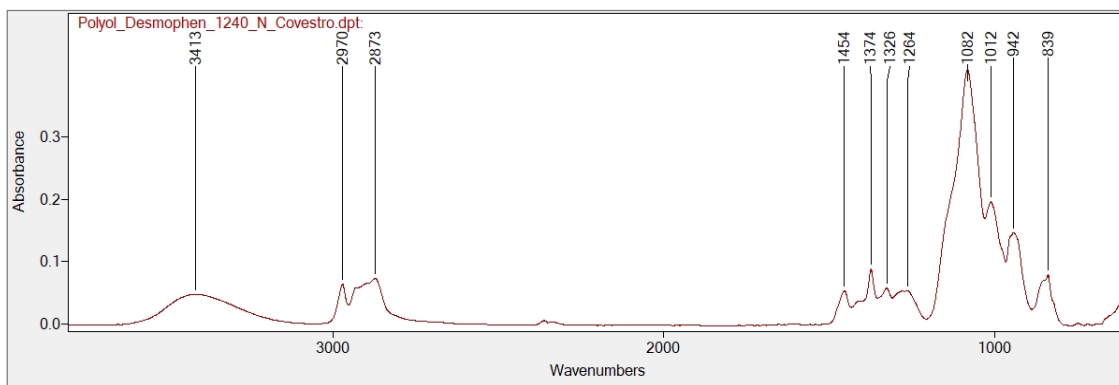


**Fig. 51 FTIR spectra of sucrose-based polyether polyol (Desmophen 1240N)**

PUR contains a basic repetitive unit urethane bond ( $\text{-NHCOO-}$ ) formed by the polymerization reaction of both components. Thus, the bond can be noticed in PUR spectra via the following characteristics:

- sharp absorption band, stretching vibration of esters  $\text{C=O}$ , from  $\text{N-CO-O}$  at  $1711\text{ cm}^{-1}$
- sharp absorption band, asymmetric stretching vibration of  $\text{C-O}$ , from  $\text{N-CO-O}$  at  $1221\text{ cm}^{-1}$
- weak band,  $\text{N-CO-O}$  asymmetric stretching vibration at  $916\text{ cm}^{-1}$

The abovementioned absorbance was attributed referred to Jiao et al. (2013). The characteristic bands of both polyol and isocyanate appear in PUR spectra, due to bonding, with less intensity of original absorbance. Because diisocyanate is the main contributor for the formation of the hard segment of PUR, the isocyanate group is observed in the PUR spectra at  $2277\text{ cm}^{-1}$ . The absorption band at  $1594\text{ cm}^{-1}$  corresponds to the vibration of  $\text{C=C}$  in the benzene ring, and the several weak bands near  $767\text{-}916.8\text{ cm}^{-1}$  belong to the out-of-plane bending vibration of  $\text{C-H}$  in the multi-substituted benzene ring (Jiao et al., 2013)

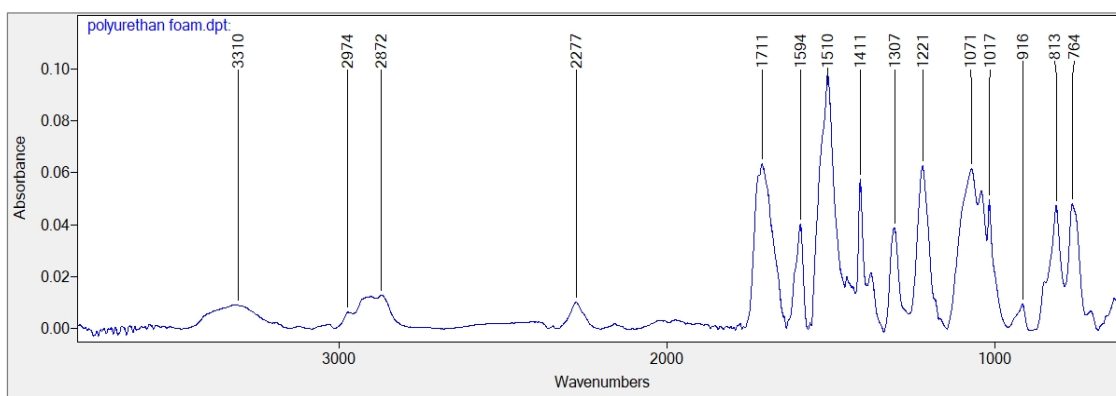


**Fig. 52 FTIR spectra of PUR foam prepared form Desmophen 1240N and Desmodur 44P16 (pMDI)**

### 5.1.4.1 Reaction of NaHSO<sub>3</sub>-blocked isocyanates with polyol

Mixtures from NaHSO<sub>3</sub>-blocked isocyanates with polyol were prepared by different isocyanate ratios, curing time, temperature and heating rate. The effects of these preparation factors will be discussed in this part via the IR results of cured mixtures.

#### **Effect of isocyanate ratio**

Fig. 53 presents the IR spectra of mixture products prepared by weight ratios between blocked MDI and polyol in 1:1 (green line), 2:1 (red line) and 3:1 (blue line). The increase of isocyanate ratios from 1:1 to 2:1 flattened the characteristic signals of polyol in the range of 2872-2974 cm<sup>-1</sup> (C-H bond) and at 1082 cm<sup>-1</sup> (ether bond C-O-C stretching). The band at 1226 cm<sup>-1</sup> (C-O from N-CO-O) became more evident in the product prepared by a 2:1 ratio. With regards to the existence of urethane bonding, the isocyanate ratio of 2:1 may induce PUR curing even better than other ratios, as can be seen from FTIR results. The optimal ratio of blocked isocyanate and polyol at 2:1 corresponded to the ratio of reactants calculated earlier in 4.1.3, in which 2.09 g NaHSO<sub>3</sub>-blocked pMDI was required for 1 g polyol for PUR preparation with an NCO index of 1.0. Furthermore, adding a higher amount of blocked pMDI up to a 3:1 mixture ratio can lead to the rise of a new signal at 961 cm<sup>-1</sup>, which was found earlier in blocked and deblocked isocyanates with NaHSO<sub>3</sub>. The signal could be assigned to di-substituted C=C bending of benzene.

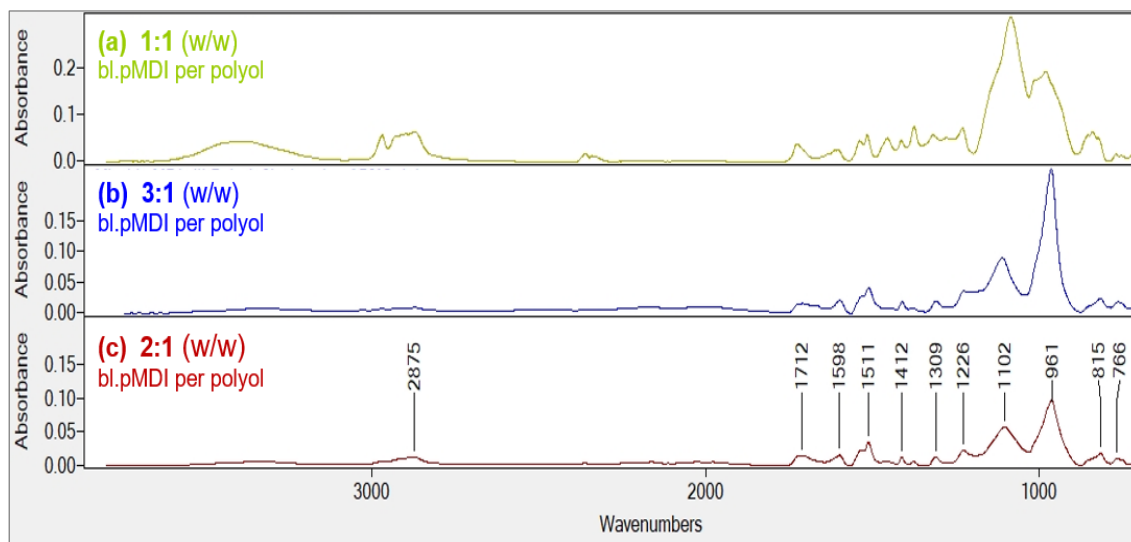


**Fig. 53 FTIR spectra of mixtures of NaHSO<sub>3</sub>-blocked pMDI and polyol cured at 250 °C prepared in different ratios (a) 1:1, (b) 3:1, (c) 2:1**

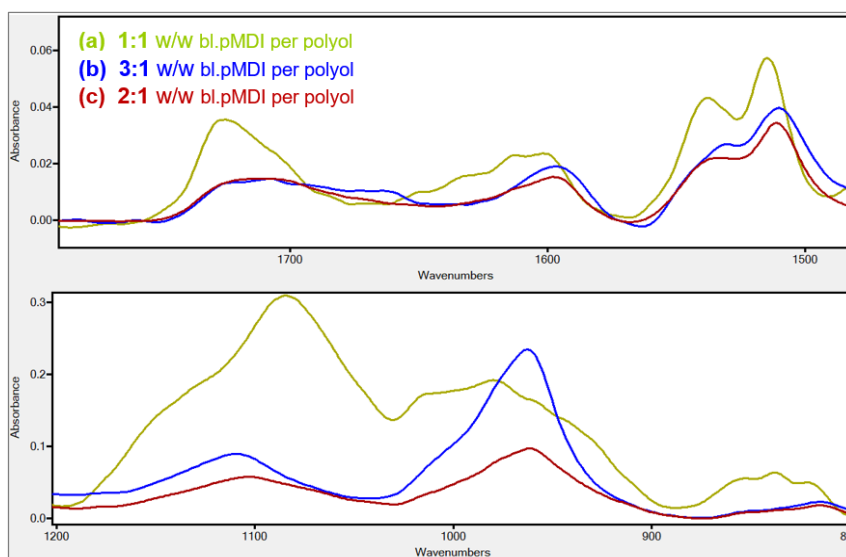


Fig. 54 Enlarged FTIR spectra of mixtures from the last figure

### ***Effect of curing temperature***

Applying two different temperatures for curing did not change IR results in the region over  $2500\text{ cm}^{-1}$ . IR results of mixture samples cured at  $150$  and  $250\text{ °C}$  in the lower region between  $2500\text{--}600\text{ cm}^{-1}$  are shown in Fig. 55. Increasing the curing temperature from  $150$  to  $250\text{ °C}$  was seen to reduce the signal intensity of  $\text{C}=\text{O}$  at  $1662\text{ cm}^{-1}$  of blocked pMDI to the higher region at  $1712\text{ cm}^{-1}$ , which conforms to the stretching vibration of esters  $\text{C}=\text{O}$  found earlier in  $\text{N-CO-O}$  of PUR. Moreover, the absorption band at  $1596\text{ cm}^{-1}$  was weakened and moved slightly to a higher wave number with the curing temperature. The absorption band corresponded to the vibration of  $\text{C}=\text{C}$  in the benzene ring in isocyanate. Its new settlement at a higher temperature agreed with the IR spectra of pure isocyanate and PUR. The absorbance at  $972\text{ cm}^{-1}$  was reduced by increasing the curing temperature.

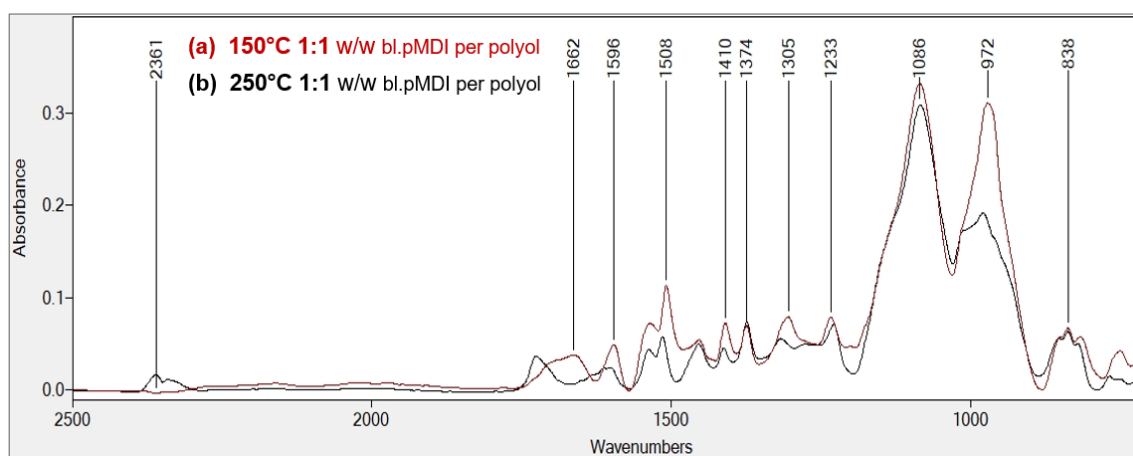
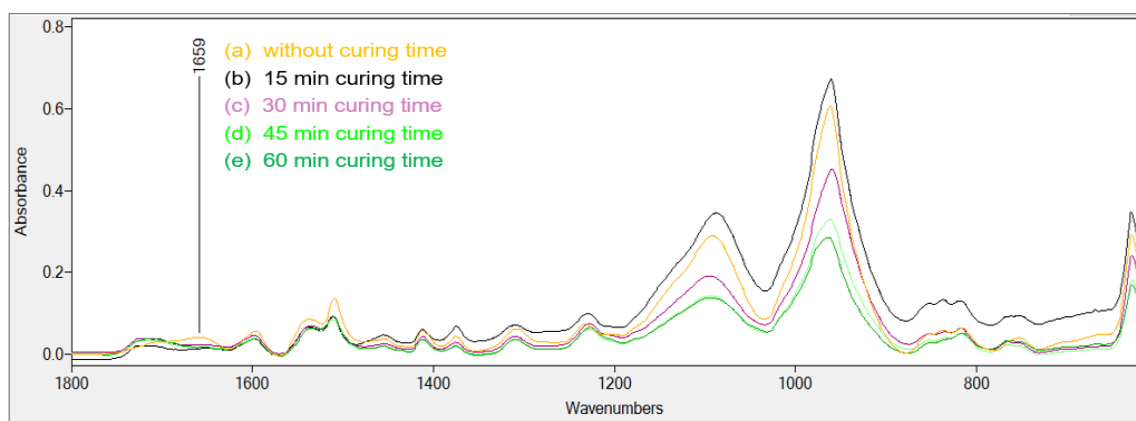


Fig. 55 FTIR spectra of mixture of  $\text{NaHSO}_3$ -blocked pMDI and polyol cured at (a)  $150\text{ °C}$  and (b)  $250\text{ °C}$

### ***Effect of curing time***

Since the curing temperature seemed to impact the IR spectra of mixture products, the curing duration was controlled in various periods to investigate their effect on IR results. Mixture samples of blocked pMDI and polyol with a ratio of 2:1 were cured at 200 °C for different periods. Fig. 56 summarizes the IR spectra of products without a continuous curing period (yellow line) and with curing periods of 15 min (black line), 30 min (violet line), 45 min (light green line), and 60 min (green line). Here, no detectable difference was observed in the formed absorption bands among samples using the various curing periods. A minor discrepancy was noticed in the shift of C=O stretching at 1659 cm<sup>-1</sup> in the mixture without curing time, which was observed to be the left in mixtures with curing time, in the same way as influenced by the curing temperature, which was discussed previously.



**Fig. 56 FTIR spectra of 2:1 w/w mixture of NaHSO<sub>3</sub>-blocked pMDI and polyol cured at 200 °C without curing time (a) and using different times (b-e)**

### ***Effect of heating rate***

The heating rate did not affect the IR results of the mixture in comparison with other factors. Mixture samples of blocked pMDI and polyol were heated up to 200 °C by using different heating rates of 5, 10 and 20 Kmin<sup>-1</sup>, as displayed in Fig. 57. It is evident that all three spectra, despite varied heating rates, exhibited an identical absorbance.

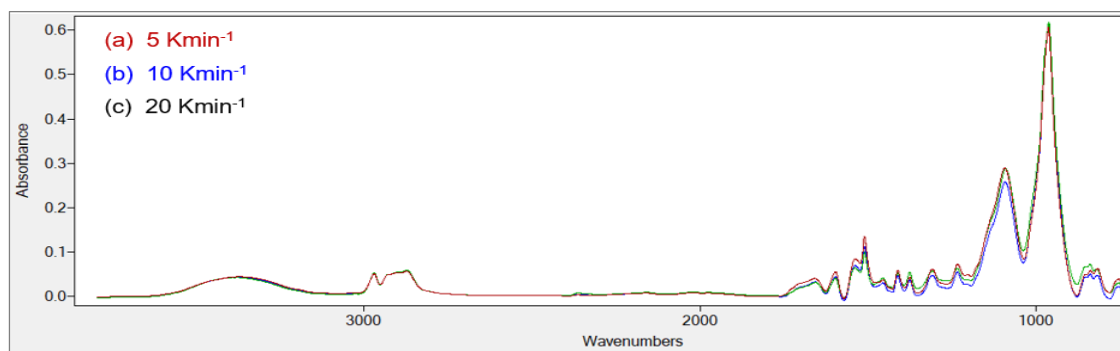


**Fig. 57 FTIR spectra of 2:1 w/w mixture of NaHSO<sub>3</sub>-blocked pMDI and polyol cured at 200 °C by different heating rates: (a) 5 Kmin<sup>-1</sup> (b) 10 Kmin<sup>-1</sup> (c) 20 Kmin<sup>-1</sup>**

### ***Effect of isocyanate type***

Mixture samples of blocked 4,4'-MDI were investigated for their IR characteristics, likewise mixtures of blocked pMDI with polyol. IR spectra of blocked 4,4'-MDI products with different mixing ratios are shown in Fig. 58. The result from blocked pMDI is plotted for comparison. Applying different isocyanate ratios in a mixture of blocked 4,4'-MDI and polyol did not lead to a distinct alteration in their IR absorbance. All spectra of blocked 4,4'-MDI still displayed the same polyol characteristics, despite the gain in isocyanate ratios, as can be seen from bands at 3413, 2970 and 2873  $\text{cm}^{-1}$ . This result responded to the mixture of blocked pMDI with a 1:1 ratio. However, polyol's characteristic signals were reduced by increasing the amount of blocked pMDI to higher levels, as discussed earlier. In the case of blocked 4,4'-MDI products, characteristic polyol bands were not changed by increasing the isocyanate level. It could be described by the boiling point of 4,4'-MDI at 196  $^{\circ}\text{C}$ , which is lower than pMDI. Therefore, the deblocked 4,4'-MDI may have partly been lost from the product during the curing reaction.

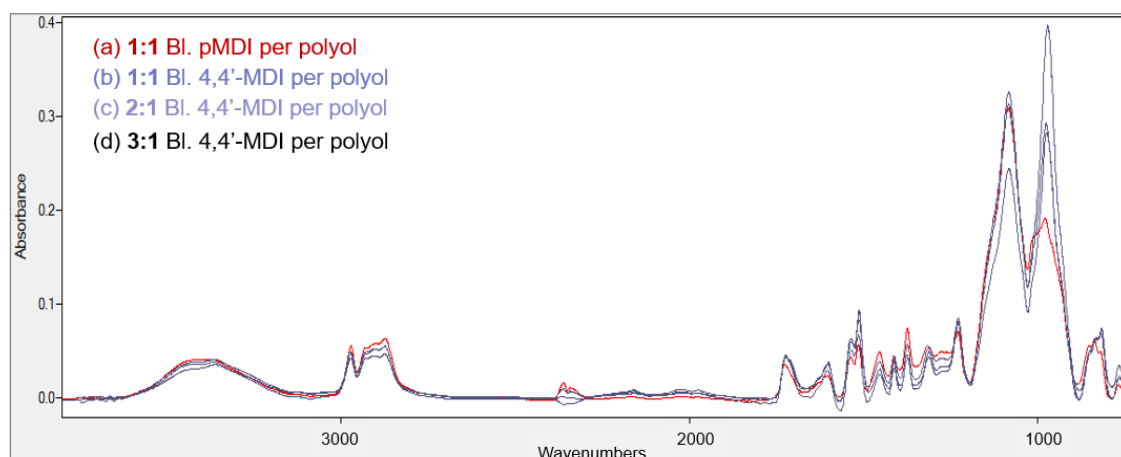


**Fig. 58 FTIR spectra of mixtures of  $\text{NaHSO}_3$ -blocked isocyanates and polyol cured at 250  $^{\circ}\text{C}$  prepared by different weight ratios**

#### **5.1.4.2 Reaction of $\epsilon$ -caprolactam-blocked isocyanates with polyol**

Likewise, the curing reaction between  $\epsilon$ -caprolactam-blocked isocyanates and polyol were investigated based on FTIR measurement. Isocyanate ratios and other curing factors were examined for their impacts on IR characteristics of cured products, except for the heating rate. Changes in IR absorbance due to curing factors are reviewed and discussed in the forthcoming section.

### ***Effect of isocyanate ratio***

The IR result of the product of caprolactam-blocked pMDI and polyol with a 1:1 ratio cured at 250  $^{\circ}\text{C}$  is represented in Fig. 59. Starting from this ratio, the cured mixture's absorption bands showed a similarity with the absorbance that appeared before in the IR result of PUR, except for the isocyanate band at 2278  $\text{cm}^{-1}$ . Strong absorbance signals

at 1711 (stretching of esters C=O) and 1221  $\text{cm}^{-1}$  (asymmetric stretching of C–O) combined with a weak band at 916  $\text{cm}^{-1}$  (N–CO–O asymmetric stretching) confirmed the formation of urethane bond (–NHCOO–). Furthermore, characteristic signals of polyol at 1017 and 1071  $\text{cm}^{-1}$  were observed in both spectra.

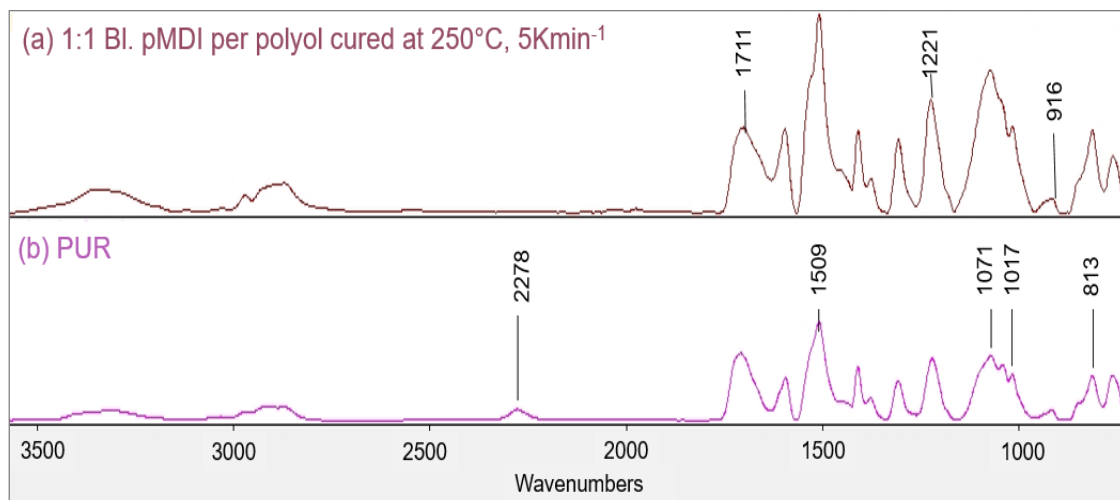


**Fig. 59 FTIR spectrum of (a) 1:1 w/w mixture of  $\epsilon$ -caprolactam-blocked pMDI and polyol compared with (b) IR result of PUR**

Surprisingly, after applying a higher amount of isocyanate ratios, the similarity in absorption bands of cured products with PUR has been decreased. The IR spectra of cured products prepared from  $\epsilon$ -caprolactam-blocked pMDI with polyol in different isocyanate ratios can be seen in Fig. 60. The intensity of absorption bands at 1711, 1221 and 916  $\text{cm}^{-1}$  were reduced by increasing isocyanate ratios from 1:1 to 2:1. The loss in those characteristic signals in mixture with 2:1 isocyanate ratios was unpredictable due to the adequate weight ratio between  $\epsilon$ -caprolactam-blocked pMDI with polyol (as calculated in 4.1.1.4).

For mixing with 1 g polyol,  $\epsilon$ -caprolactam-blocked pMDI with 2.16 g was required to produce PUR. Therefore, the sample with the 2:1 isocyanate ratio was proposed to have more related results to PUR. Moreover, the sample with the 3:1 isocyanate ratio exhibited even more differentiated results with its new sharp absorption bands, which appeared at 1109 and 962  $\text{cm}^{-1}$ . The former band is linked to C–O stretching observed earlier at 1221  $\text{cm}^{-1}$ . The latter signal at 962  $\text{cm}^{-1}$  possibly belonged to di-substituted C=C bending of benzene, as found earlier in the blocked adduct and cured products of NaHSO<sub>3</sub>-blocked pMDI (Fig. 53). However, the signal did not appear in the blocked adduct but only in the cured product with the 3:1 isocyanate ratio in the case of  $\epsilon$ -caprolactam.

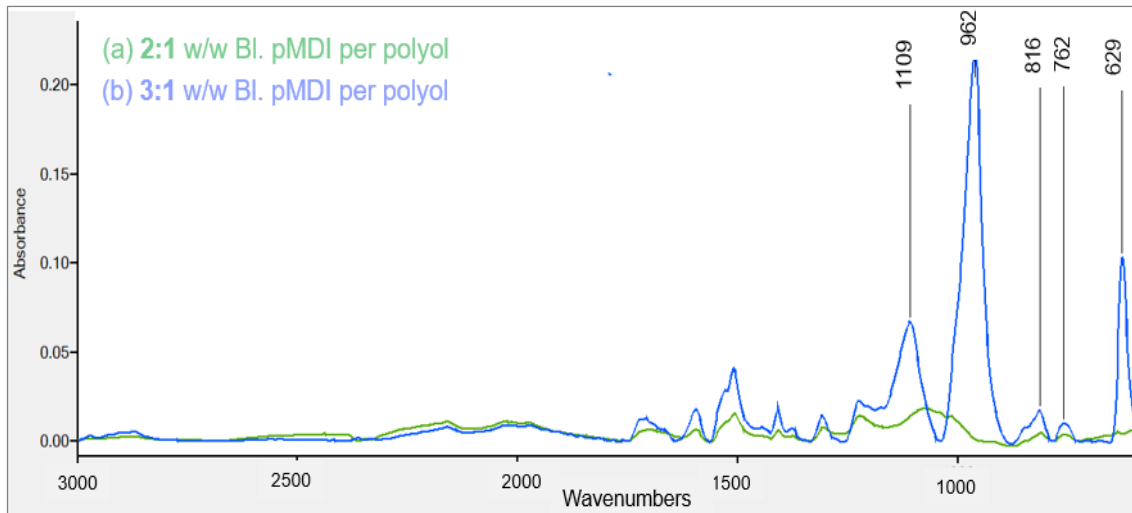


**Fig. 60** FTIR spectra of mixtures of  $\epsilon$ -caprolactam-blocked pMDI and polyol cured at 250 °C prepared in (a) 2:1, (b) 3:1 weight ratios

### ***Effect of curing temperature***

Blocked pMDI and polyol mixed by 1:1 ratio were cured at different temperatures and investigated for the IR characteristics, as illustrated by Fig. 61. Applying the higher curing temperature from 225 °C could induce the absorption band at 1703  $\text{cm}^{-1}$  (C=O stretching), which was mentioned earlier in the results of  $\text{NaHSO}_3$ -blocked pMDI. Additionally, the signal at 1225  $\text{cm}^{-1}$  (C-O stretching of C-O from N-CO-O) became more acute. However, the curing temperature of 250 °C can lead to more complimentary IR results in PUR than lower curing temperatures, regarding the similar intensity of signals at 2974  $\text{cm}^{-1}$ , 2872  $\text{cm}^{-1}$  (stretching vibration of C-H), 1074  $\text{cm}^{-1}$  (C-O-C stretching) in polyol as well as at 1508  $\text{cm}^{-1}$  (bending of N-H) in isocyanate segment.

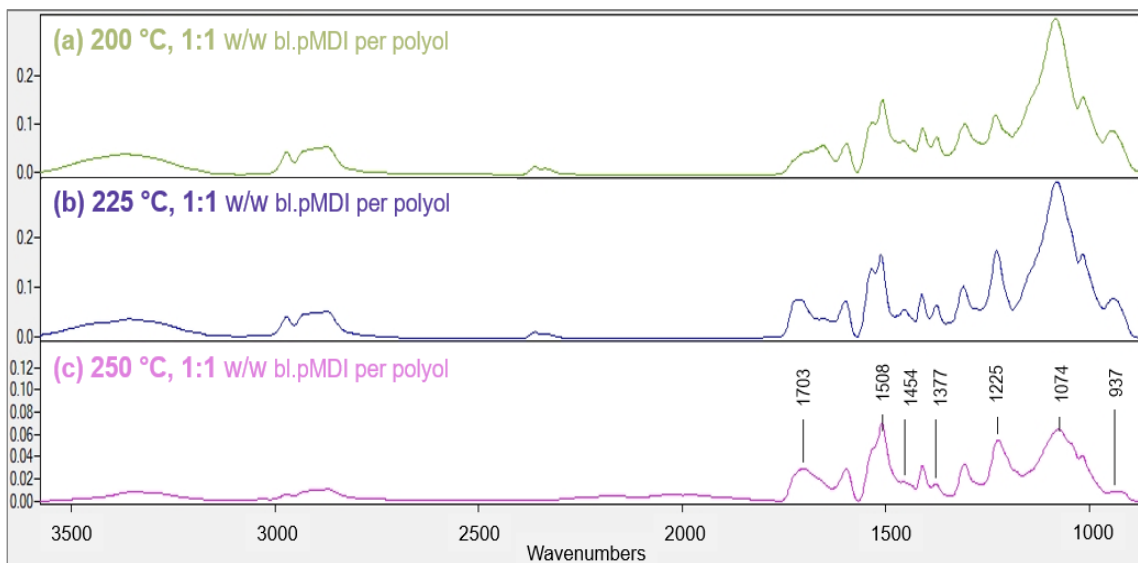
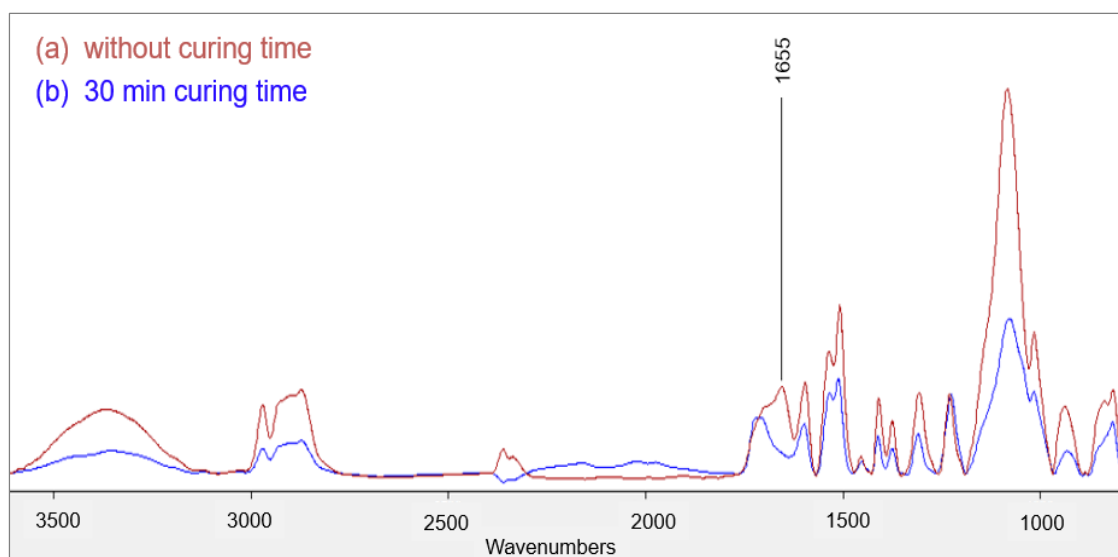


**Fig. 61** FTIR spectra of 1:1 w/w mixture of  $\epsilon$ -caprolactam-blocked pMDI and polyol cured at different temperatures: (a) 200 °C (b) 225 °C (c) 250 °C

### ***Effect of curing time***

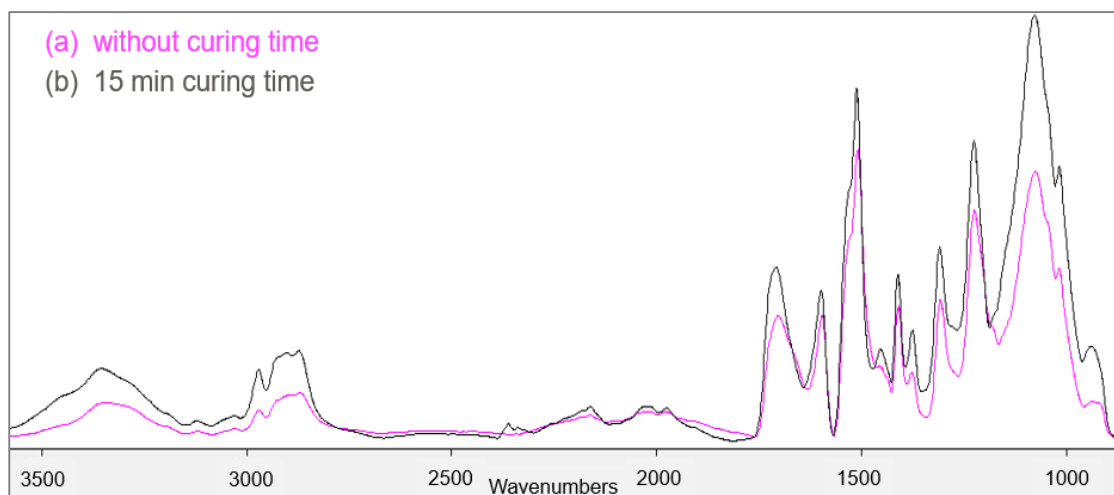
Mixture samples of blocked pMDI and polyol were cured at 200 and 250 °C as shown in Fig. 62 and 63, respectively. Both figures display the FTIR spectra of samples with and without curing periods. It appears that the curing time effected the IR results when a lower curing temperature of 200 °C was applied.

Fig. 62 reveals changes of absorbance in some signals with the existence of 30 min curing time. This transformation was found earlier in IR results affected by an increase of curing temperatures of 200 to 250 °C, for instance, the reduction of absorbance at 2974-2872 and 1074  $\text{cm}^{-1}$ , the shift of ester (C=O stretching) from 1655 to higher wave numbers. Furthermore, the absorbance in a range of 2330-1865  $\text{cm}^{-1}$  can be detected in the product with curing time. It is possibly related to the blocking agent, since the same absorbance was also found in the IR spectrum of  $\epsilon$ -caprolactam.



**Fig. 62 FTIR spectra of 1:1 mixture of  $\epsilon$ -caprolactam-blocked pMDI and polyol cured at 200 °C (a) without and (b) with curing period of 30 min**

Curing time of 15 min was added to a mixture sample heated at 250 °C, then the IR spectra of the cured product were compared to the product heated at the same temperature without curing session, as shown in Fig. 63. It appears that the curing time did not cause changes in absorption signals as high as in the lower curing temperature. IR spectrum measured from the mixed sample with curing time exhibited identical absorption bands as results from the sample without curing period. It could be assumed that some stable bonds were formed after the curing temperature of 250 °C was reached. Regardless of energy input by extended curing time afterward, the specific absorption bands rarely changed.



**Fig. 63** FTIR spectra of 1:1 mixture of  $\epsilon$ -caprolactam-blocked pMDI and polyol cured at 250 °C (a) without and (b) with curing period of 15 min

### ***Effects of isocyanate type***

$\epsilon$ -caprolactam-blocked 4,4'-MDI was investigated for PUR curing by mixing with polyol, then cured and characterized by FTIR spectrometry. The IR result is plotted and displayed in Fig. 64. The characteristic absorbance of polyol appeared to be intense despite the applied isocyanate ratio of 2:1, such as stretching vibration of C-H at 2970  $\text{cm}^{-1}$ , ether bond C-O-C stretch at 1084  $\text{cm}^{-1}$ . In contrast, the isocyanate segment did not seem to be as evident as in cured products of blocked pMDI. It can be explained by the absorbance at 1514  $\text{cm}^{-1}$  (N-H bending) and 1412  $\text{cm}^{-1}$  (O-H bending), which appeared earlier in sharp signals on the spectrum of PUR. The strong signal at 972  $\text{cm}^{-1}$  is associated with the substituted C=C bending of benzene of isocyanate as found earlier in the cured mixture of blocked pMDI with polyol.

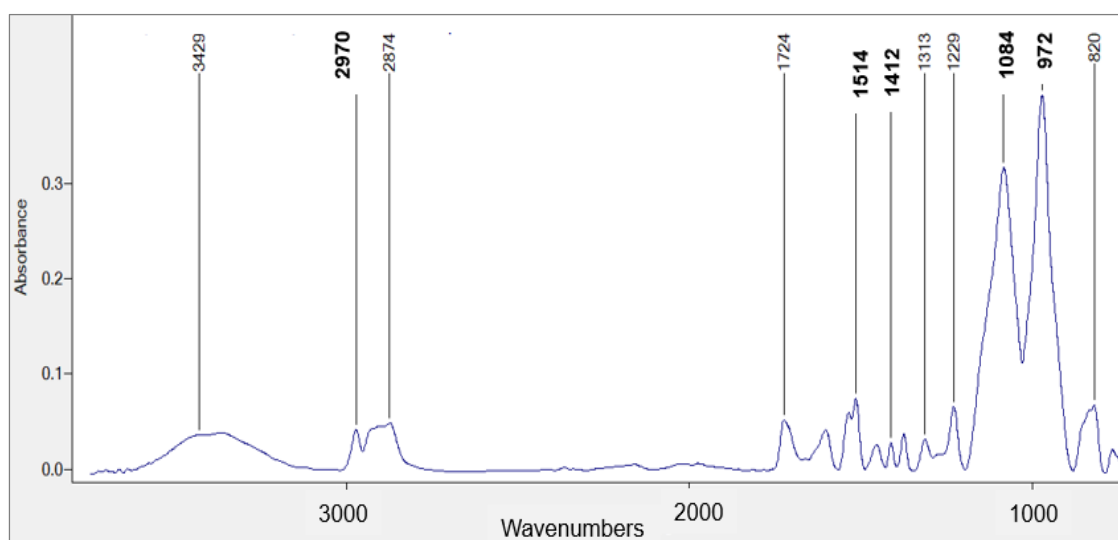


**Fig. 64** FTIR spectrum of 2:1 mixture of  $\epsilon$ -caprolactam-blocked 4,4'-MDI and polyol cured at 250 °C

### 5.1.5 Discussion

Isocyanate group of pMDI and 4,4'-MDI were successfully blocked by NaHSO<sub>3</sub> and ε-caprolactam according to the disappearance of the functional group at 2250-2265 cm<sup>-1</sup>. The deblocking temperature identified by the sharp endotherm transition in the DSC for both NaHSO<sub>3</sub>-blocked adducts was 90-127 °C, which corresponds to the optimal range for application in the one-step production process. For ε-caprolactam-blocked adducts, broad endotherm signals were observed in the thermograms between 180-226 °C. The blocking reaction was irreversible. The disappearance of the isocyanate group after heating could be described by the possible degradation reactions of the urethane bond presented by Delebecq et al. (2012). In their work, four degradation pathways of the urethane bond could be identified in a temperature range starting from 150 °C, as shown in the following diagram. The reverse reaction (a) was expected. However, dissociation (b) and amine formation (c) are possible but occur more slowly and at a higher temperature.

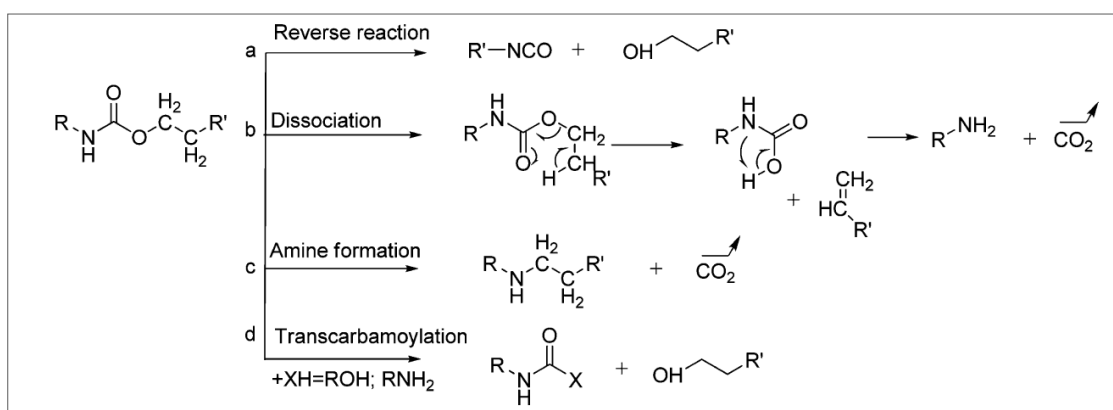


Fig. 65 Possible degradation reactions of urethane bond (Delebecq et al., 2012)

The deblocked isocyanate did not show the strong absorbance of the characteristic NCO group as intensively as the pure isocyanate. The NCO conversion rate ( $A_{NCO}/A_{ref}$ ) was identified in deblocked adducts using different times and temperatures. The NCO rate of deblocked ε-caprolactam at 225 °C was higher than that of the adduct blocked by setting it at this temperature but without a heating duration. Most of the deblocked samples show a lower NCO conversion rate than that of blocked adducts. Referred to the DSC result of commercial blocked isocyanate, the endotherm transition was also unobservable.

According to the IR result (Fig. 47), the higher the heating temperature, the more intensive the absorbance of CO<sub>2</sub> appeared to be. Furthermore, the released isocyanate can react with available active nucleophilic reagents in the system – which is amine from reaction b and c. For this reason, the low NCO conversion rate observed from the deblocked adducts is presumed to be originated from the side reactions of heating, a

potential additional reaction with the available nucleophile combined with methodic limitations e.g. impractical FTIR measurement in blocked adducts during the current deblocking status. The blocked isocyanates in solid form were then mixed with liquid polyol and heated.

The 1-C mixture from NaHSO<sub>3</sub>-blocked isocyanates exhibited the most comparable IR results to PUR when the weight ratio of blocked isocyanate per polyol of 2:1 and high curing temperature 250 °C were applied. The high curing temperature also generated the most comparable IR result to PUR in the case of ε-caprolactam-blocked adducts. On the contrary, the ε-caprolactam-blocked isocyanates showed better IR results in the mixture with a 1:1 weight ratio of blocked isocyanate per polyol. Apart from the weight ratio of blocked isocyanate and polyol, other factors (curing time, heating rate, and isocyanate types) did not appear to affect the cured mixture's IR results significantly.

## 5.2 Study II:

### Effects of wood addition and temperature on PUR foam

This section explores the effects of wood flour and temperature on PUR foam properties. In the first part, different methods for water adding were investigated for their effects on the foaming reaction. PUR foam samples were produced using different wood ratios and temperatures with regards to the selected water adding method. The following part shows the results of foam morphologies as well as chemical, physical and mechanical properties.

#### 5.2.1 PUR foam reaction analysis

In the pretest, three different methods for water adding were applied to the PUR thermal curing. The foaming reaction was measured by free rise height (FRH) and weight loss of the samples, as shown in Fig. 66. FRH is defined by the foam's height, in which the foam stops expanding as observed visually (ASTM D7487). The average (solid line) and deviation values (dashed line) of FRH are given in Fig. 66 (left). These curves indicate that the difference in FRH was not observed in both sample groups using water. However, samples without water had relatively lower FRH than both other groups. It could be attributed to the function of water as a blowing agent in PUR foam. The blowing reaction requires water to react with isocyanate for the development of CO<sub>2</sub> gas into the polymer matrix. The existence of water in the system is the main factor that induces foaming of PUR cured by heat, no matter whether it is water from wood flour or distilled water. This is described by the results of the weight loss presented in Fig. 66 (right).

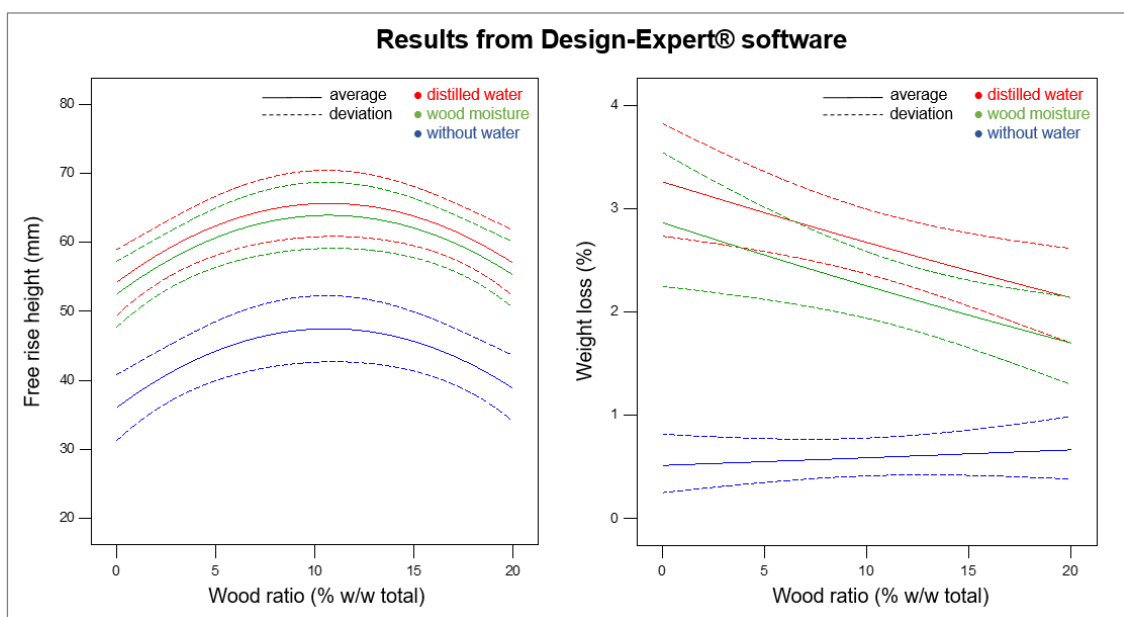


Fig. 66 (left) FRH, (right) Weight loss of PUR foam with 0-20 % wood contents (%w/w tot)

PUR samples blown by water exhibited a higher weight loss of approximately 2-3 % compared to samples without water, which had a mere with 0.5 %. Weight loss during the reaction is possibly related to water input methods and wood contents. With the increase of wood flour contents in PUR samples, the weight loss in water-blown samples declined. Although the majority of the weight loss was found at 0 % wood content in water-blown samples, the highest free rise foam appeared in samples using 10 % wood. The water evaporation could help the blowing reaction, so assumedly, weight loss can signify the foaming rate measured in FRH. Regardless of this, the highest weight loss in water-blown samples without wood did not show the greatest foam rise. It is important to notice that the foaming reaction in PUR depends on both the chemical and physical processes. The weight loss during foaming includes thermally evaporated water and the reacted CO<sub>2</sub> gas. The generated CO<sub>2</sub> may indicate the foaming rate. However, the loss of evaporated water could not suggest this, as it represents only the amount of gas coming from the polymer matrix. For that reason, no correlation between weight loss and FRH was found in this result.

## 5.2.2 PUR foam characterization

### 5.2.2.1 FTIR characterization

The FTIR spectra of pure and PUR foam with 12 % wood flour content are presented in the next figure. A new signal of formation did not arise by filling wood flour into the PUR foam, which is comparable to FTIR results of olive kernel and nutshell reinforced PUR studied by Demiroğlu et al. (2017); neither fibers caused a change in the chemical structure of PUR. Both FTIR spectrographs evidenced the urethane bond (-NHCOO-) that reacted between polyol and isocyanate. The sharp absorption bands at 1708.8 and 1223.7 cm<sup>-1</sup> correspond to the stretching vibration of -C=O and asymmetric stretching vibration of -C-O in urethane. The -NH stretching vibration of urethane is given at 3320.1 cm<sup>-1</sup>. Isocyanate and polyol segments appear via identical absorption bands, according to Jiao et al. (2013) (see Appendix I). According to the locations of functional groups in their study, absorbance units in bold numbers are represented for isocyanate and those in thinner numbers for polyol segments in Fig. 67. The signals near 2874-2966 cm<sup>-1</sup> belong to the stretching vibration of C-H in methyl or methylene. The ether bond -C-O-C from polyol is confirmed by a broad and strong band found at 1070 cm<sup>-1</sup>. For isocyanate segments, the absorption in 1594 cm<sup>-1</sup> is caused by the vibration of C=C in the benzene ring. The several weak signals between 763-915 cm<sup>-1</sup> belong to the bending vibration of C-H in the multi-substituted benzene ring. Aside from the related findings, the evident band at 2276 cm<sup>-1</sup> can show the existence of some

unreacted isocyanate monomers. This weak signal assigned to isocyanate was observed in other studies (Demiroğlu et al., 2017; Jiao et al., 2013; Trovati et al., 2010).

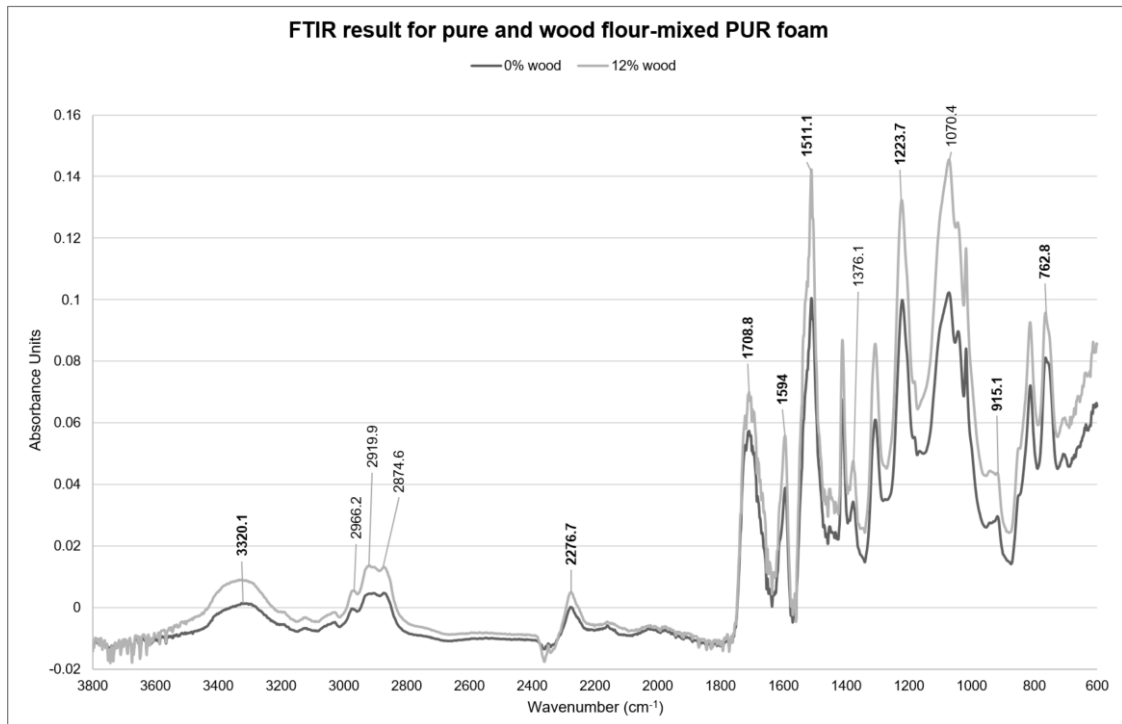


Fig. 67 FTIR spectra of pure and wood-mixed PUR foam

### 5.2.2.2 Foam morphology

An application of light microscopy and SEM can reveal cell structure and morphology. Samples cut perpendicularly to the foam rise exhibited uniformly distributed cells with the shape of irregular polyhedral. SEM showed a closed-cell structure without the connection to each other. Wood-mixed PUR exhibited some features unobserved in pure PUR samples but detected more frequently in samples with higher wood contents. This foam morphology was discovered and divided into three main characteristics: microvoid, strut with embedded filler and spotted cell wall. They are identified by the following figures and descriptions:

1. Microvoid is defined by small bubbles nucleated largely in the polymer matrix of the strut (Fig. 68) or the connection area between multiple cells (Fig. 69). It may be assumed that microvoids came into existence as they could not merge into the neighboring larger cells caused by prior consolidated polymer mass around them. For this reason, generated bubbles were unable to expand after matrix formation.



**Fig. 68** Microvoids found in 2 % wood-mixed sample built in the center of cell intersection

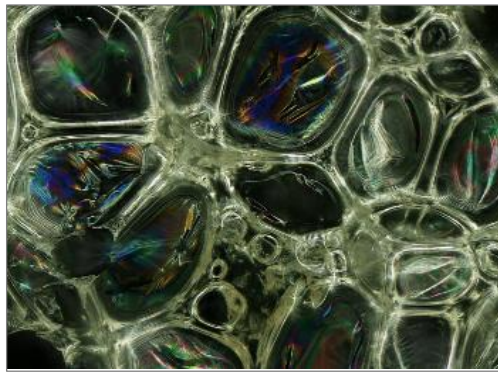


**Fig. 69** Several microvoids located in the polymer matrix in 6 % wood-mixed sample

2. Filler embedded in the struts between cells is visible in Fig. 70 and 71. The addition of filler into plastics can induce agglomeration, which existed in struts between cells, where filler and PUR components did not develop into cells. It is evidenced that fillers could not be dispersed effectively. However, grain filler, built into the struts, was also visible in a previous study (Prociak et al., 2015). From their review, it seems to be a common phenomenon when mixing filler into PUR foam, that fillers are then mostly located in the struts. Kurańska et al. (2015) confirmed the same effect of wood fiber; this being that when the amount of filler was increased, the fibers tended to be located in the thin cell walls.

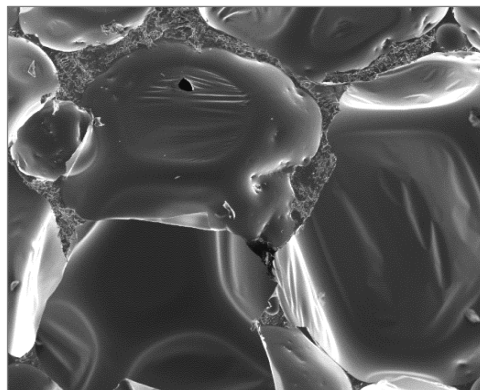


**Fig. 70** Thick cell wall formed by irregularly distributed filler from 8 % wood-mixed sample

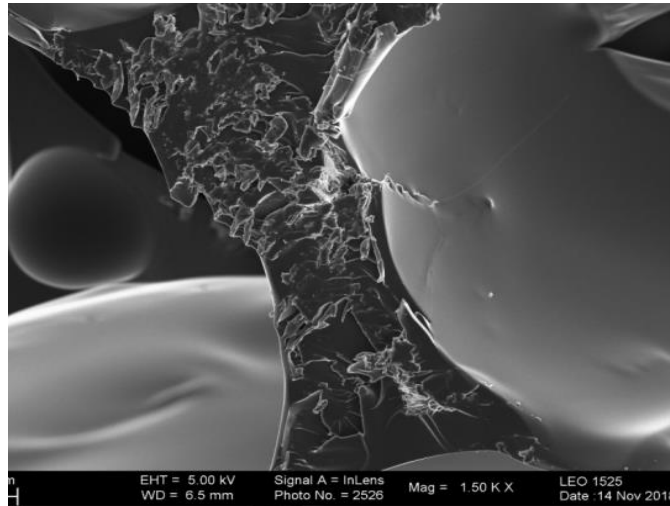


**Fig. 71** Rough surface structure of cell strut embedded by filler in 4 % wood-mixed sample

3. The spotted cell wall by filler can be seen only in the SEM analysis. Fig. 72 presents the cell wall attached by distributed small particles; it is not completely clear whether they were located within or on the cell wall. Compared to the aforementioned characteristics, this feature was reported less in the publications. It should be described by its minor effect on the mechanical strength in comparison with the last characteristic.

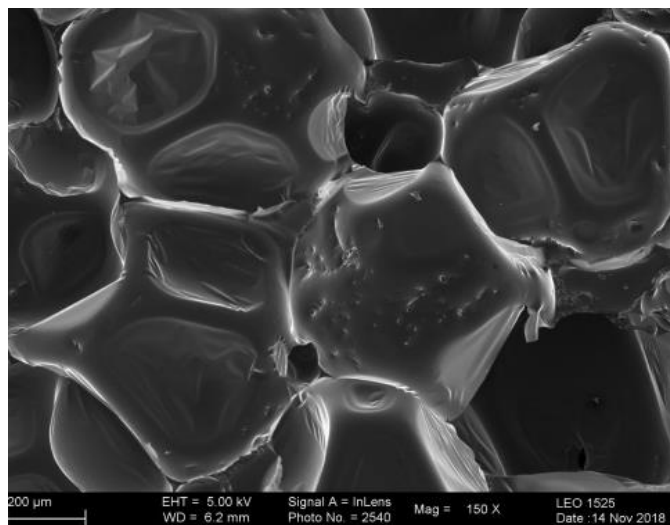


**Fig. 72** Cell appearance with spotted cell wall found in 12 % wood-mixed sample

With the increase in wood content, it was likely these characteristics in the foam structure would be observed. The appearance of microvoids and filler in the polymer matrix can signify the quality of foaming, the dispersion of filler in the polyol premix and its compatibility with PUR raw materials. It could also suggest a better method of foam preparation. As confirmed in research by Demiroğlu et al. (2017), the filler can affect the nucleation mechanism, therefore, resulting in altered foam morphologies. The incorporation of filler in struts can have an advantageous effect due to improved rigidity.

On the other hand, it can increase the amount of cell damage. However, the location of the filler is not the only factor that resulted in cell formation. Still, filler size and shape are factors that regulate the filler's location and should be taken into account. For example, overlong fiber or fillers with a size larger than the cell walls may damage the cell.

### 5.2.2.3 Material characterization by EDX

As mentioned before, images from SEM analysis have revealed cell morphology, for example, cell shape and alignment, as well as the location of wood flour within the polymer matrix. To investigate the presence of wood flour, some specific image areas were selected for element analysis. In this section, the filler distribution was divided into two groups: spotted PUR surface (Fig. 73 b-e) and embedded filler with PUR (Fig. 73 f-h). Two reference areas in Fig. 73a and i represent the PUR surface and filler, respectively.

Fig. 74 contains the atom percentage of C, N, and O of the investigated areas (Fig. 73 a-i) compared to the calculated values from reference materials. The calculation method can be found in Appendix II. From all three elements, N is the only element that is not present in cellulose filler but in isocyanate and pure PUR matrix. It corresponded to the result of investigated areas in Fig. 73 a and i, which were expected to be PUR and cellulose, respectively. N atom percentage was decreased gradually from 16.71 % in PUR > avg. 14.56 % in spotted PUR surfaces (b-e) > avg. 10.68 % in areas with PUR-embedded filler (f-h), whereas an increase in O atom percentage was observed in the same order. These findings confirmed the different distribution of cellulose flour in the polymer cell, in which poor distribution tended to arise in the strut and was noticeable as a thick cell wall. For cellular material, higher cell wall thickness can sometimes enhance mechanical properties. However, this can be disadvantageous in the case of irregular distribution. An embedded strut with high filler content constructs irregular cell walls and often leads to cell inhomogeneity, which can cause failure in the structure when absorbing force.

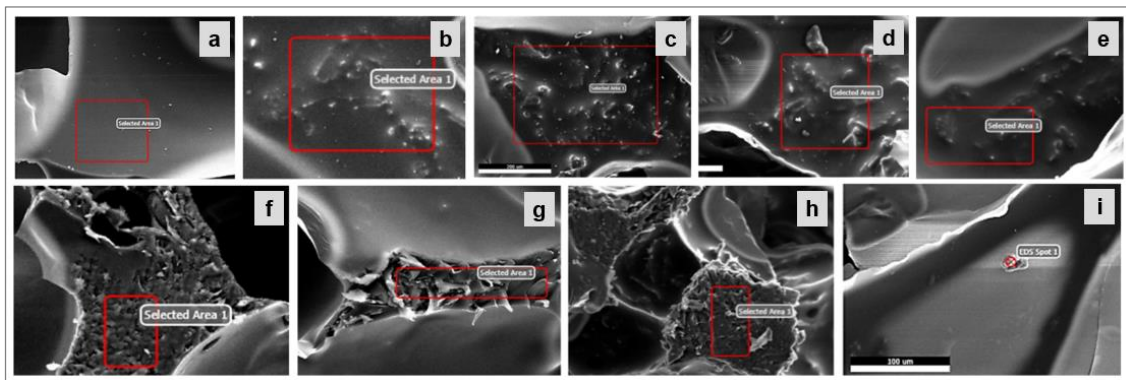
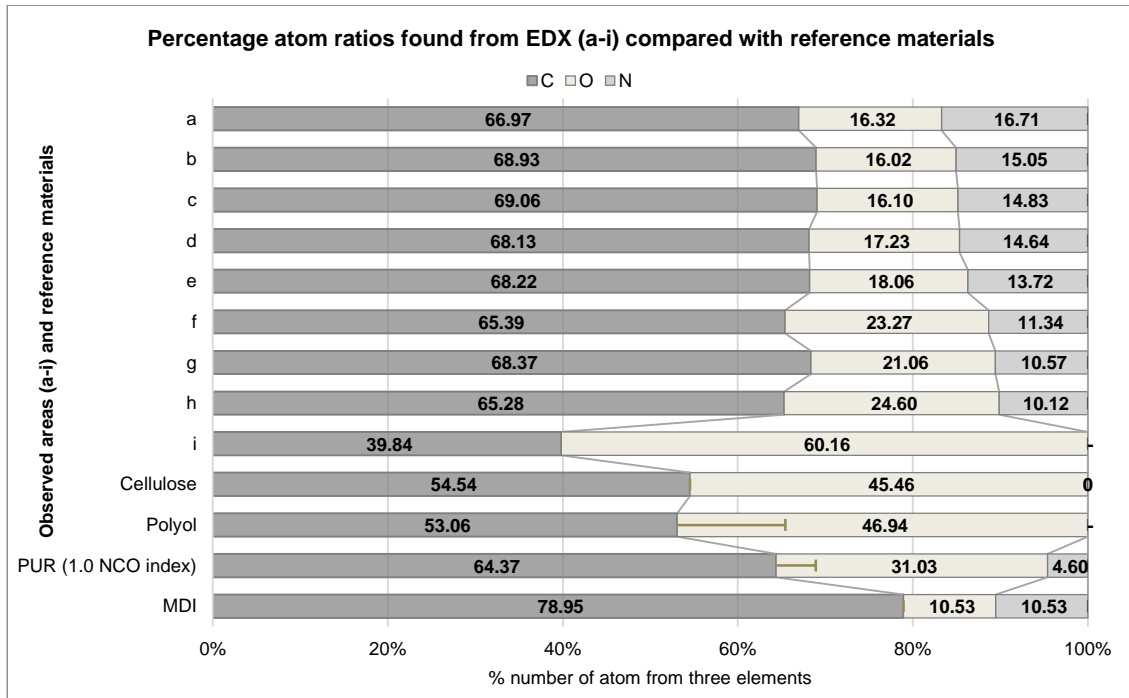


Fig. 73 a: Polymer surface, b-e: Spotted surface, f-h: Embedded filler with PUR, i: Filler particle



**Fig. 74 Percentage atom ratios of C, O, N in observed areas (Fig. 73 a-i) related to calculated values of reference materials**

#### 5.2.2.4 Open-cell content

Heat-cured PUR samples with filler contents varying from 0-10 % were composed of ca. 56-65 % of closed-cell and resin volume, as listed in Fig. 75. It is apparent that in the majority of cases, the measurement from both experiments revealed closed-cell contents lower than that of most rigid foams reviewed by Szycher (2012), which was 85-95 %. The wood flour contents did not significantly change the percentage of closed cells. However, only a minor growth of closed cells from the pure to filled PUR groups could be observed. Controlled PUR without the addition of wood flour appeared to contain more open-cell volume than PUR using various wood flour contents. This result contradicted past studies (Kurańska et al., 2015; Prociak et al., 2015) where introducing biocomponents into the reference system reduced the closed-cell content by approx. 17 % (Prociak et al., 2015). The reason given by Kurańska et al. (2015) was that the increase of wood filler contents generated an increased chance that part of them would be located in the cell walls, causing an accumulation of open cell content in these foams. The thickness of cell walls was measured in various PUR samples in this study at  $42.02 \pm 10.33 \mu\text{m}$ , while wood flour C100 has a particle size between 70-150  $\mu\text{m}$ , as described in the product information. Therefore, the former explanation would be relevant, though the current result does not show the same trend when increasing wood filler content. According to SEM analysis, it can be seen that wood flour combined with the polymer matrix into two locations: it either attached into the inner cell wall or embedded within the cell strut. The existence of the filler shown in Fig. 71 and 72 did not seem to break the cell wall.

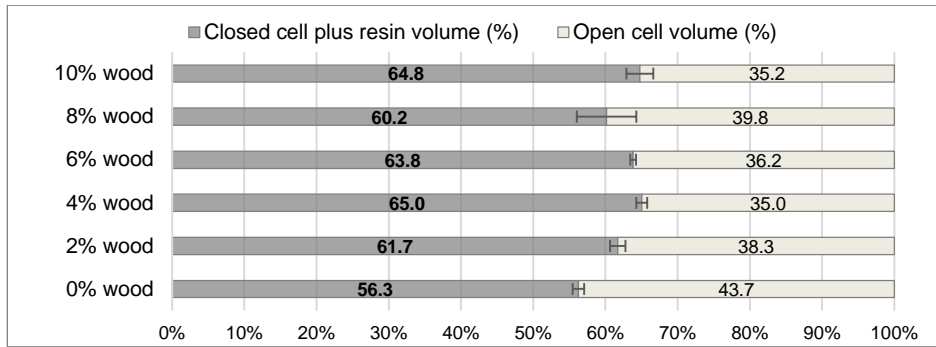


**Fig. 75 Open and closed-cell proportion of PUR foam with 0-10 % wood contents**

The results of PUR samples produced by wood flour contents of 10 and 20 % using various curing temperatures, are presented in Fig. 76. With regards to the heat-cured samples, a higher open-cell percentage was observed in samples with 20 % than those with 10 % filler content. A considerably high content of closed-cell volume between 84-89 % was evidenced in PUR samples with 10 % filler content cured at 100-140 °C. In contrast, PUR foam cured at room temperature exhibited a very low percentage of closed-cell volume at 7.5 %, which differed from past studies where the foams reacted at normal conditions. Significant lower closed-cell content was likewise found in PUR with 20 % wood content when cured at the lowest temperature of 90 °C. This result could be explained by the cell’s appearance using SEM (see Fig. 76). Some open windows with a smooth edge could be identified in the foam structure of a sample cured at room temperature. An open window was not as large as in the flexible foam, in which remained only the plateau border or strut. However, any large or small window can make a cell open, which is undesirable if low water absorption and moisture permeability are purposed for the foam application.

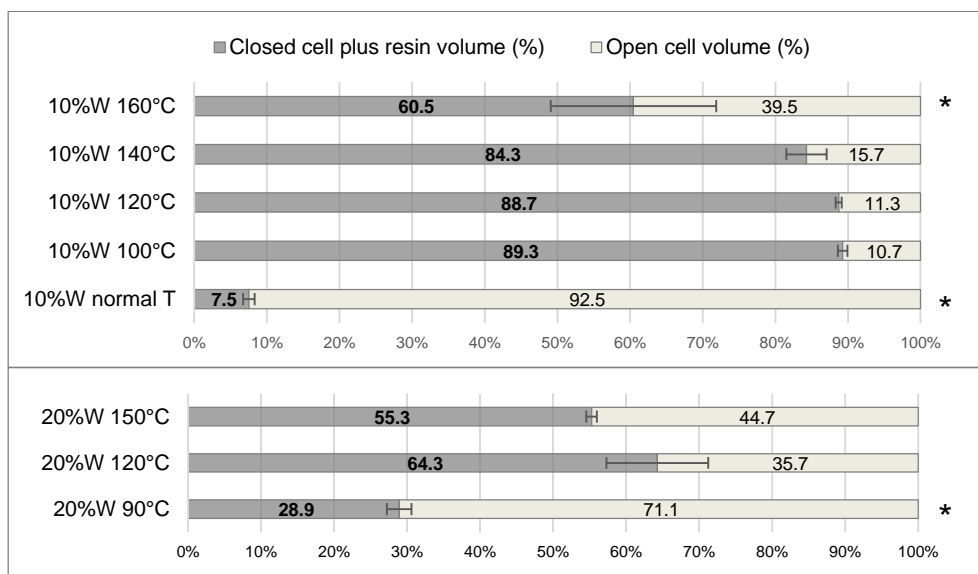


**Fig. 76 Open and closed-cell proportion of PUR foam mixed by 10, 20 % wood contents cured at different temperatures**

Lee & Ramesh (2004) described the formation of broken cell windows with different morphologies, which partly depend on window thickness distribution. For open windows with a smooth edge as found here, it originated at the early stage when the foam matrix still had high flowability. The thinner windows would rupture and flow back to the struts, and the smooth edge would be obtained. Other important factors involving the closed-cell volume are the degree of crosslinking, the surfactant used during foaming and the polyol equivalent weight. In spray applications, the degree of mixing is sometimes influential on the closed-cell content (Szycher, 2012).

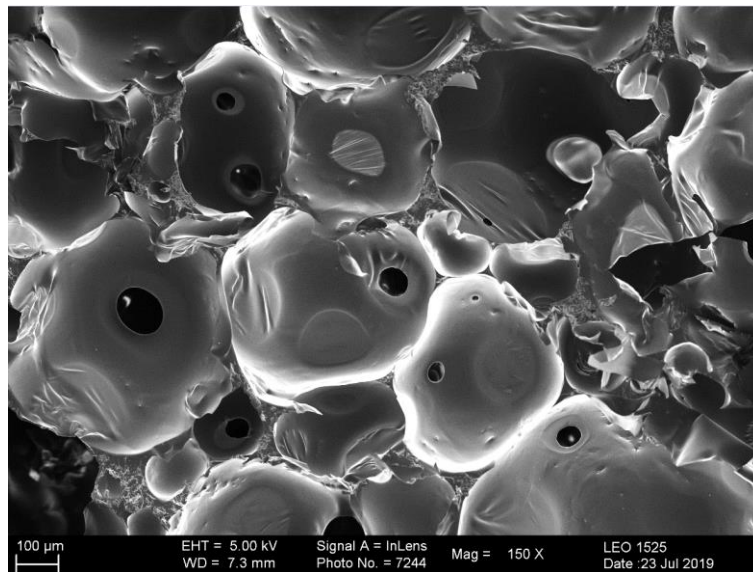


**Fig. 77 Morphology of PUR foam with 10 % wood content cured at room temperature**

On the one hand, the rise in the open cell content by higher curing temperatures i.e. 10%W 160°C, 20%W 150°C, resulted from the rapid foam expansion leading to thin cell walls that were likely to be broken during cell development. On the other hand, heat can enhance the reaction kinetics and accelerate the tack-free time, which prohibited the cell from further expansion and stabilized the cell wall. The raised curing temperature should be the reason for the increased closed-cell contents in some variables. Despite the difference in curing temperatures, the open cell content of 10%W 100°C and 10%W 120°C remained unchanged. Introducing heat into the system did not necessarily alter the contents of open and closed cells. It depended on how and when the heat contributed during the cell development and is controlled explicitly by the previously mentioned factors. It can describe the effect of a curing temperature on open and closed-cell contents in different ways.

### 5.2.2.5 Cell size

Cell size can be characterized by the diameter of foam cells and cell density. The distribution of cell diameter from both experiments is displayed in boxplots without outliers (Fig. 78-80). In most cases, the results of samples from both tests had relatively high deviation.

According to Fig. 78, the cell size of PUR foam had a distinct distribution, which was dependant on the differing wood contents. Adding a low amount of wood flour as shown in the results with a wood content of 2 and 4 %, both the cell size and cell distribution decreased. Therefore, PUR mixed with a lower content of wood, showed a higher homogeneity in cell size than in pure PUR. Zhu et al. (2012) also found that the neat PUR foam had a lower number of cells and larger cell sizes than reinforced PUR foams with fiber and nanoclays. This can be explained by the function of fillers as nucleating agents with regards to cell growth, which result in an increase in the total number of nucleated cells as well as decreased cell sizes in the reinforced foams.

A change in the average cell size was unobservable when using wood flour with contents of 6-12 %. However, the addition of wood seemed to increase the distribution in cell size, particularly in sample groups with 6 and 12 % wood contents, as shown in the boxplot (Fig. 78). The average cell size of PUR mixed by 0-12 % of wood flour appeared between 244-397  $\mu\text{m}$ , which was larger than the 180  $\mu\text{m}$  cell diameter of conventional rigid foam, according to Engels et al. (2013). The study defined cell size as a very fine cell structure, having a diameter of less than 150  $\mu\text{m}$ .

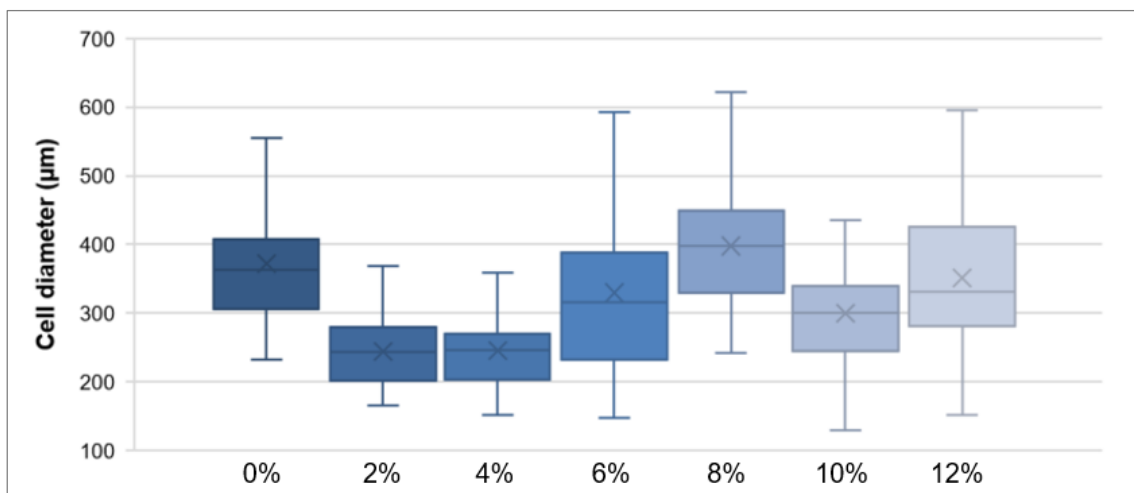
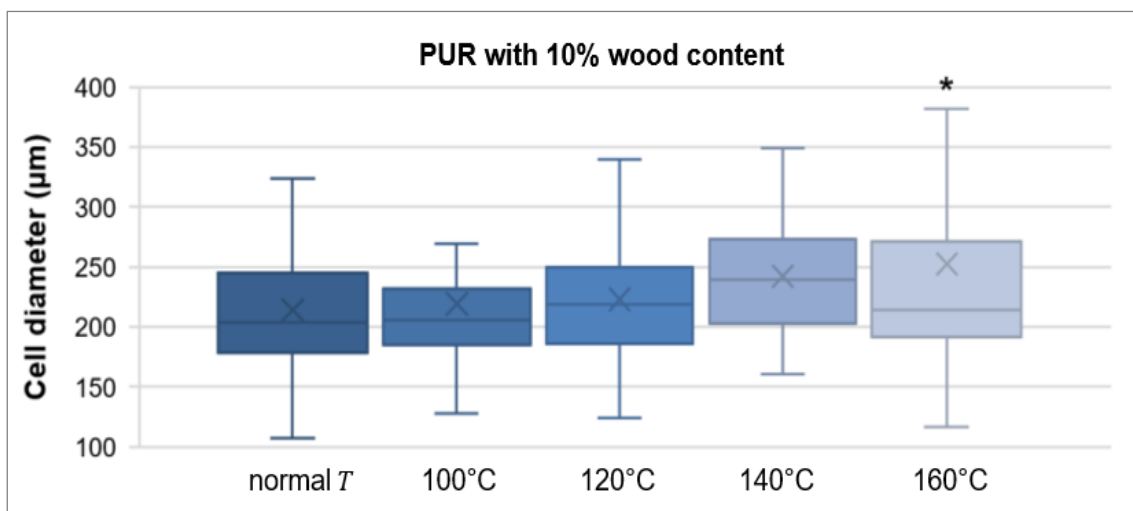


Fig. 78 Cell size distribution and averages (x) of PUR foam with 0-12 % wood contents

The results of the samples produced at different temperatures are represented in Fig. 79 and 80. It is apparent that in the majority of cases, the average cell size of samples from both PUR foam formulations with 10 and 20 % exhibited comparable values between 214-250  $\mu\text{m}$ . The standard deviation was revealed to be 100 to over 200  $\mu\text{m}$ , as high as in the last result. Using varied reaction temperatures for PUR preparation did not increase the cell diameter as expected. The largest distribution in cell size occurred at the highest test temperature of 160 °C. For PUR with 10 % wood content, no significant difference in cell size between the sample groups from room temperature to 140 °C, was found. Elevated temperatures during foam preparation were only likely to influence the cell diameter of PUR foam at 160 °C.



**Fig. 79 Cell size distribution and averages (x) of PUR foam with 10 % wood content cured at different temperatures**

In samples using a wood content of 20 %, significantly higher cell diameter was found only between sample groups using 120 and 150 °C. It is known that the reaction of PUR is exothermic and the generated heat is used to change water into steam to help expand the foam. Therefore, this transportation of water from its boiling point at 100 °C could increase the foaming rate. Despite the higher foaming rate at the elevated temperature, a change in the cell diameter was rarely found. Apart from water, applying heat for foaming also affects the polymer's viscosity, and gas concentration in the matrix. Both variables are factors that control the foam growth process (Lee & Ramesh, 2004). The influence of heat on the chemical foaming process could explain the cell diameter result more thoroughly than that on the physical foaming process.

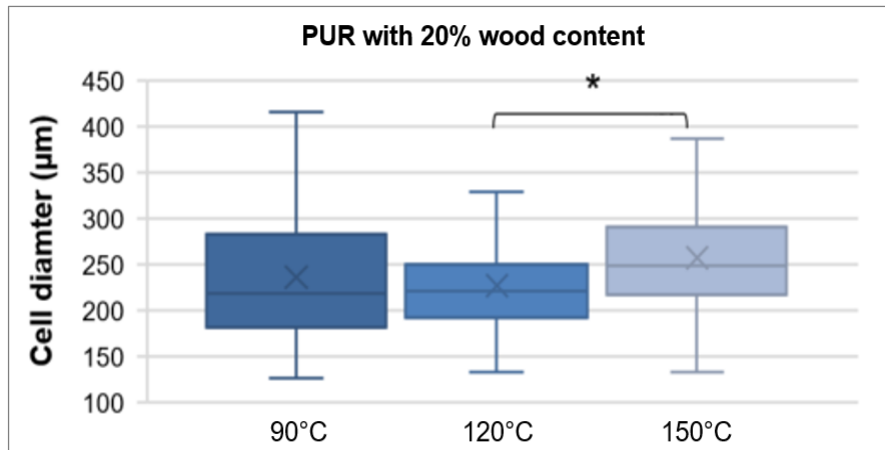


**Fig. 80 Cell size distribution and averages (x) of PUR foam with 20 % wood content cured at different temperatures**

Fig. 81 and 82 reveal the changes in cell density affected by the wood flour contents and curing temperatures, respectively. The cell density from the sample group with 20 % wood contents was undefined by SEM due to a defect in some areas; thus, their results cannot be shown here. Data in Fig. 81 suggests that the average cell size, which was larger than 300 µm, fit with cell density lower than 10,000 cells cm<sup>-3</sup>, except for the 6 % wood content group. A high variation in cell density was found in cells with a shorter diameter. Regarding cell diameter, the cell density between groups with wood contents of 2 and 4 %, differed by over 11,000 cells cm<sup>-3</sup>. Results from the group without the addition of wood and higher wood contents exhibited comparable cell diameters and densities. After all, both cell size measurements seem to have some correlations but were independent of the PUR samples' wood flour content.

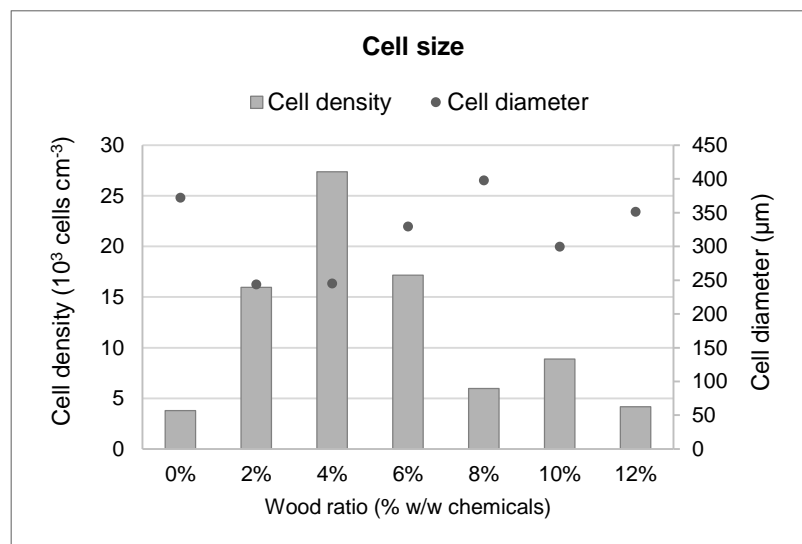


**Fig. 81 Cell density of PUR foam with 0-12 % wood contents**

Results of PUR samples cured at varying temperatures are given in Fig. 82. Despite the similar cell diameter values, the deviation in cell density still appeared in this experiment.

The difference of cell densities from the room and high-temperature curing was estimated to be ca. 10,000 cells cm<sup>-3</sup>, as discovered in the last result. It can be assumed that the thermal curing affected only the cell density but not the cell size. For heat-cured PUR foam, sample groups produced at 100, 120 and 140 °C had comparable cell diameters and densities.

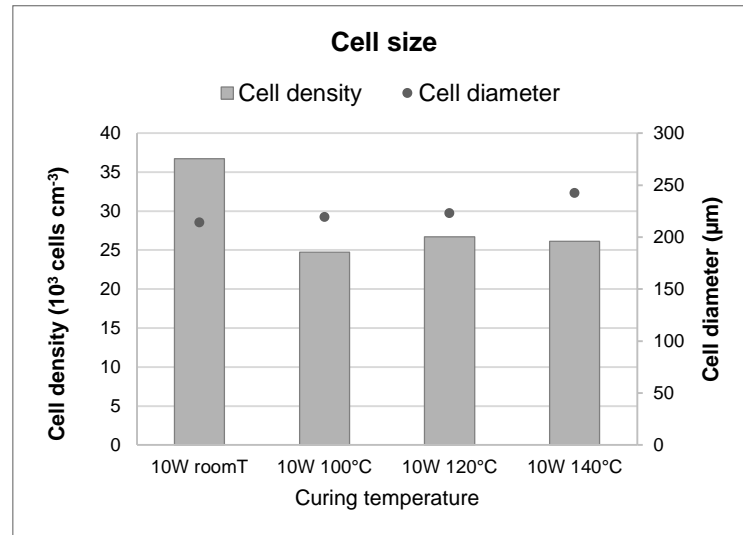


Fig. 82 Cell density of PUR foam cured at different temperatures

According to Han et al. (2003), a relation between the cell size  $D$  (diameter in cm) and cell density  $N$ , which is a number of cells per unit volume in cells cm<sup>-3</sup>, can be given as:

$$\text{Void fraction } (Vf) = \frac{\text{volume of cells}}{\text{volume of foam}} = N \cdot \left( \frac{4}{3} \pi \left( \frac{D}{2} \right)^3 \right) \quad (18)$$

$$\text{If } Vf \text{ is constant, then } D = k \cdot N^{-1/3} \quad (19)$$

The equation indicates that the cell size is inversely proportional to  $N^{1/3}$  at the same void function. Void fractions from the result mentioned above are calculated and included in Fig. 83, compared with cell size and cell density. The diagram supports the correlation between cell diameter and cell densities, which can be revealed in a power function:  $y = 542.17x^{-0.253}$ . The power of cell densities (-0.253) was higher than that value in the reference equation (20), approximately -0.333. Thus, this experiment appears to produce a higher cell diameter than estimated previously, with regards to identical cell density and void fraction. The result from samples where 6 % of wood flour is located out of the calculated area. Void fractions of heat-cured samples using 0-12 % wood contents were spread between 10-20 % in this study, except in the case of the aforementioned 6 %. The calculated void fractions are presented in Tab. 19, related to curing temperatures and wood flour contents. The alternation of a void fraction by increasing wood flour contents or curing temperature was not completely observable. The increase of wood

contents in PUR foam improved the void fraction until reaching its maximum of 6 % filler. After that, the fraction fell due to the elevated filler contents. Raised curing temperatures may increase the void fraction from 100 to 140 °C, though PUR samples cured at normal temperatures had, contra to this, a higher void fraction in this range, than those cured at 100 and 120 °C. Changes in void fraction by the use of wood flour or thermal curing were observed and found to be possible in both ways; hence the void fraction itself can change with many parameters (Han et al., 2003).

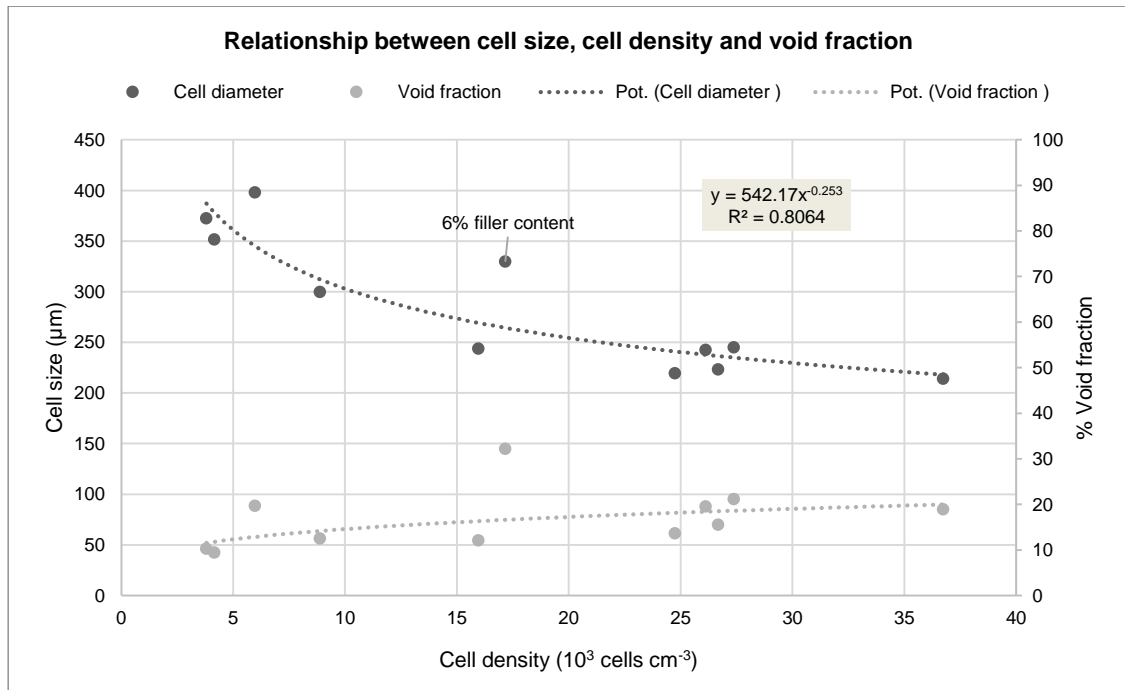


Fig. 83 Void fraction percentage and cell size in relation to cell density

Tab. 19 Void fraction percentage depending on filler contents and temperatures

| Results of different wood flour contents |        |       |       |       |       |       |      |
|--|--------|-------|-------|-------|-------|-------|------|
| Filler content (%)                       | 0      | 2     | 4     | 6     | 8     | 10    | 12   |
| Void fraction (%)                        | 10.27  | 12.11 | 21.11 | 32.21 | 19.70 | 12.52 | 9.44 |
| Results of different temperatures        |        |       |       |       |       |       |      |
| Curing temperature (°C)                  | normal | 100   | 120   | 140   |       |       |      |
| Void fraction (%)                        | 18.86  | 13.66 | 15.50 | 19.49 |       |       |      |

5.2.2.6 Foam densities

Sample densities and FRDs of specimens using varied wood contents are reviewed in this section. In the pretest, results from PUR samples blown by distilled water and wood moisture are compared by their FRDs, as shown in Fig. 84. FRD values remained constant from 0 to 10 % wood flour contents before starting to increase on higher wood flour contents, where the wood flour content had a critical impact on the FRD of samples blown by both methods. At this level, samples blown by wood moisture presented slightly higher FRD than those blown by distilled water with a difference of 20 kgm<sup>-3</sup>. According

to the dependent paired T-Test, the density was significantly higher in wood moisture groups, but the independent test showed no significant difference. Therefore, the water addition method could have a minor effect on the FRD for the same sample type.

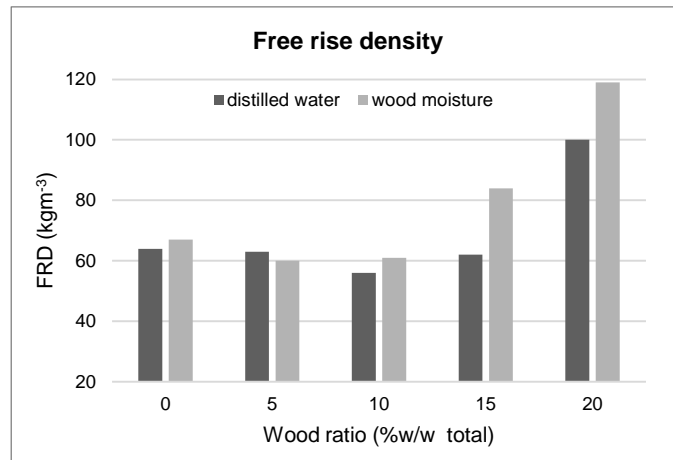


Fig. 84 FRD of PUR foam with 0-20 % wood contents

Sample densities and FRDs of PUR with a filler addition of up to 40 % are illustrated by Fig. 85. Both types of densities varied insignificantly from wood contents of 0 to 30 % until the highest contents of 40 %, where the average densities rose to ca. 90 kgm<sup>-3</sup>. In most cases, FRD and sample densities exhibited comparable values. The significant difference between sample density and FRD was unobserved according to the dependent paired T-Test. As the wood flour contents rose, change in densities could be observed from a content of 30 to 40 % of wood flour content. The ANOVA test among sample groups with 0, 20 and 40 % wood ratios showed a significantly higher sample density in the sample group with a 40 % wood ratio. The growing density in wood-mixed PUR with a higher wood content was probably attributed to the increased viscosity of the polyol mixture with the wood flour (Yuan & Shi, 2009).

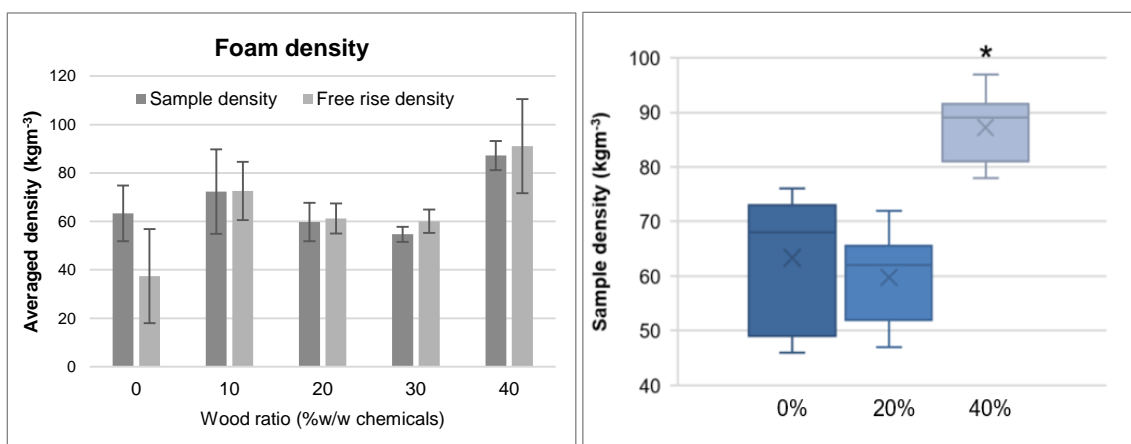
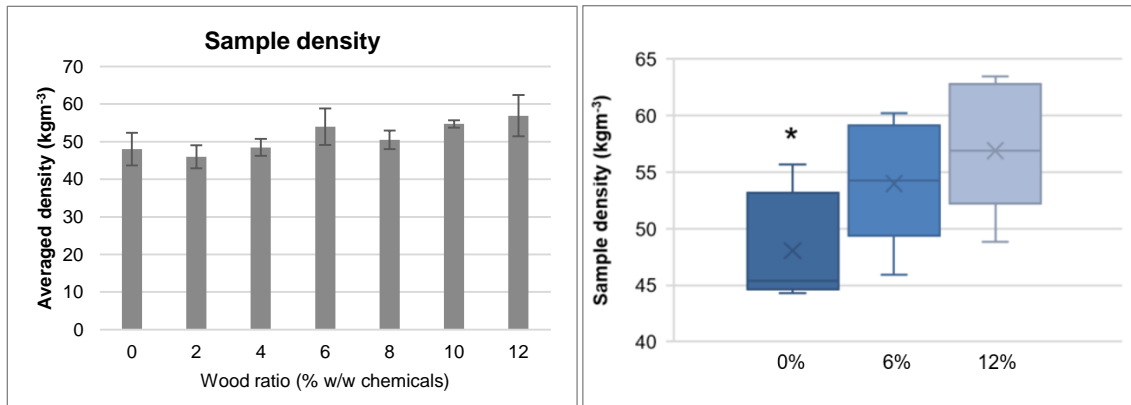


Fig. 85 Sample density and FRD of PUR foam with 0-40 % wood contents

Fig. 86 Density distribution of sample groups using 0, 20 and 40 % wood contents

In Fig. 87, the result of OVEN2 displays sample densities for every 2 % increase of wood contents between 0-12 %, where the average density appears to improve gradually by the increasing level of wood. The density remained unchanged for the small differences in wood flour ratios i.e. from 0 to 2 and 4 %. This trend conformed to the density results from OVEN1. However, neat PUR showed a significantly lower sample density than PUR containing wood contents of 6 and 12 % according to the ANOVA test among those groups, as illustrated in Fig. 88.



**Fig. 87 Sample density of PUR foam with 0-12 % wood content**

**Fig. 88 Density distribution of sample groups using 0, 6 and 12 % wood contents**

Not only wood flour content had an impact on the foam density but also the reaction temperature. Foam samples prepared at room temperature without heat input had a significantly higher density than those cured by heat, which was estimated to be twice as much when compared to results from 100 °C, as can be seen from Fig. 89. The high difference in the density level cannot be found among heat-cured samples at varied temperatures, where the densities of heat-cured foam were averaged at 48.03 to 69.17 kgm<sup>-3</sup>. Foam density tended to fall with an increase in reaction temperatures but the significant difference among heat-cured sample groups could not be verified.

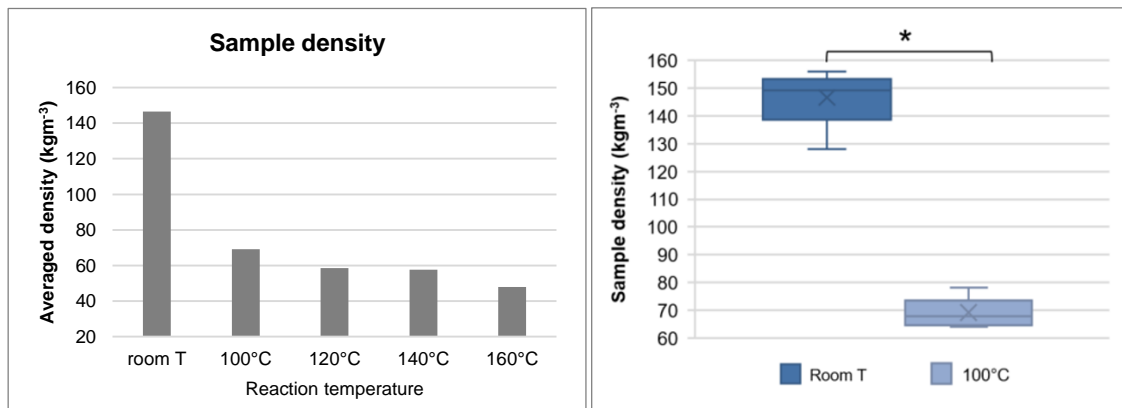


**Fig. 89 Sample density of PUR foam cured at different temperatures**

**Fig. 90 Density distribution of sample groups cured at room temperature and 100 °C**

### 5.2.2.7 Compressive properties

As illustrated in Fig. 91 and 92, compression strength and Young's modulus show the same change according to the wood concentration. Compressive properties were greatly improved from the 0 to 10 % wood-added samples, dropping afterward with higher wood contents. The average compression strength in samples with a wood content of 10 % sank from approximately 0.190 to 0.009 MPa at 40 % wood content. For all that, when adding wood flour up to 20 %, the compressive properties of PUR samples maintained acceptable values compared to the reference material. The significantly lower compressive strength was found in PUR samples with a wood content of 40 %, when compared with the groups containing wood contents of 0, 20 and 40 %.

The results confirmed the same findings from a past study (Krishnamurthi et al., 2003), where the specific compressive strength or strength-to-density ratio decreased on increased according to the wood flour content. The study explained this significant effect of filler content on relative compressive strength by these reasoning: 1) moisture contents of fillers; 2) generated initial CO<sub>2</sub> bubbles on the filler surface via the chemical reaction between isocyanate and water; the latter phenomena can create many locations called “tearing of continuity”, existing at the particle-binder. These imperfections and defects within the physical microstructure caused a drastic drop in the compression strength.

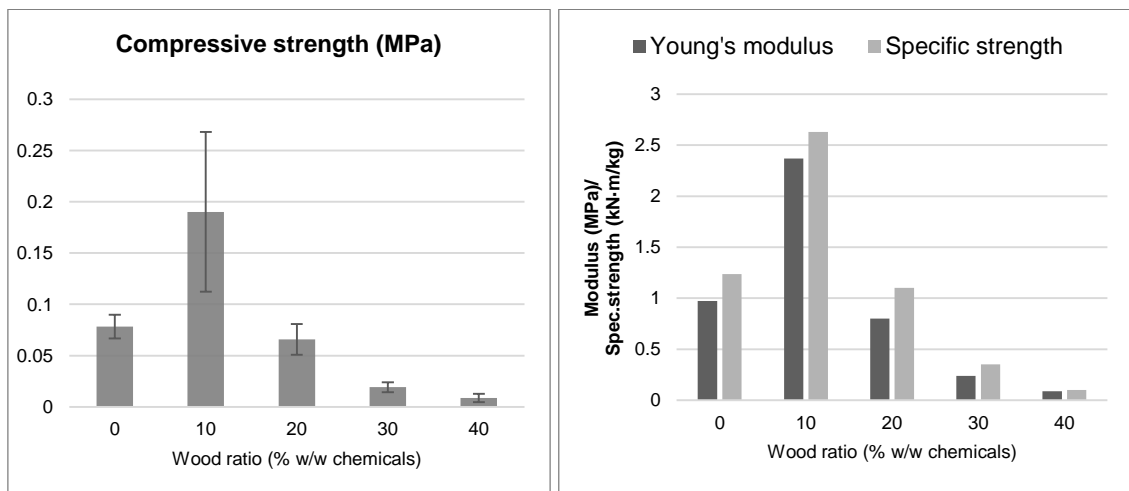


**Fig. 91 Compressive strength of PUR foam with 0-40 % wood contents**

**Fig. 92 Young's modulus and specific strength of PUR foam with 0-40 % wood contents**

Some differing results were found in Fig. 93. In the samples with an addition of wood flour up to 6 %, the properties were either the same or improved from pure PUR. Above this wood addition level, all compressive properties were reduced. However, it did not drop distinctly when considering the deviation. There was no significant difference in the compressive strength when using wood contents between 0-12 % by statistical comparison between groups with 0, 6, and 12 %. Therefore, no correlation between the compressive properties and apparent densities of samples using up to 12 % wood content existed. The overall trend showed a slight decrease in the specific strength from the increasing filler contents. Yuan & Shi (2009) also found that the compressive modulus of wood-PUR foam did not decrease until the higher wood flour content of 20 %, regardless of the increased density of the samples.

By comparing the results between OVEN1 and OVEN2 (Fig. 91 and 93), the higher averages of properties were exhibited in the latter graphic, due to the lower wood flour contents and higher NCO index that applied there. The increasing compressive strength of PUR along with the NCO index is attributed to the additional networks that arose from allophanate and biuret formation by the supplementary reactions of excess pMDI. Moreover, in most results, the 10 % wood-mixed samples in the former test and all groups in the current result, have acceptable compressive strength according to the minimum compression strength of 0.1 MPa recommended for closed-cell foam by Hee Kim et al. (2008).

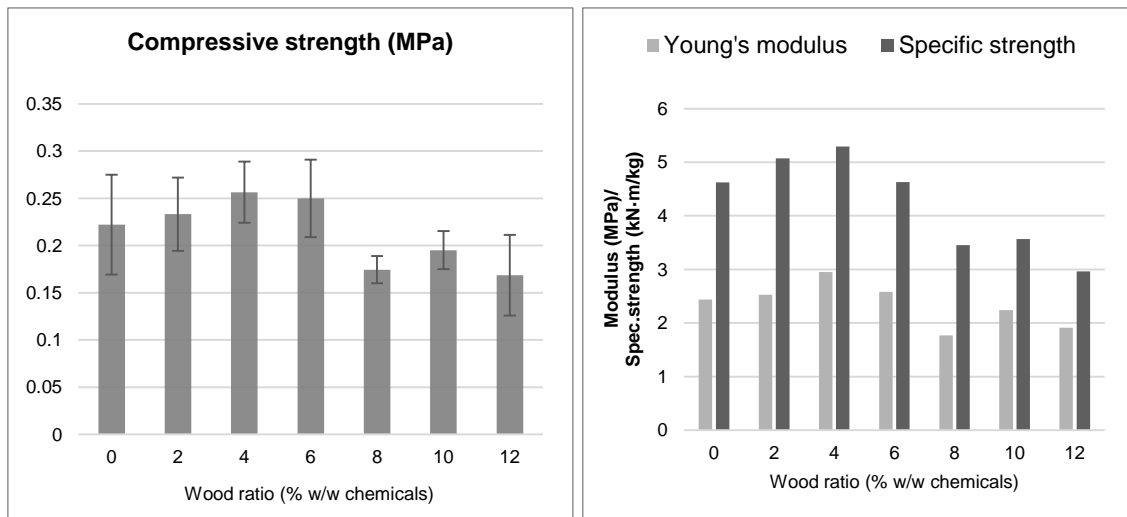


**Fig. 93 Compressive strength of PUR foam with 0-12 % wood contents**

**Fig. 94 Young's modulus and specific strength of PUR foam with 0-12 % wood contents**

Fig. 95 and 96 present the PUR foam samples' compressive properties with a wood content of 10 %, prepared at different temperatures. PUR samples cured at high temperatures had a larger decline in properties than those cured at the normal temperature. The compressive strength of samples cured at 100 °C reduced significantly to less than one-third of the samples without thermal curing, from 1.08 to 0.32 MPa. The results within heat-cured PUR samples did not differ as significantly as the results between heat-cured samples and samples cured at the normal temperature. The compressive strength dropped from 0.32 to 0.14 MPa by elevating the cure temperature from 100 to 160 °C.

Young's modulus showed the same rate of change affected by increasing curing temperatures, though the specific strength did not drop as strongly as in other properties. As the curing temperature increased, all compressive properties declined, as discussed earlier in the cell size section. Even though heat influences foam development, the cell size of PUR produced at normal and high temperatures is comparable. The heat did not significantly induce cell size changes from the mentioned results; however, it increased the foaming rate. It could be assumed that various curing temperatures may cause changes in other cell morphologies e.g. cell wall thickness or cell density that form foam structure and cell alignment for energy absorption.

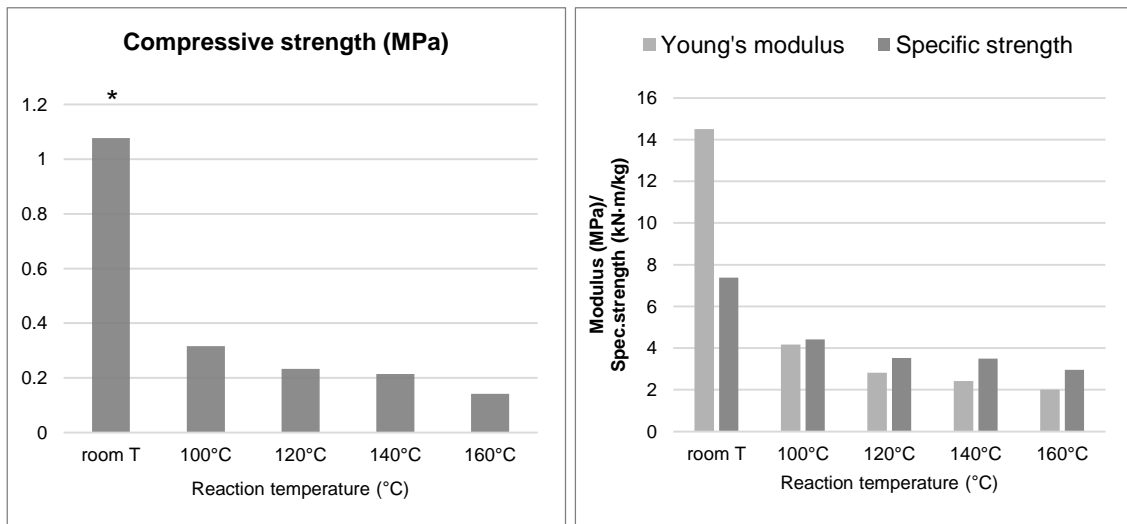


**Fig. 95 Compressive strength of wood-mixed PUR foam cured at different temperatures**

**Fig. 96 Young's modulus and specific strength of wood-mixed PUR foam cured at different temperatures**

### 5.2.2.8 Relationship between compressive strength, cell size, and densities

Previous publications have confirmed the relationship between compressive properties and cell size as well as densities of PUR foam (Yuan & Shi, 2009; Zhu et al., 2012). Mechanical properties and the material density are related in a simple power law appeared in a work by Yuan and Shi (2009), described as follows:

$$\log(\text{strength property}) = \log A + B \log(\text{density}) \quad (20)$$

where  $A$  is a constant related to the temperature and physical properties of the resin and  $B$  is related to the deformation mechanics of cellular materials.

The compressive moduli of samples with four different wood contents are presented related to their densities in Fig. 97. The slope of the log (property) plot versus log (density) is used for the determination of the density exponent value  $B$ . The evaluation results from sample groups with 10 and 20 % exhibited data alignment according to the power-law model, with over 90 % of the determination coefficient. This correlation could not be found from other filler contents, either in the group without wood or groups with 30 and 40 % filler content. PUR samples cured at 100 °C showed the different relationship of compressive moduli to the densities depending on wood flour contents. The density exponent values were calculated for ca. 1.54 and 1.66 in groups with wood flour contents of 10 and 20 %, respectively. They are comparable to values found earlier in literature, which were 1.58 (Yuan & Shi, 2009) and 1.72 (Thirumal et al., 2008).

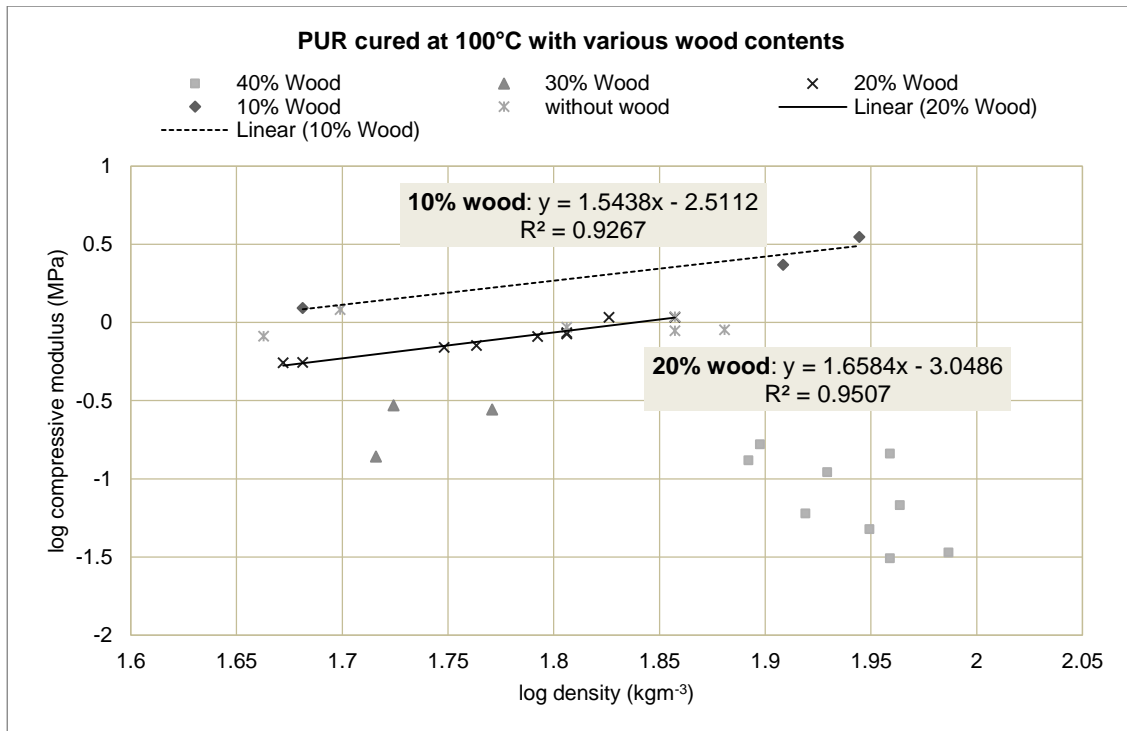
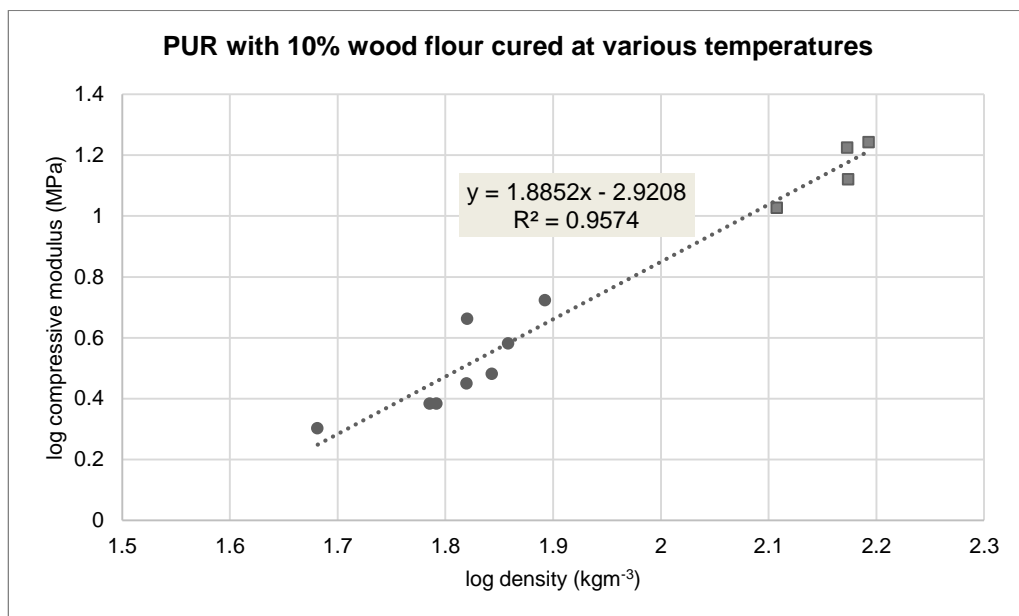


Fig. 97 Relationship between compressive modulus and density for PUR foam with different wood contents

Data from samples using wood flour contents of 10 % in the next experiment, confirmed the same dependence of the power law of compressive properties on the densities despite the variety of curing temperatures, as detailed in Fig. 98. The result showed a higher density exponent value of 1.89 than in the last one. The effect of thermal curing on the compressive properties was reviewed earlier in the previous section (Fig. 95 & 96). The specific strength of the PUR sample group cured at room temperature was measured at  $7.38 \text{ kN}\cdot\text{mkg}^{-1}$ . It was approximated to be 1.7-2.0, proportionally higher than the values from PUR groups cured by heat. Furthermore, the considerable difference in compressive moduli was approximated up to 3 to 8 times by comparison between both groups. However, the results from Fig. 98 show the similarity in the dependence of compressive moduli to the densities among PUR samples using different curing temperatures.



**Fig. 98 Relationship between compressive modulus and density for PUR foam cured at room temperature (■) and 100-160 °C (●)**

Cell size and density caused by the foaming reaction are important factors that design cell shape and structure for energy absorption. Determining the effect of both values on any mechanical properties could be tricky, as they depend on each other based on the same porosity. Gibson and Ashby (1999) assumed that cell shape is more meaningful than the cell size, when considering their effect on the mechanical and thermal properties. To investigate the dependence of compressive properties on cell size and density, the data of 10% wood-filled samples using different temperatures was plotted using the logarithm function in the power law, between density and compressive property discussed before.

Fig. 99 and 100 represent the data alignment using log (cell density) and log (cell size) for the X-axis, respectively. Heat-cured samples appeared to have a partial association of data to each other with regards to the data, while the result from the normal temperature seems to be unconnected. Because of the low coefficient of determination in both diagrams, the compressive moduli in this experiment were incompletely related to the cell size or cell density. The positive exponent value of cell density could indicate the improvement in the compressive modulus by increasing cell density. On the contrary, a larger cell size could lead to the property decreasing. As Zhu et al. (2012) verified, the addition of microfibers to the rigid foam reduced the cell size and increased the compressive strength. However, the significant correlation between the compression properties and cell size and density in this study could not be confirmed because of the high deviation observed previously.

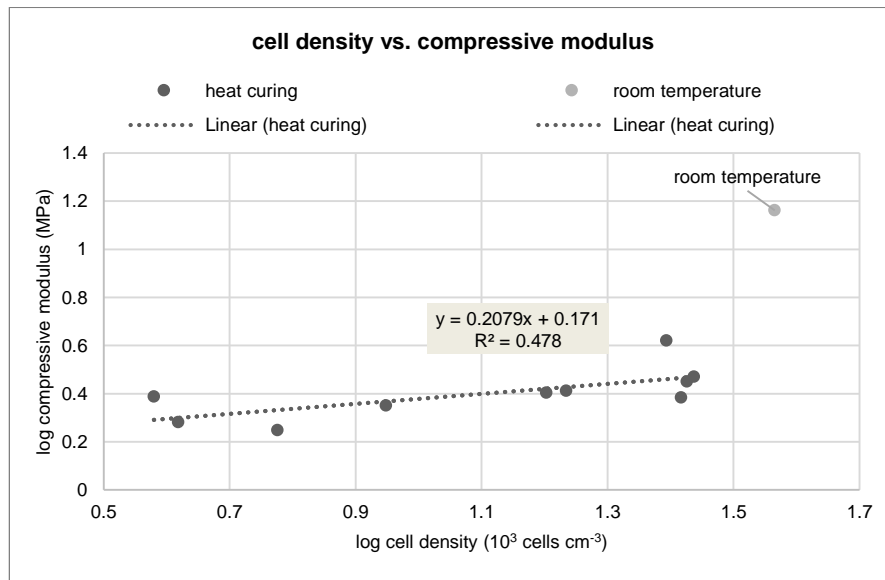


**Fig. 99 Relationship between cell density and compressive modulus of PUR foam**

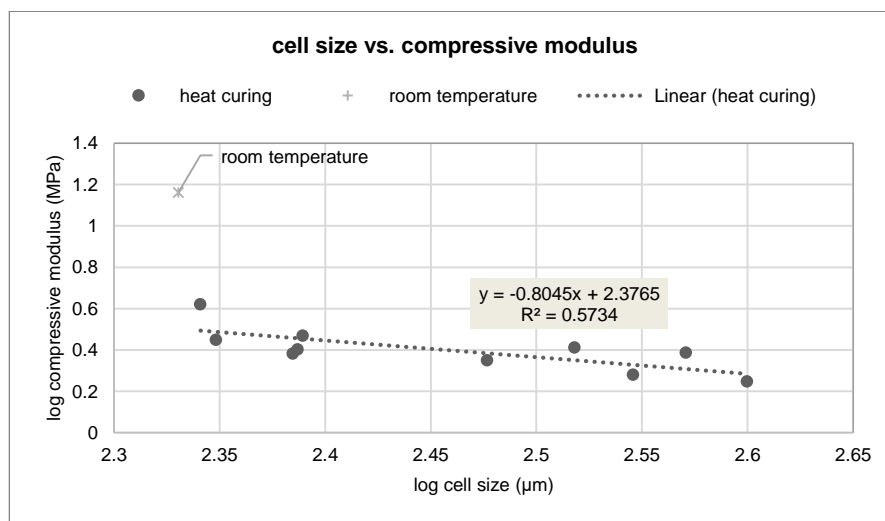


**Fig. 100 Relationship between cell size and compressive modulus of PUR foam**

### 5.3 Study III:

#### PUR foaming within the one-step panel production

PUR foam rise within the hot-pressing process was investigated via the measurement of the development of the internal temperature of the PUR mixture components. In this study, the relationship between the temperature change and foam rise was interpreted to estimate the characteristic time for plate-closing and opening, in order to have data for designing the press program. The increasing rate of the internal temperature of PUR components was affected by both the pressing temperature and the material mass used, so both parameters were varied in the foam rise analysis. The effect of different press programs on the physical and mechanical properties of the produced sandwich panels will be discussed in the final section.

##### 5.3.1 Foam rise analysis

###### 5.3.1.1 Temperature development during the foaming reaction

Fig. 101 illustrates the development in the internal temperature of the PUR mixture during foam rise. The internal temperature of the PUR mixture samples cured at 140 °C and room temperature, is presented via the red and blue lines respectively. Due to the exothermic reaction, an increase in temperature can be observed from the beginning. The internal temperature started at 20 °C then rose with a differing temperature change rate. The internal temperature of the PUR mixture cured at the normal temperature grew steadily to its maximum at ca. 36 °C with a change rate of 0.05 Ks<sup>-1</sup>.

For the sample cured at 140 °C, the internal temperature increased at a higher rate of change, 0.15 Ks<sup>-1</sup>, until the abrupt increase at 60 °C. From this critical point, the temperature rose from 60 to 120 °C within 90 s, with an average rate of change of 0.67 Ks<sup>-1</sup>. The internal temperature increased further to 160 °C, 20 °C more than the set curing temperature, the same difference being observed in the result of the PUR mixture cured at room temperature. The temperature of the sample cured at 140 °C reached its peak at 540 s. Over the rest curing time of 60 s, the temperature showed no further increase, which was assumed to be the end of the reaction. This was compared to the reference sample at room temperature, where the end of the reaction appeared later at ca. 1000 s, the temperature starting to fall and featuring a negative temperature change rate.

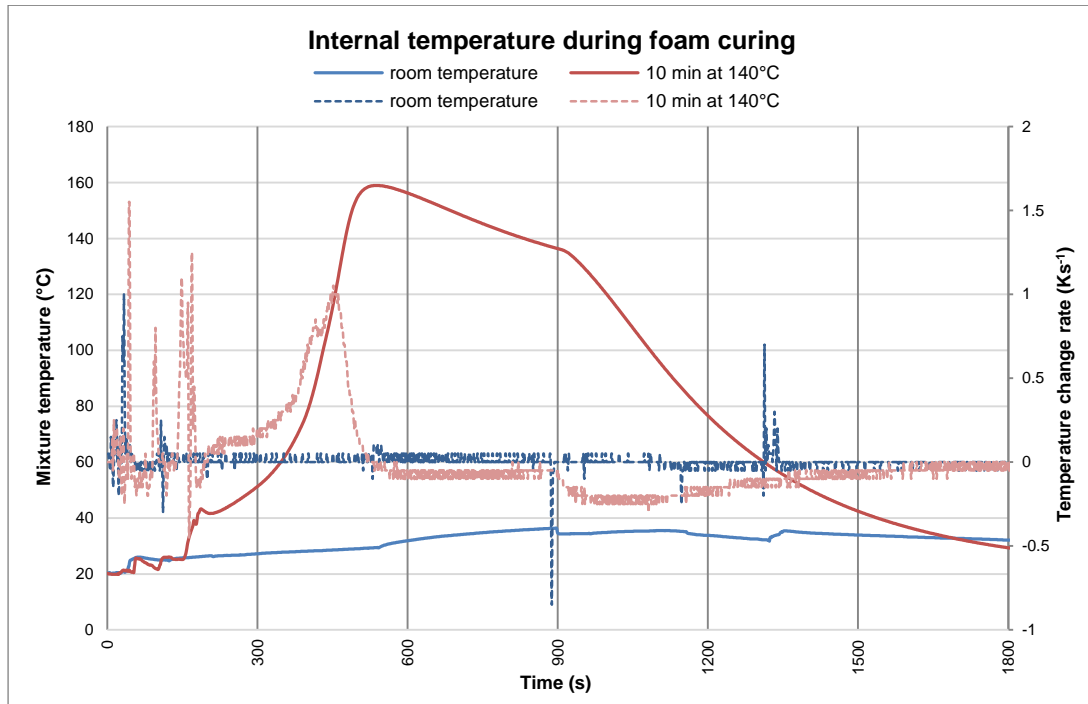


Fig. 101 Internal temperature (solid line) and temperature change rate (dashed line) of PUR mixture cured at room temperature and 140 °C

### 5.3.1.2 Relationship between internal temperature and foam rise

It is only logical to think that the internal temperature of the PUR mixture would grow faster in samples using higher curing temperatures, which was confirmed by the temperature's rate of change, as shown in Tab. 20. In most samples, the PUR mixture's internal temperature exceeded the curing temperature used, except for the group cured at 160 °C, where the maximal internal temperature of PUR had a similar value as the curing temperature.

By using lower curing temperatures, the PUR mixture required an extended period to reach the maximal internal temperature, which corresponded to the reaction's end, as discussed in the earlier result. Tab. 20 displays the average rate of change of the internal temperature. The duration from the start to the maximal internal temperature was less than 5 min when using a curing temperature of 160 °C but more than 10 min in the case of 100 °C. The same result was found for the reaction time with regards to maximal foam height.

Fig. 103 shows the foam structure at the maximal size, which expanded differently depending on the curing temperature level. However, in most cases, the foam rise terminated directly after the internal temperature had reached the maximum, the exception being the sample cured at 120 °C (red line). The internal temperature continued growing after the maximal foam height had been achieved. Despite the

divergent timing in appearance, the maximal foam height occurred at approximately the same time as the maximum internal temperature of PUR mixture in all samples. Therefore, the maximal foam height was possibly related to the maximal internal temperature.

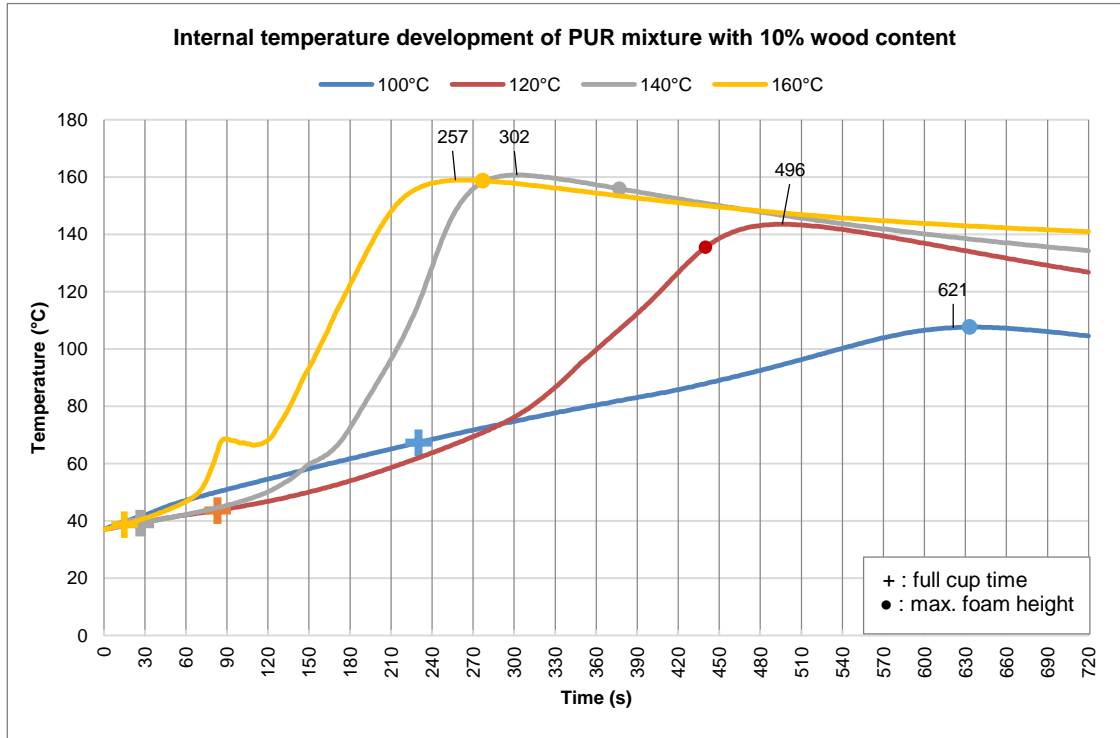


Fig. 102 Internal temperature of PUR mixture cured at different temperatures, with marks as the foam reached the full cup level (+) and the maximal foam height (•)



Fig. 103 (from left to right) Foam rise in full cup and maximum height as appeared at different curing temperatures

Tab. 20 Reaction time for full cup, maximal foam height, maximal internal temperature and temperature change rate in different samples

| Curing temperature (°C) | Full cup      |          | Max. foam height |          | Max. <i>T</i> | Average change rate from + to • (Ks <sup>-1</sup> ) |
|-------------------------|---------------|----------|------------------|----------|---------------|---|
|                         | <i>T</i> (°C) | Time (s) | <i>T</i> (°C)    | Time (s) | Time (s)      |   |
| 100                     | 38.9          | 230      | 107.6            | 632      | 621 (-11)     | 0.17  |
| 120                     | 39.3          | 80       | 135.5            | 440      | 496 (+56)     | 0.27  |
| 140                     | 43.4          | 28       | 155.7            | 383      | 302 (-81)     | 0.32  |
| 160                     | 67.3          | 16       | 158.7            | 276      | 257 (-19)     | 0.35  |

### 5.3.1.3 Effects of foam formulation on the internal temperature

PUR component mixtures with different sample weights were set in the core layer and pressed at 140 and 160 °C. Changes in the PUR mixture's internal temperature for all samples during the pressing time were calculated and shown in Fig. 104. At the beginning, the rates of change were relatively constant between 0.1-0.3 Ks<sup>-1</sup>, then they grew abruptly at a specific point in time.

By pressing at 160 °C, the PUR mixture with the highest sample weight (125 g in Test 1) had its growth point at 230 s, which was later than those with lower sample weights (100 g and 83 g in Test 2 and 3). The same findings were observed in samples prepared at a pressing temperature of 140 °C. The PUR mixture with the same weight pressed by the lower temperature (Test 4) required more reaction time than that pressed by the higher temperature (Test 2) until the growth point of the rate of change was achieved. The result indicated that the pressing temperature and total sample weight influenced the rate of change of the PUR mixture's internal temperature. Despite their differing reaction time regarding the growth point, it appeared that the increase in the temperature's rate of change was approximately found at 80 °C, as shown as by the circle marks in Fig. 105. The average rate of change in temperature in the period before and after 80 °C is summarized in Tab. 21.

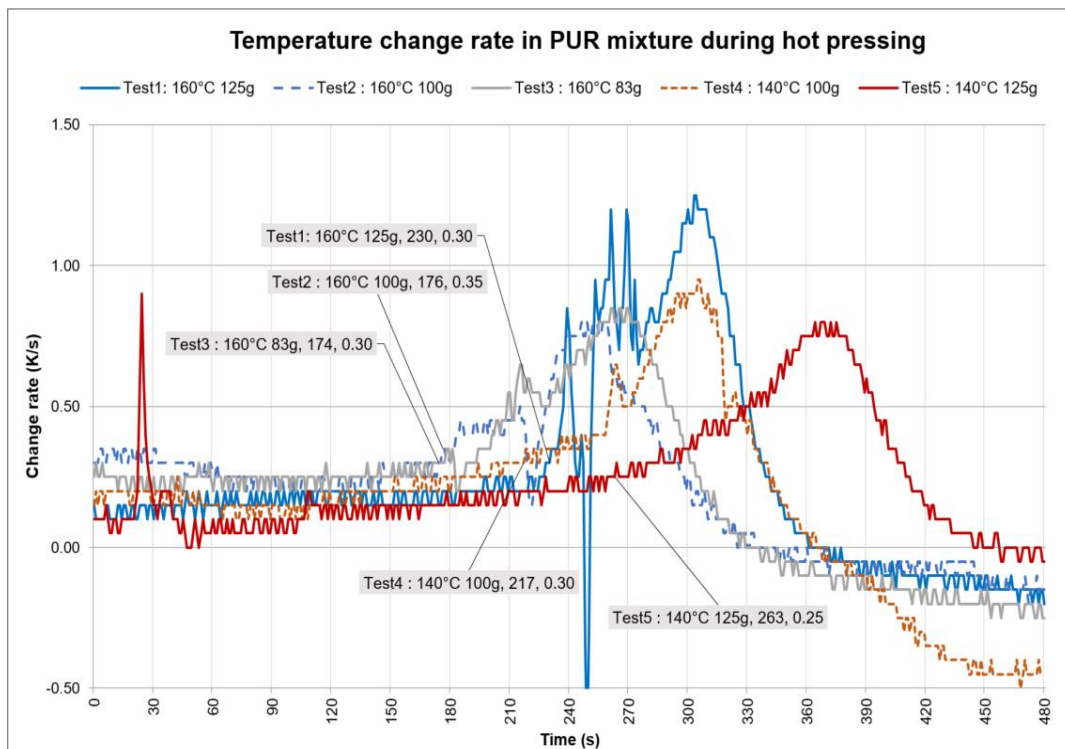


**Fig. 104** Temperature change rate in PUR mixture using different sample weights and pressing temperatures

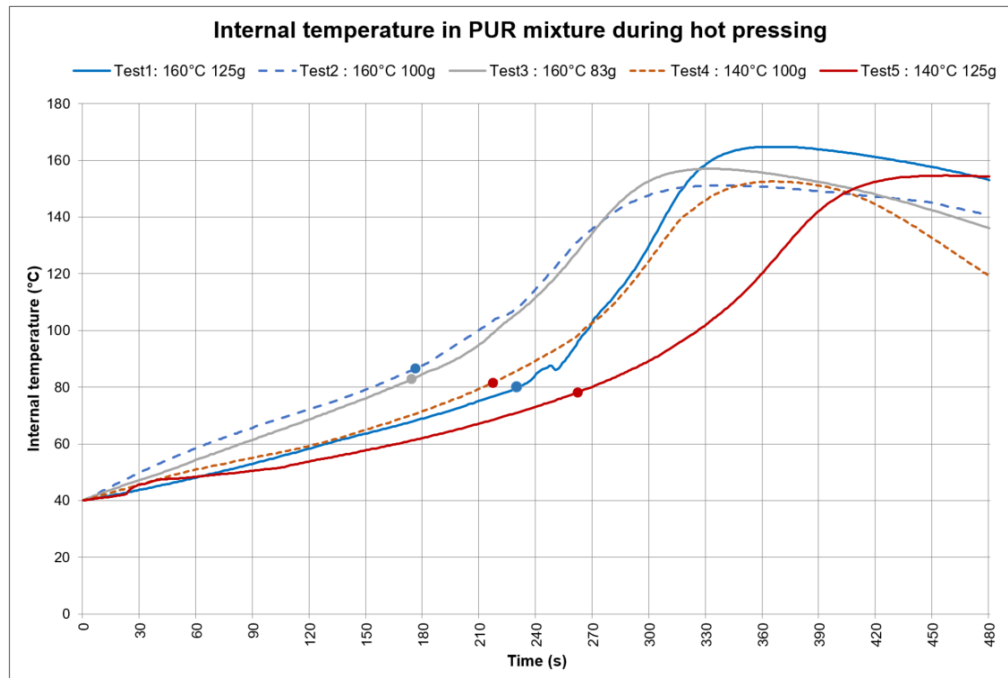


Fig. 105 Internal temperature of PUR mixture displaying the reversal point marked by •

Tab. 21 Average temperature change rate of different samples divided into three periods

| Test title    | From 40 to 80 °C |                               | From 80 to 100 °C |                               | From 100 °C to $T_{max}$ |          |                               |
|---------------|------------------|-------------------------------|-------------------|-------------------------------|--------------------------|----------|-------------------------------|
|               | Time (s)         | $T$ change rate ( $Ks^{-1}$ ) | Time (s)          | $T$ change rate ( $Ks^{-1}$ ) | $T_{max}$ (°C)           | Time (s) | $T$ change rate ( $Ks^{-1}$ ) |
| 1) 160°C 125g | 231              | 0.17                          | 36                | 0.56                          | 164.8                    | 93       | 0.70                          |
| 2) 160°C 100g | 153              | 0.26                          | 56                | 0.36                          | 151.2                    | 124      | 0.41                          |
| 3) 160°C 83g  | 164              | 0.24                          | 55                | 0.36                          | 157                      | 109      | 0.52                          |
| 4) 140°C 100g | 212              | 0.19                          | 53                | 0.38                          | 152.6                    | 99       | 0.53                          |
| 5) 140°C 125g | 269              | 0.15                          | 57                | 0.35                          | 154.7                    | 130      | 0.42                          |

The table displays the average rate of change in temperature divided into three time zones, which refer to three pressing steps within the continuous process. From the beginning up until 80 °C, the mixture started to foam slowly, as evidenced by its internal temperature. Hot plates were moved next to each other for plate closing or pressing. After that, the plates were opened, as the foaming reaction of the PUR mixture took place rapidly. Plate opening started from 80 °C, when the high reaction rate could be measured, to 100 °C, when the surface layer comprised of the wood particles compacted via the solidification of the resin (Shalbfan, 2013). It is possible for the foam to expand further at a higher temperature, so pressing was terminated to increase the volume in the core layer. Aside from this, rapid temperature changes in the PUR mixture starting from 80 °C implied the high acceleration of the foaming process. For this reason, the required time for increasing the internal temperature from 80 to 100 °C was signified for the plate-opening time. The maximal foam expansion was achieved in the last step, from 100 °C to the maximal internal temperature, therefore, were held in the aiming distance to stabilize the compacted panel during this period.

### 5.3.2 Designing the press program

PUR mixture with a wood content of 10 % was applied to the middle layer of the panel with a plate-opening distance of 100 % (20 mm), in order to monitor a change in the internal temperature and identify the time required for pressing, foaming and panel stabilizing. As can be seen from Fig. 106, acceleration in the temperature's rate change appeared at ca. 80 °C, which occurred at 210 s in both samples. This period was the maximal duration that the mixture required to accelerate the foaming reaction. Then, after a minimum of 60 s, the maximal change rate of the internal temperature was achieved. Both periods were signified for pressing and foaming time, for pressing in a further step.

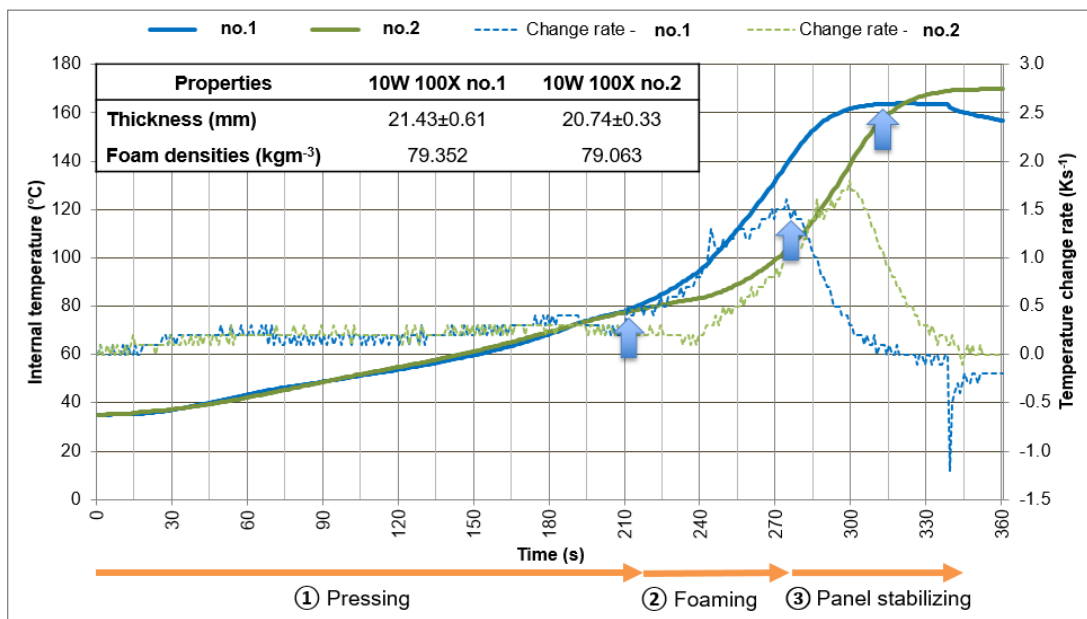


**Fig. 106 Internal temperature of PUR mixture with 10 % wood content pressed by 100 % plate-opening distance and panel properties**

A press program with a plate-opening distance of 50 % was developed and illustrated in Fig. 107. The pressing time of 210 s from the 100 % plate-opening distance program was reduced to 180 s in the new program, to compensate for the heat transfer from the pressing plates due to decreased distance between the hot plate and panel mat. Firstly, a panel using wood content of 10 %, pressed by a plate-opening distance of 50 %, with pressing time of 180 s (10W 50X180) was produced. The end panel thickness measured 11.62 mm, much lower than the stabilizing plate distance of 20 mm. The internal temperature data (see Appendix III) showed a stark internal temperature increase from the beginning, which suggested a reduction in the pressing time was needed. Consequently, the pressing time was reduced to 90 (10W 50X90) and 60 s (10W 50X60) in the following panels as well as the foaming time. The panel thickness was also improved, in which the panel pressed for 90 s showed the closest result to the aim thickness of 20 mm.

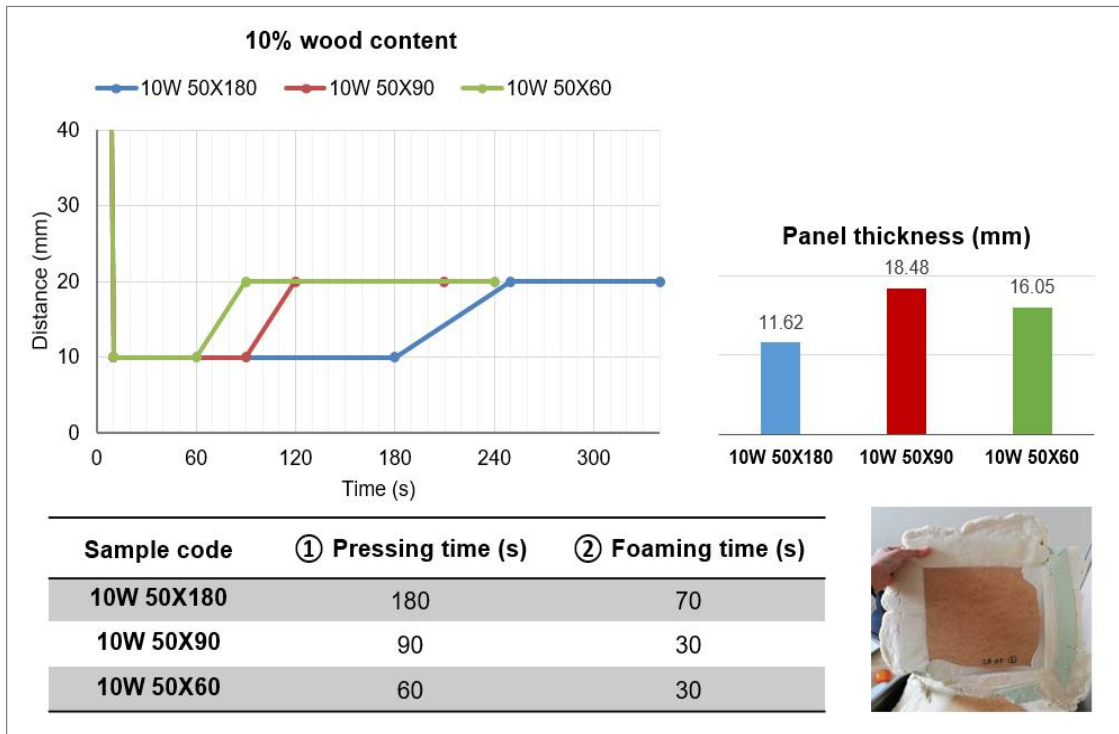


**Fig. 107 (left) Press program applied in panels with 10 % wood content mixture displaying distance of pressing plates varied in time, (right) Thickness of panel produced by different press programs**

Panels using PUR mixture with a wood content of 20 % were produced by different press programs and measured for the panel thickness, as displayed in Fig. 108. The experiment was started with a plate-opening distance of 100 % (20W 100X), to observe the internal temperature. The data (see Appendix III) suggested the pressing time of 180 s. However, the application of this in the press program exhibited a much flatter panel. Therefore, the pressing time used was set for 90 s, as in the panel made from PUR mixture with a wood content of 10 % (10W 50X90). The PUR mixture did not seem to expand as high as with the last PUR formulation. The early plate opening before the extreme rising activity (80 °C) should have supported the foam expansion. However, the mixture did not expand further after plate opening and remained 12 mm thick in both panels (20W 50X90 and 20W 50X70). It could be explained by the mixture loss from the pressing frame (see a right-corner picture of Fig. 107 and 108). In the case of 10 % wood content, this did not seem to have a high effect on the panel thickness as much as 20 % wood content. The difference in mixture formulation could have caused the foam expansion, as discussed earlier by the FRH result in chapter 5.2.1. Presumably, the foam with a wood content of 20 % became solidified as the plate opened and attached with the MDF surface panel and pressing frame. So the inner foam mixture could not expand out to enlarge the core layer as anticipated, this caused by the higher wood content.

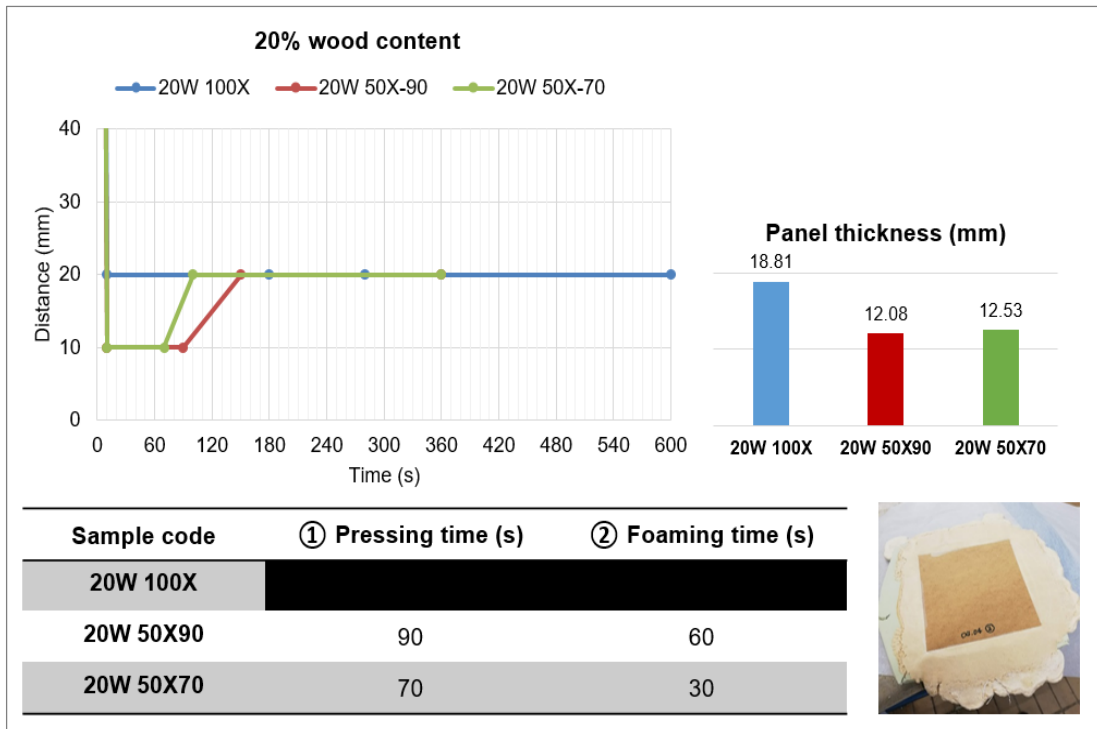


Fig. 108 Press program applied in panels with 20 % wood content mixture displaying distance of pressing plates varied in time, (right) Thickness of panel produced by different press programs

### 5.3.3 Properties of produced PUR sandwich panels

#### 5.3.3.1 Foam morphology

The PUR foam layer was investigated edgewise perpendicular to the panel pressing direction. Fig. 109-111 present the foam morphology from the different sample panels. The apparent failure was found in 10W 100X, as indicated via the large fracture in the middle of the area (Fig. 109). The cells were probably torn after foam stabilization. It can be assumed that this area solidified before the surrounding region. Then cells in other areas expanded extensively afterward and generated shear stress in the hardened area, finally inducing the cell break. A small fracture was also discovered in other samples (10W 50X90, 10W 50X180, 20W 50X90). Collapsed cells were found, though it was not obvious whether they were caused by sample preparation or the different timing of foam stabilization.

Other failures in foam structure were observed through the general inhomogeneity of cells in form and size, especially in the 20W samples (Fig. 111), depending on their position in the panel. Relatively small cells were formed on the bottom, where the mixture was spread more than in the middle or top. Cells from foam panels made of PUR mixture with 20 % wood content, generally had flatter structure than those made of 10 % wood content. It conformed to the lower foam expansion by using higher wood contents theoretically, as discussed earlier.

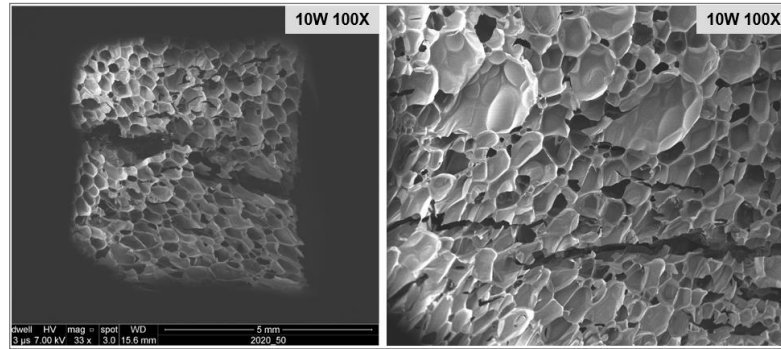


Fig. 109 SEM photos of 10W 100X samples showing the long fracture in the middle

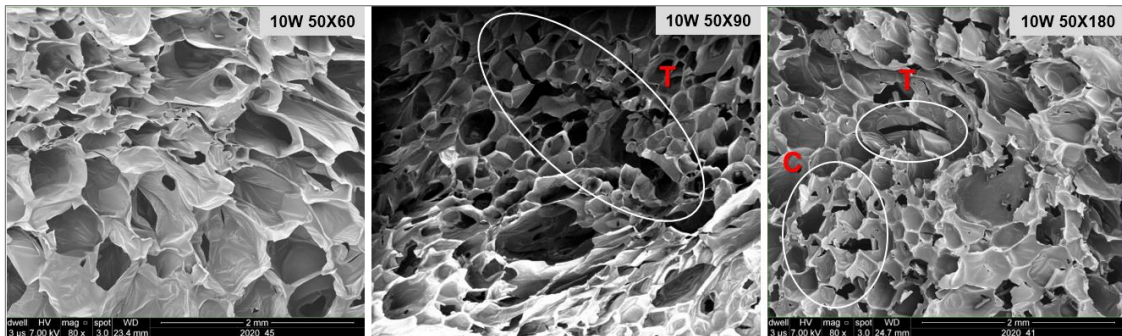


Fig. 110 SEM photos of 10W 50X samples with collapsed cell area (C) and small tears (T)

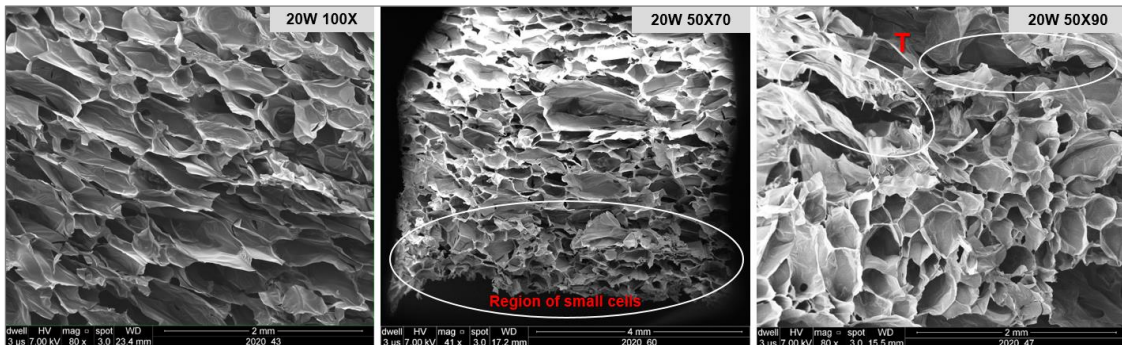


Fig. 111 SEM photos of 20W samples showing inhomogeneity, region of small cells at the bottom of panel and small breaks (T)

### 5.3.3.2 Cell size

The cell diameter from the top, parallel to the pressing direction was measured. It should be taken into account that the size results in this direction did not indicate that the foam rise had been affected by the heat from pressing plates.

The average and distribution of cell diameter measured on the 10W and 20W panels are visible in Fig. 112 and 113, respectively. There was no significant difference generally in the cell size of the 10W samples according to the ANOVA. As regards the 20W panels, the panel with a plate-opening distance of 100 % (20W 100X) had a significantly lower cell diameter than other 20W panels. It can be seen via the average value that the 20W 100X has the lowest average diameter of ca. 127 µm, while the average of

approximately 185-238  $\mu\text{m}$  was observed in other sample panels. It could be assumed that using different press programs and corresponding plate-opening distance did not alter the cell size significantly. Although a significant result was found in 20W 100X (Fig. 113), this probably resulted from the loss of PUR mixture in the other 20W panels during hot pressing.

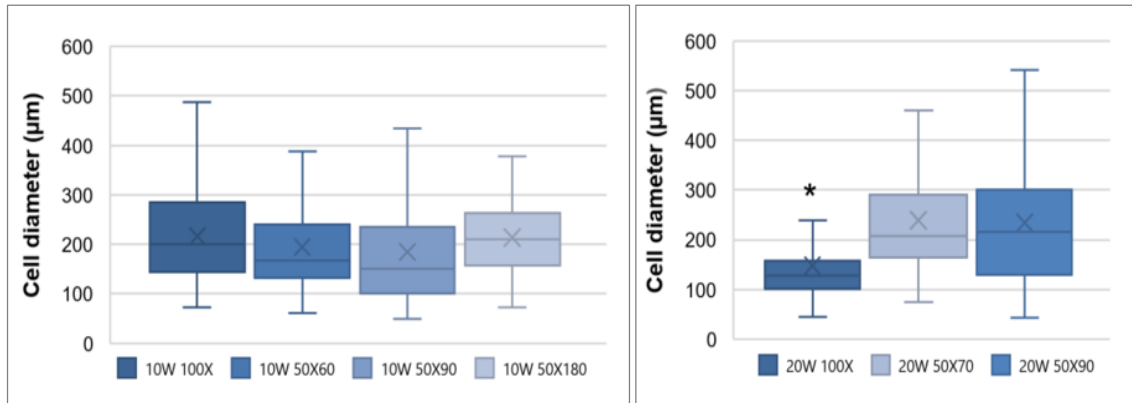


**Fig. 112 Cell size distribution of PUR foam with 10 % wood content measured in 10W panels**

**Fig. 113 Cell size distribution of PUR foam with 20 % wood content measured in 20W panels**

With regards to the homogeneity found in SEM photos in the last section, the roundness ratios of the foam cells were measured in order to evaluate the cell shape among different sample types roughly. According to Fig. 114, the roundness ratios did not differ by varying of the pressing programs. Generally, the high distribution of roundness ratios was found between 0.3 and 0.2 to 1 in 10W and 20W samples, respectively. The significantly lower roundness ratio appeared in the 20W 50X90 panel with a P-value of 0.042 when compared with other 20W panels, which was not much lower than the critical value of 0.05. Therefore, the press program did not cause a significant difference in the roundness ratio.

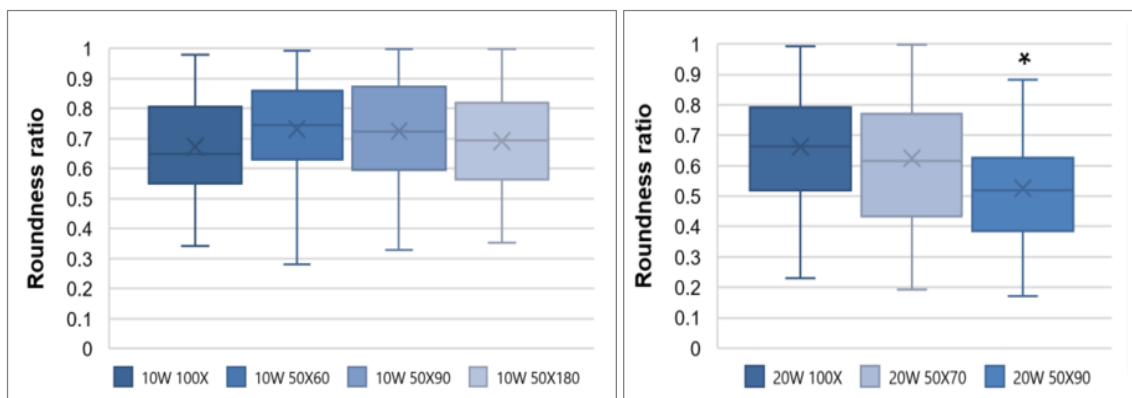


**Fig. 114 Distribution of roundness ratio of foam cells with 10 % wood content in 10W panels**

**Fig. 115 Distribution of roundness ratio of foam cells with 20 % wood content in 20W panels**

### 5.3.3.3 Foam density

The foam density was measured from the density profile of the panels. Higher wood content results in an increase in foam density, as can be seen in panels with a plate-opening distance of 100 %. Fig. 116 shows the density of PUR foam in a 10W 100X panel as 59-114  $\text{kgm}^{-3}$ , which was relatively lower than that in the 20W 100X panel with its average of ca. 120  $\text{kgm}^{-3}$ , as shown in Fig. 117. Moreover, the 20W 100X panel's foam density was significantly higher than other 20W panels when applying a plate-opening distance of 50 %. The high density of the PUR foam at 20W 100X could be related to its lowest cell diameter that was discovered earlier. In the 10W panels (see Fig. 116), an insignificant difference was only found between the 50X90 and 50X60 panels, which implied that the foam density was not affected by varying the pressing time from 60 to 90 s. Both panels had a lower foam density compared to other 10W panels. However, no significant difference in cell size was observed among 10W panels in the last result. This could be explained by the difference in foam morphology, such as cell wall thickness and void fraction.

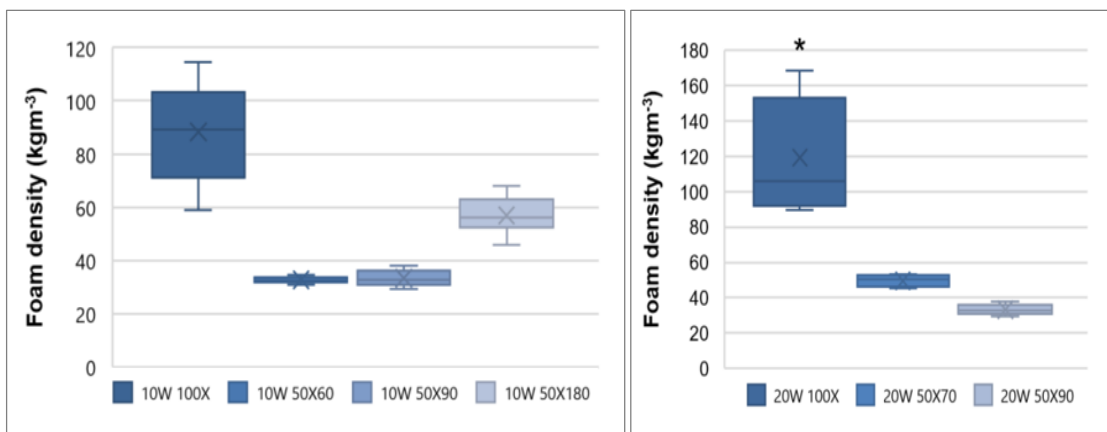


Fig. 116 Distribution of foam density from PUR core layer in 10W samples

Fig. 117 Distribution of foam density from PUR core layer in 20W samples

### 5.3.3.4 Apparent density and thickness

Regarding the constant properties of manufactured MDF surface layers, the final density of the panel depends on the density and thickness of the PUR foam, namely the expansion of the foam within the hot pressing. When considering the panel weight ( $m_p$ ) based on foam ( $m_f$ ) and surfaces ( $m_s$ ), the relationship between panel density ( $\rho_p$ ) and foam thickness ( $h_f$ ) and density ( $\rho_f$ ) can be developed as follows:

$$m_p = m_f + 2m_s \quad (21)$$

$$\begin{aligned} \xrightarrow{m=\rho V} \rho_p V_p &= \rho_f V_f + 2\rho_s V_s \xrightarrow{V=h \cdot A} \rho_p (h_p A) = \rho_f (h_f A) + 2\rho_s (h_s A) \\ \xrightarrow{\cdot A^{-1}} \rho_p h_p &= \rho_f h_f + 2\rho_s h_s \xrightarrow{\cdot h_p^{-1}} \rho_p = \frac{\rho_f h_f + 2\rho_s h_s}{h_p} \end{aligned}$$

$$\xrightarrow{h_p = h_f + 2h_s} \rho_p = \frac{\rho_f h_f + 2\rho_s h_s}{h_f + 2h_s} \quad (22)$$

Since  $h_s$  and  $\rho_s$  are constant,  $2\rho_s h_s$  and  $2h_s$  can be substituted by  $k_1$  and  $k_2$ , respectively, as follows:

$$\rho_p = \frac{\rho_f h_f + k_1}{h_f + k_2} \quad (23)$$

The equation suggests that the panel- and foam density are correlated; the opposite being true of the foam- and panel thickness, when the surface layer's properties are constant.

Panel densities are illustrated and compared with foam density and thickness, in Fig. 118 and 119. According to the ANOVA, the panel thicknesses of samples were significantly different, being associated with the difference in foam expansion resulting from plate-opening time and distance. Regarding the high variation in panel thickness, samples exhibited significantly different panel densities within the 10W and 20W groups, except for the panel density between 100W 50X60 and 100W 50X90. Both panels possessed an insignificantly different density despite their differing thicknesses, which was possibly related to the similarity in foam density found earlier. The overall trend of panel density grew from a plate-opening distance of 100% to 50% with a higher pressing time. This was probably induced by the great reduction in panel thickness rather than the change in foam density, as panels showed decreased foam density by extension of the pressing time.

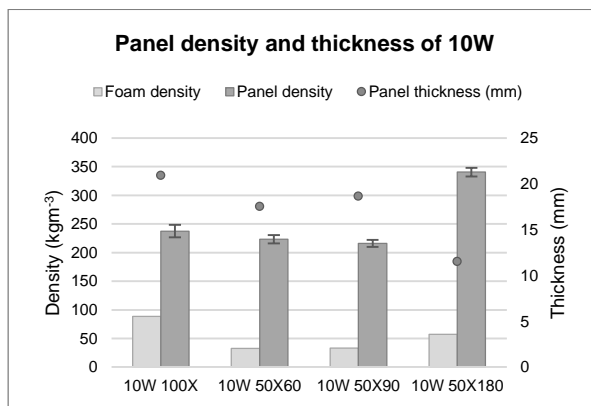


Fig. 118 Panel density and thickness of 10W panels compared with foam density

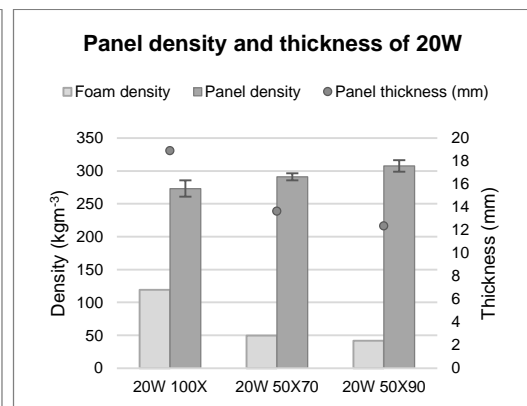


Fig. 119 Panel density and thickness of 20W panels compared with foam density

### 5.3.3.5 Compression properties

Compressive strength and Young's modulus of 10W panels are represented in Fig. 120 and 121. The highest average strength of ca. 0.1 MPa appeared in the 10W 100X panel with a high deviation, which corresponded to the compression strength of PUR foam with a wood content of 10 % produced in the cup test from Study II. The similar Young's modulus also appeared in the 10 % wood-mixed PUR foam from both studies. The specific strength of the 10W 100X panel ( $0.423 \text{ kN}\cdot\text{mkg}^{-1}$ ) was much lower than that of the PUR foam from the cup test ( $2.629 \text{ kN}\cdot\text{mkg}^{-1}$ ), due to the increasing density of the existing MDF surfacing in the panels. But when considering only a part of PUR foam, the specific strength thereof PUR foam in 10W 100X averaged at  $1.15 \text{ kN}\cdot\text{mkg}^{-1}$ , which was still lower than that from the cup test.

By comparing 10W panels, lower compressive properties were observed in panels with a plate-opening distance of 50 % (50X panels), especially in the 10W 50X60 and 50X90 panels, that had values more than five times lower than those of the 100X panel. However, the 10W 50X180 panel displayed better properties than those of other 50X panels, which corresponded to its higher foam density as discussed earlier. A longer plate-closing time of 180 s possibly forced the cell expansion to be limited in volume and therefore created a cell structure with increased cell wall thickness, which could support more stress than foam produced with a shorter plate-closing time.

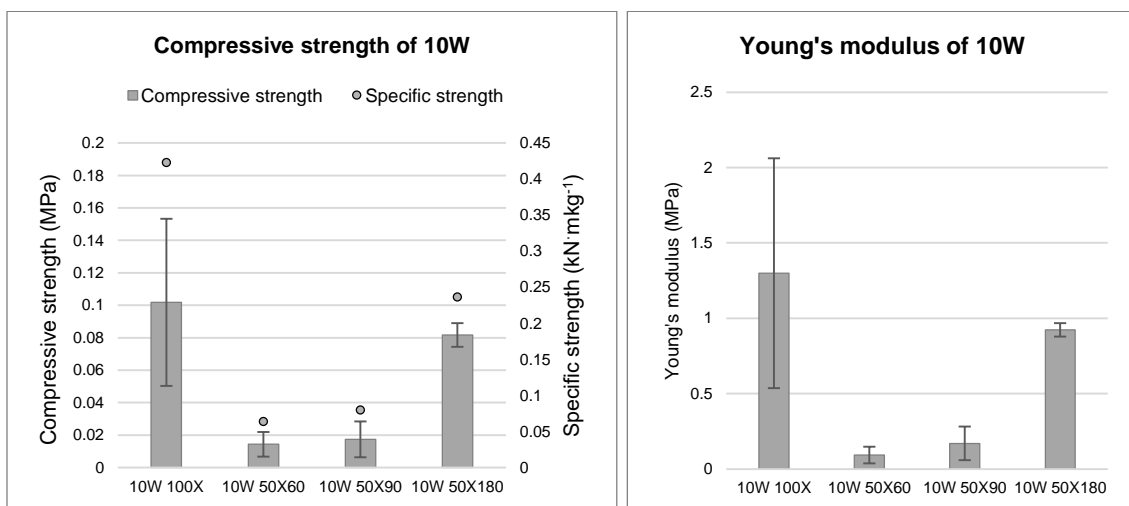


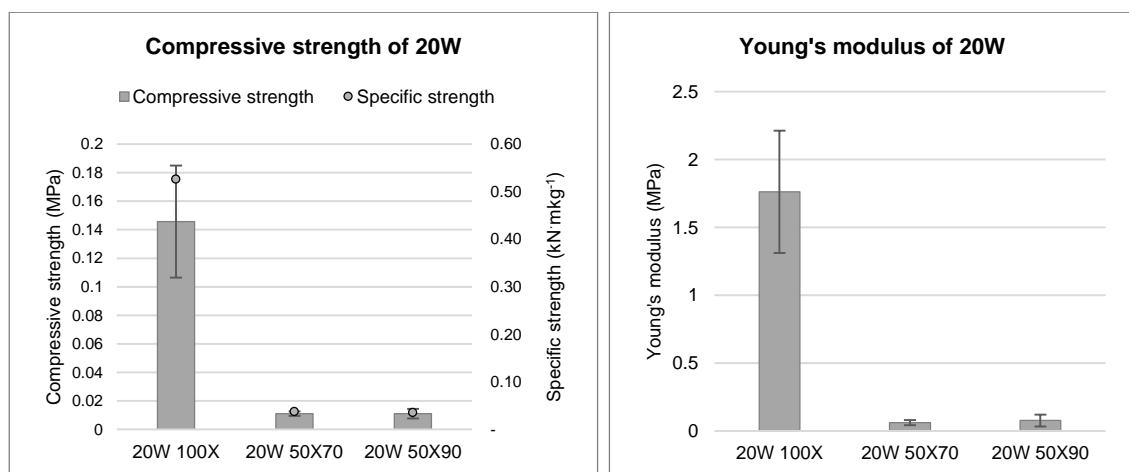
Fig. 120 Compressive and specific strength of 10W panels

Fig. 121 Young's modulus of 10W panels

The compressive properties of 20W panels are illustrated in Fig. 122 and 123. The 20W 100X panel had a slightly higher average strength than the 10W 100X panel, which contradicted the earlier findings in Study II, where the compressive properties became decreased with higher wood contents. The high deviation in both results could explain this insignificant difference. By comparing samples from different press programs, remarkably higher compressive properties were observed in the panel with a plate-opening distance of 100 %. The 20W 100X had values more than ten times higher in all compressive properties than the 20W 50X70 and 20W 50X90. Higher foam density in the 20W 100X was assumedly not the only reason for this high value, due to not only the marked difference in specific strength but also its significantly smaller cell diameter and distribution. The homogeneity in the cell diameter can construct a matrix structure that absorbs higher stress than heterogeneity does.

However, the average compressive properties measured on the 10W and 20W panels appeared to be lower than the typical value for PUR sandwich panels foam of 0.18-0.20 MPa (Randall & Lee, 2002). According to the reference, only the 20W 100X panel would exhibit an acceptable compressive strength, whereas the 10W 100X panel almost achieved this value with its deviation, while other panels had much lower properties.

It can be concluded that the compressive properties were not improved by the pressing process, in this case, by the addition of a plate-opening distance of 50 %. PUR could expand freely with more cavities in the 100X panels than in 50X panels. The plate-closing process may affect the free expansion, causing changes in cell structure during the matrix formation and solidification of the foam.



**Fig. 122 Compressive and specific strength of 20W panels**

**Fig. 123 Young's modulus of 20W panels**

### 5.3.3.6 Internal bond

The internal bond properties of the 10W and 20W panels are shown in Fig. 124 and 125, respectively. The general trend appears to be related to the result of compressive properties. The average internal bond of panels with a plate-opening distance of 100 % (100X) was higher than those with a plate-opening distance of 50 % (50X) in both groups, though, a noticeably high deviation was found in the 10W 100X panel. Tab. 22 displays the failure mode observed in specimens after the internal bond testing. Since the failure only took place in the middle foam layer in the 10W 100X panel, the high variation is caused by the inhomogeneity of the foam matrix. Thus, there was no significant difference when comparing the 10W 100X panel with the other 10W panels. Additionally, shear failure appeared mostly in the PUR layer of the 20W 50X70 and 20W 50X90 panels; both of which had a significantly lower internal bond, amounting to a quarter of the 20W 100X panel.

Panels using a plate-opening distance of 100 % exhibited higher deviation than panels with a plate-closing step related to the compression results. As discussed earlier, adding a pressing step could potentially alter the cell structure during the foam formation, resulting in a decreased internal bond. On the other hand, panels without the plate-closing step allowed for more expansion of the PUR foam, which led to a high deviation in properties due to the uneven development of the foam volume.

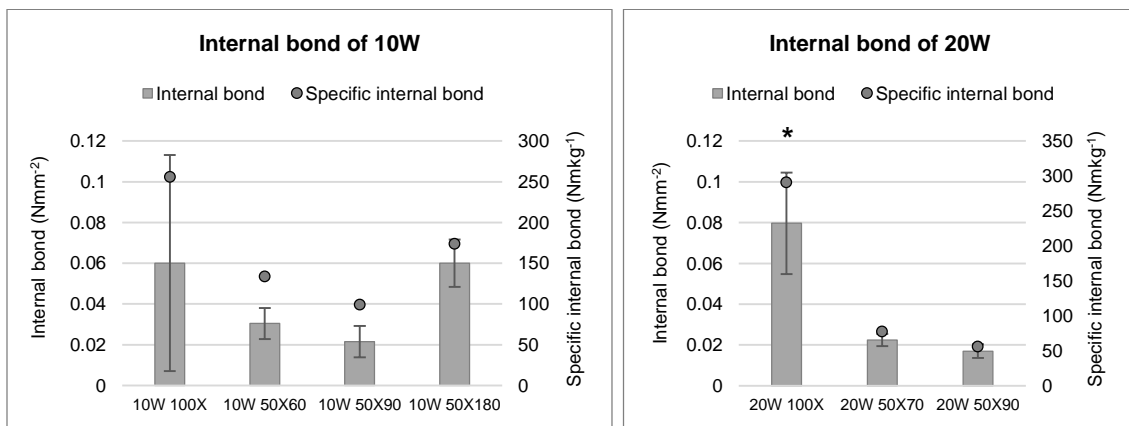


Fig. 124 Internal bond of 10W panels

Fig. 125 Internal bond of 20W panels

Tab. 22 Locations of failure observed from the tensile shear in different panels

| Panel sample | Failure mode                                   |
|--------------|--|
| 10W 100X     | only in foam layer                             |
| 10W 50X60    | only between surface and foam layer            |
| 10W 50X90    | between surface and foam layer > in foam layer |
| 10W 50X180   | only between surface and foam layer            |
| 20W 100X     | between surface and foam layer > in foam layer |
| 20W 50X70    | in foam layer > between surface and foam layer |
| 20W 50X90    | in foam layer > between surface and foam layer |

### 5.3.3.7 Thermal resistance and conductivity

Thermal conductivity ( $\lambda$ ) is reduced with the decreased density of a material. The insulating PUR foam of  $0.024 \text{ Wm}^{-1}\text{K}^{-1}$  amounts to thermal conductivity ten times lower than solid PUR, which is  $0.250\text{-}0.330 \text{ Wm}^{-1}\text{K}^{-1}$  (Engels et al., 2013; Szycher, 2012). The thermal conductivity of PUR foam and panels are shown in Fig. 126 and 127, in comparison with material densities. As evident in the foam properties of both results, the thermal conductivity exhibited the same change in value as the foam density. PUR foam from the 10W panels with a density range of  $33\text{-}88 \text{ kgm}^{-3}$ , exhibited thermal conductivity between  $0.036\text{-}0.037 \text{ Wm}^{-1}\text{K}^{-1}$ , whereas those from the 20W panels showed comparable values of  $0.037\text{-}0.043 \text{ Wm}^{-1}\text{K}^{-1}$  based on the higher density range of  $42\text{-}120 \text{ kgm}^{-3}$ .

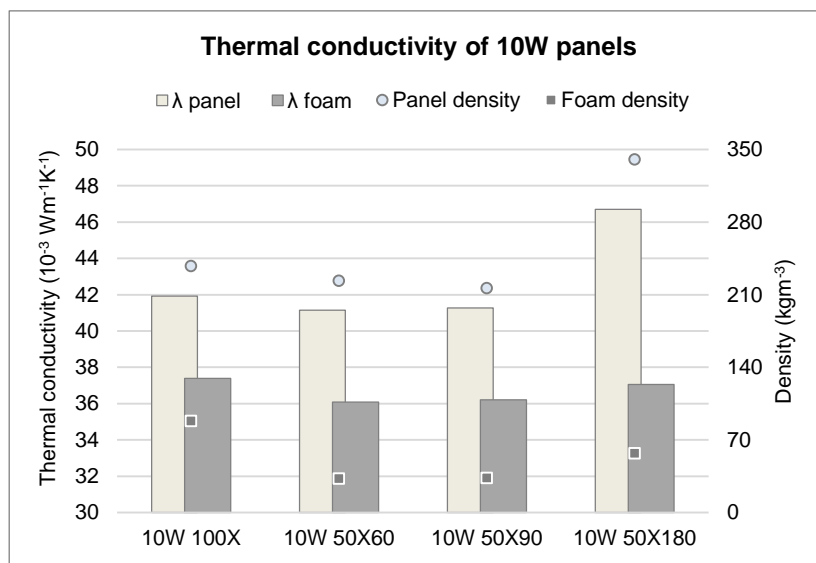


Fig. 126 Thermal conductivity related to densities of 10W panels

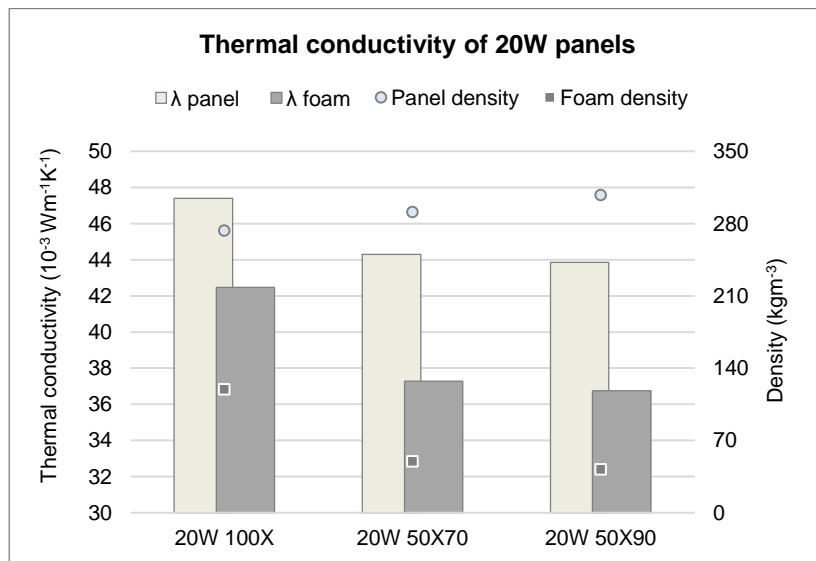


Fig. 127 Thermal conductivity related to densities of 20W panels

A similar trend was noticed in the relationship between thermal conductivity and densities of the 10W panels, where an increase in panel densities led to a rise in thermal conductivity. A different result appeared in the 20W panels. As the densities of the 20W 50X70 and 20W 50X90 panels rose higher than the 20W 100X panel, their thermal conductivities decreased. The composition of the MDF sheet, with its thermal conductivity of  $0.0889 \text{ Wm}^{-1}\text{K}^{-1}$  – higher than that of the PUR foam – commonly increased both the density and the thermal conductivity of the panel, as observed in each sample result. With regards to the different thickness of the expanded PUR layer, the increase in the panel density of said layer, varied in each panel. Therefore, the 20W 50X70 and 20W 50X90 panels with their lower foam density, had higher panel density than the 20W 100X panel. However, the difference in their panel densities was not considered as high as that of their foam densities. Hence, it did not lead to the increase in thermal conductivity. Furthermore, the panel's thermal conductivity depends on the thickness and thermal conductivity of combined layers, as shown in the following equations.

According to the formula (13):  $R_{tot} = 2 \cdot R_{MDF} + \frac{d_{PUR}}{\lambda_{PUR}}$ ,

$$\frac{d_{tot}}{\lambda_{tot}} = 2 \cdot R_{MDF} + \frac{d_{PUR}}{\lambda_{PUR}} \quad (24)$$

$$\lambda_{tot} = \frac{d_{tot}}{2 \cdot R_{MDF} + \frac{d_{PUR}}{\lambda_{PUR}}} = \frac{d_{tot}}{\frac{(2 \cdot R_{MDF} \cdot \lambda_{PUR}) + d_{PUR}}{\lambda_{PUR}}}$$

$$\lambda_{tot} = \frac{d_{tot} \cdot \lambda_{PUR}}{(2 \cdot R_{MDF} \cdot \lambda_{PUR}) + d_{PUR}} \quad (25)$$

Since  $\lambda_{PUR}$  is low, increasing PUR thickness ( $d_{PUR}$ ) will lead to reduced  $\lambda_{tot}$ . Seeing that  $R_{MDF}$  is a constant value,  $\lambda_{tot}$  becomes decreased with higher  $d_{PUR}$  and lower  $d_{tot}$ , or with a higher thickness ratio of PUR core to panel.

This ratio from the 20W 50X70 and 20W 50X90 panels was lower than the 20W 100X panel; however, their thermal conductivities dropped instead of rising. It could be assumed that the thermal conductivity of the PUR in 20W 50X70 and 50X90 was very low compared with the 20W 100X panel, the overall thermal conductivity being marginally affected by the reduced foam thickness as a result.

Additionally, the thermal conductivity of PUR foam is determined partly by the pore structure of the foam and its cell size. The smaller the cell diameter, the lower the thermal conductivity (Engels et al., 2013). However, in this study, the relationship between cell

size and thermal conductivity was not found. The 20W 100X panel, with its lower cell diameter, still had higher thermal conductivity due to its higher foam density.

The thermal resistance or  $R$ -value is a requirement in the building industry, which is related directly to the thickness and conversely to the thermal conductivity. In Fig. 128 and 129,  $R$ -value and panel thickness are shown for comparison. The  $R$ -Value decreased with a lower panel thickness as the plate-closing time grew in each type of panel. However, when regarding the panel thickness, the 20W 100X showed lower thermal resistance than the 10W 50X60 and 10W 50X90, which implied lower insulating property for building purposes.

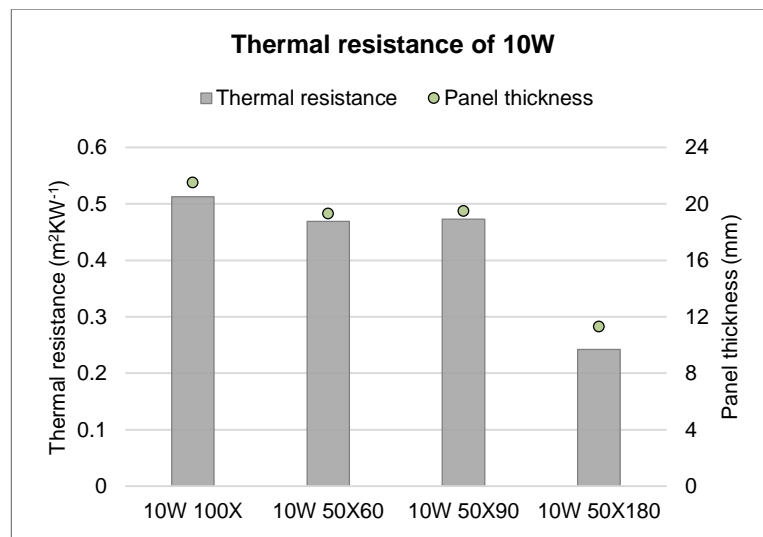


Fig. 128 Thermal resistance of 10W panels

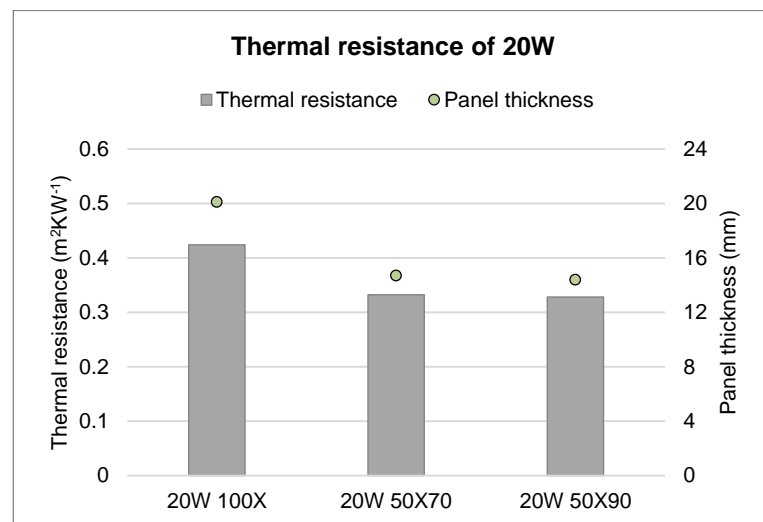


Fig. 129 Thermal resistance of 20W panels

## 5.4 Overall discussion

1-C PUR products were developed for the foaming process in the core layer during continuous panel production. The critical requirement of the core layer necessitates that foaming be triggered by the controlling of parameters. Blocked isocyanates facilitate the blending of polyol in isocyanates without the spontaneous reaction. In Study I, two types of blocked isocyanates were successfully prepared and mixed with polyol for PUR curing by setting at specific high temperatures. The cured products did not show polymerization of the PUR as regards the material appearance. The reactivity of isocyanates was prevented in the form of a blocked adduct. It was supposed to be reactive on heat curing for foaming products. Because of the low reactivity of NCO, unblocked isocyanates were used in further studies. Study II focused on the characteristics of PUR foam, that could be affected by the temperature in the hot-pressing machine. Aside from this, wood flour was added with different contents, to enhance the applicability of the PUR components owing to their liquidity. Heat-cured PUR foam with added wood flour shows the acceptable properties at specific levels. Study II confirmed the application of developed PUR formulations at high temperatures, so the components were investigated in the sandwich panel production in Study III. Since the foaming process of PUR could not be triggered by high temperatures in Study I, it was inspected temporally in Study III. The press program was designed by measuring the change in foam rise related to the internal temperature of foam. Panels produced by the varying press programs had their properties tested.

Although the mixtures cured at 250 °C presented similar IR absorbance to PUR, they did not change into the polymerized structure, as observed visibly. The end product was powdery and brittle (see Fig. 130), which could be attributed to the available blocking agents' side effects. To summarize, the prepared 1-C PUR mixture appeared to be cross-linked at the higher temperature rather than the target range between 90-120 °C, and the properties of the cured sample did not meet the requirement of the foaming reaction at curing temperature.



**Fig. 130 Cured product of mixture of blocked pMDI and polyol prepared by (left) NaHSO<sub>3</sub>-blocked pMDI (right) ε-caprolactam-blocked pMDI**

When comparing both blocking agents, a larger amount of isocyanate reacted to the water content during the blocking reaction by ε-caprolactam (34.71 %) than that of NaHSO<sub>3</sub> (3.94 %) according to the CO<sub>2</sub> detection test. The reaction between isocyanate and water forms amine (R-NH<sub>2</sub>), that further reacts with isocyanate to generate urea (R<sub>1</sub>-NH-CO-NH-R<sub>2</sub>); there was a notable absence of amine signals in the IR result of ε-caprolactam-blocked products. The existing urea can consume the available isocyanate in the system, becoming biuret and inducing a higher degree of cross-linking (Fig. 131). The generation of additional urea means greater possibilities for cross-linking. Consequently, curing ε-caprolactam-blocked isocyanates required a lower isocyanate/polyol ratio than the NaHSO<sub>3</sub>-blocked adducts, producing a more analogous IR result to PUR.

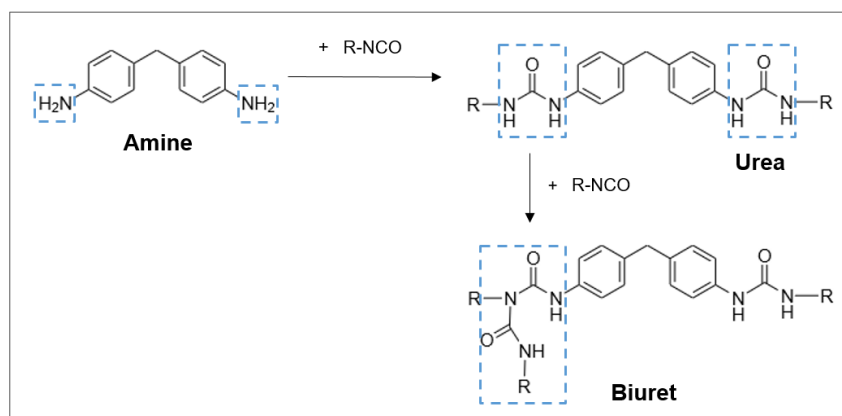


**Fig. 131 Possible reactions of MDI-amine side product with isocyanate to bond urea and biuret groups**

Another possibility for applying PUR in the one-step production process, was the addition of wood flour into the PUR mixture. In Study II, the properties of PUR rigid foam were investigated for the effects resulting from both the curing temperature and wood contents. Firstly, PUR samples blown by the addition of different water types (distilled water vs. wood moisture) exhibited no difference in FRH and weight loss during foaming. Still, they had significantly higher foaming ability compared to samples filled with moistureless, oven-dried wood flour. Presumably, foam curing at 100 °C releases

moisture from bound water – located within the wood's cell wall – and into the mixture to take part in the reaction, leading to a similar foaming result with samples blown by distilled water. Further tests were thus executed only by using distilled water for blowing.

The addition of wood did not affect the PUR foam's chemical characteristics, according to the consistency in IR results observed between wood-added and neat PUR foam, only its physical and mechanical properties. PUR containing a wood content of 40 % achieved a remarkably high density of ca.  $90 \text{ kgm}^{-3}$  in the OVEN1 test, with an NCO index of 1.0. Using this level of wood content increased the PUR densities due to the higher viscosity of the mixture (Yuan & Shi, 2009), which conformed to the foam morphology observed by SEM. Wood filler embedded in the struts tended to be found more regularly in higher wood flour contents because of the agglomeration. In other publications (Demiroğlu et al., 2017; Rodrigue et al., 2006), wood filler was observed to act as a nucleating agent that substantially reduced cell size and increased cell density. However, the significance of the cell size of PUR filled with wood contents of 0-12 % was not observed in this study. The chemical reaction between the isocyanate and water initially generated many fine  $\text{CO}_2$  bubbles on the surfaces of the fillers which would create a tearing of continuity at the particle-binder border (Krishnamurthi et al., 2003). It should describe the significant decline of compressive strength in PUR foam containing a wood concentration of 40 % with an average of 0.009 MPa, compared to that of 10 % filler containing PUR, which is 0.19 MPa. Yet, by adding up to 12 % of wood flour content in the OVEN2 test, the compressive properties did not vary significantly.

Curing temperature appears to have a greater influence on foam properties than the wood filler content. The density of wood-mixed PUR foam significantly decreased from an approximate average of  $146$  to  $70 \text{ kgm}^{-3}$ , when the curing temperature of  $100 \text{ }^\circ\text{C}$  was applied compared to room temperature. The difference in curing temperature showed remarkable results, especially between PUR cured at room temperature and  $100 \text{ }^\circ\text{C}$ . PUR samples cured at room temperature achieved the highest compressive strength (ca. 1 MPa) when compared with heat-cured samples at  $100\text{-}160 \text{ }^\circ\text{C}$  (0.14-0.32 MPa), in which the lowest compressive property was observed in samples using the highest curing temperature. The same findings were noticed in Young's modulus and the specific strength when the sample density was compensated. Based on the consistency in cell size between both groups (room temperature vs.  $100 \text{ }^\circ\text{C}$ ), the decreased compressive properties in heat-cured PUR were presumably caused by changes in other cell morphologies e.g. the cell shape and anisotropy, that create the cell alignment and corresponding structure for force absorption. A comparison of micrographs (Fig. 132) shows that PUR foam cured at high temperatures produced more anisotropic cells than

samples cured at lower temperatures, which had a more consistent cell shape and more spherical cells.

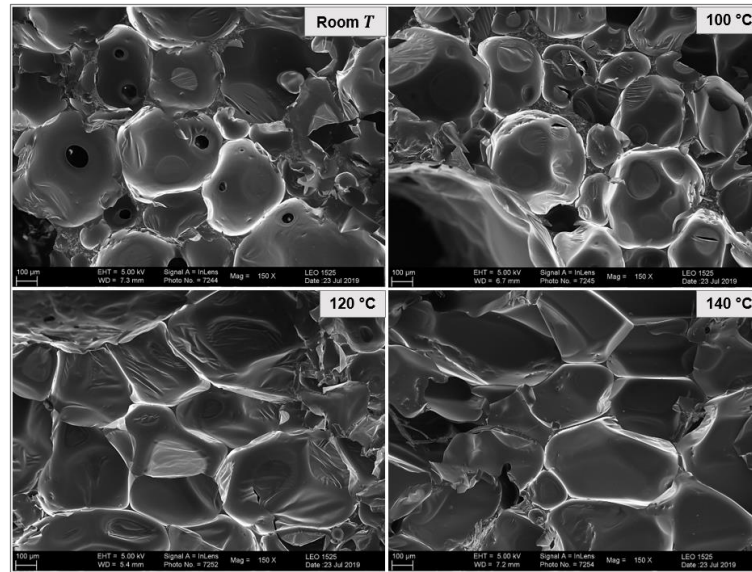


**Fig. 132 SEM micrographs of PUR foam with 10% wood content cured at different temperatures**

The cell size measurement showed a significantly higher cell diameter distribution when the curing temperature 160 °C was applied. For closed-cell content, the wood addition in this research induced PUR foam with lower closed-cell contents (56-65 % in 0-10 % wood-mixed PUR) than the value of PUR in the literature (85-95 %) (Szycher, 2012), which was possibly caused by a thermal curing process impacting the foam morphology. As shown in Fig. 73, the appearance of microvoids on the polymer matrix's cell wall implied irregular thickness distribution, which could be influenced by both the wood filler and curing temperature alike. Using different curing temperatures, sample groups cured at room temperature and 160 °C had relatively lower closed-cell contents than those cured at 100, 120 and 140 °C.

The wood particle's existence in the PUR component simplified the application due to the liquid mixture's reduced ratio being substituted by wood filler. An obstacle that appeared in the PUR formulation was the increase of viscosity in the mix once the components been combined, which complicated the regular distribution. In this study, the mixing proceeded until the components' homogeneous mass was reached, which supported the foam's slow expansion rate. The result from Study II provided a possible PUR application solution for in one-step production. From the most results the study could tell, that the addition of 10 % wood flour and curing temperature of 100 °C, appeared to be optimal parameters for further studies.

The concept of adding wood flour was investigated in Study II. It would make it possible to increase the solidity of mixture's components and simplify the distribution within the sandwich panels' middle layer. Since it was not possible to activate the reaction thermally by using the blocked isocyanate for the creation of PUR foam as found in Study I, the process, instead of being controlled by thermal activation, was controlled by the relationship between pressing time and foam rise in Study III. Foam rise was estimated related to the internal temperature of PUR to design the press program. The investigation in the case of cup testing (through video recording), indicated that maximal foam height was possibly related to the components' maximal internal temperature. The plate-closing or the pressing time was identified by time to foam rise. In this study, different press programs were created using various plate-closing times for: 50 % distance from the final plate-opening distance (50X), this being compared with the press program without plate-closing (100X). The goal thickness was not achieved in the 50X panels or when the plate-closing distance was applied. The PUR did not seem to offer sufficient resistance against pressing, which led to material loss during production.

The hot-pressing process produced a lower panel thickness than expected, as the foam could not expand naturally and therefore deviated from the foam density. Generally, 100X panels had higher foam density and panel thickness than 50X panels produced by different plate-closing times. With a longer pressing period, the panels tended to have reduced end thickness and corresponding density due to material loss by pressure. The 100X panels prepared from both sets of wood contents revealed a high level of deviation, compared to 50X panels from the same group; for varying compressive strength, the levels lay between 0.05-0.15 and 0.10-0.18 MPa in the 10W 100X and 20W 100X panels respectively. It could be explained by the free expansion of the mixture in 100X panels without the plate-closing step. The high deviation in the 100X panels was also found in the internal bond, which implied the foam structure's inhomogeneity expanded in their middle layer. The inhomogeneity of the foam could be attributed to the varying fractures in the structure observed by the SEM, which were short and long tears and collapsed cells. They appeared even before the mechanical testing, which could be related to the difference in the foams' expansion rate in each position, as well as deconstruction of the foam during formation by abrupt pressing.

PUR with wood contents of 10 and 20 % was applied to the middle layer of sandwich panels surfaced by MDF sheets. Higher density was found in the PUR layer with a higher wood content as expected. The foam densities were measured at between 33-90 and 32-153 kgm<sup>-3</sup> from the PUR cores, with 10 and 20 % wood content respectively. The compressive properties changed in direct conjunction with the foam densities. Higher

specific strength was also found in sample groups with higher foam densities. The internal bond and specific strength also varied in direct conjunction with the foam density. Failure mode via tension was observed within the foam layer and more regularly in the interconnection between the foam and MDF surfaces.

After all was said and done, a significant difference among different samples with regards to both the cell size and roundness ratio of the PUR foam, was not observed. The 100X panel with wood content of 20 %, showed a significantly smaller cell diameter, differing from other 20W panels. With regards to thermal conductivity, panels with a higher foam density exhibited higher or inferior thermal conductivity. Like the other property measurements, foam density appeared to impact the thermal conductivity rather than the panel density. The 10W panels had a lower thermal conductivity of 0.036-0.037  $\text{Wm}^{-1}\text{K}^{-1}$ , which is lower than that of the 20W panels, at 0.037-0.043  $\text{Wm}^{-1}\text{K}^{-1}$ ; this most likely depended on the foam density. Compared with the value of insulating PUR foam at 0.024  $\text{Wm}^{-1}\text{K}^{-1}$  (Engels et al., 2013), panels in this study had a slightly higher value.

# 6 Conclusion

---

The thesis provided solutions for creating new PUR formulations, for application in the one-step production process of sandwich wood-based panels. The chemical and physical development of the formulation was investigated in Study I and II, respectively. Active isocyanates were successfully blocked, both by  $\text{NaHSO}_3$  and  $\epsilon$ -caprolactam, these being tested independently of each other. The chemical characteristics and deblocking temperatures of blocked adducts conformed with past studies. The effects of wood contents and curing temperature on foam properties in Study II, suggested alternatives for cases when wood flour is added as well as thermal curing in PUR production, and what the optimal degree of addition is.

In the development of 1-C PUR formulation, results from both studies can lead to the following main conclusions:

- The deblocking temperature of isocyanates blocked by  $\text{NaHSO}_3$  was detected at a range of 90-127 °C, lower than with  $\epsilon$ -caprolactam (180-226 °C); the lower value corresponds with the application range within the pressing process.
- Curing the 1-C mix of blocked adducts and polyol at the temperatures up to 250 °C, did not lead to enough cross-linking in the PUR polymerization, though the cured product displays a similar IR result as PUR rigid foam.
- The thermal curing resulted in PUR foam densities being ca. 2-3 times lower than the sample cured at room temperature.
- An acceptable compressive strength of at least 0.14 MPa was achieved with a wood flour content of 10 % by thermal curing up to 160 °C; however, the compressive properties were reduced at higher curing temperatures, particularly the specific strength.
- A significant change in cell size, influenced by the addition of wood flour and thermal curing was rarely observed. The PUR mixture's viscosity increased on the addition of wood flour yet decreased by thermal curing, leading to counterbalanced results.
- The higher viscosity of wood flour reduces the miscibility between the polyol and the isocyanate, therefore deaccelerating the foam expansion.

The extended time to foam expansion could be advantageous in continuous production. It provides sufficient time for panel pressing prior to the opening of the hot plates for core expansion. However, the application of the PUR components as a result of the pressure

resistance was not clarified. To investigate both assumptions, PUR with added wood was introduced into the process in Study III, where the press program had been designed from the foam rise rate. The study confirmed previous findings, that the maximal foam height was related to the maximal internal temperature of the components. Panels with a pressing step (50X panels) were produced for property comparison with panels without a pressing step (100X panels). The results are summed up as follows:

- The target panel thickness was achieved only in 100X panels.
- Decreases in panel thickness and density were observed with a longer pressing period due to material loss by pressing.
- 100X panels exhibited a higher deviation in foam properties (compression and internal bond) than the 50X panels due to the free but irregular foam expansion.

Despite an excessive isocyanate ratio, the 1-C PUR mix containing blocked isocyanate lacked sufficient reactivity for PUR polymerization. Hence, the concept of PUR foam production being reactivated by the hot press's temperature is still impractical. The low release of isocyanate found by the FTIR measurement after deblocking, can describe the low rate of PUR activity, which can be reasoned by the following consumptions.

- I. Possible degradation pathways of urethane bonds at high temperature (Fig. 65).
- II. Low content of isocyanate in the blocked adducts and side effects from chemical characteristics of existing blocking agents.

Creating a press program was possible following the PUR mixture's internal temperature; however, only an exact timing for the press opening could prevent the PUR foam from cell collapse and deconstruction. The convective heat transfers from the varying distance between hot plates should be considered because of their effects on viscosity, foam rise rate and corresponding morphologies of the produced foam. To implement the PUR mix components in the industrial process, a temperature measurement and camera system should be installed in the core layer, in order to monitor the foam expansion for opening of the hot pressing plates at the precise moment. At the same time, the compaction of the surface layer is challenging due to the flowability of components. The typical high level of pressure used to compress the wood-based surfaces in the first stage, could lead to material loss and irregular distribution of foam components in the core layer. The applicable press program should be designed to hold the hot plate distance following the foam rise yet not introduce additional pressure too early. After the foam's stabilization, the pressure can be applied. Simultaneously, a low pressing temperature is suggested in the first stage, being increased afterward in order to avoid stabilization of the panel before foam expansion.

# 7 Outlook

---

PUR is advantageous due to its thermosetting properties, since it would allow the production of foam core panels at an industrial scale; in principle with existing production lines and without a cooling unit. On the contrary, PUR as a chemical reactive polymer, challenges utilization as the core material in the process as regards the required characteristics for the one-step production i.e. expandable under heat, regularly distributed and pressure-resistant in its unexpanded state. This thesis showed problems arising from the application of the concepts. Chemically blocked isocyanate could provide good storage stability and prevent the PUR reacting before its application. In this thesis, the blocked isocyanate could not form the PUR's foam structure due to the low release rate of isocyanate and assumedly the side effects of the blocking agents. In future research, the chemical effects of blocking agents on 1-C PUR mixture and the cured products' correspondent properties should be thoroughly determined. Besides that, some promising aspects could be suggested below for future research, to enhance the activity of the NCO groups:

- The prepolymer is possibly a solution for cross-linking by transcaramoylation reaction (Fig. 65 d) with polyols. As presented by Delebecq et al. (2012), urethane can rearrange into a new urethane or urea compound in the presence of a more nucleophilic molecule. The approach is regularly used in the coating industry for a one-pot, slow polymerization process.
- The microencapsulation of isocyanate or physically blocked isocyanate, in which isocyanate is separated in the shell. As mentioned in chapter 2.3, the shell wall, made of PUR or polyurea, could be formed by the interfacial polymerization of isocyanate with active hydrogen. Instead of activation by temperature, pressure was employed to control the release of the isocyanate from the core when applied for plywood production by Ma et al. (2019).

Still, pressure resistance could be a concerning point. The shell of the microcapsule must be designed to resist more pressure and, at the same time, release a sufficient rate of NCO under activated conditions. Assuming that the highly cross-linked polymerization could be generated, PBAs would be added to the mixture during the PUR exothermic reaction for foaming the structure. Another trend in the PUR industry is non-isocyanate polyurethanes (NIPU) from cyclic carbonate functional polymers. The concept appears as an attractive alternative to solve the toxicity problems from isocyanate functions,

especially NIPU from renewable resources. NIPU is initiated by the synthesis of cyclic carbonates, followed by their reaction with amines or polyamine compounds (Kathalewar et al., 2013). However, the rate of this reaction is relatively slow compared to the common PUR reaction. Methods are available nowadays to circumvent this lack of reactivity (Delebecq et al., 2012).

PUR has many advantages because of its versatility, and the polyol as the PUR main component could be garnered from renewable resources. The excellent insulating property and tailor-made characteristic depending on selected ingredients and processing parameters, make PUR an attractive core layer for bio-based sandwich wood panels. The PUR components' feasibility within the existing production line by the one-step process, will give it an economic advantage. This gap is not currently being fulfilled by the raw material available on the market. PUR's adjustment as the core material for the sandwich panel's continuous process is still intriguing as regards further research. Regarding the constant development in the PUR industry, advanced approaches are worth knowing for utilizing PUR in its different forms within the wood-based panels, to increase economic and ecological advantages and extend application areas.

## Appendix I: FTIR absorbance units of PUR

Tab. 23 FTIR absorbance units of PUR as reviewed in Jiao et al. (2013)

| Frequency<br>(cm <sup>-1</sup> )      | Functional groups  |
|---------------------------------------|--|
| <u>Isocyanate segment</u>             |  |
| 3389                                  | Broad absorption bands, stretching vibrations of N-H                       |
| 3322.9                                | Broad absorption bands, stretching vibrations of N-H                       |
| 1526.4                                | Medium-strong band, in-plane bending vibration of N-H                      |
| 1726.3                                | Sharp absorption band, typical for the stretching vibration of esters C=O  |
| 1221.9                                | Sharp absorption band, asymmetric stretching vibration of C-O, from N-CO-O |
| 916.8                                 | Weak band, N-CO-O symmetric stretching vibration                           |
| 1604.4                                | vibration of C=C in benzene ring   |
| 767-916.8                             | out-of-plane bending vibration of C-H in multi-substituted benzene ring    |
| <u>polyether polyols soft segment</u> |  |
| 2979.5                                | stretching vibration of C-H in methyl                                      |
| 2929                                  | stretching vibration of C-H in methylene                                   |
| 2873                                  | stretching vibration of C-H in methylene                                   |
| 1380                                  | symmetric bending vibration of -CH <sub>3</sub>                            |
| 1082.7                                | broad and strong band from ether bond C-O-C stretch                        |

## Appendix II: Calculation of atom ratios in different materials

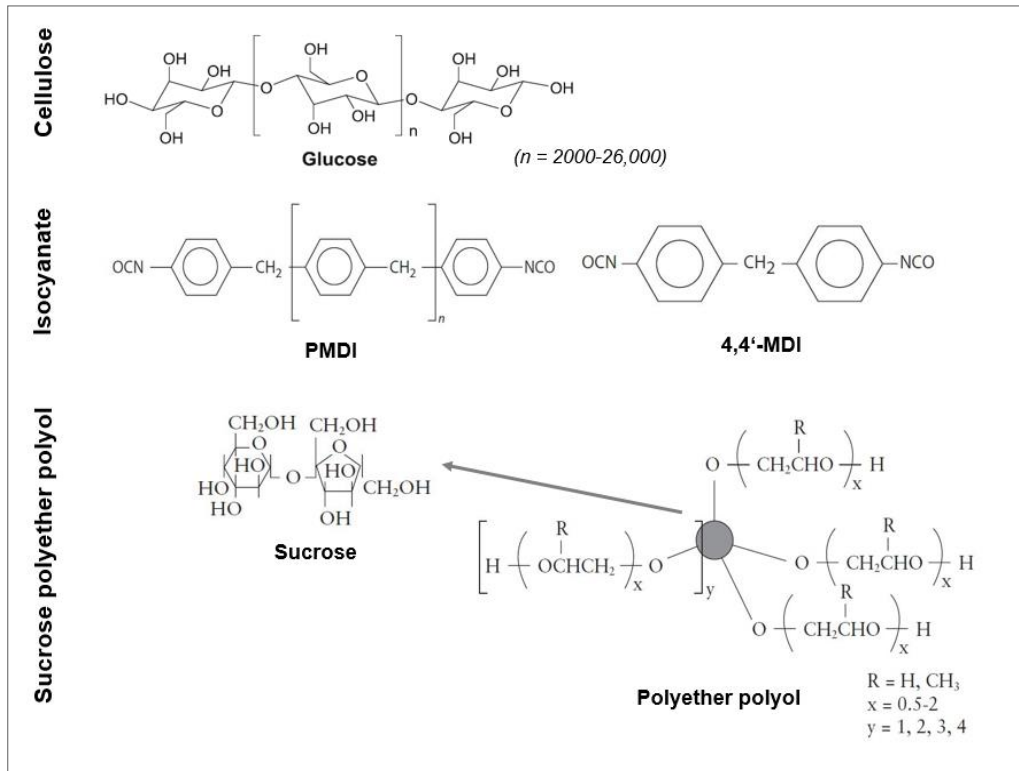


Fig. 133 Structure of cellulose (Abdellaoui et al., 2018), isocyanate and polyol modified from Szycher (2012)

- For polyether polyol structure without sucrose,  
no. of C atom =  $2xy$  or  $3xy$  when R is H or CH<sub>3</sub>, respectively  
no. of O atom =  $(x+1)y$
- Added with sucrose with 12 C atoms and 11 O atoms reduced by  $y$  O atoms for bonding,  
total no. of C atom =  $2xy + 12$  or  $3xy + 12$   
total no. of O atom =  $(x+1)y + 11 - y = xy + 11$
- In case of minimum C atoms ( $x = 0.5$ ,  $y = 1$ ),  
C atoms would be  $\rightarrow 2xy + 12 = 13$  with O atoms for  $xy+11 = 11.5$
- In case of maximum C atoms ( $x = 2$ ,  $y = 4$ )  
C atoms would be  $\rightarrow 3xy + 12 = 36$  with O atoms for  $xy+11 = 19$

Tab. 24 Calculated atom number and percentage of C, O, N containing in reference materials

| Material type                         | n      | C             |       | O        |       | N        |       |
|---------------------------------------|--------|---------------|-------|----------|-------|----------|-------|
|                                       |        | atom no.      | %     | atom no. | %     | atom no. | %     |
| <b>Cellulose</b>                      | 2000   | 12012         | 54.54 | 10011    | 45.46 | n.a.     | n.a.  |
|                                       | 26000  | 156012        | 54.55 | 130011   | 45.45 | n.a.     | n.a.  |
| <b>Sucrose-based polyether polyol</b> | min. C | 13            | 53.06 | 11.5     | 46.94 | n.a.     | n.a.  |
|                                       | max. C | 36            | 65.45 | 19       | 34.55 | n.a.     | n.a.  |
| <b>MDI</b>                            |        | 15            | 78.95 | 2        | 10.53 | 2        | 10.53 |
| <b>PMDI</b>                           |        | >MDI (=15+7n) |       | 2        | <MDI  | 2        | <MDI  |
| <b>PUR</b>                            | min. C | 28            | 64.37 | 13.5     | 31.03 | 2        | 4.60  |
| <b>1.0 NCO index</b>                  | max. C | 51            | 68.92 | 21       | 28.38 | 2        | 2.70  |

### Appendix III: Internal temperature of PUR mixture during pressing

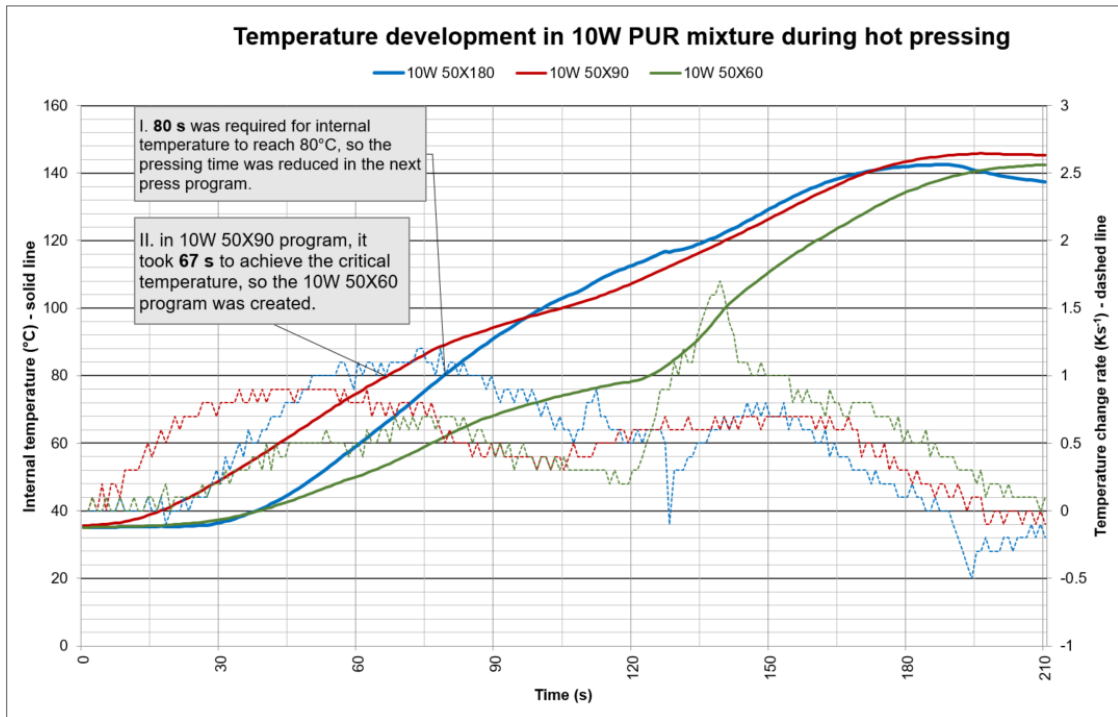


Fig. 134 Internal temperature and change rate of PUR mixture with 10 % wood content

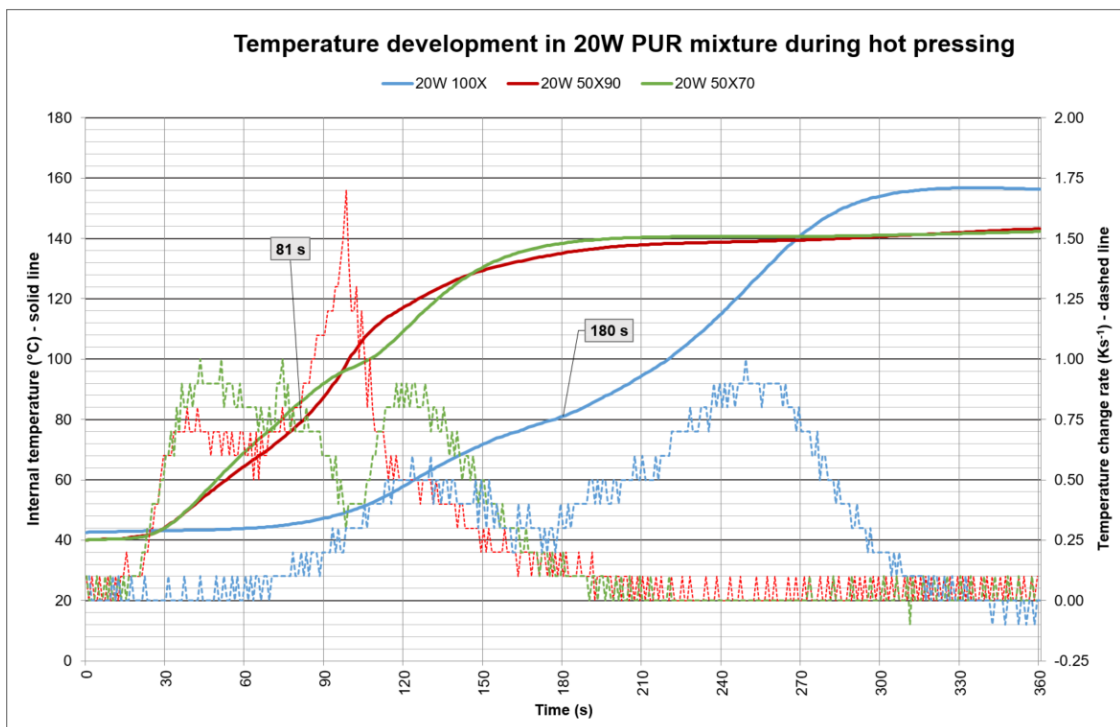


Fig. 135 Internal temperature and change rate of PUR mixture with 20 % wood content

## List of Tables

|         |  |     |
|---------|--|-----|
| Tab. 1  | Properties of polymer core materials (Klein, 2009; Kollmann et al., 1975) .....  | 11  |
| Tab. 2  | Product examples of sandwich wood panel with plastic foam core and their application areas.....  | 12  |
| Tab. 3  | Typical properties of PUR rigid foams transformed in the metric system (Szycher, 2012).....  | 23  |
| Tab. 4  | Advantages and disadvantages of commonly used techniques.....  | 39  |
| Tab. 5  | General ambient conditions and requirements for the core layer material .....  | 43  |
| Tab. 6  | Overview of Study I.....   | 45  |
| Tab. 7  | Overview of Study II.....  | 45  |
| Tab. 8  | Overview of Study III.....   | 46  |
| Tab. 9  | Specifications of polyol (Desmophen 1240N) and isocyanates (Desmodur 44P16, 4,4'-MDI).....   | 47  |
| Tab. 10 | Specifications of blocking agents.....   | 47  |
| Tab. 11 | Weight ratios of raw chemicals used for preparation of blocked isocyanates .....   | 48  |
| Tab. 12 | Heating programs applied on deblocked isocyanates for the measurement of NCO conversion rate .....   | 50  |
| Tab. 13 | Mixture samples prepared by different factors for PUR curing.....  | 51  |
| Tab. 14 | Applied parameters in experiments of PUR foam production.....  | 53  |
| Tab. 15 | Formulations of PUR components used for panel production .....   | 55  |
| Tab. 16 | Absorbance of C=O and NCO frequencies in pure and NaHSO <sub>3</sub> -blocked isocyanates .....  | 69  |
| Tab. 17 | Absorbance of C-H and NCO frequencies in pure and ε-caprolactam-blocked isocyanates .....  | 74  |
| Tab. 18 | Summary of deblocking temperatures measured in the research compared to reported values from literature a. Zhang et al. (2011), b. Lee et al. (2005) ..... | 77  |
| Tab. 19 | Void fraction percentage depending on filler contents and temperatures .....   | 107 |
| Tab. 20 | Reaction time for full cup, maximal foam height, maximal internal temperature and temperature change rate in different samples.....                        | 118 |
| Tab. 21 | Average temperature change rate of different samples divided into three periods .....  | 120 |
| Tab. 22 | Locations of failure observed from the tensile shear in different panels .....   | 130 |
| Tab. 23 | FTIR absorbance units of PUR as reviewed in Jiao et al. (2013).....  | 144 |
| Tab. 24 | Calculated atom number and percentage of C, O, N containing in reference materials.....  | 145 |

## List of Figures

|         |  |    |
|---------|--|----|
| Fig. 1  | Development of world population and global wood-based panel production compared with woody crop area over 1992-2018 (FAOSTAT, 2020).....   | 5  |
| Fig. 2  | Density of wood-based materials and cell wall (Monteiro et al., 2018).....   | 8  |
| Fig. 3  | Classification of measured employed to maintain the properties of wood-reduced particleboards at those of commercially manufactured panels (Benthien et al., 2019) ...           | 9  |
| Fig. 4  | Homogeneous and structured core materials (Pflug et al., 2002) .....   | 11 |
| Fig. 5  | Failure modes of sandwich beam (Gibson & Ashby, 1999).....   | 14 |
| Fig. 6  | Failure mode map loaded in 3-point bending (Gibson & Ashby, 1999) .....  | 15 |
| Fig. 7  | Continuous line of foam production (Davies, 2008).....   | 18 |
| Fig. 8  | Schematic of (a) the conventional particleboard process in comparison to (b) the foam core panel process (Thoemen, 2008).....  | 19 |
| Fig. 9  | Development of a production process for foam core particleboards in an industrial scale (Shalbafan et al., 2016) .....   | 21 |
| Fig. 10 | (left) European plastic converter demand by polymer types in 2017 adapted from PlasticsEurope, (right) PUR consumption in different forms 2016 adapted from PlasticInsight ..... | 22 |
| Fig. 11 | Thermal conductivity values of various insulating materials (Engels et al., 2013)  |    |
| Fig. 12 | MDI and MDI polymer .....  | 24 |
| Fig. 13 | Important PUR reactions (blowing and polymerization) adapted from Demharter (1998).....  | 26 |
| Fig. 14 | Production of PUR rigid foam adapted from Kapps & Buschkamp (2004) .....   | 28 |
| Fig. 15 | Rise rate, volume expansion, and reaction exotherm of a water-blown rigid foam (Lee & Ramesh, 2004) .....  | 29 |
| Fig. 16 | (a) Symbols represent experimental results for foam height (b) Bubble pressure simulation (Al-Moameri et al., 2016). .....   | 30 |
| Fig. 17 | Probable reaction between isocyanate group of PUR and cellulosic fiber adapted from Mothé et al. (2009).....   | 33 |
| Fig. 18 | Cellulose structure (Siqueira et al., 2010).....   | 34 |
| Fig. 19 | Reaction schemes of isocyanate with or bonded to wood containing water (Gao et al., 2005) .....  | 35 |
| Fig. 20 | Common reactions used in PUR chemistry (Delebecq et al., 2012).....  | 37 |
| Fig. 21 | a Blocking and deblocking reaction of isocyanate, b Curing reaction (Delebecq et al., 2012) .....  | 38 |
| Fig. 22 | Blocking agents divided into O-based and N-based compounds, considered by the atom that reacts to C-atom of NCO group in the formation of blocked adducts .....                  | 40 |
| Fig. 23 | Blocking and deblocking reaction of isocyanate and NaHSO <sub>3</sub> .....  | 41 |
| Fig. 24 | Blocking and deblocking reaction of isocyanate and ε-caprolactam .....   | 42 |
| Fig. 25 | Procedure for designing press program divided in four steps .....  | 54 |
| Fig. 26 | Component mixture, scattering on the surface layers, compaction of surface layers, a finished panel with frame   |    |
| Fig. 27 | Press programs, without pressing and with 50% plate-opening distance .....   | 56 |
| Fig. 28 | Procedure for the development of press program   |    |
| Fig. 29 | Preparation steps of PUR samples for property testing.....   | 57 |
| Fig. 30 | Sample cutting profile for panel characterization .....  | 58 |

|  |    |
|--|----|
| Fig. 31 Schematic diagram of gas pycnometer (ASTM D6226) .....   | 63 |
| Fig. 32 DSC curve of commercial blocked TDI .....  | 67 |
| Fig. 33 FTIR spectra of commercial blocked TDI before and<br>after heating up to 250 °C by DSC.....  | 68 |
| Fig. 34 FTIR spectra of pure pMDI and NaHSO <sub>3</sub> -blocked adduct   |    |
| Fig. 35 FTIR spectra of pure 4,4'-MDI and NaHSO <sub>3</sub> -blocked adduct .....   | 69 |
| Fig. 36 DSC curve of NaHSO <sub>3</sub> -blocked pMDI  |    |
| Fig. 37 DSC curve of NaHSO <sub>3</sub> -blocked 4,4'-MDI .....  | 70 |
| Fig. 38 DSC curve of NaHSO <sub>3</sub> -blocked pMDI and 4,4'-MDI in the range of 0-150 °C with<br>cooling-down and reheating phases, measured by heating rate of 4 Kmin <sup>-1</sup> .....                      | 71 |
| Fig. 39 TGA and DTG curve of NaHSO <sub>3</sub> -blocked pMDI  |    |
| Fig. 40 TGA and DTG curve of NaHSO <sub>3</sub> -blocked 4,4'-MDI .....  | 72 |
| Fig. 41 FTIR spectra of pure pMDI and ε-caprolactam-blocked adduct   |    |
| Fig. 42 FTIR spectra of pure 4,4'-MDI and ε-caprolactam-blocked adduct .....   | 73 |
| Fig. 43 DSC curve of ε-caprolactam-blocked pMDI and 4,4'-MDI .....   | 74 |
| Fig. 44 TGA and DTG curve of ε-caprolactam-blocked pMDI  |    |
| Fig. 45 TGA and DTG curve of ε-caprolactam-blocked 4,4'-MDI .....  | 76 |
| Fig. 46 FTIR spectra of NaHSO <sub>3</sub> -blocked pMDI and after heating at 120 °C by DSC .....  | 79 |
| Fig. 47 FTIR curves of NaHSO <sub>3</sub> -blocked pMDI at different temperatures  |    |
| Fig. 48 FTIR curves of NCO absorption band from ε-caprolactam-blocked pMDI<br>at different time and temperatures .....   | 80 |
| Fig. 49 Absorbance ratios of NCO normalized to C-H in blocked and deblocked pMDI .....   | 81 |
| Fig. 50 Absorbance ratios of NCO normalized to C-H in blocked and deblocked 4,4'-MDI .....   | 82 |
| Fig. 51 FTIR spectra of sucrose-based polyether polyol (Desmophen 1240N)   |    |
| Fig. 52 FTIR spectra of PUR foam prepared from Desmophen 1240N and<br>Desmodur 44P16 (pMDI) .....  | 83 |
| Fig. 53 FTIR spectra of mixtures of NaHSO <sub>3</sub> -blocked pMDI and polyol cured at 250 °C<br>prepared in different ratios (a) 1:1, (b) 3:1, (c) 2:1 .....  | 84 |
| Fig. 54 Enlarged FTIR spectra of mixtures from the last figure   |    |
| Fig. 55 FTIR spectra of mixture of NaHSO <sub>3</sub> -blocked pMDI and polyol cured at<br>(a) 150 °C and (b) 250 °C .....   | 85 |
| Fig. 56 FTIR spectra of 2:1 w/w mixture of NaHSO <sub>3</sub> -blocked pMDI and polyol<br>cured at 200 °C without curing time (a) and using different times (b-e) .....  | 86 |
| Fig. 57 FTIR spectra of 2:1 w/w mixture of NaHSO <sub>3</sub> -blocked pMDI and polyol cured at 200 °C<br>by different heating rates: (a) 5 Kmin <sup>-1</sup> (b) 10 Kmin <sup>-1</sup> (c) 20 Kmin <sup>-1</sup> |    |
| Fig. 58 FTIR spectra of mixtures of NaHSO <sub>3</sub> -blocked isocyanates and polyol cured at 250 °C<br>prepared by different weight ratios .....  | 87 |
| Fig. 59 FTIR spectrum of (a) 1:1 w/w mixture of ε-caprolactam-blocked pMDI and polyol<br>compared with (b) IR result of PUR .....  | 88 |
| Fig. 60 FTIR spectra of mixtures of ε-caprolactam-blocked pMDI and polyol cured at 250 °C<br>prepared in (a) 2:1, (b) 3:1 weight ratios  |    |
| Fig. 61 FTIR spectra of 1:1 w/w mixture of ε-caprolactam-blocked pMDI and polyol<br>cured at different temperatures: (a) 200 °C (b) 225 °C (c) 250 °C .....  | 89 |
| Fig. 62 FTIR spectra of 1:1 mixture of ε-caprolactam-blocked pMDI and polyol cured<br>at 200 °C (a) without and (b) with curing period of 30 min.....  | 90 |
| Fig. 63 FTIR spectra of 1:1 mixture of ε-caprolactam-blocked pMDI and polyol cured<br>at 250 °C (a) without and (b) with curing period of 15 min.....  | 91 |

|  |     |
|--|-----|
| Fig. 64 FTIR spectrum of 2:1 mixture of $\epsilon$ -caprolactam-blocked 4,4'-MDI and polyol cured at 250 °C .....                  | 91  |
| Fig. 65 Possible degradation reactions of urethane bond (Delebecq et al., 2012) .....  | 92  |
| Fig. 66 FRH, Weight loss of PUR foam with 0-20 % wood contents (%w/w tot) .....  | 94  |
| Fig. 67 FTIR spectra of pure and wood-mixed PUR foam .....   | 96  |
| Fig. 68 Microvoids found in 2 % wood-mixed sample built in the center of cell intersection   |     |
| Fig. 69 Several microvoids located in the polymer matrix in 6 % wood-mixed sample  |     |
| Fig. 70 Thick cell wall formed by irregularly distributed filler from 8 % wood-mixed sample .....                                  | 97  |
| Fig. 71 Rough surface structure of cell strut embedded by filler in 4 % wood-mixed sample  |     |
| Fig. 72 Cell appearance with spotted cell wall found in 12 % wood-mixed sample .....   | 98  |
| Fig. 73 a: Polymer surface, b-e: Spotted surface, f-h: Embedded filler with PUR, i: Filler particle .....                          | 99  |
| Fig. 74 Percentage atom ratios of C, O, N in observed areas (Fig. 73 a-i) related to calculated values of reference materials..... | 100 |
| Fig. 75 Open and closed-cell proportion of PUR foam with 0-10 % wood contents  |     |
| Fig. 76 Open and closed-cell proportion of PUR foam mixed by 10, 20 % wood contents cured at different temperatures .....          | 101 |
| Fig. 77 Morphology of PUR foam with 10 % wood content cured at room temperature .....  | 102 |
| Fig. 78 Cell size distribution and averages ( $\bar{x}$ ) of PUR foam with 0-12 % wood contents .....                              | 103 |
| Fig. 79 Cell size distribution and averages ( $\bar{x}$ ) of PUR foam with 10 % wood content cured at different temperatures ..... | 104 |
| Fig. 80 Cell size distribution and averages ( $\bar{x}$ ) of PUR foam with 20 % wood content cured at different temperatures       |     |
| Fig. 81 Cell density of PUR foam with 0-12 % wood contents .....   | 105 |
| Fig. 82 Cell density of PUR foam cured at different temperatures .....   | 106 |
| Fig. 83 Void fraction percentage and cell size in relation to cell density.....  | 107 |
| Fig. 84 FRD of PUR foam with 0-20 % wood contents  |     |
| Fig. 85 Sample density and FRD of PUR foam with 0-40 % wood contents   |     |
| Fig. 86 Density distribution of sample groups using 0, 20 and 40 % wood contents.....  | 108 |
| Fig. 87 Sample density of PUR foam with 0-12 % wood content  |     |
| Fig. 88 Density distribution of sample groups using 0, 6 and 12 % wood contents  |     |
| Fig. 89 Sample density of PUR foam cured at different temperatures   |     |
| Fig. 90 Density distribution of sample groups cured at room temperature and 100 °C .....   | 109 |
| Fig. 91 Compressive strength of PUR foam with 0-40 % wood contents   |     |
| Fig. 92 Young's modulus and specific strength of PUR foam with 0-40 % wood contents .....  | 110 |
| Fig. 93 Compressive strength of PUR foam with 0-12 % wood contents   |     |
| Fig. 94 Young's modulus and specific strength of PUR foam with 0-12 % wood contents .....  | 111 |
| Fig. 95 Compressive strength of wood-mixed PUR foam cured at different temperatures  |     |
| Fig. 96 Young's modulus and specific strength of wood-mixed PUR foam cured at different temperatures .....                         | 112 |
| Fig. 97 Relationship between compressive modulus and density for PUR foam with different wood contents.....                        | 113 |
| Fig. 98 Relationship between compressive modulus and density for PUR foam cured at room temperature (■) and 100-160 °C (●) .....   | 114 |
| Fig. 99 Relationship between cell density and compressive modulus of PUR foam  |     |
| Fig. 100 Relationship between cell size and compressive modulus of PUR foam .....  | 115 |
| Fig. 101 Internal temperature and temperature change rate of PUR mixture cured at room temperature and 140 °C .....                | 117 |

|          |  |     |
|----------|--|-----|
| Fig. 102 | Internal temperature of PUR mixture cured at different temperatures, with marks as the foam reached the full cup level (+) and the maximal foam height (●)                         |     |
| Fig. 103 | Foam rise in full cup and maximum height as appeared at different curing temperatures.....   | 118 |
| Fig. 104 | Temperature change rate in PUR mixture using different sample weights and pressing temperatures.....   | 119 |
| Fig. 105 | Internal temperature of PUR mixture displaying the reversal point .....  | 120 |
| Fig. 106 | Internal temperature of PUR mixture with 10 % wood content pressed by 100 % plate-opening distance and panel properties .....  | 121 |
| Fig. 107 | Press program applied in panels with 10 % wood content mixture displaying distance of pressing plates varied in time, Thickness of panel produced by different press programs..... | 122 |
| Fig. 108 | Press program applied in panels with 20 % wood content mixture displaying distance of pressing plates varied in time, Thickness of panel produced by different press programs..... | 123 |
| Fig. 109 | SEM photos of 10W 100X samples showing the long fracture in the middle   |     |
| Fig. 110 | SEM photos of 10W 50X samples with collapsed cell area (C) and small tears (T)   |     |
| Fig. 111 | SEM photos of 20W samples showing inhomogeneity, region of small cells at the bottom of panel and small breaks (T) .....   | 124 |
| Fig. 112 | Cell size distribution of PUR foam with 10 % wood content measured in 10W panels   |     |
| Fig. 113 | Cell size distribution of PUR foam with 20 % wood content measured in 20W panels   |     |
| Fig. 114 | Distribution of roundness ratio of foam cells with 10 % wood content in 10W panels   |     |
| Fig. 115 | Distribution of roundness ratio of foam cells with 20 % wood content in 20W panels .....   | 125 |
| Fig. 116 | Distribution of foam density from PUR core layer in 10W samples  |     |
| Fig. 117 | Distribution of foam density from PUR core layer in 20W samples .....  | 126 |
| Fig. 118 | Panel density and thickness of 10W panels compared with foam density   |     |
| Fig. 119 | Panel density and thickness of 20W panels compared with foam density .....   | 127 |
| Fig. 120 | Compressive and specific strength of 10W panels  |     |
| Fig. 121 | Young's modulus of 10W panels .....  | 128 |
| Fig. 122 | Compressive and specific strength of 20W panels  |     |
| Fig. 123 | Young's modulus of 20W panels .....  | 129 |
| Fig. 124 | Internal bond of 10W panels  |     |
| Fig. 125 | Internal bond of 20W panels .....  | 130 |
| Fig. 126 | Thermal conductivity related to densities of 10W panels  |     |
| Fig. 127 | Thermal conductivity related to densities of 20W panels.....   | 131 |
| Fig. 128 | Thermal resistance of 10W panels   |     |
| Fig. 129 | Thermal resistance of 20W panels .....   | 133 |
| Fig. 130 | Cured product of mixture of blocked pMDI and polyol prepared by NaHSO <sub>3</sub> -blocked pMDI, ε-caprolactam-blocked pMDI   |     |
| Fig. 131 | Possible reactions of MDI-amine side product with isocyanate to bond urea and biuret groups.....   | 135 |
| Fig. 132 | SEM micrographs of PUR foam with 10% wood content cured at different temperatures.....   | 137 |
| Fig. 133 | Structure of cellulose (Abdellaoui et al., 2018), isocyanate and polyol modified from Szycher (2012) .....   | 145 |
| Fig. 134 | Internal temperature and change rate of PUR mixture with 10 % wood content   |     |
| Fig. 135 | Internal temperature and change rate of PUR mixture with 20 % wood content.....  | 146 |

## References

- Abdellaoui, H., Bouhfid, R., & Qaisw-1s, A. E. K. (2018). Lignocellulosic Fibres Reinforced Thermoset Composites: Preparation, Characterization, Mechanical and Rheological Properties. In S. Kalia (Ed.), *Springer Series on Polymer and Composite Materials. Lignocellulosic Composite Materials* (Vol. 33, pp. 215–270). Springer International Publishing. [https://doi.org/10.1007/978-3-319-68696-7\\_5](https://doi.org/10.1007/978-3-319-68696-7_5)
- Al-Moameri, H., Zhao, Y., Ghoreishi, R., & Suppes, G. J. (2016). Simulation Blowing Agent Performance, Cell Morphology, and Cell Pressure in Rigid Polyurethane Foams. *Industrial & Engineering Chemistry Research*, 55(8), 2336–2344. <https://doi.org/10.1021/acs.iecr.5b04711>
- ASTM D1622. *Test Method for Apparent Density of Rigid Cellular Plastics* (ASTM D1622 - 08). West Conshohocken, PA. ASTM International.
- ASTM D6226. *Test Method for Open Cell Content of Rigid Cellular Plastics* (ASTM D6226 - 10). West Conshohocken, PA. ASTM International.
- ASTM D7487. *Practice for Polyurethane Raw Materials: Polyurethane Foam Cup Test* (ASTM D7487-18). West Conshohocken, PA. ASTM D7487-18.
- ASTM D883. *Terminology Relating to Plastics* (ASTM D883 - 20a). West Conshohocken, PA. ASTM International.
- Atiqah, A., T Mastura, M., A Ahmed Ali, B., Jawaid, M., & M Sapuan, S. (2017). A review on polyurethane and its polymer composites. *Current Organic Synthesis*, 14(2), 233–248. <https://www.ingentaconnect.com/content/ben/cos/2017/00000014/00000002/art00011>
- Barbu, M. C., Lüdtke, J., Thömen, H., & Welling, J. (2010). Innovative production of wood-based lightweight panels. *Processing Technologies for the Forest and Biobased Products Industries, MC Barbu, Ed*, 115–122. [http://conference.fh-salzburg.ac.at/fileadmin/files/documents/PTF\\_BPI\\_2010.pdf#page=120](http://conference.fh-salzburg.ac.at/fileadmin/files/documents/PTF_BPI_2010.pdf#page=120)
- Barruet, J., Gaillet, C., & Penelle, J. (2007). Easy One-Pot Synthesis of a Reactive Hydrogel from Commercially Available 2-Isocyanatoethyl Methacrylate and K<sub>2</sub>S<sub>2</sub>O<sub>5</sub>. *Macromolecular Rapid Communications*, 28(20), 2007–2011. <https://doi.org/10.1002/marc.200700355>
- Benthien, J. T., Lüdtke, J., & Ohlmeyer, M. (2019). Effect of increasing core layer particle thickness on lightweight particleboard properties. *European Journal of Wood and Wood Products*, 77(6), 1029–1043. <https://doi.org/10.1007/s00107-019-01452-5>
- Bodig, J., & Jayne, B. A. (1982). *Mechanics of wood and wood composites*. Van Nostrand Reinhold New York.
- Casado, U., Marcovich, N. E., Aranguren, M. I., & Mosiewicki, M. A. (2009). High-strength composites based on tung oil polyurethane and wood flour: Effect of the filler concentration on the mechanical properties. *Polymer Engineering & Science*, 49(4), 713–721. <https://doi.org/10.1002/pen.21315>
- Choe, K. H., Lee, D. S., Seo, W. J., & Kim, W. N. (2004). Properties of rigid polyurethane foams with blowing agents and catalysts. *Polymer Journal*, 36(5), 368–373. <https://doi.org/10.1295/polymj.36.368>
- Choupani Chaydarreh, K., Shalbfan, A., & Welling, J. (2017). Effect of ingredient ratios of rigid polyurethane foam on foam core panels properties. *Journal of Applied Polymer Science*, 134(17). <https://doi.org/10.1002/app.44722>
- Davies, J. M. (2008). *Lightweight sandwich construction*. John Wiley & Sons.

- Delebecq, E., Pascault, J.-P., Boutevin, B., & Ganachaud, F. (2012). On the versatility of urethane/urea bonds: reversibility, blocked isocyanate, and non-isocyanate polyurethane. *Chemical Reviews*, 113(1), 80–118. <https://doi.org/10.1021/cr300195n>
- Demharter, A. (1998). Polyurethane rigid foam, a proven thermal insulating material for applications between+ 130 C and- 196 C. *Cryogenics*, 38(1), 113–117. [https://doi.org/10.1016/S0011-2275\(97\)00120-3](https://doi.org/10.1016/S0011-2275(97)00120-3)
- Demiroğlu, S., Erdoğan, F., Akin, E., KARAVANA, H. A., & SEYDİBEYOĞLU, M. Ö. (2017). Natural Fiber Reinforced Polyurethane Rigid Foam. *Gazi University Journal of Science*, 30(2). <https://api.semanticscholar.org/CorpusID:136256568>
- DIN CEN/TS 16368:2014-06. *Leichte Spanplatten\_- Anforderungen; Deutsche Fassung CEN/TS\_16368:2014*. Berlin. Beuth Verlag GmbH.
- DIN EN 319. *DIN EN 319:1993-08, Spanplatten und Faserplatten; Bestimmung der Zugfestigkeit senkrecht zur Plattenebene; Deutsche Fassung EN\_319:1993* (DIN EN 319:1993-08 DIN EN 319:1993-08). Berlin. Beuth Verlag GmbH.
- Engels, H.-W., Pirkl, H.-G., Albers, R., Albach, R. W., Krause, J., Hoffmann, A., Casselmann, H., & Dormish, J. (2013). Polyurethanes: versatile materials and sustainable problem solvers for today's challenges. *Angewandte Chemie International Edition*, 52(36), 9422–9441. <https://doi.org/10.1002/anie.201302766>
- FAOSTAT. (2020). *FAO. Food and Agriculture Organization of the United Nations*. <http://www.fao.org/faostat/en/#data>
- Gama, N., Ferreira, A., & Barros-Timmons, A. (2018). Polyurethane Foams: Past, Present, and Future. *Materials*, 11. <https://doi.org/10.3390/ma11101841>
- Gao, Z. H., Gu, J. Y., Wang, X.-M., Li, Z. G., & Bai, X. D. (2005). FTIR and XPS study of the reaction of phenyl isocyanate and cellulose with different moisture contents. *Pigment & Resin Technology*, 34(5), 282–289. <https://doi.org/10.1108/03699420510620300>
- Gibson, L. J., & Ashby, M. F. (1999). *Cellular solids: structure and properties*. Cambridge university press.
- Gu, R., & Sain, M. M. (2013). Effects of wood fiber and microclay on the performance of soy based polyurethane foams. *Journal of Polymers and the Environment*, 21(1), 30–38. <https://doi.org/10.1007/s10924-012-0538-y>
- Han, X., Zeng, C., Lee, L. J., Koelling, K. W., & Tomasko, D. L. (2003). Extrusion of polystyrene nanocomposite foams with supercritical CO<sub>2</sub>. *Polymer Engineering & Science*, 43(6), 1261–1275. <https://doi.org/10.1002/pen.10107>
- Hee Kim, S., Lim, H., Chul Song, J., & Kyu Kim, B. (2008). Effect of blowing agent type in rigid polyurethane foam. *Journal of Macromolecular Science, Part a: Pure and Applied Chemistry*, 45(4), 323–327. <https://doi.org/10.1080/10601320701864260>
- Hellmann, T. (Ed.) (2012). *Ressourceneffizienz in der Möbelproduktion – ein Lei(ch)tfaden*.
- ISO 844. *DIN EN ISO 844:2014-11, Harte Schaumstoffe\_- Bestimmung der Druckeigenschaften (ISO\_844:2014); Deutsche Fassung EN\_ISO\_844:2014*. Berlin. Beuth Verlag GmbH.
- Jiao, L., Xiao, H., Wang, Q., & Sun, J. (2013). Thermal degradation characteristics of rigid polyurethane foam and the volatile products analysis with TG-FTIR-MS. *Polymer Degradation and Stability*, 98(12), 2687–2696. <https://doi.org/10.1016/j.polymdegradstab.2013.09.032>
- Jones, R. (2008). Cross-linking organic coatings with blocked isocyanates. *Transactions of the IMF*, 86(2), 75–79. <https://doi.org/10.1179/174591908X264464>

- Kanner, B., & Decker, T. G. (1969). Urethane foam formation—role of the silicone surfactant. *Journal of Cellular Plastics*, 5(1), 32–39. <https://doi.org/10.1177%2F0021955X6900500104>
- Kapps, M., & Buschkamp, S. (2004). The production of rigid polyurethane foam. *Bayer Materials Science*, 20, 3–12. <http://www.sabro.com.pk/wp-content/uploads/2018/05/Poly-Urethane-Foaming-Technical-Catalogue.pdf>
- Karlsson, K. F., & TomasÅström, B. (1997). Manufacturing and applications of structural sandwich components. *Composites Part a: Applied Science and Manufacturing*, 28(2), 97–111. [https://doi.org/10.1016/S1359-835X\(96\)00098-X](https://doi.org/10.1016/S1359-835X(96)00098-X)
- Kathalewar, M. S., Joshi, P. B., Sabnis, A. S., & Malshe, V. C. (2013). Non-isocyanate polyurethanes: from chemistry to applications. *RSC Advances*, 3(13), 4110–4129. <https://doi.org/10.1039/C2RA21938G>
- Kharazipour, A., & Bohn, C. (2013). Use of popcorn for timber and composite materials(8,568,895). Washington, DC: U.S. Patent and Trademark Office.
- Klein, B. (2009). *Leichtbau-Konstruktion*. Springer.
- Kollmann, F. F. P., Kuenzi, E. W., & Stamm, A. J. (1975). Principles of wood science and technology. Wood based materials.
- Krishnamurthi, B., Bharadwaj-Somaskandan, S., Sergeeva, T., & Shutov, F. (2003). Effect of wood flour fillers on density and mechanical properties of polyurethane foams. *Cellular Polymers*, 22(6), 371–381. <https://doi.org/10.1177%2F026248930302200602>
- Kuranska, M., & Prociak, A. (2012). Porous polyurethane composites with natural fibres. *Composites Science and Technology*, 72(2), 299–304. <https://doi.org/10.1016/j.compscitech.2011.11.016>
- Kurańska, M., Aleksander, P., Mikelis, K., & Ugis, C. (2013). Porous polyurethane composites based on bio-components. *Composites Science and Technology*, 75, 70–76. <https://doi.org/10.1016/j.compscitech.2012.11.014>
- Kurańska, M., Prociak, A., Cabulis, U., & Kirpluks, M. (2015). Water-blown polyurethane-polyisocyanurate foams based on bio-polyols with wood fibers. *Polimery*, 60. <https://doi.org/10.14314/polimery.2015.705>
- Lee, & Ramesh, N. S. (2004). *Polymeric foams: Mechanisms and materials. Polymeric foams series*. CRC Press.
- Lee, J. M., Subramani, S., Lee, Y. S., & Kim, J. H. (2005). Thermal decomposition behavior of blocked diisocyanates derived from mixture of blocking agents. *Macromolecular Research*, 13(5), 427–434. <https://doi.org/10.1007/BF03218476>
- Libni, G., Ali, B. M., Sathiyaraj, S., & Nasar, A. S. (2018). Catalysis of cure reaction of  $\epsilon$ -caprolactam-blocked polyisocyanate with diol using non-tin catalysts. *Journal of Macromolecular Science, Part a: Pure and Applied Chemistry*, 55(7), 552–558. <https://doi.org/10.1080/10601325.2018.1481346>
- Lim, H., Kim, E. Y., & Kim, B. K. (2010). Polyurethane foams blown with various types of environmentally friendly blowing agents. *Plastics, Rubber and Composites*, 39(8), 364–369. <https://doi.org/10.1179/174328910X12691245469835>
- Lubis, M. A. R., Park, B.-D., & Lee, S.-M. (2017). Modification of urea-formaldehyde resin adhesives with blocked isocyanates using sodium bisulfite. *International Journal of Adhesion and Adhesives*, 73, 118–124. <https://doi.org/10.1016/j.ijadhadh.2016.12.001>
- Lüdtke, J. (2011). Entwicklung und Evaluierung eines Konzepts für die kontinuierliche Herstellung von Leichtbauplatten mit polymerbasiertem Kern und Holzwerkstoffdecklagen.

- Lüdtke, J., Welling, J., Thömen, H., & Barbu, M. C. (2007). Verfahren zum Herstellen einer Sandwichplatte bzw. Leichtbau-Holzwerkstoffplatte. *Leichtbau-Holzwerkstoffplatte. Application for European Patent DE*, 10(2007), 12.
- Ma, Y., Jiang, Y., Tan, H., Zhang, Y., & Gu, J. (2017). A rapid and efficient route to preparation of isocyanate microcapsules. *Polymers*, 9(7), 274. <https://doi.org/10.3390/polym9070274>
- Ma, Y., Zhang, Y., Liu, X., & Gu, J. (2019). Synthesis of isocyanate microcapsules as functional crosslinking agent for wood adhesive. *The Journal of Adhesion*, 1–15. <https://doi.org/10.1080/00218464.2019.1625039>
- Mantau, U., Saal, U., Prins, K., Steierer, F., Lindner, M., Verkerk, H., Eggers, J., Leek, N., Oldenburger, J., & Asikainen, A. (2010). Real potential for changes in growth and use of EU forests. *Hamburg: EUwood, Methodology Report*.
- Matuana, L. M., & Mengeloglu, F. (2002). Manufacture of rigid PVC/wood-flour composite foams using moisture contained in wood as foaming agent. *Journal of Vinyl and Additive Technology*, 8(4), 264–270. <https://doi.org/10.1002/vnl.10373>
- Monteiro, S., Martins, J., Magalhães, F. D., & Carvalho, L. (2018). Lightweight wood composites: challenges, production and performance. In *Lignocellulosic Composite Materials* (pp. 293–322). Springer. [https://doi.org/10.1007/978-3-319-68696-7\\_7](https://doi.org/10.1007/978-3-319-68696-7_7)
- Mosiewicki, M. A., Casado, U., Marcovich, N. E., & Aranguren, M. I. (2012). Moisture dependence of the properties of composites made from tung oil based polyurethane and wood flour. *Journal of Polymer Research*, 19(2), 9776. <https://doi.org/10.1007/s10965-011-9776-2>
- Mosiewicki, M. A., Dell'Arciprete, G. A., Aranguren, M. I., & Marcovich, N. E. (2009). Polyurethane Foams Obtained from Castor Oil-based Polyol and Filled with Wood Flour. *Journal of Composite Materials*, 43(25), 3057–3072. <https://doi.org/10.1177/0021998309345342>
- Mothé, C. G., Araujo, C. R. de, & Wang, S. H. (2009). Thermal and mechanical characteristics of polyurethane/curaua fiber composites. *Journal of Thermal Analysis and Calorimetry*, 95(1), 181–185. <https://doi.org/10.1007/s10973-008-9091-2>
- Nilsson, E., & Nilsson, A. C. (2002). Prediction and measurement of some dynamic properties of sandwich structures with honeycomb and foam cores. *Journal of Sound and Vibration*, 251(3), 409–430. <https://doi.org/10.1006/jsvi.2001.4007>
- Nolte Holzwerkstoff GmbH & Co. KG. (2009, March 26). *Nolte Holzwerkstoff GmbH & Co KG stellt „AirMaxx“ vor: Neues Leichtgewicht* [Press release]. Gernersheim, Germany. <https://www.bm-online.de/allgemein/neues-leichtgewicht/#slider-intro-3>
- Parker, B. A. (1986). Structural insulated panel system(4,628,650). Washington, DC: U.S. Patent and Trademark Office.
- Petrović, Z. S. (2008). Polyurethanes from vegetable oils. *Polymer Reviews*, 48(1), 109–155. <https://doi.org/10.1080/15583720701834224>
- Pflug, J., Xinyu, F., Vangrimde, B., Verpoest, I., Brattfisch, P., & Vandepitte, D. (Eds.) (2002). *Development of a sandwich material with polypropylene/natural fibre skins and paper honeycomb core*.
- PlasticInsight. *Polyurethane Properties, Production, Price, Market, and Uses* [Press release]. <https://www.plasticsinsight.com/resin-intelligence/resin-prices/polyurethane/#what>
- PlasticsEurope. *Plastics – the Facts 2018: An analysis of European plastics production, demand and waste data* [Press release]. [https://www.plasticseurope.org/application/files/6315/4510/9658/Plastics\\_the\\_facts\\_2018\\_AF\\_web.pdf](https://www.plasticseurope.org/application/files/6315/4510/9658/Plastics_the_facts_2018_AF_web.pdf)

- Premkumar, S., Chozhan, C. K., & Alagar, M. (2008). Studies on thermal, mechanical and morphological behaviour of caprolactam blocked methylenediphenyl diisocyanate toughened bismaleimide modified epoxy matrices. *European Polymer Journal*, *44*(8), 2599–2607. <https://doi.org/10.1016/j.eurpolymj.2008.05.031>
- Prociak, A., Kurańska, M., Malewska, E., Szczepkowski, L., Zieleniewska, M., Ryszkowska, J., Ficoń, J., & Rząsa, A. (2015). Biobased polyurethane foams modified with natural fillers. *Polimery*, *60*. <https://doi.org/10.14314/polimery.2015.592>
- Randall, D., & Lee, S. (2002). *The polyurethanes book*. Wiley.
- Reich, O. (1962). Die Biegung der Sandwichbalken. *Wiss. Zeitschrift Der TU-Dresden*, *11*(1), 71–86.
- Rizvi, G., Matuana, L. M., & Park, C. B. (2000). Foaming of PS/wood fiber composites using moisture as a blowing agent. *Polymer Engineering & Science*, *40*(10), 2124–2132. <https://doi.org/10.1002/pen.11345>
- Rodrigue, D., Souici, S., & Twite-Kabamba, E. (2006). Effect of wood powder on polymer foam nucleation. *Journal of Vinyl and Additive Technology*, *12*(1), 19–24. <https://doi.org/10.1002/vnl.20062>
- Rolph, M. S., Markowska, A. L. J., Warriner, C. N., & O'Reilly, R. K. (2016). Blocked isocyanates: From analytical and experimental considerations to non-polyurethane applications. *Polymer Chemistry*, *7*(48), 7351–7364. <https://doi.org/10.1039/C6PY01776B>
- Shalbfan, A. (2013). Investigation of foam materials to be used in lightweight wood based composites.
- Shalbfan, A., Chaydarreh, K. C., & Welling, J. (2016). Development of a One-Step Process for Production of Foam Core Particleboards using Rigid Polyurethane Foam. *BioResources*, *11*(4), 9480–9495. <https://doi.org/10.15376/biores.11.4.9480-9495>
- Silverstein, R. M., & Bassler, G. C. (1962). Spectrometric identification of organic compounds. *Journal of Chemical Education*, *39*(11), 546. <https://doi.org/10.1021/ed039p546>
- Simon, J., Barla, F., Kelemen-Haller, A., Farkas, F., & Kraxner, M. (1988). Thermal stability of polyurethanes. *Chromatographia*, *25*(2), 99–106. <https://doi.org/10.1007/BF02259024>
- Siqueira, G., Bras, J., & Dufresne, A. (2010). Cellulosic bionanocomposites: a review of preparation, properties and applications. *Polymers*, *2*(4), 728–765. <https://doi.org/10.3390/polym2040728>
- Sponholz, K. (2017, January 13). *Spanplatte aus Popcorn ist leicht und spart Ressourcen*. EnBauSa.de. <https://www.enbausa.de/daemmung/aktuelles/artikel/spanplatte-aus-popcorn-ist-leicht-und-spart-ressourcen-4828.html>
- Stosch, M. (Ed.). (2009). *BM Special: Lightweight Design - Material, Technology, Processing* [Special issue]. Konradin Verlag.
- Subramani, S., Cheong, I. W., & Kim, J. H. (2004). Chain extension studies of water-borne polyurethanes from methyl ethyl ketoxime/ $\epsilon$ -caprolactam-blocked aromatic isocyanates. *Progress in Organic Coatings*, *51*(4), 328–338. <https://doi.org/10.1016/j.porgcoat.2004.08.004>
- Szycher, M. (2012). *Szycher's handbook of polyurethanes*. CRC Press.
- Tang, Y.-F., Liu, J., Li, Z., Chen, B.-Y., & Mei, S.-F. (2013). Study on blocking and deblocking kinetics of diisocyanate with  $\epsilon$ -caprolactam using ftir spectroscopy. *Asian Journal of Chemistry*, *25*, 5703–5706. <https://doi.org/10.14233/ajchem.2013.OH67>

- Thirumal, M., Khastgir, D., Singha, N. K., Manjunath, B. S., & Naik, Y. P. (2008). Effect of foam density on the properties of water blown rigid polyurethane foam. *Journal of Applied Polymer Science*, *108*(3), 1810–1817. <https://doi.org/10.1002/app.27712>
- Thoemen, H. (Ed.) (2008). *Lightweight panels for the European furniture industry: Some recent developments*.
- Trovati, G., Sanches, E. A., Neto, S. C., Mascarenhas, Y. P., & Chierice, G. O. (2010). Characterization of polyurethane resins by FTIR, TGA, and XRD. *Journal of Applied Polymer Science*, *115*(1), 263–268. <https://doi.org/10.1002/app.31096>
- Wicks, D. A., & Wicks, Z. W. (2001). Blocked isocyanates III: Part B: Uses and applications of blocked isocyanates. *Progress in Organic Coatings*, *41*(1), 1–83. [https://doi.org/10.1016/S0300-9440\(00\)00164-8](https://doi.org/10.1016/S0300-9440(00)00164-8)
- Wicks, D. A., & Wicks Jr, Z. W. (1999). Blocked isocyanates III: Part A. Mechanisms and chemistry. *Progress in Organic Coatings*, *36*(3), 148–172. [https://doi.org/10.1016/S0300-9440\(99\)00042-9](https://doi.org/10.1016/S0300-9440(99)00042-9)
- Wiedemann, J. (2007). *Leichtbau: Elemente und Konstruktion*. Springer-Verlag.
- Yang, J., Keller, M. W., Moore, J. S., White, S. R., & Sottos, N. R. (2008). Microencapsulation of isocyanates for self-healing polymers. *Macromolecules*, *41*(24), 9650–9655. <https://doi.org/10.1021/ma801718v>
- Yuan, J., & Shi, S. Q. (2009). Effect of the addition of wood flours on the properties of rigid polyurethane foam. *Journal of Applied Polymer Science*, *113*(5), 2902–2909. <https://doi.org/10.1002/app.30322>
- Zenkert, D. (1995). *An introduction to sandwich construction*. Engineering materials advisory services.
- Zhang, Y., Gu, J., Jiang, X., Zhu, L., & Tan, H. (2011). Investigation on blocking and deblocking isocyanates by sodium bisulphite. *Pigment & Resin Technology*, *40*(6), 379–385. <https://doi.org/10.1108/03699421111180527>
- Zhao, Y., Gordon, M. J., Tekeei, A., Hsieh, F.-H., & Suppes, G. J. (2013). Modeling reaction kinetics of rigid polyurethane foaming process. *Journal of Applied Polymer Science*, *130*(2), 1131–1138. <https://doi.org/10.1002/app.39287>
- Zhou, Z., Lv, H., Wang, X., Ren, F., & Xu, W. (2013). Deblocking of the water-soluble isophorone diisocyanate blocked by sodium bisulfite and its application. *Journal of Applied Polymer Science*, *128*(1), 597–599. <https://doi.org/10.1002/app.38238>
- Zhu, M., Bandyopadhyay-Ghosh, S., Khazabi, M., Cai, H., Correa, C., & Sain, M. (2012). Reinforcement of soy polyol-based rigid polyurethane foams by cellulose microfibers and nanoclays. *Journal of Applied Polymer Science*, *124*(6), 4702–4710. <https://doi.org/10.1002/app.35511>
- Zuckerstätter, G., WOLLBOLDT, P., SCHILD, G., WEBER, H. K., & Sixta, H. (2010). Advanced NMR based characterization of wood and wood products. *Processing Technologies for the Forest and Biobased Products Industries*, 90. [http://conference.fh-salzburg.ac.at/fileadmin/files/documents/PTF\\_BPI\\_2010.pdf#page=95](http://conference.fh-salzburg.ac.at/fileadmin/files/documents/PTF_BPI_2010.pdf#page=95)

# Acknowledgements

---

This thesis becomes a reality despite the continuing COVID-19 pandemic with the kind support and help of many individuals.

Foremost, I am highly indebted to the Ministry of Higher Education, Science, Research and Innovation of Thailand for supporting me with a full-term scholarship from Bachelor to Ph.D. since my arrival in Germany in 2008. My special thanks are extended to the staff of the Office of Educational Affairs, Germany, for facilitating the basic requirements for my studying life here.

The completion of my dissertation would not have been possible without the support, guidance, and nurturing of Prof. Dr. Andreas Krause, my research project supervisor. He recommended the topic and provided me with precious experience. I am incredibly grateful to him.

Special thanks should be given to Dr. Jan Lüdtkke for his practical suggestions and constructive criticism and Dr. Ralph Lehnen for the chemical knowledge. I wish to thank both mentors for their contribution to this work.

I am incredibly grateful for the assistance given by Johannes Beruda, Dörte Annett Bielenberg, and Stefani Warsaw as regards their valuable technical support. The experiments could not have been executed smoothly without general help from Johannes in the laboratory, Dörte on property measurements, and Steffi for the sample preparation.

I would like to recognize the assistance that I received from Tanya Potsch for the SEM analysis and Sergej Kaschuro to facilitate the Keyence microscope. The PUR foam structure would not be well investigated without their effort.

I also had the great pleasure of working with Martina Heitmann. She assisted me in preparing blocked isocyanates, especially in handling with the DSC and FTIR instruments.

Furthermore, I wish to acknowledge the external help provided by the following individuals:

- Uta Sazama (Institut für Anorganische und Angewandte Chemie, UHH) for the thermoanalysis of blocked isocyanates.

- Ranate Walter (Institut für Zoologie for SEM, UHH) for the preparation and SEM analysis of PUR foam specimens.
- Dr. Thomas Emmeler (Institute of Membrane Research, Helmholtz-Zentrum Geesthacht) for facilitating the gas pycnometer and assisting me with measurement of open-cell content.

I appreciate the support from my WPC group colleagues (Bright, Emilin, Goran, Julien, Julius, Linh, Marco, Martin, Michael, Pourya, Sylvia) who were happy and ready to help and discuss the related topics. The advice and corrections given by Martin have been a great help in TGA.

I would like to offer my special thanks to Bettina Steffen and Valentina Zemke for moral support and the great friendship that cannot be underestimated.

Thanks should also go to Thai friends in Hamburg, my roommates Som, Tutoo or sharing experience and simplifying my life aboard, and Bennet, who always listens and encourages me with a positive attitude.

Finally, I wish to thank my family for their support and encouragement throughout my study for their profound belief in my abilities, primarily my brother Udom, who has inspired and supported me with his guidance all along my academic way.

*Ph.D. study can be harder than PUR rigid foam.*

*Support from people around me is like PUR adhesive that combines the strength of different materials into the reinforced structure.*

*Fear from falling fades away with the backup from beloved ones, in the same way, the mattress from PUR flexible foam does.*